Deciphering PLN-R14del Cardiomyopathy

From Pathological Mechanisms to Therapeutic Modulation

Liu Sun

Stellingen behorende bij het proefschrift:

Deciphering PLN-R14del Cardiomyopathy:

From Pathological Mechanisms to Therapeutic Modulation

Liu Sun

1. Distinct pathogenic phospholamban variants may drive cardiomyopathy through mechanisms that extend beyond impaired SERCA regulation, including maladaptive protein interactions and structural remodeling of the sarco/endoplasmic reticulum – *this thesis*
2. In a mouse model of PLN-R14del cardiomyopathy, common cardiac remodeling pathways are not sufficient to accelerate disease onset. – *this thesis*
3. In PLN-R14del cardiomyopathy, disruption of sarco/endoplasmic reticulum organization and proteome homeostasis occurs early and precedes major functional deterioration – *this thesis*
4. The therapeutic benefit of PLN-ASO in PLN-R14del cardiomyopathy appears to be driven primarily by restoration of SR structure rather than by correction of calcium cycling. – *this thesis*
5. PLN silencing is a promising targeted therapeutic strategy because interventions aimed at the primary molecular defect are more likely to succeed than those aimed only at downstream consequences – *this thesis*
6. Computational modeling of PLN complexes can complement experimental biology and improve our mechanistic understanding of variant-specific cardiomyopathy – *this thesis*
7. Difficult circumstances may slow a person down, but they do not determine the final destination.
8. *Per aspera ad astra.* – Latin proverb

Deciphering PLN-R14del Cardiomyopathy: From Pathological Mechanisms to Therapeutic Modulation

Liu Sun

孙 柳

Liu Sun
Deciphering PLN-R14del Cardiomyopathy: From Pathological Mechanisms to Therapeutic Modulation

PhD dissertation University of Groningen, the Netherlands
The publication of this thesis was financially supported by University of Groningen, University Medical Center Groningen, and Graduate School of Medical Sciences.

Cover design: Liu Sun
Lay-out: Liu Sun
Printed by: ProefschriftMaken.nl
Copyright © 2026 by Liu Sun

All rights reserved. No part of this publication may be reproduced, stored in a retrieval system, or transmitted in any form or by any means, electronic, mechanical, photocopying, recording or otherwise, without prior permission.

university of groningen

Deciphering PLN-R14del Cardiomyopathy: From Pathological Mechanisms to Therapeutic Modulation

PhD thesis

to obtain the degree of PhD at the
University of Groningen
on the authority of the
Rector Magnificus Prof. E. Sterken
and in accordance with
the decision by the College of Deans.

This thesis will be defended in public on

Wednesday 27 May 2026 at 16:15 hours

by

Liu Sun
Born on 11 August 1993

Supervisor
Prof. H. H. W. Silljé

Co-supervisor
Dr. V. Oliveira Nunes Teixeira

Assessment committee
Prof. R.A. de Boer
Prof. A. J. A. van de Sluis
Prof. J. P. van Tintelen

Paranymphs
Rani Puspitarani
Xuanxuan Guo

TABLE OF CONTENTS

Chapter 1	Introduction and aims	*2*
Chapter 2	Beyond SERCA: Emerging mechanisms of pathogenic PLN variants in cardiomyopathy	*16*
Chapter 3	Cardiac remodeling pathways do not accelerate disease onset and severity in a mouse model of PLN-R14del cardiomyopathy	*42*
Chapter 4	An inducible mouse model of PLN-R14del cardiomyopathy reveals early proteomic changes in the sarco/endoplasmic reticulum	*80*
Chapter 5	In PLN-R14del mice, SR structure restoration, rather than calcium cycling, is the dominant effector of PLN-ASO treatment	*108*
Chapter 6	Simulating the impact of phospholamban (PLN) silencing on PLN complexes in PLN-R14del cardiomyopathy	*142*
Chapter 7	General discussion and future perspectives	*160*
Appendices		*174*

Netherlandse samenvatting	Dutch summary
Dankwoord	Acknowledgements
Curriculum vitae	About the author

Chapter 1

Introduction and aims

General introduction

Introduction to Cardiomyopathy

Cardiomyopathy comprises a heterogeneous group of disorders affecting the myocardium, and is characterized by structural and/or functional abnormalities of the heart muscle. These changes may cause enlargement of the heart, thickening of heart walls, or increased stiffness, ultimately reducing cardiac performance and reducing the ability to pump blood efficiently. The etiology of cardiomyopathy is diverse and includes genetic mutations, viral infections, metabolic or autoimmune disorders, as well as prolonged exposure to cardiotoxic agents such as alcohol and certain medications.

Genetically determined cardiomyopathies, also referred to as inherited cardiomyopathies, constitute a subset of heart muscle diseases caused by pathogenic variants transmitted within families. These conditions typically arise from mutations in genes involved in sarcomere structure, desmosome integrity, or ion channel function. As a result, they can lead to progressive myocardial dysfunction and an increased risk of heart failure, arrhythmias, and sudden cardiac death.[1,2]

Cardiomyopathies can broadly be classified into several types of which the major forms are summarized here. ***I)*** Hypertrophic cardiomyopathy (HCM) is primarily characterized by abnormal thickening of the heart muscle, which can lead to left ventricular outflow obstruction, diastolic dysfunction, and arrhythmias. It is most commonly associated with mutations in sarcomeric genes such as MYH7 (β-myosin heavy chain) and MYBPC3 (myosin-binding protein C).[3] ***II)*** Dilated cardiomyopathy (DCM), is marked by ventricular dilation and systolic dysfunction, often resulting from mutations in a diverse set of genes, including amongst others, TTN (titin), LMNA (lamin A/C), and PLN (phospholamban).[4-6] ***III)*** Arrhythmogenic cardiomyopathy (ACM) primarily affects the right ventricle and is characterized by the replacement of myocardial tissue with fibrofatty deposits. It is commonly associated with mutations in desmosomal genes such as PKP2, DSG2, DSC2, JUP and DSP.[7] ***IV)*** Restrictive cardiomyopathy (RCM) is a rarer form, distinguished by abnormal diastolic function that leads to severe heart stiffness and restricted ventricular filling. This condition is often linked to mutations in troponin genes (TNNC1, TNNT2, and TNNI3), which impair myocardial relaxation.[8] Although the different cardiomyopathy subtypes were originally defined by phenotypic characteristics, specific genetic variants do not always confirm to a single classification. In some cases, the same pathogenic variant may give rise to distinct cardiomyopathy phenotypes depending on the individual carrier. Furthermore, different variants of the same gene may also cause different types of cardiomyopathies. Thus, there can be considerable complexity and overlap between cardiomyopathies.

Introduction to PLN-Related Genetic Cardiomyopathy

Despite its small size, the phospholamban (PLN or PLB) gene harbors numerous mutations that have been implicated in inherited cardiomyopathies. Over the past

decades, a number of human PLN variants have been identified as disease causing, including E2stop,[9] R9C,[10] R9H,[11] R9L,[11] R14del,[12] R25C,[13] and L39stop,[14] Although the exact pathological mechanisms of the PLN variants are still incompletely understood, we do have comprehensive knowledge on the physiological function of PLN. This tiny 52-amino acid protein is located in the sarcoplasmic reticulum (SR) membrane of ventricular myocytes **(Figure 1)**. It plays a crucial role in regulating calcium (Ca^{2+}) homeostasis in ventricular cardiomyocytes by modulating the activity of the sarcoplasmic reticulum calcium ATPase 2a (SERCA2a). PLN can assemble into pentamers or exist as monomers, with the monomeric form being the primary functional inhibitor of SERCA2a. In its dephosphorylated state under resting conditions, monomeric PLN binds to SERCA2a and lowers its apparent affinity for Ca^{2+}, thereby limiting Ca^{2+} reuptake into the sarcoplasmic reticulum (SR) during diastole.

The inhibitory action of PLN on SERCA2a is dynamically regulated by the β-adrenergic pathway. Upon β-adrenergic stimulation, PLN is phosphorylated by the cAMP-dependent protein kinase (PKA) at serine 16 and undergoes a conformational change that relieves its inhibitory effect on SERCA2a, thereby enhancing calcium reuptake into the SR.[15] This phosphorylation-dependent regulation of SERCA2a by PLN is important for maintaining proper calcium cycling, ensuring efficient cardiac muscle relaxation and contraction **(Figure 1)**.

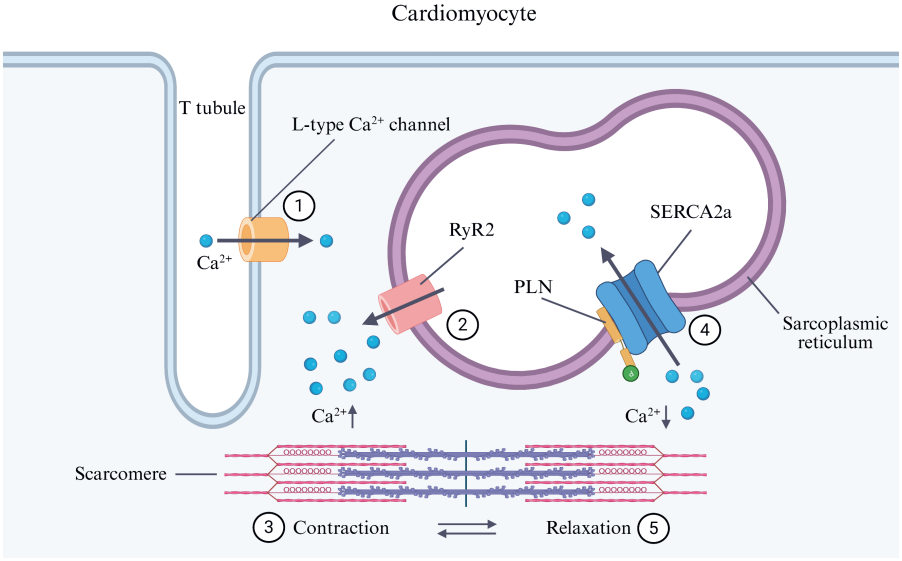

Figure 1. Schematic representation of the function of Ca^{2+} flow in healthy cardiac myocytes.
Upon an action potential in late diastole, **(1)** extracellular Ca^{2+} enters cardiomyocytes and **(2)** triggers the release of large amounts of Ca^{2+} via the Ryonodine Receptor 2 (RyR2) from the sarcoplasmic reticulum (SR). This causes the **(3)** contraction of sarcomeres. **(4)** SERCA2a mediated SR Ca^{2+} uptake, results in reduced cytoplasmic Ca^{2+} concentration and hence **(5)** relaxation of sarcomeres. The Ca^{2+} reuptake by SERCA2a (**4**) is regulated by PLN, which on its turn is controlled by reversible phosphorylation (P).

PLN-R14del cardiomyopathy

Among the different pathological PLN variants, the most prevalent one is the deletion of amino acid residue arginine 14 (p.Arg14del) also termed PLN-R14del. This variant was first described in 2006 to be present in a Greek family.[12] A screening study by van der Zwaag et al. on Dutch patients with DCM and ACM found that approximately 12% of ACM patients and 15% of DCM patients carry the PLN-R14del mutation in the Netherlands, with over 1,500 carriers identified.[16] The relative high presence of the PLN-R14del variant in the northern Netherlands, turned out be due to a novel founder mutation, which is believed to have originated around 1400 A.D..[16,17] All known carriers in the Netherlands therefore share the same haplotype.[16,18,19] This variant has also been reported worldwide, including in other European countries such as Norway,[20] Germany,[21] Belgium,[20] and the UK,[20] as well as in the United States,[22] Canada,[23] and China.[24] Its presence across multiple populations suggests a broader global distribution beyond its originally identified founder region.

To date, no homozygous individuals have been unequivocally identified. Clinical manifestations among heterozygous PLN-R14del carriers exhibit significant variability. While some individuals develop inherited DCM, experience impaired cardiac contractility, abnormal electrocardiography, frequent ventricular arrhythmias, and heart failure leading to early mortality, others remain asymptomatic with normal echocardiographic findings, particularly at a young age.[25,26] Others may experience an ACM phenotype, with potential risk of sudden cardiac death. This variability indicates that additional factors may play a role in modulating disease penetrance.

Histopathological analyses of PLN-R14del patients revealed extensive ventricular fibrosis, a common characteristic often observed in DCM and ACM. Moreover, fibrofatty replacement, often present in ACM, has also been observed in PLN-R14del cardiomyopathy.[27,28] Electrocardiographic abnormalities commonly observed in carriers include low QRS voltages, inverted T waves, and decreased R-wave amplitudes, regardless of echocardiographic findings.[12,16] Notably, PLN protein aggregation has been identified in the myocardial tissue of PLN-R14del-associated DCM patients but not in other forms of DCM, suggesting a distinct pathophysiological mechanism **(Figure 2)**.[29] These pathological and electrical abnormalities are absent in unaffected family members, reinforcing the direct association of this variant with disease development.

Potential mechanisms and novel therapy of PLN-R14del cardiomyopathy

The absence of the amino acid arginine at position 14 in the PLN protein prevents its phosphorylation by PKA. As a result, PLN-R14del was believed to remain in a persistently dephosphorylated state, leading to sustained inhibition of SERCA activity.[12] This constitutive inhibition was hypothesized to cause SERCA super-inhibition, significantly impairing calcium reuptake into the sarcoplasmic reticulum (SR). Consequently, intracellular calcium handling would be impaired increasing the susceptibility to arrhythmias and heart failure.[12]

However, studies on the topology and conformational dynamics of PLN-R14del in isolated *in vitro* systems revealed that while WT-PLN inhibited SERCA activity, the inhibitory effect of PLN-R14del was significantly weaker.[30,31] Calcium measurements in isolated mouse cardiomyocytes further demonstrated accelerated relaxation and enhanced Ca^{2+} uptake into the sarcoplasmic reticulum (SR) in PLN-R14del mice compared to WT cardiomyocytes.[32-34] Also in human iPSC (induced pluripotent stem cell) derived PLN-R14del cardiomyocytes no enhanced inhibition of calcium uptake was observed.[33] Taking together, this suggests that PLN-R14del could be a (partial) loss-of-function variant rather than a SERCA2a super-inhibitor.

Immunohistochemistry revealed an abnormal cytoplasmic distribution and perinuclear accumulation of PLN protein in myocardial sections from PLN-R14del carriers' biopsies. Notably, this aberrant PLN localization was not observed in myocardial sections from patients with other forms of DCM.[29,35] A mouse model exhibiting similar characteristics was utilized to investigate this hallmark of PLN-R14del cardiomyopathy.[36] In this model, PLN-R14del protein initially forms small speckles, which progressively develop into larger clusters as the disease advances. Immunofluorescence microscopy revealed these abnormal protein distributions suggests that they likely represent abnormal sarcoplasmic/endoplasmic reticulum (S/ER) clusters rather than PLN-specific protein aggregates.[32] PLN-R14del can also induce endoplasmic reticulum (ER) stress and activation of the unfolded protein response (UPR).[37,38] In PLN-R14del cardiomyopathy, UPR activation may act protectively by reducing ER stress, which in turn helps maintain cellular function and may attenuate disease progression. These findings highlight the critical role of pathological S/ER alterations as a key underlying mechanism in PLN-R14del cardiomyopathy.

In PLN-R14de iPSCs, proteomic analysis revealed a reduction in endoplasmic reticulum (ER), ribosomal, and mitochondrial proteins. Electron microscopy further demonstrated ER dilation and the presence of large lipid droplets closely associated with mitochondria.[39] The reduced mitochondrial content and altered metabolic profile in PLN-R14del cardiomyopathy were accompanied by impaired mitochondrial respiration, significantly elevated steady-state levels of reactive oxygen and nitrogen species (ROS/RNS), and compromised adenosine triphosphate (ATP) synthesis. The latter changes are commonly observed in heart failure and may also be related to secondary effects.[39]

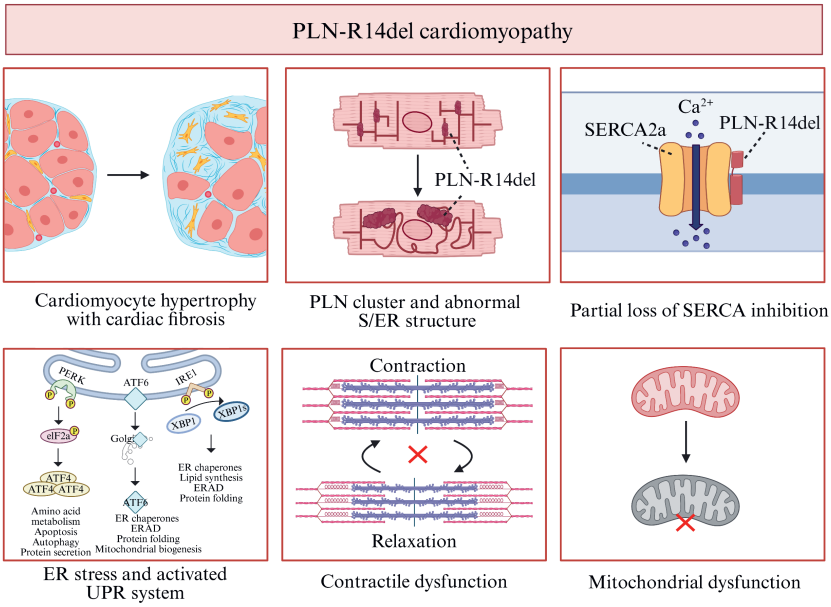

Figure 2. Six pathological features of PLN R14del cardiomyopathy that have been identified on a cellular and sub-cellular level.

Current and novel treatments

Due to the limited understanding of the pathogenic mechanisms underlying PLN-R14del cardiomyopathy, there are currently no targeted therapies available. Clinical management is primarily supportive and aligned with guideline-directed therapy for heart failure and arrhythmia control. Treatment typically includes pharmacological agents such as beta-blockers, angiotensin-converting enzyme (ACE) inhibitors, and anti-arrhythmic drugs. Implantable cardioverter-defibrillators (ICDs) are frequently utilized to mitigate the risk of sudden cardiac death. In cases of end-stage heart failure, heart transplantation remains the definitive therapeutic option.[19]

Ongoing research continues to explore novel therapeutic strategies, including gene editing, pharmacological therapeutics targeting improve cardiac contractility, and molecular chaperone therapies, hold promise for directly targeting the underlying genetic causes of inherited cardiomyopathy, paving the way for improved long-term outcomes.[40,41] Among these strategies, PLN silencing has already been tested in preclinical PLN-R14del cardiomyopathy models, where partial PLN knockdown produced robust improvements in cardiac function and reduced the size of pathological PLN clusters, thereby underscoring the translational potential of this approach.[38,42,43]

Aims and outline of this thesis

The overall aim of this thesis is to elucidate the molecular and pathophysiological mechanisms underlying PLN-R14del cardiomyopathy and to explore potential therapeutic strategies. Specifically, this work aimed to:

- Provide an overview of shared and mutation-specific disease mechanisms across different PLN variants.
- Examine cardiac stress as a potential modifier influencing disease onset and progression.
- Identify early molecular alterations that drive disease progression.
- Assess the dose-dependent therapeutic effects of PLN-ASO and investigate the underlying mechanisms of PLN-R14del cardiomyopathy.

In **Chapter 2**, we provide a comprehensive overview of all PLN-related mutations discovered worldwide that lead to cardiomyopathy. Alterations in this small protein, consisting of only 52 amino acids, can significantly impact cardiac function. In this chapter, we describe the clinical manifestations and key findings of animal and cellular models of various pathogenic PLN variants and discuss their potential pathogenic mechanisms. By comparing these mutations, we aim to provide new insights and perspectives for developing targeted approaches to PLN cardiomyopathy.

In **Chapter 3**, we address the pronounced heterogeneity in disease onset and severity among PLN-R14del carriers. We investigate whether cardiac stress may contribute to the variable disease penetrance observed in humans by using a PLN-R14del mouse model. We employed transverse aortic constriction (TAC), a well-established method for imposing cardiac afterload, to determine whether pressure overload accelerates disease onset and development in PLN-R14del cardiomyopathy.

In **Chapter 4**, we develop a novel inducible PLN-R14del mouse model based on the MerCreMer system with tamoxifen injections. This “inducible system” allows for synchronized transition from the wild-type PLN to the pathogenic PLN-R14del variant. This approach allows for a more precise identification of disease development and temporal pathological changes, providing a solid foundation for further investigation into the pathophysiological mechanisms of PLN-R14del cardiomyopathy.

In **Chapter 5**, we use a homozygous PLN-R14del mouse model to investigate the effects of antisense oligonucleotide (ASO)-mediated silencing in PLN-R14del cardiomyopathy, focusing on both outcome and underlying mechanisms. Previous studies established that silencing the pathogenic PLN gene using ASO therapy can have beneficial effects. However, neither the optimal dose, nor the underlying mechanisms of PLN silencing improved cardiac function were explored. In this chapter, we explore the potential molecular and cellular mechanisms underlying this therapeutic effect.

In **Chapter 6**, we simulate the effect of PLN depletion on the different forms of PLN-WT and PLN-R14del, namely monomer, pentamer and complexed to SERCA2a. This computer modelling reveals that different PLN forms show distinct sensitivity to PLN silencing. This may be important for future therapeutic developments.

In **Chapter 7**, we summarize the main findings and implications of this thesis, along with future perspectives for PLN cardiomyopathy.

References

1. Towbin JA. Inherited cardiomyopathies. Circ J 2014;78:2347-2356.
2. McKenna WJ, Judge DP. Epidemiology of the inherited cardiomyopathies. Nat Rev Cardiol 2021;18:22-36.
3. Velicki L, Jakovljevic DG, Preveden A, Golubovic M, Bjelobrk M, Ilic A, Stojsic S, Barlocco F, Tafelmeier M, Okwose N, Tesic M, Brennan P, Popovic D, Ristic A, MacGowan GA, Filipovic N, Maier LS, Olivotto I. Genetic determinants of clinical phenotype in hypertrophic cardiomyopathy. BMC Cardiovasc Disord 2020;20:516.
4. Kayvanpour E, Sedaghat-Hamedani F, Amr A, Lai A, Haas J, Holzer DB, Frese KS, Keller A, Jensen K, Katus HA, Meder B. Genotype-phenotype associations in dilated cardiomyopathy: meta-analysis on more than 8000 individuals. Clin Res Cardiol 2017;106:127-139.
5. Pankuweit S. Lamin A/C mutations in patients with dilated cardiomyopathy. Eur Heart J 2018;39:861-863.
6. Ware JS, Li J, Mazaika E, Yasso CM, DeSouza T, Cappola TP, Tsai EJ, Hilfiker-Kleiner D, Kamiya CA, Mazzarotto F, Cook SA, Halder I, Prasad SK, Pisarcik J, Hanley-Yanez K, Alharethi R, Damp J, Hsich E, Elkayam U, Sheppard R, Kealey A, Alexis J, Ramani G, Safirstein J, Boehmer J, Pauly DF, Wittstein IS, Thohan V, Zucker MJ, Liu P, Gorcsan J, 3rd, McNamara DM, Seidman CE, Seidman JG, Arany Z, Imac, Investigators I. Shared Genetic Predisposition in Peripartum and Dilated Cardiomyopathies. N Engl J Med 2016;374:233-241.
7. Costa S, Cerrone M, Saguner AM, Brunckhorst C, Delmar M, Duru F. Arrhythmogenic cardiomyopathy: An in-depth look at molecular mechanisms and clinical correlates. Trends Cardiovasc Med 2021;31:395-402.
8. Tadros HJ, Life CS, Garcia G, Pirozzi E, Jones EG, Datta S, Parvatiyar MS, Chase PB, Allen HD, Kim JJ, Pinto JR, Landstrom AP. Meta-analysis of cardiomyopathy-associated variants in troponin genes identifies loci and intragenic hot spots that are associated with worse clinical outcomes. J Mol Cell Cardiol 2020;142:118-125.
9. Li Z, Chen P, Xu J, Yu B, Li X, Wang DW, Wang DW. A PLN nonsense variant causes severe dilated cardiomyopathy in a novel autosomal recessive inheritance mode. Int J Cardiol 2019;279:122-125.
10. Schmitt J, Kamisago M, Asahi M, Li G, Ahmad F, Mende U, Kranias E, MacLennan D, Seidman J, Seidman C. Dilated cardiomyopathy and heart failure caused by a mutation in phospholamban. Science (New York, NY) 2003;299:1410-1413.
11. Medeiros A, Biagi DG, Sobreira TJ, de Oliveira PS, Negrao CE, Mansur AJ, Krieger JE, Brum PC, Pereira AC. Mutations in the human phospholamban gene in patients with heart failure. Am Heart J 2011;162:1088-1095 e1081.
12. Haghighi K, Kolokathis F, Gramolini A, Waggoner J, Pater L, Lynch R, Fan G, Tsiapras D, Parekh R, Dorn G, MacLennan D, Kremastinos D, Kranias E. A mutation in the human phospholamban gene, deleting arginine 14, results in lethal, hereditary cardiomyopathy. Proceedings of the National Academy of Sciences of the United States of America 2006;103:1388-1393.
13. Liu GS, Morales A, Vafiadaki E, Lam CK, Cai WF, Haghighi K, Adly G, Hershberger RE, Kranias EG. A novel human R25C-phospholamban mutation is associated with super-inhibition of calcium cycling and ventricular arrhythmia. Cardiovasc Res 2015;107:164-174.

14. Haghighi K, Kolokathis F, Pater L, Lynch RA, Asahi M, Gramolini AO, Fan G-C, Tsiapras D, Hahn HS, Adamopoulos S, Liggett SB, Dorn GW, MacLennan DH, Kremastinos DT, Kranias EG. Human phospholamban null results in lethal dilated cardiomyopathy revealing a critical difference between mouse and human. Journal of Clinical Investigation 2003;111:869-876.
15. Mattiazzi A, Mundina-Weilenmann C, Guoxiang C, Vittone L, Kranias E. Role of phospholamban phosphorylation on Thr17 in cardiac physiological and pathological conditions. Cardiovasc Res 2005;68:366-375.
16. van der Zwaag PA, van Rijsingen IA, Asimaki A, Jongbloed JD, van Veldhuisen DJ, Wiesfeld AC, Cox MG, van Lochem LT, de Boer RA, Hofstra RM, Christiaans I, van Spaendonck-Zwarts KY, Lekanne dit Deprez RH, Judge DP, Calkins H, Suurmeijer AJ, Hauer RN, Saffitz JE, Wilde AA, van den Berg MP, van Tintelen JP. Phospholamban R14del mutation in patients diagnosed with dilated cardiomyopathy or arrhythmogenic right ventricular cardiomyopathy: evidence supporting the concept of arrhythmogenic cardiomyopathy. Eur J Heart Fail 2012;14:1199-1207.
17. van der Zwaag PA, van Rijsingen IA, de Ruiter R, Nannenberg EA, Groeneweg JA, Post JG, Hauer RN, van Gelder IC, van den Berg MP, van der Harst P, Wilde AA, van Tintelen JP. Recurrent and founder mutations in the Netherlands-Phospholamban p.Arg14del mutation causes arrhythmogenic cardiomyopathy. Neth Heart J 2013;21:286-293.
18. van der Heijden JF, Hassink RJ. The phospholamban p.Arg14del founder mutation in Dutch
19. Hof IE, van der Heijden JF, Kranias EG, Sanoudou D, de Boer RA, van Tintelen JP, van der Zwaag PA, Doevendans PA. Prevalence and cardiac phenotype of patients with a phospholamban mutation. Neth Heart J 2019;27:64-69.
20. Te Rijdt WP, Hoorntje ET, de Brouwer R, Oomen A, Amin A, van der Heijden JF, Karper JC, Westenbrink BD, Sillje HHW, Te Riele A, Wiesfeld ACP, van Gelder IC, Willems TP, van der Zwaag PA, van Tintelen JP, Hillege JH, Tan HL, van Veldhuisen DJ, Asselbergs FW, de Boer RA, Wilde AAM, van den Berg MP. Rationale and design of the PHOspholamban RElated CArdiomyopathy intervention STudy (i-PHORECAST). Neth Heart J 2022;30:84-95.
21. Posch MG, Perrot A, Geier C, Boldt LH, Schmidt G, Lehmkuhl HB, Hetzer R, Dietz R, Gutberlet M, Haverkamp W, Ozcelik C. Genetic deletion of arginine 14 in phospholamban causes dilated cardiomyopathy with attenuated electrocardiographic R amplitudes. Heart Rhythm 2009;6:480-486.
22. DeWitt MM, MacLeod HM, Soliven B, McNally EM. Phospholamban R14 deletion results in late-onset, mild, hereditary dilated cardiomyopathy. J Am Coll Cardiol 2006;48:1396-1398.
23. Cheung CC, Healey JS, Hamilton R, Spears D, Gollob MH, Mellor G, Steinberg C, Sanatani S, Laksman ZW, Krahn AD. Phospholamban cardiomyopathy: a Canadian perspective on a unique population. Neth Heart J 2019;27:208-213.
24. Jiang X, Xu Y, Sun J, Wang L, Guo X, Chen Y. The phenotypic characteristic observed by cardiac magnetic resonance in a PLN-R14del family. Sci Rep 2020;10:16478.
25. Groeneweg JA, van der Zwaag PA, Olde Nordkamp LR, Bikker H, Jongbloed JD, Jongbloed R, Wiesfeld AC, Cox MG, van der Heijden JF, Atsma DE, de Boer K, Doevendans PA, Vink A, van Veen TA, Dooijes D, van den Berg MP, Wilde AA, van Tintelen JP, Hauer RN. Arrhythmogenic right ventricular dysplasia/cardiomyopathy according to revised 2010 task force criteria with inclusion of non-desmosomal phospholamban mutation carriers. Am J Cardiol 2013;112:1197-1206.
26. van Rijsingen IA, van der Zwaag PA, Groeneweg JA, Nannenberg EA, Jongbloed JD,

Zwinderman AH, Pinto YM, Dit Deprez RH, Post JG, Tan HL, de Boer RA, Hauer RN, Christiaans I, van den Berg MP, van Tintelen JP, Wilde AA. Outcome in phospholamban R14del carriers: results of a large multicentre cohort study. Circ Cardiovasc Genet 2014;7:455-465.

27. Gho JM, van Es R, Stathonikos N, Harakalova M, te Rijdt WP, Suurmeijer AJ, van der Heijden JF, de Jonge N, Chamuleau SA, de Weger RA, Asselbergs FW, Vink A. High resolution systematic digital histological quantification of cardiac fibrosis and adipose tissue in phospholamban p.Arg14del mutation associated cardiomyopathy. PLoS One 2014;9:e94820.
28. Eijgenraam TR, Sillje HHW, de Boer RA. Current understanding of fibrosis in genetic cardiomyopathies. Trends Cardiovasc Med 2020;30:353-361.
29. Te Rijdt WP, van der Klooster ZJ, Hoorntje ET, Jongbloed JDH, van der Zwaag PA, Asselbergs FW, Dooijes D, de Boer RA, van Tintelen JP, van den Berg MP, Vink A, Suurmeijer AJH. Phospholamban immunostaining is a highly sensitive and specific method for diagnosing phospholamban p.Arg14del cardiomyopathy. Cardiovasc Pathol 2017;30:23-26.
30. Ceholski DK, Trieber CA, Young HS. Hydrophobic imbalance in the cytoplasmic domain of phospholamban is a determinant for lethal dilated cardiomyopathy. J Biol Chem 2012;287:16521-16529.
31. Hughes E, Middleton DA. Comparison of the structure and function of phospholamban and the arginine-14 deficient mutant associated with dilated cardiomyopathy. PLoS One 2014;9:e106746.
32. Stege NM, Eijgenraam TR, Oliveira Nunes Teixeira V, Feringa AM, Schouten EM, Kuster DWD, van der Velden J, Wolters AHG, Giepmans BNG, Makarewich CA, Bassel-Duby R, Olson EN, de Boer RA, Sillje HHW. DWORF Extends Life Span in a PLN-R14del Cardiomyopathy Mouse Model by Reducing Abnormal Sarcoplasmic Reticulum Clusters. Circ Res 2023;133:1006-1021.
33. Badone B, Ronchi C, Lodola F, Knaust AE, Hansen A, Eschenhagen T, Zaza A. Characterization of the PLN p.Arg14del Mutation in Human Induced Pluripotent Stem Cell-Derived Cardiomyocytes. Int J Mol Sci 2021;22.
34. Maniezzi C, Eskandr M, Florindi C, Ferrandi M, Barassi P, Sacco E, Pasquale V, Maione AS, Pompilio G, Teixeira VON, de Boer RA, Sillje HHW, Lodola F, Zaza A. Early consequences of the phospholamban mutation PLN-R14del(+/-) in a transgenic mouse model. Acta Physiol (Oxf) 2024;240:e14082.
35. Te Rijdt WP, van Tintelen JP, Vink A, van der Wal AC, de Boer RA, van den Berg MP, Suurmeijer AJ. Phospholamban p.Arg14del cardiomyopathy is characterized by phospholamban aggregates, aggresomes, and autophagic degradation. Histopathology 2016;69:542-550.
36. Eijgenraam TR, Boukens BJ, Boogerd CJ, Schouten EM, van de Kolk CWA, Stege NM, Te Rijdt WP, Hoorntje ET, van der Zwaag PA, van Rooij E, van Tintelen JP, van den Berg MP, van der Meer P, van der Velden J, Sillje HHW, de Boer RA. The phospholamban p.(Arg14del) pathogenic variant leads to cardiomyopathy with heart failure and is unreponsive to standard heart failure therapy. Sci Rep 2020;10:9819.
37. Feyen DAM, Perea-Gil I, Maas RGC, Harakalova M, Gavidia AA, Arthur Ataam J, Wu TH, Vink A, Pei J, Vadgama N, Suurmeijer AJ, Te Rijdt WP, Vu M, Amatya PL, Prado M, Zhang Y, Dunkenberger L, Sluijter JPG, Sallam K, Asselbergs FW, Mercola M, Karakikes I. Unfolded Protein Response as a Compensatory Mechanism and Potential Therapeutic Target in PLN

R14del Cardiomyopathy. Circulation 2021;144:382-392.
38. Eijgenraam TR, Stege NM, Oliveira Nunes Teixeira V, de Brouwer R, Schouten EM, Grote Beverborg N, Sun L, Spater D, Knoll R, Hansson KM, Amilon C, Janzen D, Yeh ST, Mullick AE, van der Meer P, de Boer RA, Sillje HHW. Antisense Therapy Attenuates Phospholamban p.(Arg14del) Cardiomyopathy in Mice and Reverses Protein Aggregation. Int J Mol Sci 2022;23.
39. Cuello F, Knaust AE, Saleem U, Loos M, Raabe J, Mosqueira D, Laufer S, Schweizer M, van der Kraak P, Flenner F, Ulmer BM, Braren I, Yin X, Theofilatos K, Ruiz-Orera J, Patone G, Klampe B, Schulze T, Piasecki A, Pinto Y, Vink A, Hubner N, Harding S, Mayr M, Denning C, Eschenhagen T, Hansen A. Impairment of the ER/mitochondria compartment in human cardiomyocytes with PLN p.Arg14del mutation. EMBO Mol Med 2021;13:e13074.
40. Vafiadaki E, Glijnis PC, Doevendans PA, Kranias EG, Sanoudou D. Phospholamban R14del disease: The past, the present and the future. Front Cardiovasc Med 2023;10:1162205.
41. Deiman FE, Bomer N, van der Meer P, Grote Beverborg N. Review: Precision Medicine Approaches for Genetic Cardiomyopathy: Targeting Phospholamban R14del. Curr Heart Fail Rep 2022;19:170-179.
42. Sun L, Eijgenraam TR, Amilon C, Janzen D, Hansson KM, Kubli DA, Spater D, Mullick AE, van der Meer P, Nunes Teixeira VO, Sillje HHW. In PLN-R14del mice, SR structure restoration, rather than calcium cycling, is the dominant effector of PLN-ASO treatment. Cardiovasc Res 2025;121:2042-2054.
43. Grote Beverborg N, Spater D, Knoll R, Hidalgo A, Yeh ST, Elbeck Z, Sillje HHW, Eijgenraam TR, Siga H, Zurek M, Palmer M, Pehrsson S, Albery T, Bomer N, Hoes MF, Boogerd CJ, Frisk M, van Rooij E, Damle S, Louch WE, Wang QD, Fritsche-Danielson R, Chien KR, Hansson KM, Mullick AE, de Boer RA, van der Meer P. Phospholamban antisense oligonucleotides improve cardiac function in murine cardiomyopathy. Nat Commun 2021;12:5180.
44. Kranias EG, Hajjar RJ. Modulation of cardiac contractility by the phospholamban/SERCA2a regulatome. Circ Res 2012;110:1646-1660.

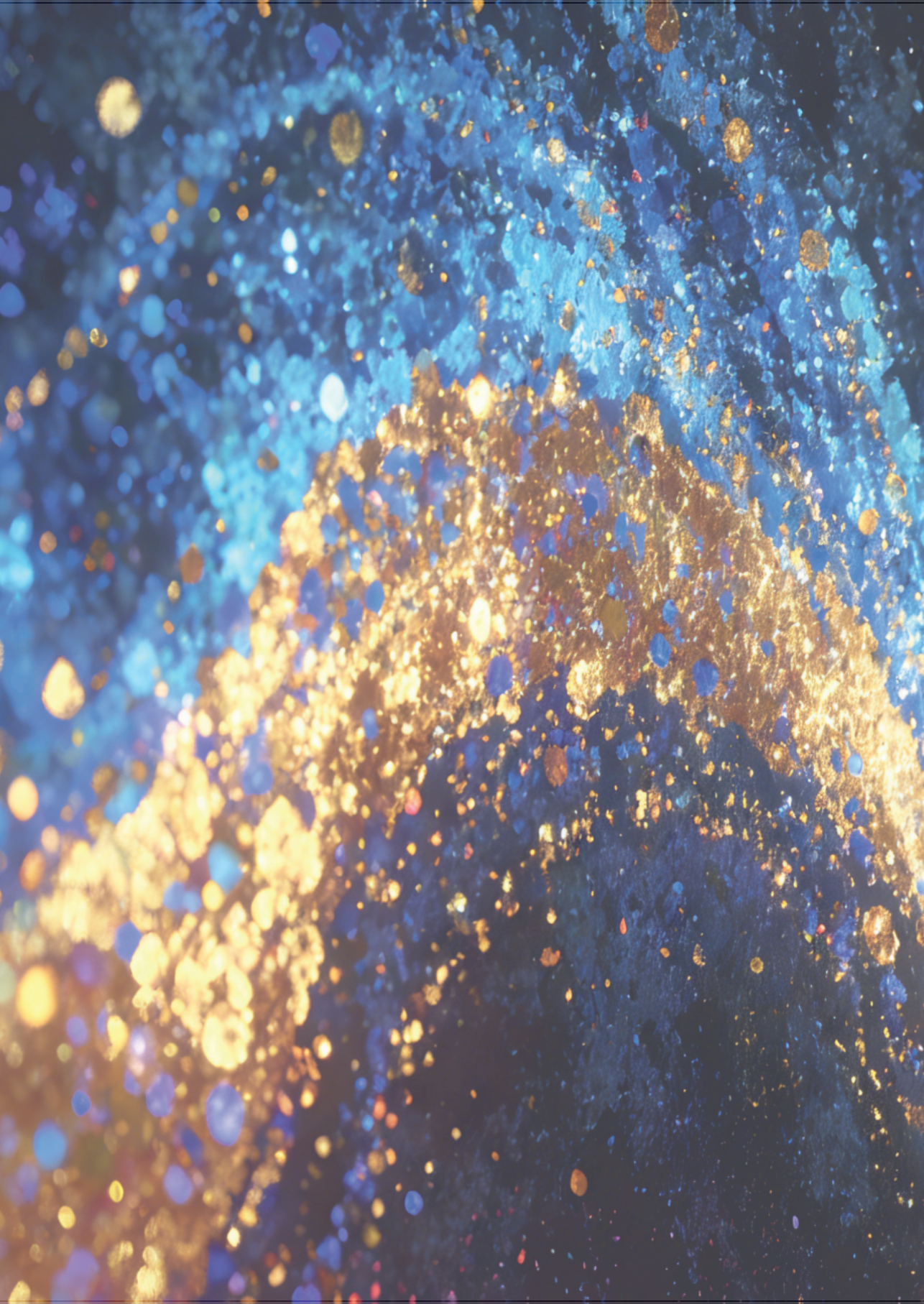

Chapter 2

Beyond SERCA: Emerging mechanisms of pathogenic PLN variants in cardiomyopathy

Distinct pathogenic mechanisms of PLN variants require different therapeutic solutions

Liu Sun, Vivian Oliveira Nunes Teixeira, Herman H.W. Silljé*

Department of Cardiology, University of Groningen, University Medical Center Groningen, Groningen, the Netherlands

(In preparation)

Abstract

The heart is a vital circulatory pump, and its dysfunction remains one of the leading causes of death worldwide. The fundamental mechanism of calcium-controlled and sarcomere-mediated cardiac contraction and relaxation is well established. However, our understanding of the pathological processes that disrupt this essential contraction/relaxation cycle remains limited. In this review we focus on phospholamban (PLN) protein, encoded by the PLN gene. PLN is predominantly expressed in the heart, where it modulates the activity of sarco/endoplasmic reticulum Ca^{2+}-ATPase 2a (SERCA2a) and thereby regulates calcium uptake into the sarcoplasmic reticulum (SR), a key determinant of sarcomere relaxation. Importantly, numerous pathogenic PLN variants have been identified that cause inherited cardiomyopathies, including arrhythmogenic cardiomyopathy (ACM), dilated cardiomyopathy (DCM), and subsequent heart failure. Despite intensive investigations, the precise molecular consequences of these pathogenic variants remain incompletely understood. Pathogenic PLN variants can lead to either gain- or loss-of-function effects, altered phosphorylation, or even acquisition of novel deleterious properties that impair cardiac function. Here, we summarize the basic principles of PLN function, and highlight that different PLN variants disrupt distinct molecular mechanisms, suggesting that tailored therapeutic strategies may be required to address the spectrum of PLN-associated cardiomyopathies.

Introduction

Cardiac contraction (systole) and relaxation (diastole) rely on tightly regulated intracellular calcium cycling between sarcoplasmic reticulum (SR) and cytosol in cardiomyocytes. Relaxation of the myocardium requires efficient reuptake of cytosolic calcium into the SR, primarily mediated by the sarco/endoplasmic reticulum Ca^{2+}-ATPase 2a (SERCA2a).[1] Phospholamban (PLN) is a small, single-pass transmembrane protein of the SR that modulates SERCA2a activity and thereby plays a central role in cardiac calcium homeostasis.[2]

PLN was first identified as a key substrate of protein kinase A (PKA) in cardiac SR fractions. It was subsequently established that this small 52 amino acid protein can consist in a monomeric and pentameric configuration and control SERCA2a mediated SR calcium uptake and hence serve as a canonical regulator of beat-to-beat Ca^{2+} handling **(Figure 1)**.[3-5]

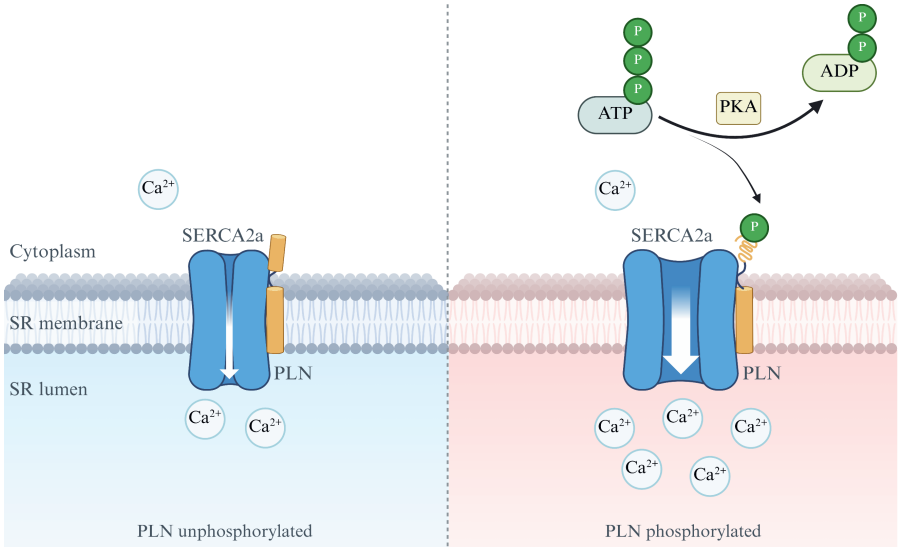

Figure 1. Schematic representation of PLN-dependent regulation of SERCA2a.

Panels show SERCA2a in the sarcoplasmic reticulum (SR) membrane together with unphosphorylated (left) or phosphorylated (right) phospholamban (PLN). In the unphosphorylated state, PLN reduces SERCA2a calcium affinity, limiting Ca^{2+} reuptake into the SR lumen. Upon phosphorylation of PLN by protein kinase A (PKA), this inhibitory action is relieved, leading to enhanced SERCA2a-mediated Ca^{2+} uptake and increased SR Ca^{2+} load.

Structurally, PLN comprises a cytoplasmic regulatory hydrophilic region domain I (residues 1-30) and a transmembrane hydrophobic domain II (residues 31-52).[2,6] PLN

adopts an L-shaped conformation formed by two α-helices connected by a β-turn (Thr[17], Ile[18], Glu[19], and Met[20]).[7] Domain I can be further subdivided into domain Ia (residues 1-16) containing the Ser16 PKA phosphorylation site, a loop structure (residues 17-22) containing the Thr17 Ca^{2+}/calmodulin-dependent protein kinase II (CaMKII) phosphorylation site, and domain Ib (residues 23-30) which is positioned at the lipid head group/water interface.[2,7,8] This modular architecture couples signal reception in the cytosol with assembly interfaces in the membrane, enabling conformational and topological changes of PLN and its regulatory influence on SERCA2a **(Figure 2)**.

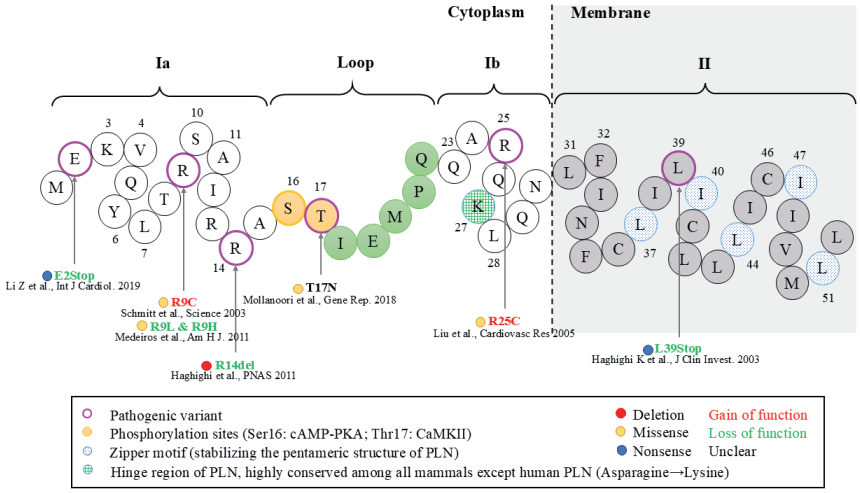

Figure 2. Schematic representation of human phospholamban (PLN) sequence, structural domains, functional sites, and clinical variants.

Diagram of human PLN showing residues 1-52 grouped into the cytosolic domains Ia, loop, Ib and membrane domain II. The left part represents the cytoplasmic portion of PLN, whereas the shaded region on the right corresponds to the transmembrane segment. Circles denote individual amino acids, with magenta-outlined residues indicating reported pathogenic variants. Two phosphorylation sites, Ser16 (PKA) and Thr17 (Ca^{2+}-calmodulin-dependent protein kinase II, CaMKII), are highlighted in yellow. Blue-shaded residues mark the canonical leucine/isoleucine zipper motif that stabilizes the pentameric structure of PLN. The green-hatched region indicates the hinge region of PLN, which is highly conserved across mammals, with the exception that lysine (K) in human PLN is replaced by asparagine (N) in most other mammals, including mice. Reported human pathogenic variants are mapped to their corresponding positions along the sequence and annotated with the original references. Colored circles indicate mutation type (red for deletion, yellow for missense, blue for nonsense), whereas the color of the variant labels denotes the proposed functional consequence (red for gain of function, green for loss of function, black for unclear).

Unphosphorylated PLN interacts with SERCA2a through intramembrane contacts, thereby reducing the affinity of SERCA2a for calcium. This inhibitory effect can be alleviated either by an increase in intracellular Ca^{2+} concentration or by phosphorylation of PLN.[4,9-11] The regulatory role of PLN in SERCA2a activity has therefore long been considered the major mechanism linking PLN to cardiac physiology and disease. Based on this framework, mechanistic studies of PLN cardiomyopathy historically focus on dysregulated calcium handling and impaired myocardial relaxation as the primary drivers of pathology. However, this perspective has increasingly been challenged. Emerging evidence suggests that abnormalities in PLN structure, altered oligomerization dynamics, and S/ER clustering may also exert pathogenic effects, potentially independently of PLN inhibitory interaction with SERCA2a.[12]

In this review, we discuss how pathogenic PLN variants affect PLN structure and topology, thereby altering its monomer-pentamer equilibrium and interactions with SERCA2a and other proteins, and potentially leading to acquisition of novel deleterious properties that impair cardiac function.

PLN pentamer-monomer structure and regulatory balance

Structurally, PLN exists in a dynamic equilibrium between a monomeric and a pentameric state. The monomer is generally regarded as the functionally active inhibitory form, directly binding to SERCA2a and reducing its Ca^{2+} affinity, whereas the pentameric form is often regarded as an inactive or storage state that serves as a molecular reservoir predominating under resting conditions.[13] Each PLN monomer comprises a cytoplasmic regulatory domain and a transmembrane α-helix that mediates oligomerization through hydrophobic interactions, most notably involving residues within the leucine/isoleucine zipper motif (Leu37, Ile40, Leu44, Ile47, Leu51) **(Figure 2)**. The predominant structural conformation of pentameric phospholamban mainly adopts a “pinwheel” topology, in which the cytoplasmic domains extend along and interact intimately with the SR membrane surface.[14] PLN pentamerization modulates the sensitivity and dynamic range of the SERCA-PLN regulatory system during physiological stress.[13] The pentamer-monomer balance is highly sensitive to multiple regulatory factors, including phosphorylation,[15] calcium concentration, lipid composition,[16] oxidative modifications, temperature and PLN variants.[17-19] Genetic or biochemical perturbations that promote pentamer formation alter the kinetics and the extent to which SERCA2a inhibition is relieved during β-adrenergic stimulation, thereby influencing cardiac relaxation (lusitropy) under load.[13] Thus, the delicate equilibrium between PLN pentamers and monomers constitutes a key regulatory node for fine-tuning cardiac Ca^{2+} cycling, and its disruption, such as through pathogenic mutations, that may contribute to the development of cardiomyopathy.

In contrast to domain II, which exhibits a similar structure in different structural studies, domain I displays markedly greater conformational flexibility. Phospholamban can adopt three distinct conformational states, two inhibitory conformations, T state and R

state, and a non-inhibitory conformation B state. The T state is characterized by a helical, membrane-associated domain Ia, whereas the excited R state corresponds to an unfolded, membrane-detached configuration.[7,20] Although both R and T state are inhibitory, the R state has weaker inhibitory action and adopts a conformation more similar to structural effects observed for Ser16-phosphorylated PLN, including the more dynamic and disordered conformation.[6,21] By shifting the equilibrium between T and R states, the extent of SERCA2a inhibition by PLN can be tuned.[22] When PLN is bound to SERCA2a and becomes phosphorylated on Ser16, PLN shifts the populations toward the "B state", which is non-inhibitory, further illustrating the complexity of its regulatory cycle. The reversible inhibition of SERCA2a activity by PLN can be divided into two steps. One is the association/dissociation of pentamer of PLN. And second is the association/dissociation of monomeric PLN and SERCA2a **(Figure 3)**.[10] PLN mutations alter either one or more steps of the regulation process, which may lead to the gain or loss of SERCA2a activity inhibition.

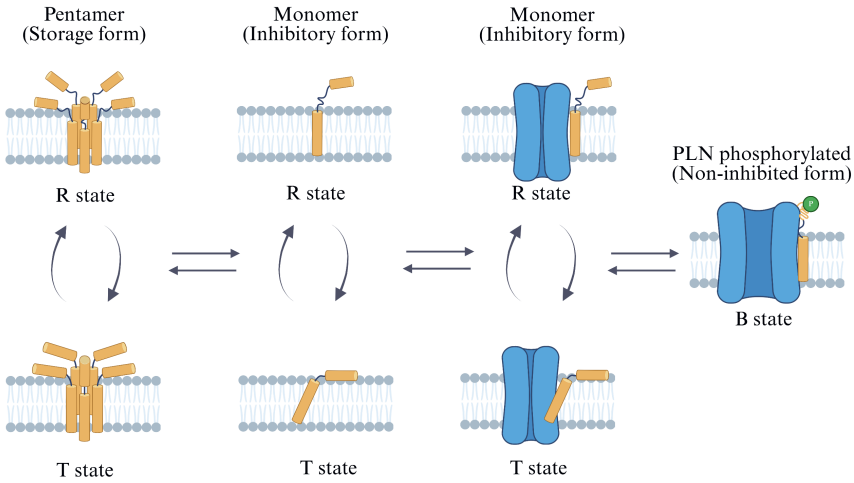

Figure 3. Conformational changes and transitions of PLN and SERCA2a inhibitory effects.
Schematic depiction illustrating the dynamic interconversion of PLN (yellow) between pentameric and monomeric states and its functional interaction with SERCA2a (blue). The left panel shows PLN in a pentameric "storage" form, which exists in equilibrium between R and T conformations within the SR membrane. Dissociation of the pentamer yields monomeric PLN, which in its R and T states acts as an inhibitory species. Transition to the B state (right), in which PLN is phosphorylated by PKA and displaced from its inhibitory site on SERCA2a, relieves inhibition and restores full SERCA2a function. Arrows indicate the reversible equilibria between these conformational and oligomeric states.

While PLN monomers directly inhibit SERCA2a through physical interaction, pentamers function as phosphorylation buffers owing to their higher affinity for PKA,

thereby delaying monomer phosphorylation and ensuring a more gradual and controlled regulation of SERCA2a activity.[23-25] Mutational studies have highlighted the importance of residues 37-52 (which constitute leucine/isoleucine zipper motif) for this balance. Substitutions such as L37A and I40A destabilize pentamer formation, increase the proportion of monomeric PLN, and result in a "super-inhibitory" effect on SERCA2a activity. In contrast, the C41F mutation also favors a monomeric state but paradoxically exhibits weaker inhibitory capacity than wild-type PLN, suggesting that monomerization alone is not sufficient to account for functional regulation of SERCA2a activity.[26] Collectively, these findings indicate that PLN's regulatory role cannot be explained solely by the presence of monomers, but rather by the dynamic interplay between monomeric and pentameric states, the structural integrity of the coiled-coil domain, and their responsiveness to phosphorylation. Notably, most monomer mutational studies to date have been performed in a PLN-null background, which provides a clear mechanistic readout but may not fully capture the complexity of PLN regulation under physiological conditions. Introducing these variants into a wild-type background could therefore yield deeper insights into how monomer-pentamer equilibrium and cooperative interactions fine-tune SERCA2a function *in vivo*.

Molecular network and protein-protein interactions of PLN

Because of the relationship of PLN/SERCA2a, myocardial contractility and relaxation are highly dependent on PLN phosphorylation. PKA phosphorylation on Ser16 was shown to be sufficient for mediating the maximal cardiac responses to beta-adrenergic stimulation.[27] The role of CaMKII-mediated Thr17 phosphorylation is less well established and most likely involves adaptation to altered cytoplasmic calcium concentraties.[28] Recent evidence further suggests a regulatory "locking" mechanism in which Ser16 and Thr17 phosphorylation together generate a binding site for 14-3-3 proteins, thereby limiting dephosphorylation by protein phosphatase 1c. Thr17 phosphorylation appears to provide a more energetically favorable 14-3-3 interaction, implying that CaMKII-mediated PLN modification may produce a longer-lasting, "memory-like" effect.[29] Functionally, phosphorylation of PLN relieves its inhibitory effect on SERCA2a, but the precise structural basis of this regulation has long been debated. Structural studies suggest that phosphorylation does not cause PLN to dissociate from SERCA2a but instead induces local conformational changes, particularly within the cytoplasmic regulatory domain, thereby weakening the affinity of PLN monomers for SERCA2a.[30-32] Importantly, several pathogenic PLN variants, including R9C, R9H, and R14del, appear to be unresponsive to phosphorylation, such that PKA or CaMKII mediated signaling fails to modify SERCA2a inhibition.[33-35] Mechanistically, these mutations may alter the accessibility of phosphorylation sites or impair the conformational transition that normally follows phosphorylation, thereby locking PLN in an specific state. Additionally, S-palmitoylation at Cys36, through the attachment of a 16-carbon palmitate, increases PLN hydrophobicity and has been suggested to enhance phosphorylation and favor pentamer formation.[36] Together, these findings underscore that the inability of PLN to respond to phosphorylation represents

an important disease mechanism, while restoration or mimicking of phosphorylation can provide therapeutic benefit.

Recent studies reveal that PLN mutations perturb protein-protein interaction networks that extend beyond SERCA2a. HAX-1, an anti-apoptotic protein present in the outer mitochondrial membrane, has been reported to enhance the inhibitory effect of PLN on SERCA2a. The interaction with HAX-I may also serve an important role in mediating SR/mitochondrial communication and influencing mitochondrial calcium concentartions.[37] AKAP18δ (A-kinase anchoring protein 18δ) also functionally regulates CaMKII at both the PLN-SERCA and ryanodine receptor (RyR) complexes.[38] Furthermore, protein phosphatase 1 (PP1) and its regulatory subunit interact with PLN complexes thereby mediating PLN dephosphorylation and thereby suppressing SERCA2a activity.[39] Additionally, PLN together with sarcolipin (SLN) and DWORF points to a broader micropeptide network that shapes SERCA2a regulation.[40] These findings indicate that the regulation and function of PLN are more complex than originally appreciated, as alterations in PLN oligomerization, membrane organization, and interactions with protein beyond SERCA2a can reshape pathophysiological behavior of PLN.

Clinical pathogenic PLN variants

Since the first variant PLN R9C was found in 2003, numerous other PLN variants have been identified with proven relation to cardiac function, in addition a variant of uncertain significance.[33,41] Pathogenic variation comprises deletions, missense, and nonsense, with phenotypes ranging from asymptomatic presentation to dilated cardiomyopathy, hypertrophic cardiomyopathy, and ventricular tachycardia.[41] The clinical observations highlight the diverse pathogenic mechanisms of PLN variants beyond altered SERCA2a inhibition alone. Given that PLN is highly conserved across vertebrate species, mechanistic insights from model organisms have been instrumental in elucidating how distinct PLN variants disrupt Ca^{2+} handling and contribute to cardiomyopathy.[42] Notably, human and mouse PLN differ at only one residue (position 27, Lys in human versus Asn in mouse), supporting the translational relevance of experimental findings across species.[43]

Pathogenic missense variants

PLN R9C, R9L and R9H

Several human missense variants affect PLN codon 9, including c.25C>T (p.Arg9Cys, R9C), c.26G>T (p.Arg9Leu, R9L), and c.26G>A (p.Arg9His, R9H), indicating that Arg9 is a mutational hotspot in phospholamban.[33,34] Located in the cytosolic regulatory

segment (domain Ia). This residue enhances the efficiency of Ser16 phosphorylation and is essential for proper protein kinase A recognition, particularly in the context of the PLN pentamer.[45]

The PLN p.Arg9Cys (R9C) variant was initially identified in patients with dilated cardiomyopathy and heart failure. Consistent with these clinical observations, transgenic mice carrying the PLN-R9C mutation develop DCM at 4 months of age resulting in heart failure death at 5 months of age on average.[33,46] Additionally, Schmitt et al. demonstrated the association between the dose-dependent inhibition effect of PLN-R9C using transgenic mice carrying 2 ($PLN^{+/+}$+$TgPLN^{R9C}$), 1 ($PLN^{+/-}$+$TgPLN^{R9C}$) or 0 ($PLN^{-/-}$+$TgPLN^{R9C}$) endogenous PLN alleles.[47] Mice carrying both endogenous wild-type PLN and transgenic PLN-R9C exhibit DCM with the shortest lifespan, suggesting a dominant-negative or gain-of-toxic-function effect of the R9C mutation in the presence of wild-type PLN. In contrast, $PLN^{-/-}$+$TgPLN^{R9C}$ mice survive significantly longer, indicating that the pathogenicity of R9C is amplified by the presence of wild-type PLN. In the presence of PLN^{wt}, a reduced SR Ca^{2+} uptake rate was observed in $TgPLN^{R9C}$ mouse cardiomyocytes, indicative for enhanced SERCA2a inhibition. However, in the absence of PLN^{wt}, the SR Ca^{2+} reuptake rate of $TgPLN^{R9C}$ mouse cardiomyocytes is even higher than control WT cardiomyocytes, suggesting that PLN^{R9C} reduces SERCA2a activity on its own.[47] Thus PLN-R9C alone reduces SERCA2a activity, but in the presence of WT PLN it enhances SERCA2a inhibition. One potential explanation for the loss of inhibition is that cysteine disulfide bridges in the cytoplasmic domains of PLN-R9C stabilize the pentamer, making it unable to deoligomerize and regulate SERCA2a.[18] An engineered monomeric (AFA) variant of PLN-R9C does show stronger SERCA2a inhibition as compared to WT PLN, indicating that stable pentamer formation is indeed the likely cause of reduced PLN-R9C SERCA2a inhibition in the absence of WT PLN.[48] Since $PLN^{-/-}$+$TgPLN^{R9C}$ mice do develop disease, whereas PLN KO mice are disease free in the absence of SERCA2a regulation, this suggests that stable pentamers could have detrimental actions in these mice. An explanation of the inhibitory action in the presence of WT PLN may come from the observation that PLN^{R9C} can trap PKA and inhibit WT PLN phosphorylation of PKA thereby generating a constitutive SERCA2a inhibitory WT PLN pool.[33] Thus, multiple mechanisms may contribute to disease development in PLN-R9C carriers.

Similar to R9C, both R9L and R9H variants were linked to idiopathic dilated cardiomyopathy (DCM) and reduced ejection fraction, ultimately resulting in premature death.[44] The R9H variant is considered a low-penetrant allele in humans, as not all carriers within the same family exhibit clinical manifestations of cardiac

disease.[44] This same PLN-R9H mutation is also identified in a family of Welsh Springer Spaniels. In contrast to humans, R9H in dogs is highly penetrant and frequently associated with biventricular dilation, systolic dysfunction, ventricular arrhythmias, and sudden death.[49] This difference in severity, may reflect species-dependent differences in PLN structure and protein-protein interaction networks. PLN-R9L substitutes a hydrophobic residue for the positively charged Arg9, a physicochemical change that may underlie comparable cardiac dysfunction.[50] Consistent with this, R9L is reported to largely abolish PLN's regulatory inhibition of SERCA2a.[45] Previous study suggests the pathological effect of R9C may due to increased hydrophobicity at position 9 of domain Ia,[50] which causes the cytoplasmic amphipathic helix of PLN-R9C to adopt a more extended and disordered conformation.[51,52] However, if the PLN-R9C structure preferentially assumes the "R state", it would be difficult to reconcile this with its reported gain-of-function phenotype. Opposing with this, several studies have proposed that PLN-R9C, rather than stabilizing the R state, favors a transition toward the membrane-associate state, enriching the T state.[53] Furthermore, the hydrophobic imbalance hypothesis seems not appliable on R9H, since the amino acid of R9H is less hydrophobic.[50] The functional consequences of the rare R9L and R9H variants remain largely unknown. These substitutions were detected in cardiomyopathy patients, but their effects on PLN oligomerization and the pentamer-monomer equilibrium were not experimentally characterized. Finally, a suggested hypothesis is that the absence of Arg9 in disease-causing mutants of PLN (such as R9C, R9H, and R9L) could alter the conformational selection by PKA, thereby creating a kinetic trap for PKA and affecting the phosphorylation of other cellular targets.[45] Therefore, these variants may contribute to disease via alternative mechanisms, beyond SERCA2a regulation.

PLN-T17N

Heterozygous PLN variant, c.50C>A (p.Thr17Asn; T17N), was identified in an idiopathic dilated cardiomyopathy case and argues that substituting Thr17 may abolish the Thr17 phosphorylation site and potentially perturb PLN function (including effects in/near the HAX1-interacting region), with in-silico predictions supporting likely pathogenicity. However, since this variant was identified in only a single case, the evidence is insufficient to draw any definitive conclusions about causality or clinical significance.[54]

PLN-R25C

Another heterozygous substitution c.73C>T (p.Arg25Cys, R25C) was identified in patients with DCM with non-sustained ventricular tachycardia (NSVT), and requiring heart transplantation.[55] PLN-R25C is associated with "super-inhibition" of SERCA2a. Overexpressing PLN-R25C in rat myocytes exhibit significant inhibition of SR Ca^{2+}-

transport, depressed contraction, prominent arrhythmias. This inhibitory effect can be completely relieved by isoproterenol-mediated PKA phosphorylation of this PLN variant.[55]

Different from PLN-R9C, PLN-R25C mutant shifts the conformational equilibrium toward the R state confirmation.[53] This means R25C mutant preferentially binds to SERCA2a and might interfere with the recognition mechanism of PLN. These structural differences further suggest that altered interactions between PLN and the membrane bilayer play an essential role in the dysregulation of Ca^{2+} cycling in cardiomyocytes.

PLN R14del

The PLN deletion c.40_42delAGA, (p.Arg14del, R14del) was initially identified in a Greek family with DCM and cardiac arrythmias.[56] PLN-R14del is the most prevalent mutation in Netherlands, around 12% in patients with ACM and 15% in DCM patients, and over 1500 carriers have been identified.[57] Additionally, this variant was also reported in other European countries,[58,59] as well as in the United States,[60] China,[61] and Canada.[62,63] Heterozygous carriers exhibit marked phenotypic heterogeneity, ranging from asymptomatic individuals with normal echocardiograms at advanced age to those who develop severe dilated cardiomyopathy with impaired systolic function, frequent ventricular arrhythmias, heart failure, and premature death at early adulthood.[64] Most carriers do, however, develop symptoms at middle age. Homozygous carriers have up to now not been identified. Most probands carrying PLN-R14del exhibited similar electrocardiographic features with low QRS voltages, inverted T waves, and attenuated R wave amplitudes.[56-58] Notably, abnormal PLN protein aggregation or clusters are a hallmark of PLN-R14del cardiomyopathy, and are not present in DCM hearts of other etiologies.[65-67]

Mechanistically, PLN-R14del was initially believed to be a SERCA2a super-inhibitor, compromising sarcoplasmic reticulum Ca^{2+} reuptake and consequently promote diastolic dysfunction, Ca^{2+} overload, and increased arrhythmogenic susceptibility.[35] Badone et al, however, contradicted this super-inhibition theory using human PLN-R14del iPSC derived cardiomyocytes and reported reduced inhibitory activity.[68] In parallel, studies using mice with a genomic PLN-R14del locus also show reduced SERCA2a inhibition in both heterozygous and homozygous cardiomyocytes.[69-71] Instead of SERCA2a calcium handling, altered S/ER structure may therefore be the primary driver of PLN-R14del cardiomyopathy.[12,69] This conceptual shift has recently been reviewed.[12]

Recent studies demonstrated that silencing PLN-R14del with antisense oligonucleotides (ASOs) could significantly improve survival in homozygous PLN-R14del mice.[72,73] In cardiomyocytes isolated from PLN-R14del mice, Ca^{2+} uptake was enhanced and ASO treatment did not have additional effects on calcium handling in

PLN-R14del cardiomyocytes.[74] Nevertheless, the mice exhibited remarkable therapeutic benefit with prolonged life spam and better cardiac function. Importantly, ASO treatment did resolve the abnormal PLN clustering, a hallmark of this cardiomyopathy, strongly pointing towards this as the pathological problem. Together, these findings further support that PLN-R14del is an abnormal PLN clustering disease and importantly, highlight ASO therapy as a promising treatment strategy for this disease.

In comparison to WT PLN, computational simulations suggest that the PLN-R14del variant may exhibit a higher affinity for itself, potentially shifting the pentamer/monomer equilibrium toward a more pentameric form.[17] However, this prediction requires direct experimental validation in relevant *in vitro* and *in vivo* systems. If confirmed, these pentamers may lead to the observed increased ER stress, and activate the unfolded protein response (UPR), which potentially initially exert a protective, adaptive role by enhancing protein quality control.[75] Markers of autophagy, including P62 and LC3 are also repeatedly reported in different study models and in human cardiac tissue, indicating that autophagy is activated and/or hampered. An, *in vitro* study suggested impaired autophagosome-lysosome fusion upon ectopic PLN-R14del overexpression studies in cell lines, which may compromise the clearance of PLN clusters.[76]

Taken together, these observations support a disease mechanism that is not driven by the loss of PLN function, but by mutation-induced alterations in PLN structure and potentially imbalance in the monomer-pentamer equilibrium. These changes promote abnormal S/ER membrane clustering and enhanced Ca^{2+} handling into SR, progressively injuring cardiomyocytes and ultimately driving pathological remodeling towards dilated and/or arrhythmogenic cardiomyopathy.

Pathogenic nonsense variants

PLN L39Stop

The PLN nonsense mutation c.116T>G (p.Leu39*, L39Stop), also referred as L39X or Leu39Ter, is a T116G transversion that converts the codon for leucine at position 39 (TTA) into a premature stop codon (TGA).[77] The truncation of PLN and the resulting loss of its transmembrane domain II contribute to the pathogenesis of DCM, HCM, ACM, progressive heart failure, and premature death.[78,79] Heterozygous individuals display a broad spectrum of phenotypes, ranging from asymptomatic carriers to those presenting with HCM characterized by preserved left ventricular systolic function and a delay transition to DCM, while others develop sustained ventricular tachycardia.[77,80,81] In contrast, homozygous individuals develop severe DCM at a very young age and required cardiac transplantation. These findings indicate that the PLN-L39Stop mutation exhibits a dosage-dependent effect and follows an autosomal dominant inheritance pattern, while also implying that additional genetic or environmental factors may contribute to its pathogenic mechanism. Although PLN

mRNA is readily detectable in the myocardium of these homozygous carriers, no corresponding PLN protein could be observed.[77] Using human stem-cell-derived cardiomyocytes it was demonstrated that the L39Stop transcript is stable and actively translated, but that the resulting truncated protein undergoes rapid proteasomal degradation, indicating that enhanced protein turnover rather than mRNA instability accounts for the reduced detectability of PLN protein. This continuous production and clearance of a misfolded PLN species have been suggested to contribute to disease in L39Stop carriers.[82]

E2Stop

Another nonsense variant, p.Glu2Ter (c.4G>T, E2Stop), was identified in a homozygous patient who undergoes nonsense-mediated mRNA decay, resulting in absent PLN protein expression. This individual developed dilated cardiomyopathy and severe heart failure. In contrast, heterozygous family members, who express approximately 50% of normal PLN levels, appear asymptomatic and display normal ECG.[83] Unlike L39Stop, the E2Stop mutation can be regarded as a true null allele that does not generate any PLN protein, supporting the notion that PLN haploinsufficiency is likely tolerated in humans. Notably, only one homozygous E2Stop patient has been reported to date. Given the consanguineous background, additional genetic or non-genetic contributors cannot be excluded. Therefore, while complete loss of PLN expression remains a plausible disease driver in homozygosity, the pathogenic mechanism of E2Stop still remains to be clarified.

Unlike in humans, complete absence of PLN in mice does not result in cardiac disease, but enhances Ca^{2+} transient amplitude, myocardial contractility and exercise endurance.[84-86] PLN ablation can even attenuate cardiac dysfunction and partially normalize disease-associated molecular and transcriptional changes in several transgenic mouse models, including calsequestrin-related heart failure, hypertrophic cardiomyopathy, and PLN-R14del cardiomyopathy.[87-90] In humans, by contrast, the consequences of complete PLN deficiency, E2Stop, may be detrimental, but this remains poorly defined due to only one reported homozygous patient . One potential explanation for the apparent interspecies differences is higher baseline heart rate and the relative contribution of the SERCA/PLN axis to Ca^{2+} handling, suggesting that PLN requirements for Ca^{2+} homeostasis could diverge between mice and humans.

These findings indicate that PLN silencing is beneficial in the murine heart, even when PLN is completely ablated, but also highlight a dose dependence in humans. Thus, therapeutic strategies targeting PLN should aim for finely tuned, partial inhibition rather than complete loss of function to maximize benefit while minimizing the risk of

maladaptive Ca^{2+} overload and arrhythmogenesis.

Discussion

Despite its small size, the PLN gene harbors a disproportionately large number of pathogenic variants that give rise to inherited cardiomyopathies. However, it has become increasingly clear that these variants do not converge on a single pathogenic mechanism. Instead, they perturb PLN structure, Ca^{2+} handling and intracellular signaling through several partially overlapping processes, including altered SR Ca^{2+} cycling, disturbed interactions with other proteins, induction of abnormal S/ER clustering, and potential secondary effects on mitochondrial function.

With regard to Ca^{2+} cycling, different variants can either accelerate or slow SR Ca^{2+} uptake. Reduced SR Ca^{2+} uptake is well-known from animal models to have detrimental consequences and is thought to contribute to heart-failure progression in general.[91] Conversely, enhanced Ca^{2+} uptake improves contractile performance, constitutively elevated uptake may also be harmful, as high SR Ca^{2+} content can promote Ca^{2+} sparks and trigger arrhythmias.[92] Loss of dynamic regulation is a further layer of complexity: all pathogenic variants appear to impair the finely tuned beat-to-beat modulation of PLN-SERCA2a to some extent. This may have limited consequences in mice, which operate within a relative narrow physiological heart-rate range, but can be much more relevant in humans. Indeed, while PLN knockout mice do not develop overt cardiomyopathy, complete loss of PLN in humans (E2Ter) is associated with severe cardiac dysfunction, underscoring a s species- and dose-dependence of PLN biology.

Many pathogenic variants act primarily through mutation-induced changes in PLN structure affecting monomer-pentamer formation and interaction with SERCA2a,[17] which in turn influence Ca^{2+} handling and/or protein interactions. The R9C variant stabilizes the pentamer via disulfide bridges,[18] limiting access to SERCA2a and reducing phosphorylation accessibility, and has also been proposed to sequester PKA. Other protein partners, such as HAX-1, may further modulate the impact of individual variants.[93] In addition, increased PLN clustering-particularly in the context of R14del has been linked to abnormal S/ER membrane organization and impaired autophagosome-lysosome fusion, thereby engaging maladaptive proteostasis pathways and contributing to pathological remodeling.[76] Mutations beyond the classical deletion, missense and nonsense variants, including insertions and promoter variants, have also been reported in association with PLN-related disease, although current evidence remains insufficient to establish a direct causal relationship.[41] Disturbed Ca^{2+} handling and S/ER architecture are likely to propagate towards mitochondria, via mitochondria-associated membranes, where altered Ca^{2+} transfer and stress signaling may further exacerbate energetic failure and cell death.[94]

These mechanistic insights have important therapeutic implications and help explain why interventions cannot be uniformly applied across all PLN variants. For example, the selective SERCA2a activator PST3093 enhances calcium reuptake and cardiac performance, possibly by attenuating the PLN-SERCA2a interaction.[95] This approach may therefore be most relevant for superinhibitory PLN variants, but not other variants. Additional therapeutic opportunities arise from modulation of the PP1 regulatory axis. Inhibiting PP1 activity or enhancing its endogenous inhibitor I-1 may enhance PLN phosphorylation and improve calcium handling, while AAV-mediated delivery of a constitutively active I-1 (I-1c) has shown favorable effects on cardiac remodeling and function in both preclinical and early clinical studies.[96] One potential solution might be the development of a gene-editing approach that replaces the entire PLN coding sequence, which is feasible given its relatively small size (156 bp). Yet, current TALEN and CRISPR/Cas9 studies have not replaced the full coding sequence and instead require variant-specific targeting, which limits broad clinical scalability.[65,97] PLN silencing has been shown to exert protective effects in PLN-R14del cardiomyopathy in a mouse model by resolving pathogenic S/ER protein clusters.[74] Such a strategy may also be beneficial in other forms of heart failure, including PLN-R25C cardiomyopathy, through improved calcium cycling. Similarly, in PLN-R9C, which functions as a dominant-negative variant, PLN silencing is potentially to be effective. However, a key unresolved issue is the tolerable extent of PLN suppression in humans, as excessive silencing could potentially generate detrimental effects.

Conclusion

It has become clear that the pathogenicity of PLN variants should not be regarded only as a problem of altered Ca^{2+} homeostasis. Instead, accumulating evidence highlights a broader and more complex framework that includes toxic effects of truncated or mislocalized proteins, disruption of protein-protein interaction networks and proteostasis pathways, aberrant oligomerization and clustering within the SR membrane, and variant-specific modulation of post-translational modifications and stress signaling. Consequently, therapeutic strategies for PLN cardiomyopathies are unlikely to follow a universal “one-size-fits-all” approach, even though such a solution would be preferable and more cost-effective. From a translational standpoint, these insights underscore the need for therapeutic strategies that go beyond restoration of SERCA2a activity. While SERCA2a activators and antisense oligonucleotides targeting mutant alleles remain promising, complementary approaches directed at reducing protein aggregation, alleviating ER stress, or enhancing autophagic clearance may prove equally important.

Authorship contribution statement

L.S. and H.H.W.S. defined the concept of this manuscript. L.S. drafted a concept manuscript; L.S., V.O.N.T. and H.H.W.S. edited and revised the manuscript; all authors approved the final version of this manuscript.

Reference

1. Eisner DA, Caldwell JL, Kistamás K, Trafford AW. Calcium and Excitation-Contraction Coupling in the Heart. Circulation Research. 2017;121:181-195. doi: 10.1161/circresaha.117.310230
2. David H M, Evangelia G K. Phospholamban: a crucial regulator of cardiac contractility. Nat Rev Mol Cell Biol. 2003;4. doi: 10.1038/nrm1151
3. Tada M, Kirchberger MA, Katz AM. Phosphorylation of a 22,000-dalton component of the cardiac sarcoplasmic reticulum by adenosine 3':5'-monophosphate-dependent protein kinase. Journal of Biological Chemistry. 1975;250:2640-2647. doi: 10.1016/s0021-9258(19)41650-5
4. J F, A U, K K, S T, M K, M T. Complete complementary DNA-derived amino acid sequence of canine cardiac phospholamban. J Clin Invest. 1987;79. doi: 10.1172/jci112799
5. Fujii J, Zarain-Herzberg A, Willard HF, Tada M, MacLennan DH. Structure of the rabbit phospholamban gene, cloning of the human cDNA, and assignment of the gene to human chromosome 6. Journal of Biological Chemistry. 1991;266:11669-11675. doi: 10.1016/s0021-9258(18)99009-5
6. Gustavsson M, Traaseth NJ, Veglia G. Probing ground and excited states of phospholamban in model and native lipid membranes by magic angle spinning NMR spectroscopy. Biochim Biophys Acta. 2012;1818:146-153. doi: 10.1016/j.bbamem.2011.07.040
7. Nathaniel J T, Lei S, Raffaello V, Daniel G M, George B, Gianluigi V. Structure and topology of monomeric phospholamban in lipid membranes determined by a hybrid solution and solid-state NMR approach. Proc Natl Acad Sci U S A. 2009;106. doi: 10.1073/pnas.0904290106
8. Akin BL, Hurley TD, Chen Z, Jones LR. The structural basis for phospholamban inhibition of the calcium pump in sarcoplasmic reticulum. J Biol Chem. 2013;288:30181-30191. doi: 10.1074/jbc.M113.501585
9. P J, M I, M T, M C, E C. Nature and site of phospholamban regulation of the Ca2+ pump of sarcoplasmic reticulum. Nature. 1989;342. doi: 10.1038/342090a0
10. Kimura Y, Kurzydlowski K, Tada M, MacLennan DH. Phospholamban inhibitory function is activated by depolymerization. J Biol Chem. 1997;272:15061-15064. doi: 10.1074/jbc.272.24.15061
11. Simmerman HK, Collins JH, Theibert JL, Wegener AD, Jones LR. Sequence analysis of phospholamban. Identification of phosphorylation sites and two major structural domains. Journal of Biological Chemistry. 1986;261:13333-13341. doi: 10.1016/s0021-9258(18)69309-3
12. Stege NM, de Boer RA, Makarewich CA, van der Meer P, Sillje HHW. Reassessing the Mechanisms of PLN-R14del Cardiomyopathy: From Calcium Dysregulation to S/ER Malformation. JACC Basic Transl Sci. 2024;9:1041-1052. doi: 10.1016/j.jacbts.2024.02.017
13. Funk F, Kronenbitter A, Hackert K, Oebbeke M, Klebe G, Barth M, Koch D, Schmitt JP. Phospholamban pentamerization increases sensitivity and dynamic range of cardiac relaxation. Cardiovasc Res. 2023;119:1568-1582. doi: 10.1093/cvr/cvad037
14. Nathaniel J T, Raffaello V, Kurt D T, Christine B K, David D T, Gianluigi V. Spectroscopic validation of the pentameric structure of phospholamban. Proc Natl Acad Sci U S A. 2007;104. doi: 10.1073/pnas.0701016104

15. Hou Z, Kelly EM, Robia SL. Phosphomimetic mutations increase phospholamban oligomerization and alter the structure of its regulatory complex. J Biol Chem. 2008;283:28996-29003. doi: 10.1074/jbc.M804782200
16. Cao Y, Yang R, Wang W, Jiang S, Yang C, Wang Q, Liu N, Xue Y, Lee I, Meng X, et al. Effects of membrane lipids on phospholamban pentameric channel structure and ion transportation mechanisms. Int J Biol Macromol. 2023;224:766-775. doi: 10.1016/j.ijbiomac.2022.10.164
17. Cleary SR, Teng ACT, Kongmeneck AD, Fang X, Phillips TA, Cho EE, Smith RA, Karkut P, Makarewich CA, Kekenes-Huskey PM, et al. Dilated cardiomyopathy variant R14del increases phospholamban pentamer stability, blunting dynamic regulation of calcium. J Biol Chem. 2025;301:108118. doi: 10.1016/j.jbc.2024.108118
18. Ha KN, Masterson LR, Hou Z, Verardi R, Walsh N, Veglia G, Robia SL. Lethal Arg9Cys phospholamban mutation hinders Ca2+-ATPase regulation and phosphorylation by protein kinase A. Proc Natl Acad Sci U S A. 2011;108:2735-2740. doi: 10.1073/pnas.1013987108
19. Robia SL, Campbell KS, Kelly EM, Hou Z, Winters DL, Thomas DD. Forster transfer recovery reveals that phospholamban exchanges slowly from pentamers but rapidly from the SERCA regulatory complex. Circ Res. 2007;101:1123-1129. doi: 10.1161/CIRCRESAHA.107.159947
20. Ablorh ND, Thomas DD. Phospholamban phosphorylation, mutation, and structural dynamics: a biophysical approach to understanding and treating cardiomyopathy. Biophys Rev. 2015;7:63-76. doi: 10.1007/s12551-014-0157-z
21. Gustavsson M, Traaseth NJ, Karim CB, Lockamy EL, Thomas DD, Veglia G. Lipid-mediated folding/unfolding of phospholamban as a regulatory mechanism for the sarcoplasmic reticulum Ca2+-ATPase. J Mol Biol. 2011;408:755-765. doi: 10.1016/j.jmb.2011.03.015
22. Gustavsson M, Verardi R, Mullen DG, Mote KR, Traaseth NJ, Gopinath T, Veglia G. Allosteric regulation of SERCA by phosphorylation-mediated conformational shift of phospholamban. Proc Natl Acad Sci U S A. 2013;110:17338-17343. doi: 10.1073/pnas.1303006110
23. Fujii J, Maruyama K, Tada M, MacLennan DH. Expression and Site-specific Mutagenesis of Phospholamban. Journal of Biological Chemistry. 1989;264:12950-12955. doi: 10.1016/s0021-9258(18)51579-9
24. I T A, P D A, K R M, M A L, A T B, D M E. Structural organization of the pentameric transmembrane alpha-helices of phospholamban, a cardiac ion channel. EMBO J. 1994;13. doi: 10.1002/j.1460-2075.1994.tb06801.x
25. Simmerman HK, Kobayashi YM, Autry JM, Jones LR. A leucine zipper stabilizes the pentameric membrane domain of phospholamban and forms a coiled-coil pore structure. J Biol Chem. 1996;271:5941-5946. doi: 10.1074/jbc.271.10.5941
26. Chu G, Li L, Sato Y, Harrer JM, Kadambi VJ, Hoit BD, Bers DM, Kranias EG. Pentameric assembly of phospholamban facilitates inhibition of cardiac function in vivo. J Biol Chem. 1998;273:33674-33680. doi: 10.1074/jbc.273.50.33674
27. Chu G, Lester JW, Young KB, Luo W, Zhai J, Kranias EG. A single site (Ser16) phosphorylation in phospholamban is sufficient in mediating its maximal cardiac responses to beta -agonists. J Biol Chem. 2000;275:38938-38943. doi: 10.1074/jbc.M004079200
28. Mattiazzi A, Mundina-Weilenmann C, Guoxiang C, Vittone L, Kranias E. Role of phospholamban phosphorylation on Thr17 in cardiac physiological and pathological conditions. Cardiovasc Res. 2005;68:366-375. doi: 10.1016/j.cardiores.2005.08.010

29. Julia M, Daniel K-D, Sergiy T, Alice B, Kirsten U-F, Markus K, Christof L, Henning U, Mattia M, Christian O, et al. 14-3-3 binding creates a memory of kinase action by stabilizing the modified state of phospholamban. Sci Signal. 2020;13. doi: 10.1126/scisignal.aaz1436
30. Traaseth NJ, Thomas DD, Veglia G. Effects of Ser16 phosphorylation on the allosteric transitions of phospholamban/Ca(2+)-ATPase complex. J Mol Biol. 2006;358:1041-1050. doi: 10.1016/j.jmb.2006.02.047
31. Kimura Y, Kurzydlowski K, Tada M, MacLennan DH. Phospholamban regulates the Ca2+-ATPase through intramembrane interactions. J Biol Chem. 1996;271:21726-21731. doi: 10.1074/jbc.271.36.21726
32. Karim CB, Zhang Z, Howard EC, Torgersen KD, Thomas DD. Phosphorylation-dependent conformational switch in spin-labeled phospholamban bound to SERCA. J Mol Biol. 2006;358:1032-1040. doi: 10.1016/j.jmb.2006.02.051
33. Joachim P S, Mitsuhiro K, Michio A, Guo Hua L, Ferhaan A, Ulrike M, Evangelia G K, David H M, J G S, Christine E S. Dilated cardiomyopathy and heart failure caused by a mutation in phospholamban. Science. 2003;299. doi: 10.1126/science.1081578
34. Ceholski DK, Turnbull IC, Kong CW, Koplev S, Mayourian J, Gorski PA, Stillitano F, Skodras AA, Nonnenmacher M, Cohen N, et al. Functional and transcriptomic insights into pathogenesis of R9C phospholamban mutation using human induced pluripotent stem cell-derived cardiomyocytes. J Mol Cell Cardiol. 2018;119:147-154. doi: 10.1016/j.yjmcc.2018.05.007
35. Kobra H, Fotis K, Anthony O G, Jason R W, Luke P, Roy A L, Guo-Chang F, Dimitris T, Rohan R P, Gerald W 2nd D, et al. A mutation in the human phospholamban gene, deleting arginine 14, results in lethal, hereditary cardiomyopathy. Proc Natl Acad Sci U S A. 2006;103. doi: 10.1073/pnas.0510519103
36. Zhou T, Li J, Zhao P, Liu H, Jia D, Jia H, He L, Cang Y, Boast S, Chen YH, et al. Palmitoyl acyltransferase Aph2 in cardiac function and the development of cardiomyopathy. Proc Natl Acad Sci U S A. 2015;112:15666-15671. doi: 10.1073/pnas.1518368112
37. Bidwell PA, Haghighi K, Kranias EG. The antiapoptotic protein HAX-1 mediates half of phospholamban's inhibitory activity on calcium cycling and contractility in the heart. J Biol Chem. 2018;293:359-367. doi: 10.1074/jbc.RA117.000128
38. Carlson CR, Aronsen JM, Bergan-Dahl A, Moutty MC, Lunde M, Lunde PK, Jarstadmarken H, Wanichawan P, Pereira L, Kolstad TRS, et al. AKAP18delta Anchors and Regulates CaMKII Activity at Phospholamban-SERCA2 and RYR. Circ Res. 2022;130:27-44. doi: 10.1161/CIRCRESAHA.120.317976
39. Vafiadaki E, Arvanitis DA, Sanoudou D, Kranias EG. Identification of a protein phosphatase-1/phospholamban complex that is regulated by cAMP-dependent phosphorylation. PLoS One. 2013;8:e80867. doi: 10.1371/journal.pone.0080867
40. Phillips TA, Hauck GT, Pribadi MP, Cho EE, Cleary SR, Robia SL. Micropeptide hetero-oligomerization adds complexity to the calcium pump regulatory network. Biophys J. 2023;122:301-309. doi: 10.1016/j.bpj.2022.12.014
41. Vafiadaki E, Chaudhari I, Soliman KM, Eliopoulos AG, Kranias EG, Sanoudou D. Genetic landscape of phospholamban cardiomyopathies. Front Cell Dev Biol. 2025;13:1626242. doi: 10.3389/fcell.2025.1626242
42. Bers DM. Calcium cycling and signaling in cardiac myocytes. Annu Rev Physiol. 2008;70:23-49. doi: 10.1146/annurev.physiol.70.113006.100455

43. Zhao W, Yuan Q, Qian J, Waggoner JR, Pathak A, Chu G, Mitton B, Sun X, Jin J, Braz JC, et al. The presence of Lys27 instead of Asn27 in human phospholamban promotes sarcoplasmic reticulum Ca2+-ATPase superinhibition and cardiac remodeling. Circulation. 2006;113:995-1004. doi: 10.1161/CIRCULATIONAHA.105.583351
44. Fish M, Shaboodien G, Kraus S, Sliwa K, Seidman CE, Burke MA, Crotti L, Schwartz PJ, Mayosi BM. Mutation analysis of the phospholamban gene in 315 South Africans with dilated, hypertrophic, peripartum and arrhythmogenic right ventricular cardiomyopathies. Sci Rep. 2016;6:22235. doi: 10.1038/srep22235
45. Ceholski DK, Trieber CA, Holmes CF, Young HS. Lethal, hereditary mutants of phospholamban elude phosphorylation by protein kinase A. J Biol Chem. 2012;287:26596-26605. doi: 10.1074/jbc.M112.382713
46. Burke MA, Chang S, Wakimoto H, Gorham JM, Conner DA, Christodoulou DC, Parfenov MG, DePalma SR, Eminaga S, Konno T, et al. Molecular profiling of dilated cardiomyopathy that progresses to heart failure. JCI Insight. 2016;1. doi: 10.1172/jci.insight.86898
47. Schmitt JP, Ahmad F, Lorenz K, Hein L, Schulz S, Asahi M, Maclennan DH, Seidman CE, Seidman JG, Lohse MJ. Alterations of phospholamban function can exhibit cardiotoxic effects independent of excessive sarcoplasmic reticulum Ca2+-ATPase inhibition. Circulation. 2009;119:436-444. doi: 10.1161/CIRCULATIONAHA.108.783506
48. Weber DK, Reddy UV, Robia SL, Veglia G. Pathological mutations in the phospholamban cytoplasmic region affect its topology and dynamics modulating the extent of SERCA inhibition. Biochim Biophys Acta Biomembr. 2024;1866:184370. doi: 10.1016/j.bbamem.2024.184370
49. Yost O, Friedenberg SG, Jesty SA, Olby NJ, Meurs KM. The R9H phospholamban mutation is associated with highly penetrant dilated cardiomyopathy and sudden death in a spontaneous canine model. Gene. 2019;697:118-122. doi: 10.1016/j.gene.2019.02.022
50. Ceholski DK, Trieber CA, Young HS. Hydrophobic imbalance in the cytoplasmic domain of phospholamban is a determinant for lethal dilated cardiomyopathy. J Biol Chem. 2012;287:16521-16529. doi: 10.1074/jbc.M112.360859
51. Yu X, Lorigan GA. Probing the interaction of Arg9Cys mutated phospholamban with phospholipid bilayers by solid-state NMR spectroscopy. Biochim Biophys Acta. 2013;1828:2444-2449. doi: 10.1016/j.bbamem.2013.07.003
52. Yu X, Lorigan GA. Secondary structure, backbone dynamics, and structural topology of phospholamban and its phosphorylated and Arg9Cys-mutated forms in phospholipid bilayers utilizing 13C and 15N solid-state NMR spectroscopy. J Phys Chem B. 2014;118:2124-2133. doi: 10.1021/jp500316s
53. Nelson SED, Ha KN, Gopinath T, Exline MH, Mascioni A, Thomas DD, Veglia G. Effects of the Arg9Cys and Arg25Cys mutations on phospholamban's conformational equilibrium in membrane bilayers. Biochim Biophys Acta Biomembr. 2018;1860:1335-1341. doi: 10.1016/j.bbamem.2018.02.030
54. Mollanoori H, Naderi N, Amin A, Hassani B, Shahraki H, Teimourian S. A novel human T17N-phospholamban variation in idiopathic dilated cardiomyopathy. Gene Reports. 2018;12:122-127. doi: 10.1016/j.genrep.2018.06.014
55. Liu GS, Morales A, Vafiadaki E, Lam CK, Cai WF, Haghighi K, Adly G, Hershberger RE, Kranias EG. A novel human R25C-phospholamban mutation is associated with super-inhibition

of calcium cycling and ventricular arrhythmia. Cardiovasc Res. 2015;107:164-174. doi: 10.1093/cvr/cvv127

56. Haghighi K, Kolokathis F, Gramolini A, Waggoner J, Pater L, Lynch R, Fan G, Tsiapras D, Parekh R, Dorn G, et al. A mutation in the human phospholamban gene, deleting arginine 14, results in lethal, hereditary cardiomyopathy. Proceedings of the National Academy of Sciences of the United States of America. 2006;103:1388-1393. doi: 10.1073/pnas.0510519103
57. van der Zwaag PA, van Rijsingen IA, Asimaki A, Jongbloed JD, van Veldhuisen DJ, Wiesfeld AC, Cox MG, van Lochem LT, de Boer RA, Hofstra RM, et al. Phospholamban R14del mutation in patients diagnosed with dilated cardiomyopathy or arrhythmogenic right ventricular cardiomyopathy: evidence supporting the concept of arrhythmogenic cardiomyopathy. Eur J Heart Fail. 2012;14:1199-1207. doi: 10.1093/eurjhf/hfs119
58. Posch M, Perrot A, Geier C, Boldt L, Schmidt G, Lehmkuhl H, Hetzer R, Dietz R, Gutberlet M, Haverkamp W, et al. Genetic deletion of arginine 14 in phospholamban causes dilated cardiomyopathy with attenuated electrocardiographic R amplitudes. Heart rhythm. 2009;6:480-486. doi: 10.1016/j.hrthm.2009.01.016
59. Lopez-Ayala JM, Boven L, van den Wijngaard A, Penafiel-Verdu P, van Tintelen JP, Gimeno JR. Phospholamban p.arg14del mutation in a Spanish family with arrhythmogenic cardiomyopathy: evidence for a European founder mutation. Rev Esp Cardiol (Engl Ed). 2015;68:346-349. doi: 10.1016/j.rec.2014.11.012
60. DeWitt MM, MacLeod HM, Soliven B, McNally EM. Phospholamban R14 deletion results in late-onset, mild, hereditary dilated cardiomyopathy. J Am Coll Cardiol. 2006;48:1396-1398. doi: 10.1016/j.jacc.2006.07.016
61. Chen L, Song J, Chen X, Chen K, Ren J, Zhang N, Rao M, Hu Z, Zhang Y, Gu M, et al. A novel genotype-based clinicopathology classification of arrhythmogenic cardiomyopathy provides novel insights into disease progression. Eur Heart J. 2019;40:1690-1703. doi: 10.1093/eurheartj/ehz172
62. Cheung CC, Healey JS, Hamilton R, Spears D, Gollob MH, Mellor G, Steinberg C, Sanatani S, Laksman ZW, Krahn AD. Phospholamban cardiomyopathy: a Canadian perspective on a unique population. Neth Heart J. 2019;27:208-213. doi: 10.1007/s12471-019-1247-0
63. Doevendans PA, Glijnis PC, Kranias EG. Leducq Transatlantic Network of Excellence to Cure Phospholamban-Induced Cardiomyopathy (CURE-PLaN). Circ Res. 2019;125:720-724. doi: 10.1161/CIRCRESAHA.119.315077
64. Hof IE, van der Heijden JF, Kranias EG, Sanoudou D, de Boer RA, van Tintelen JP, van der Zwaag PA, Doevendans PA. Prevalence and cardiac phenotype of patients with a phospholamban mutation. Neth Heart J. 2019;27:64-69. doi: 10.1007/s12471-018-1211-4
65. Karakikes I, Stillitano F, Nonnenmacher M, Tzimas C, Sanoudou D, Termglinchan V, Kong CW, Rushing S, Hansen J, Ceholski D, et al. Correction of human phospholamban R14del mutation associated with cardiomyopathy using targeted nucleases and combination therapy. Nat Commun. 2015;6:6955. doi: 10.1038/ncomms7955
66. Te Rijdt WP, van der Klooster ZJ, Hoorntje ET, Jongbloed JDH, van der Zwaag PA, Asselbergs FW, Dooijes D, de Boer RA, van Tintelen JP, van den Berg MP, et al. Phospholamban immunostaining is a highly sensitive and specific method for diagnosing phospholamban p.Arg14del cardiomyopathy. Cardiovasc Pathol. 2017;30:23-26. doi: 10.1016/j.carpath.2017.05.004

67. Te Rijdt WP, van Tintelen JP, Vink A, van der Wal AC, de Boer RA, van den Berg MP, Suurmeijer AJ. Phospholamban p.Arg14del cardiomyopathy is characterized by phospholamban aggregates, aggresomes, and autophagic degradation. Histopathology. 2016;69:542-550. doi: 10.1111/his.12963
68. Badone B, Ronchi C, Lodola F, Knaust AE, Hansen A, Eschenhagen T, Zaza A. Characterization of the PLN p.Arg14del Mutation in Human Induced Pluripotent Stem Cell-Derived Cardiomyocytes. Int J Mol Sci. 2021;22. doi: 10.3390/ijms222413500
69. Stege NM, Eijgenraam TR, Oliveira Nunes Teixeira V, Feringa AM, Schouten EM, Kuster DWD, van der Velden J, Wolters AHG, Giepmans BNG, Makarewich CA, et al. DWORF Extends Life Span in a PLN-R14del Cardiomyopathy Mouse Model by Reducing Abnormal Sarcoplasmic Reticulum Clusters. Circ Res. 2023;133:1006-1021. doi: 10.1161/CIRCRESAHA.123.323304
70. Maniezzi C, Eskandr M, Florindi C, Ferrandi M, Barassi P, Sacco E, Pasquale V, Maione AS, Pompilio G, Teixeira VON, et al. Early consequences of the phospholamban mutation PLN-R14del(+/-) in a transgenic mouse model. Acta Physiol (Oxf). 2024;240:e14082. doi: 10.1111/apha.14082
71. Claudia M, Marem E, Chiara F, Mara F, Paolo B, Elena S, Valentina P, Angela S M, Giulio P, Vivian Oliveira Nunes T, et al. Early consequences of the phospholamban mutation PLN-R14del(+/-) in a transgenic mouse model. Acta Physiol (Oxf). 2024;240. doi: 10.1111/apha.14082
72. Grote Beverborg N, Spater D, Knoll R, Hidalgo A, Yeh ST, Elbeck Z, Sillje HHW, Eijgenraam TR, Siga H, Zurek M, et al. Phospholamban antisense oligonucleotides improve cardiac function in murine cardiomyopathy. Nat Commun. 2021;12:5180. doi: 10.1038/s41467-021-25439-0
73. Eijgenraam TR, Stege NM, Oliveira Nunes Teixeira V, de Brouwer R, Schouten EM, Grote Beverborg N, Sun L, Spater D, Knoll R, Hansson KM, et al. Antisense Therapy Attenuates Phospholamban p.(Arg14del) Cardiomyopathy in Mice and Reverses Protein Aggregation. Int J Mol Sci. 2022;23. doi: 10.3390/ijms23052427
74. Sun L, Eijgenraam TR, Amilon C, Janzen D, Hansson KM, Kubli DA, Spater D, Mullick AE, van der Meer P, Nunes Teixeira VO, et al. In PLN-R14del mice, SR structure restoration, rather than calcium cycling, is the dominant effector of PLN-ASO treatment. Cardiovasc Res. 2025. doi: 10.1093/cvr/cvaf156
75. Feyen DAM, Perea-Gil I, Maas RGC, Harakalova M, Gavidia AA, Arthur Ataam J, Wu TH, Vink A, Pei J, Vadgama N, et al. Unfolded Protein Response as a Compensatory Mechanism and Potential Therapeutic Target in PLN R14del Cardiomyopathy. Circulation. 2021;144:382-392. doi: 10.1161/CIRCULATIONAHA.120.049844
76. Vafiadaki E, Kranias EG, Eliopoulos AG, Sanoudou D. The phospholamban R14del generates pathogenic aggregates by impairing autophagosome-lysosome fusion. Cell Mol Life Sci. 2024;81:450. doi: 10.1007/s00018-024-05471-1
77. Haghighi K, Kolokathis F, Pater L, Lynch RA, Asahi M, Gramolini AO, Fan G-C, Tsiapras D, Hahn HS, Adamopoulos S, et al. Human phospholamban null results in lethal dilated cardiomyopathy revealing a critical difference between mouse and human. Journal of Clinical Investigation. 2003;111:869-876. doi: 10.1172/jci17892

78. Abrol N, Smolin N, Ceholski DK, Young HS, Robia SL. Phospholamban C-Terminal Truncations Including Heart Failure Mutation L39Stop Decrease Membrane Localization and Oligomerization and Alter the Structure of the PLB-Serca Complex. Biophysical Journal. 2014;106:566a-567a.
79. Abrol N, Smolin N, Stefonowicz C, Robia SL. Abstract 282: Phospholamban Truncation Mutations Including Heart Failure Mutant L39stop Disrupt Membrane Localization. Circulation Research. 2013;113:293–304.
80. Sanoudou D, Kolokathis F, Arvanitis D, Al-Shafai K, Krishnamoorthy N, Buchan RJ, Walsh R, Tsiapras D, Barton PJ, Cook SA, et al. Genetic modifiers to the PLN L39X mutation in a patient with DCM and sustained ventricular tachycardia? Glob Cardiol Sci Pract. 2015;2015:29. doi: 10.5339/gcsp.2015.29
81. Landstrom AP, Adekola BA, Bos JM, Ommen SR, Ackerman MJ. PLN-encoded phospholamban mutation in a large cohort of hypertrophic cardiomyopathy cases: Summary of the literature and implications for genetic testing. American Heart Journal. 2011;161:165-171. doi: 10.1016/j.ahj.2010.08.001
82. Rohner E, Witman N, Sohlmer J, De Genst E, Louch WE, Sahara M, Chien KR. An mRNA assay system demonstrates proteasomal-specific degradation contributes to cardiomyopathic phospholamban null mutation. Mol Med. 2021;27:102. doi: 10.1186/s10020-021-00362-8
83. Li Z, Chen P, Xu J, Yu B, Li X, Wang DW, Wang DW. A PLN nonsense variant causes severe dilated cardiomyopathy in a novel autosomal recessive inheritance mode. Int J Cardiol. 2019;279:122-125. doi: 10.1016/j.ijcard.2018.12.075
84. Slack JP, Grupp IL, Dash R, Holder D, Schmidt A, Gerst MJ, Tamura T, Tilgmann C, James PF, Johnson R, et al. The enhanced contractility of the phospholamban-deficient mouse heart persists with aging. J Mol Cell Cardiol. 2001;33:1031-1040. doi: 10.1006/jmcc.2001.1370
85. Luo W, Grupp IL, Harrer J, Ponniah S, Grupp G, Duffy JJ, Doetschman T, Kranias EG. Targeted ablation of the phospholamban gene is associated with markedly enhanced myocardial contractility and loss of beta-agonist stimulation. Circulation Research. 1994;75:401.
86. Desai, Kavin H, Schauble, Eric. Phospholamban deficiency does not compromise exercise capacity. American Journal of Physiology. 1999.
87. Kaneko M, Hashikami K, Yamamoto S, Matsumoto H, Nishimoto T. Phospholamban Ablation Using CRISPR/Cas9 System Improves Mortality in a Murine Heart Failure Model. PLoS One. 2016;11:e0168486. doi: 10.1371/journal.pone.0168486
88. Bai Y, Jones PP, Guo J, Zhong X, Clark RB, Zhou Q, Wang R, Vallmitjana A, Benitez R, Hove-Madsen L, et al. Phospholamban knockout breaks arrhythmogenic Ca(2)(+) waves and suppresses catecholaminergic polymorphic ventricular tachycardia in mice. Circ Res. 2013;113:517-526. doi: 10.1161/CIRCRESAHA.113.301678
89. Rajan S, Pena JR, Jegga AG, Aronow BJ, Wolska BM, Wieczorek DF. Microarray analysis of active cardiac remodeling genes in a familial hypertrophic cardiomyopathy mouse model rescued by a phospholamban knockout. Physiological Genomics. 2013;45:764-773.
90. Haghighi K, Pritchard T, Bossuyt J, Waggoner JR, Yuan Q, Fan GC, Osinska H, Anjak A, Rubinstein J, Robbins J, et al. The human phospholamban Arg14-deletion mutant localizes to plasma membrane and interacts with the Na/K-ATPase. J Mol Cell Cardiol. 2012;52:773-782. doi: 10.1016/j.yjmcc.2011.11.012

91. Bers DM, Eisner DA, Valdivia HcH. Sarcoplasmic Reticulum Ca2+ and Heart Failure. Circulation Research. 2003;93:487-490. doi: 10.1161/01.Res.0000091871.54907.6b
92. Sato D, Uchinoumi H, Bers DM. Increasing SERCA function promotes initiation of calcium sparks and breakup of calcium waves. J Physiol. 2021;599:3267-3278. doi: 10.1113/JP281579
93. Vafiadaki E, Sanoudou D, Arvanitis DA, Catino DH, Kranias EG, Kontrogianni-Konstantopoulos A. Phospholamban interacts with HAX-1, a mitochondrial protein with anti-apoptotic function. J Mol Biol. 2007;367:65-79. doi: 10.1016/j.jmb.2006.10.057
94. Ruiz-Meana M, Fernandez-Sanz C, Garcia-Dorado D. The SR-mitochondria interaction: a new player in cardiac pathophysiology. Cardiovasc Res. 2010;88:30-39. doi: 10.1093/cvr/cvq225
95. Arici M, Ferrandi M, Barassi P, Hsu SC, Torre E, Luraghi A, Ronchi C, Chang GJ, Peri F, Ferrari P, et al. Istaroxime Metabolite PST3093 Selectively Stimulates SERCA2a and Reverses Disease-Induced Changes in Cardiac Function. J Pharmacol Exp Ther. 2023;384:231-244. doi: 10.1124/jpet.122.001335
96. Kranias EG, Hajjar RJ. Modulation of cardiac contractility by the phospholamban/SERCA2a regulatome. Circ Res. 2012;110:1646-1660. doi: 10.1161/CIRCRESAHA.111.259754
97. Dave J, Raad N, Mittal N, Zhang L, Fargnoli A, Oh JG, Savoia ME, Hansen J, Fava M, Yin X, et al. Gene editing reverses arrhythmia susceptibility in humanized PLN-R14del mice: modelling a European cardiomyopathy with global impact. Cardiovasc Res. 2022;118:3140-3150. doi: 10.1093/cvr/cvac021

Chapter 3

Cardiac remodeling pathways do not accelerate disease onset and severity in a mouse model of PLN-R14del cardiomyopathy

Liu Sun, Elisabeth M. Schouten, Karla. Arevalo Gomez, Vivian Oliveira Nunes Teixeira*, Herman H.W. Silljé*

Department of Cardiology, University Medical Center Groningen, University of Groningen, the Netherlands

Scientific Reports volume 15, Article number: 33393 (2025)

Abstract:

PLN-R14del is a pathogenic Phospholamban (PLN) gene variant, characterized by ventricular arrhythmias and dilated cardiomyopathy in heterozygous carriers. Disease development is highly heterogeneous, indicating involvement of additional disease triggers, influencing both the onset and severity of the disease. A heterozygous PLN-R14del mouse model ($R14^{\Delta/+}$) was used to investigate whether cardiac pressure, induced by transverse aortic constriction (TAC), could accelerate disease onset. Wild-type littermates and sham operated animals were used as controls. At 6-week, both TAC groups exhibited increased left ventricular wall thickness, ventricular and atrial weights, and reduced ejection fraction, with comparable hypertrophic and fibrotic responses. Furthermore, differential gene expression showed activation of cardiac remodeling and stress pathways, and changes in metabolic genes expression in TAC groups. Importantly, TAC did not induce sarco-endoplasmic reticulum malformation in $R14^{\Delta/+}$ mice, suggesting that general cardiac stress and remodeling pathways are insufficient to trigger PLN-R14del cardiomyopathy.

In conclusion, TAC induced pressure overload provoked robust cardiac remodeling with activation of common stress pathways in young adult WT and $R14^{\Delta/+}$ mice. It did not trigger PLN-R14del-specific sarco-endoplasmic malformation or accelerate disease progression. These findings imply that activation of common cardiac stress pathways alone may be insufficient to accelerate the onset of PLN-R14del cardiomyopathy early adulthood.

Keywords: Phospholamban arginine 14 deletion cardiomyopathy; cardiac pressure overload; cardiomyocytes hypertrophy; cardiac remodeling

Introduction

Phospholamban (PLN) is a small protein that regulates the major Sarco/Endoplasmic Reticulum Calcium ATPase (SERCA2a), thereby controlling the rate of Ca^{2+} uptake into the sarcoplasmic reticulum (SR).[1] PLN therefore acts as a modulator of the cardiomyocyte contraction-relaxation cycle. Numerous PLN pathogenic variants have been identified and PLN-R14del, which lacks the codon for arginine residue 14, is the most prevalent known pathogenic variant and has been extensively studied.[2] Heterozygous carriers of PLN-R14del can develop arrhythmogenic cardiomyopathy (ACM) and/or dilated cardiomyopathy (DCM), which can lead to severe heart failure (HF).[3,4] Although it was originally hypothesized that this pathogenic variant would cause super-inhibition of SERCA, resulting in cytosolic calcium overload, more recent results suggest that this may not be the case.[5] Mouse PLN-R14del studies, revealed that abnormal S/ER malformation with strong perinuclear localization of PLN positive S/ER clusters was associated with cardiomyocyte cell death and consequent heart failure.[6] This strong perinuclear PLN localization has been shown to be a hallmark of this disease both in patients and PLN-R14del mice and has not been observed in other forms of ACM/DCM.[7]

PLN-R14del cardiomyopathy shows a high variability in disease onset and disease severity. Although, on average, disease develops around middle age, some carriers already develop severe disease at early adulthood, whereas others only develop mild symptoms at advanced age. This heterogeneity is even present between family members and is poorly understood.[8,9] Exercise, which can be a risk factor in other inherited cardiomyopathies, was not associated with PLN-R14del cardiomyopathy.[10] Similarly psychological stress or personality traits do not appear to be associated with PLN-R14del disease. Investigation of polymorphisms as secondary disease drivers has so far also not been promising, but this could also be a consequence of the relatively small cohorts.[11,12]

We previously generated a heterozygous mouse model ($R14^{\Delta/+}$) that shows key features of human PLN-R14del cardiomyopathy, which allows to investigate potential secondary disease drivers.[13] This mouse model develops characteristic cardiomyocyte perinuclear PLN clustering at one year of age with subsequent decrease in cardiac function, cardiomyocyte hypertrophy, fibrotic tissue replacement, and cardiac dilatation.[13] This disease onset corresponds with the disease onset in middle aged humans and together with the relative slow disease progression makes it an ideal model to investigate potential modifying factors that could enhance disease onset and severity. In a recent study, using a transgenic PLN mouse model unable to form naturally occurring PLN pentamers, it was shown that cardiac pressure overload induced by transverse aortic constriction (TAC), decreased survival in these mice. This was attributed to the narrower range of SERCA2a activity modulation in these transgenic mice causing more pronounced cardiac dysfunction after TAC.[14] Recent data indicate that also in PLN-R14del cardiomyopathy altered balances between PLN complexes

may exist, resulting in a less dynamic behavior.[15] It is therefore tempting to believe that the TAC induced stress pathways may also trigger PLN-R14del cardiomyopathy. Pressure overload induced cardiac stress has also been shown to accelerate disease development in several other genetic mouse models probably by activating pathways involving Ca^{2+} homeostasis, myofibrillar protein,[16] oxidative stress[17] and mitochondrial autophagy,[18] amongst others. Cardiomyocyte hypertrophy and fibrotic remodeling are features observed both in TAC and PLN-R14del cardiomyopathy and activation by TAC may lower the threshold for subsequent PLN-R14del cardiomyopathy development.[6] With the hypothesis that elevated cardiac stress could accelerate the course of PLN-R14del cardiomyopathy, we conducted TAC in $R14^{\Delta/+}$ mice and investigated cardiac remodeling and function as well as abnormal PLN-R14del clustering.

Method

Study design and animal model

At the age of 10 weeks, baseline echocardiography was performed and mice were randomly divided for sham or TAC operation. This resulted in four groups with 7 mice in the sham-WT group, 6 in the sham-R14del group, 10 in the TAC-WT group, and 13 in the TAC-R14del group. To enhance the consistency of the procedure and minimize variability introduced by operators, we used a refined TAC procedure by implementing rubber O-rings with a fixed inner diameter.[19] General appearance and body weight was monitored weekly. Mice were sacrificed 6 weeks post-surgery, after which organs, tissue and plasma were collected for subsequent histological and molecular analyses. All in vivo procedures were conducted under sustained anesthesia with 2-2.5% isoflurane in oxygen. This study was approved by the Dutch Central Committee for animal experiments (CCD; license number AVD1050020199105) and the animal ethical committee of the University of Groningen (permit numbers IVD199105-02-004) and followed the guidelines set out in the Directive 2010/63/EU of the European Parliament for using animals in research. It also followed the Animal Research: Reporting of In Vivo Experiments (ARRIVE) guidelines for reporting on experiments done with animals.[20] All methods were performed in accordance with the relevant guidelines and regulations. The minimum number of animals required for each experiment was calculated based on G*power (3.1.9.7) analyses, setting the significance level at 5% and the power at 80%. PLN-R14del cardiomyopathy is a monogenic disease caused by a pathogenic variant located on an autosomal chromosome and it affects males and females similarly.[5] Previous studies have demonstrated comparable clinical phenotypes in both male and female patients and also cardiac imaging revealed similar pathological changes, but males with low-voltage ECGs showed somewhat worse prognostic value.[21,22] Also, in PLN-R14del mice, male and female characteristics have been investigated and revealed comparable pathological phenotypes.[6,13,23] Since the effect of TAC is dependent on the aortic diameter, which is related to rodent age and weight, it is essential to use a similar group of mice.[24] Combining male and female mice, that have different weights, would

complicate this study by generating more variability necessitating much larger group numbers.[19] Since this is ethically not desired and the pathology of this monogenic disorder is similar in males and females we decided to use male mice only.

Echocardiography

M-mode and 2-dimensional echocardiography were performed before surgery and 6 weeks after TAC/Sham procedure, using a Vevo 3100 preclinical imaging system with a 40-MHz MXX550D linear array transducer (FUJIFILM VisualSonics, Canada) to monitor LV morphology and function as described previously.[6] Follow-up hemodynamic assessment was evaluated by Vevo LAB software version 5.5.0 (FUJIFILM VisualSonics). The data acquisition and analysis followed the guidelines provided by the European Society of Cardiology Working Group on Myocardial Function[25] and were performed in a blinded manner.

To verify the effectiveness and consistency of TAC, pressure gradient doppler echocardiography was performed 1-week after surgery. Using the suprasternal view, pulsed-wave doppler recordings were obtained at the site of the aortic arch to measure the peak velocity of blood flow across the constriction. The pressure gradient was calculated using the modified Bernoulli equation.

Histological staining

Transverse bi-ventricular slices were fixated in 4% formaldehyde solution (4% formalin; Klinipath, the Netherlands) for a minimum of 24 hours. Subsequently, the fixed hearts were dehydrated in an automated system (Leica TP1020; Leica Microsystems, Germany) embedded in paraffin (Klinipath) and sliced into 4-µm sections for histological staining. The slides underwent deparaffinization prior to advancing to the subsequent staining procedure.

Masson trichrome staining was performed to identify collagen deposition, adhering to the standard protocol. Subsequently, the entire stained sections were scanned using a Nanozoomer 2.0-HT digital slide scanner (Hamamatsu Photonics, Japan). Quantification of fibrosis in each section was accomplished by analyzing the percentage of the total section area occupied by fibrotic tissue using the positive Pixel Count v9 algorithm of Aperio's ImageScope software (version 12.4.0; Leica Microsystem).
To assess the size of cardiomyocytes, ventricular tissue was stained with fluorescein isothiocyanate (FITC)-conjugated wheat germ agglutinin (WGA, Sigma-Aldrich, MO, USA) and DAPI (4',6-diamidino-2 phenylindole, DAPI, blue) to visualized the extracellular matrix, and nuclei. 30-50 transversally cut cardiomyocytes of each animal were measured for size quantification. The whole stained sections were imaged using an Olympus VS200 ASW digital fluorescent slide scanner (Olympus- Life Science, Japen) at 40x magnification. QuPath Open Software for Bioimage Analysis (version 0.4.3) was used to measure the surface area. Cardiomyocytes area is displayed as a μm^2.
To reveal the localization of PLN in mouse cardiac tissue samples, the 2D12 anti-PLN antibody (Invitrogen, CA, USA) were used. Subsequently incubated with secondary

antibody donkey anti-rabbit Alexa FluorTM 555 (A31572, Invitrogen). In addition, DAPI (4′,6-diamidino-2-phenylindole; Invitrogen, CA, USA), and WGA (Sigma-Aldrich, MO, USA) were co-stained to visualize the cell nuclei and boundary.

Quantitative Polymerase Chain Reaction (q-PCR)

Total RNA was extracted from snap frozen left ventricular tissue using TRI Reagent (Sigma-Aldrich, MO, USA) according to the manufacturer's protocol. cDNA synthesis was conducted utilizing the QuantiTect reverse transcription kit (Qiagen, Germany). q-PCR was performed using iQ SYBR green supermix (Bio-Rad, CA, USA) and C1000 Thermal cycler CFX 384 Real-Time PCR Detection System (Bio-Rad).

Gene expression levels were determined by qPCR analysis using iQ SYBR green supermix (BioRad) and, C1000 Thermal cycler CFX 384 Real-Time PCR Detection system (Bio-Rad) with the manufacturer's instructions and recommended protocol. Gene expression data was normalized to the reference gene values from one of the components of the large 60S ribosomal subunit (Rplp0, encoding 36B4) using CFX Manager software (version 3.0; Bio-Rad). The resulting values were then expressed relative to the wild-type (WT) sham group. Primer sequences are listed in **Table S1**.

Protein isolation and immunoblotting

Total proteins were extracted from snap frozen left ventricles (LVs) using Radioimmunoprecipitation assay lysis buffer as described previously.[13] Protein concentration was measured using a Pierce bicinchoninic acid (BCA) protein assay kit (Thermo Scientific, MA, USA). The protein was then adjusted to a consistent concentration for subsequent Western blot analysis. Samples were heated to 95°C for 5 minutes, followed by loading onto a sodium dodecyl sulfate-polyacrylamide gel electrophoresis (SDS-PAGE) system. Load 5ug of protein per well for PLN gel and 20 ug of protein for SERCA gel. Proteins separated by SDS-PAGE were then transferred to an Immun-Blot polyvinylidene fluoride (PVDF) membrane using a semi-dry transfer system (Amersham Biosciences, UK). Revert 700 total protein stain (LI-COR # 926-11021) was applied for total protein detection and subsequent western blot normalization. Following staining, the membranes were blocked with blocking buffer, then incubated overnight at 4°C with a primary antibody, followed by a one-hour incubation at room temperature with a secondary antibody. Detection was accomplished through enhanced chemiluminescence using Western Lightning Ultra Chemiluminescent Substrate (204-22101) and Cytiva Amersham ImageQuant 800. To prepare 1X working solution, equal volumes Reagent A and Reagent B were combined. Targeting protein quantification is performed using Image Studio Lite Software Ver.5.2. The primary and secondary antibodies that were used are presented in **Table S2**.

RNA Sequencing

RNA isolation was performed as mentioned above. RNA Library preparation and sequencing of 5 RNA samples from each group of animals was perfomed by Lexogen NGS services (Vienna, Austria). The QuantSeq reads (fastq files) were mapped to the Ensembl Mus Musculus genome (GRCh38). Data filtering, normalization, principal

component (PC) analysis and differential expression analysis were performed using the DESeq package in R. Differentially expressed genes (DEGs) were defined by a Benjamini-Hochberg adjusted P value of <0.1 and an absolute fold change of >0.5. Pathway analysis of DEGs was performed using g:Profiler (https://biit.cs.ut.ee/gprofiler/gost).

Statistical Analyses

Data are presented as means ± standard error of the mean (SEM). Because of the low variability observed in the sham groups, a smaller number of mice were included in the sham group. Due to the small group sizes, nonparametric comparisons were conducted between groups. The Kruskal-Wallis test followed by Dunn's multiple comparisons test was employed for multigroup comparisons. Statistical analysis of DEGs was done in R version 4.3.1. All statistical analyses were performed using the GraphPad Prism (version 10.1.2). Statistical significance was considered at a level of $P<0.05$.

Results

1.1 TAC induced cardiac hypertrophy and cardiac dysfunction in both WT and R14$^{\Delta/+}$ mice

Echocardiographic assessment of trans-TAC pressure gradients demonstrated a clear increased higher value in TAC-operated groups compared to the sham group and no difference between the TAC groups (**Fig.S1**). At six weeks post-TAC surgery, revealed a significant decrease in the ejection fraction (%LVEF) and increase in the thickness of diastolic left ventricular anterior wall (LVAWd), and diastolic left ventricular posterior wall (LVPWd) after TAC in both the R14$^{\Delta/+}$ and WT groups (**Fig.1A-C**). However, more variation was apparent in %LVEF and not all mice showed a similar decline in %LVEF, indicating that at this stage mice had either compensated or decompensated heart failure (**Fig.1A**). The increase in echo determined ventricular wall thickness was corroborated by a significant higher LV mass in all TAC mice (**Fig.1E**). Moreover, atria weights were also strongly increased (**Fig.1F**) indicative for a hypertrophic stress response in both LV and atria, which is common to pressure overload. There was, however, no difference between the wildtype and the R14$^{\Delta/+}$ group in these responses. Together, R14$^{\Delta/+}$ mice did show similar cardiac hypertrophy and cardiac dysfunction as compared to WT mice, indicating that pressure overload does not accelerate or aggravate cardiac dysfunction in PLN-R14del cardiomyopathy.

1.2 TAC induced cardiac remodeling to a similar extend in WT and R14$^{\Delta/+}$ mice

In response to cardiac pressure overload, the heart undergoes both structural and functional remodeling. WGA staining of LV histological slices revealed significant cardiomyocyte hypertrophy in the TAC groups as compared to their sham groups (**Fig.2A-B**). This aligns with the increased LV wall thickness and cardiac weights (**Fig.1**). In addition, Masson trichrome staining of midventricular sections demonstrated an excessive extracellular matrix deposition within the ventricles in both WT and R14$^{\Delta/+}$ mice TAC groups as compared with the sham groups (**Fig.2C-D**). These cardiac

remodeling features were also reflected by changes in gene expression.

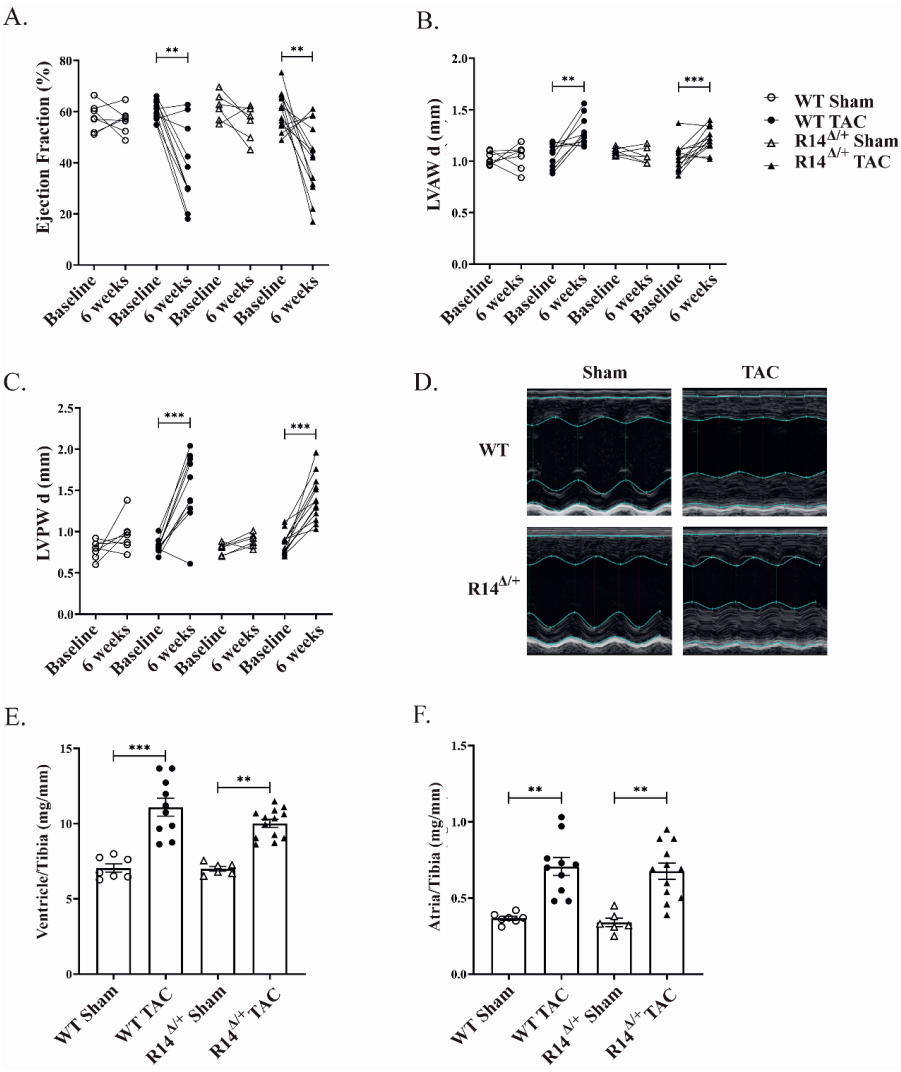

Figure 1. TAC induced cardiac hypertrophy and cardiac dysfunction to a similar extend in WT and R14del mice

(A) Ejection fraction (EF%) of individual mice in each group, **(B)** diastolic left ventricular anterior wall thickness (LVAWd), and **(C)** diastolic left ventricular posterior wall thickness (LVPWd). **(D)** Representative cardiac echo graphic images of mice in sham and TAC groups. **(E)** The ratio of ventricle/tibia and **(F)** atria/tibia. The data significance was analyzed using Kruskal-Wallis tests, followed by Dunn's multiple comparisons test. **p<0.01, ***p<0.001.

The relative mRNA expression of *NPPA*, encoding Atrial Natriuretic Peptide (ANP), a common cardiac wall stress and hypertrophy marker was elevated by more than 20-fold in both TAC groups. Similarly, increased expression of fibrotic genes, including Tissue Inhibitor of Metalloproteinases 1 (Timp1) and collagen type I alpha 1 (Col1a1), corresponded with the histological staining data (**Fig.2E-G**). Again, there was no difference in the response to TAC in both groups and cardiac pressure overload therefore induced a similar extent of cardiac remodeling in both genotypes.

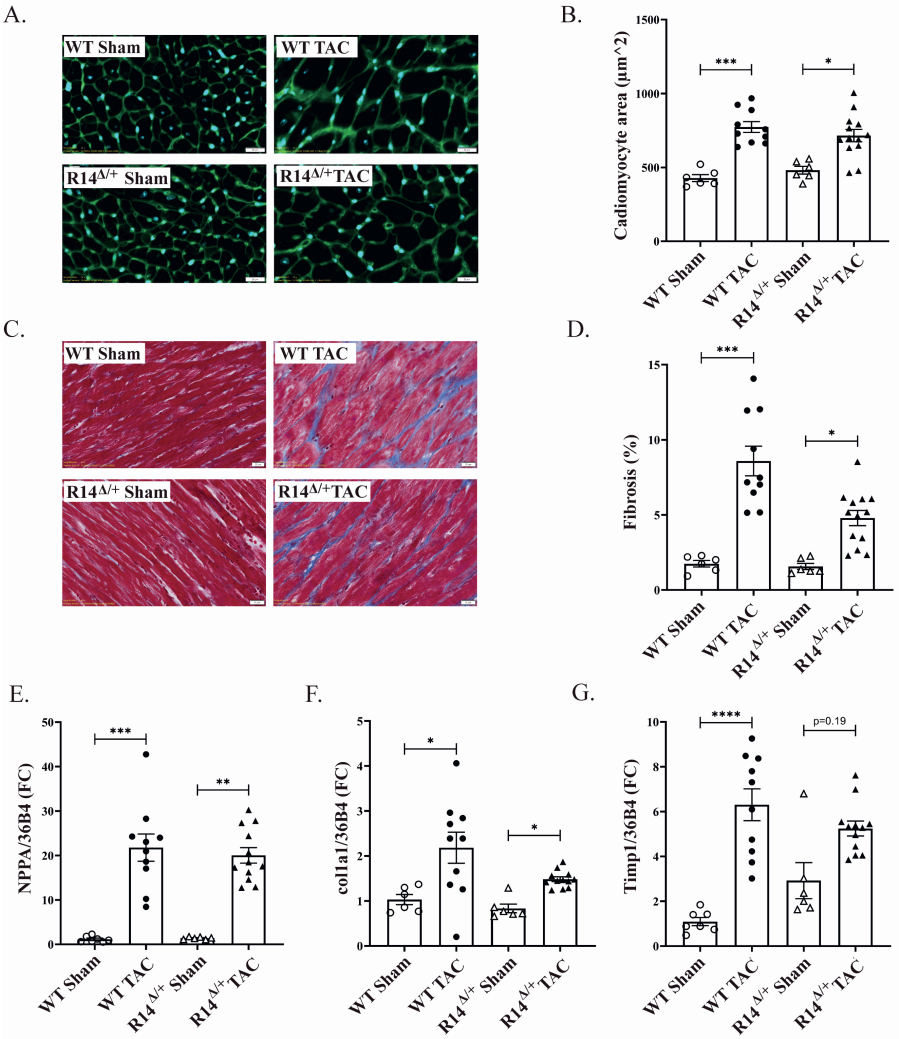

Figure 2. Cardiomyocytes hypertrophy and cardiac fibrosis are induced to a similar extend in both WT and PLN-R14del mice post TAC

(A) Representative images of extracellular Matrix (wheat germ agglutinin, WGA, green) and nuclei (4',6-diamidino-2 phenylindole, DAPI, blue) staining on left ventricular (LV) sections and **(B)**

cardiomyocytes size measurement on transversally cut cardiomyocytes (scale bar 20 µm). **(C)** Representative (average based) Masson trichrome-staining on LV sections (scale bar 20 µm), and **(D)** quantification of fibrosis area. Relative mRNA level of **(E)** cardiac stress (NPPA) and **(F, G)** fibrosis-related genes (col1a1 and Timp). The data significance was analyzed using Kruskal-Wallis tests, followed by Dunn's multiple comparisons test. *p<0.05, ***p<0.001, ****p<0.0001.

1.3 TAC did not imbalance the PLN and SERCA mRNA and protein level

The SERCA2a/PLN ratio has been suggested to be important for cardiac function and to be altered in heart failure.[26] We therefore also analyzed the level of SERCA2a, PLN and their ratio in WT and R14$^{\Delta/+}$ mice (**Fig.3A-E**). There is a mild, but statistically non-significant, decrease in the expression levels of SERCA2a in TAC surgery group compared to the sham mice (**Fig.3A, C**), while the expression levels of PLN protein remained unchanged (**Fig.3B, D**). Moreover, no marked differences were found in the SERCA2a/PLN ratios could be observed (**Fig.3E**). This indicates that TAC did not disturb the ratio between PLN and SERCA2a levels and that this remains similar between WT and R14$^{\Delta/+}$ mice.

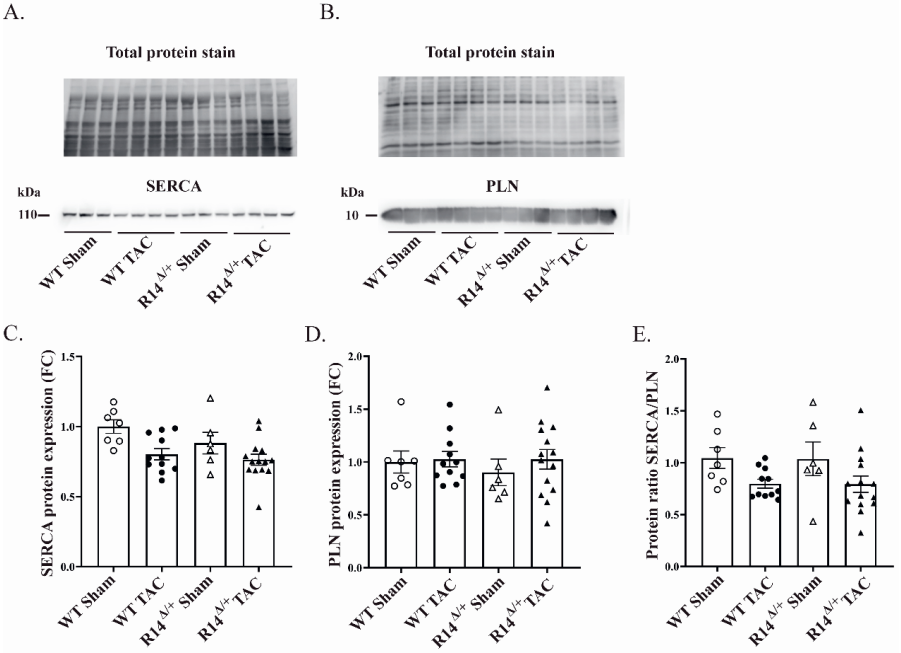

Figure 3. PLN and SERCA level remain similar in both WT and PLN-R14del mice

(A, B) Representative Western blot images of total protein, SERCA protein, and PLN protein levels in LVs. **(C, D)** SERCA and PLN protein quantification corrected by total protein. **(E)** SERCA/PLN protein ratio. The data significance was analyzed using Kruskal-Wallis tests, followed by Dunn's multiple comparisons test. PVDF (polyvinylidene fluoride) membranes were sectioned according to the molecular

weights of the target proteins and incubated with the corresponding antibodies. Full-length, uncropped Western blot images are included in the supplemental material for reference.

1.4 TAC did not induce abnormal PLN-R14del SER clustering

Malformation of the cardiac SER, with characteristic perinuclear PLN localization, is a hallmark of PLN-R14del cardiomyopathy. This has been observed in human patient biopsies, and in cardiac tissue of $R14^{\Delta/+}$ mice and homozygous $R14^{\Delta/\Delta}$ mice.[13] We were wondering if cardiac stress induced by TAC would be able to induce and accelerate this abnormal SER clustering in $R14^{\Delta/+}$. Histological staining with anti-PLN antibody together with WGA and DAPI staining did not reveal any abnormal SER clusters in 14-week-old $R14^{\Delta/+}$mice, which is in accordance with our earlier observation that these appear only after 12 month in these mice. Importantly, cardiac stress induced by TAC did also not induce abnormal SER cluster formation in any $R14^{\Delta/+}$ mice at this age (**Fig.4A**). PLN staining in these R14del mice was indistinguishable from that observed in WT mice. As a control we also performed immunofluorescence staining in LV tissue of 21 months PLN-$R14^{\Delta/+}$ mice, confirming earlier observations of abnormal SER clusters in cardiomyocytes in these old mice (**Fig.S2**). Previously, we showed that P62 is elevated together with SER cluster formation and this has recently been attributed to impaired autophagy.[23,27] Although P62 Western blotting revealed a significant increase in p62 in WT group after TAC, this was not additionally elevated in $R14^{\Delta/+}$ (**Fig. S3**) confirming that TAC was not able to further induce this process and trigger $R14^{\Delta/+}$ specific disease processes, including abnormal SER formation.

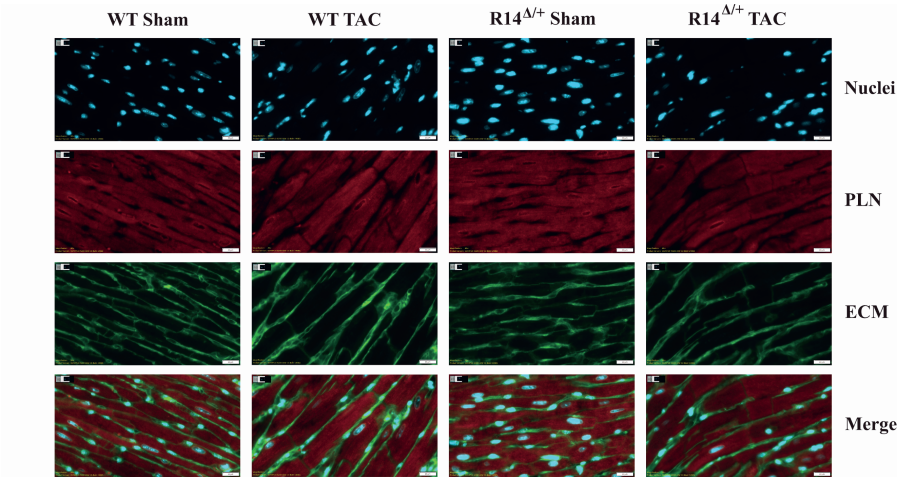

Figure 4. TAC did not induce PLN-R14del S/ER clustering

Representative images immunofluorescence staining of PLN (red), together with extracellular matrix (green) and nuclei (blue) of the LV sections of WT Sham, WT TAC, $R14^{\Delta/+}$ Sham and $R14^{\Delta/+}$ TAC (scale bar 20 μm).

1.5 Whole genome gene expression profiling reveals similar pathway changes between $R14^{\Delta/+}$ and WT after TAC

To further investigate potential cardiac differences between WT and R14$^{\Delta/+}$ mice and the effect of TAC induced cardiac stress on signaling pathways in these mice total RNA-sequencing on LV tissues was performed on 5 mice of each group. Principal component analysis revealed a strong clustering of the sham groups on one side and the TAC groups on the other side (**Fig.5A**). However, no separation between WT TAC vs R14$^{\Delta/+}$ TAC and WT sham vs R14$^{\Delta/+}$ sham were observed (**Fig.S4**). We subsequently conducted functional enrichment analysis to discern gene programs exhibiting differential regulation between disease states and their respective controls. Examining the most significantly enriched gene ontology (GO) terms for biological processes revealed common terms for both the WT and R14$^{\Delta/+}$ TAC groups. The shared biological processes between WT TAC vs WT Sham and R14$^{\Delta/+}$ TAC vs R14$^{\Delta/+}$ Sham were investigated. Common positive enriched biological processes included developmental, extracellular matrix, morphogenesis and response to stimulus terms and reflect the cardiac remodeling process observed after TAC (**Fig.5B**). Not surprisingly, the genes enriched in these biological pathways are predominantly associated with hypertrophy (e.g., NPPA, NPPB, and MYH7) and fibrosis (e.g., COL4A3, COL8A1, TIMP1, MMP2). In addition, immune response-related genes are enriched (IL4RA, and Ccl21a) (**Table S3**). Negative enriched biological processes are dominated by metabolism and ion-transport related genes, including genes for mitochondrial processes (ATP5pf, PINK1, MT-ND5, SLC25A4), amino acid metabolism (MTR and GPT), fatty acid and lipid metabolism (ACADVL, HADHA, and ACSS1) (**Table S4**). Again, the gene expression profiles after TAC were equally altered in WT and PLN-R14$^{\Delta/+}$ mice, yet these did not influence the progression of PLN-R14del cardiomyopathy.

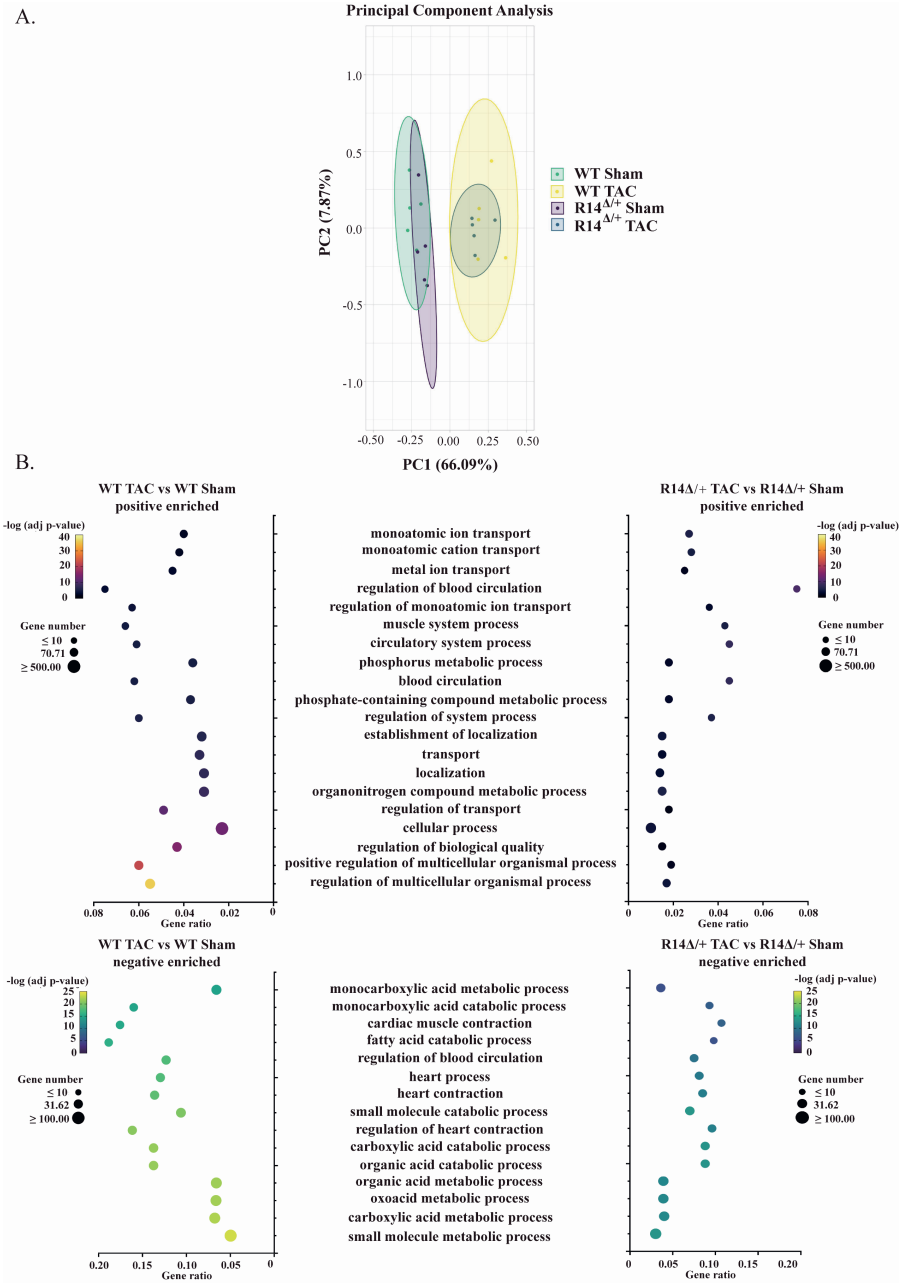

Figure 5. RNA sequencing identified common biological processes activated in WT and R14del mice in response to TAC

(A) Principal component (PC) analysis plot of RNA sequencing results on mice LV tissue (n=5 per group). Genes contributing to the variance in PC1, represent 66.09% of the total variance, and genes contributing to the PC2 is 7.87% of the total variance. **(B)** Top 20 most positive enriched gene biological processes in

WT mice and R14$^{\Delta/+}$ TAC mice. Top 15 most negative enriched gene biological processes in WT and R14$^{\Delta/+}$ TAC mice.

Discussion

The onset and severity of disease manifestation in human PLN-R14del carriers exhibit considerable variability, but underlying mechanisms explaining this variation have not been identified. In this study, we investigated whether cardiac stress could accelerate disease onset and exacerbate disease progression in a R14$^{\Delta/+}$ mouse model, which displays similar disease characteristics to those observed in human patients. Although, transverse aortic constriction induced cardiac wall stress and activated numerous cardiac remodeling pathways, it did not accelerate PLN-R14del disease progression in heterozygous R14$^{\Delta/+}$ mice. Importantly, it also did not provoke abnormal sarcoplasmic reticulum (SER) formation in R14$^{\Delta/+}$ mice, a key characteristic of PLN-R14del cardiomyopathy in both humans and mice. These results suggest that cardiac wall stress and concomitant activation of common cardiac stress and remodeling pathways are unlikely to act as common triggers for PLN-R14del cardiomyopathy.

The appearance of sporadic abnormal SER clusters and subsequent disease development in heterozygous PLN-R14del mouse model does not start before one year of age and cardiomyopathy features become visible by 18 months of age.[13] Also clinical studies indicate a potential link with aging, as symptoms typically manifest in the fifth decade of life.[21] However, disease development is rather heterogeneous and it is unclear which factors are involved. Accumulating cellular stress is a common factor during ageing and cardiomyocytes, are also affected by age related factors, like hypertension, oxidative stress, genomic stress, metabolic stress and reduction of protein quality controls systems. Applying cardiac wall stress to the heart can stimulate stress pathways and often trigger or accelerate disease. This has been shown in numerous genetic animal models that by themselves do not directly show disease phenotypes, but only after stress induced by cardiac pressure overload.[16-18] This was also shown in a transgenic mouse strain in which a mutant PLN protein was expressed that had lost the ability to form pentamers (TgAFA-PLN) and in PLN-KO mice.[14] These mice showed decreased survival rate after TAC (within 4 weeks) and increased myocardial fibrosis. It was suggested that the diminished range of SERCA2a mediated calcium handling in TgAFA-PLN and in PLN-KO mice was responsible for enhanced disease development under pressure overload. We did not observe accelerated disease development in PLN-R14del mice, suggesting that altered calcium handling may not be the driving force in this disease. This is in agreement with recent finding indicating that in PLN-R14del abnormal SER formation is most likely the main disease driver for this cardiomyopathy.[6] Our observation that pressure overload was not able to induce abnormal SER formation in PLN-R14del mice, is in line with the absence of disease acceleration in mice after TAC. This further supports the notion that PLN-R14del cardiomyopathy is not just a calcium related disease, but involves other pathological processes, like abnormal SER formation.

Cardiac remodeling pathways were similarly activated by cardiac pressure overload in WT and PLN-R14del mice. This includes hypertrophic response and alteration in metabolic gene expression profiles, indicative for the well know switch to fetal gene expression and a shift from fatty acid to glucose metabolism.[28] PLN-R14del cardiomyopathy has been linked to metabolic alterations,[2] but our observation reveals that a change into a fetal-like metabolic state does not trigger PLN-R14del disease. Furthermore, the activation of cardiac remodeling pathways after TAC did not provoke specific features of PLN-R14del cardiomyopathy in these mice. Therefore, cardiac remodeling, which also occurs upon ageing,[29] does not appear to be a trigger factor for this disease.

A few mouse studies did report about induction of ER stress pathways after TAC,[30,31] but we were not able to confirm this and did not observe potent activation of these pathways. Since ER stress was not clearly triggered in the experiment, the study doesn't provide enough evidence to understand its involvement in this specific heart condition (**Fig.S5**). This will require further investigation in other disease models, since activation of the ER stress unfolded protein response (UPR) is a common feature of PLN-R14del cardiomyopathy in human and mice.[32] So far, we do not know if UPR activation is contributing to disease or is a protective response to PLN-R14del induced ER malformation. At least in vitro, using human iPSC derived cardiomyocytes, was shown that drug induced ER chaperone BiP expression was able to improve PLN-R14del cardiomyocyte function, suggestive for a protective action. [32] Since ER malformation is a hallmark of PLN-R14del cardiomyopathy, this clearly needs further attention and will require in vivo studies with specific ER stress activators.

While this study demonstrates that TAC induced pressure overload in young adult PLN-R14del mice does not accelerate disease onset, it is important to acknowledge that the manifestation of PLN-R14del cardiomyopathy is likely influenced by multiple converging factors beyond mechanical stress alone. The lack of phenotype induction under TAC may reflect the need for additional or alternative disease triggers that more closely mimic the clinical complexity observed in human mutation carriers. Such as applying TAC at an older age, when age-associated stressors are more pronounced, could offer a more sensitive condition for phenotype induction. Moreover, other physiological or pharmacological stressors may serve as relevant accelerants. These include chronic β-adrenergic stimulation via isoproterenol-loaded osmotic mini-pumps, intense physical exertion through forced swimming or treadmill model, or nutrient deprivation models to induce autophagy. This would not only improve our understanding of PLN-R14del cardiomyopathy but may also guide the development of targeted intervention strategies tailored to specific disease modifiers.

This study also has some limitations. First, only males were included in this study and potential sex-specific effects cannot be excluded. Although no obvious sex differences have been observed in this PLN-R14del mouse model, so far,[23] male sex has been

suggested to influence heart failure outcomes in human phospholamban mutation carriers.[33] Therefore, the use of male mice was considered justified for this study, but future research should aim to address potential sex-related differences more specifically. We cannot completely exclude potential sex-dependent differences in response to pressure overload. Future studies including both sexes are warranted to explore this further. Secondly, we cannot exclude that activation of pressure overload stress pathways at a later age may provoke PLN-R14del cardiomyopathy features and accelerate disease. If so, it would mean that additional age-related priming factors are required. So far, we have no evidence for this. Finally, we did only investigate DCM related processes and cannot exclude that ACM related features may be affected in these mice upon pressure overload. This would, however, require ex vivo investigations after TAC, since, so far arrythmia could not be detected in vivo in these mice.

In conclusion, cardiac stress induced cardiac remodeling pathways do not trigger PLN-R14del cardiomyopathy features in a mouse model with this pathogenic variant. It therefore remains elusive which factors may promote this cardiomyopathy and this may require investigation of other ageing and stress related pathways, like oxidative stress or ER stress.

Additional Information

Data Availability

The datasets generated and/or analyzed during the current study are available from the corresponding author, Dr. Herman H.W. Silljé (h.h.w.sillje@umcg.nl), upon reasonable request. The RNA-sequencing data of the current study is available in the NCBI Sequence Read Archive (SRA) under the accession number PRJNA1285300. https://www.ncbi.nlm.nih.gov/sra/?term=PRJNA1285300

Funding

This work was supported by the Dutch Heart Foundation [2018-30 (CVON-PREDICT2) to H.H.W.S. and V.O.N.T., 01-003-2022-0358 (CarMa) to H.H.W.S. and V.O.N.T]; China Scholarship Council Grant [202008230186 to L.S.].

Competing Interests

None of the authors have any conflicts of interest, financial or otherwise, to disclose.

Autor contributions

L.S, V.O.N.T and H.H.W.S. conceived and designed research; L.S., V.O.N.T. and E.M.S. performed experiments; L.S. and K.A.G. analyzed data; L.S., V.O.N.T, and H.H.W.S. interpreted results of experiments; L.S. and K.A.G. prepared figures; L.S. drafted manuscript; L.S., E.M.S., K.A.G., V.O.N.T. and H.H.W.S. edited and revised manuscript; all authors approved final version of manuscript.

References

1. Glaves JP, Primeau JO, Espinoza-Fonseca LM, Lemieux MJ, Young HS. The Phospholamban Pentamer Alters Function of the Sarcoplasmic Reticulum Calcium Pump SERCA. Biophys J. 2019;116:633-647. doi: 10.1016/j.bpj.2019.01.013
2. Vafiadaki E, Glijnis PC, Doevendans PA, Kranias EG, Sanoudou D. Phospholamban R14del disease: The past, the present and the future. Front Cardiovasc Med. 2023;10:1162205. doi: 10.3389/fcvm.2023.1162205
3. Haghighi K, Kolokathis F, Gramolini AO, Waggoner JR, Pater L, Lynch RA, Fan GC, Tsiapras D, Parekh RR, Dorn GW, 2nd, et al. A mutation in the human phospholamban gene, deleting arginine 14, results in lethal, hereditary cardiomyopathy. Proc Natl Acad Sci U S A. 2006;103:1388-1393. doi: 10.1073/pnas.0510519103
4. van der Zwaag PA, van Rijsingen IA, de Ruiter R, Nannenberg EA, Groeneweg JA, Post JG, Hauer RN, van Gelder IC, van den Berg MP, van der Harst P, et al. Recurrent and founder mutations in the Netherlands-Phospholamban p.Arg14del mutation causes arrhythmogenic cardiomyopathy. Neth Heart J. 2013;21:286-293. doi: 10.1007/s12471-013-0401-3
5. Stege NM, de Boer RA, Makarewich CA, van der Meer P, Silljé HHW. Reassessing the Mechanisms of PLN-R14del Cardiomyopathy. JACC: Basic to Translational Science. 2024. doi: 10.1016/j.jacbts.2024.02.017
6. Stege NM, Eijgenraam TR, Oliveira Nunes Teixeira V, Feringa AM, Schouten EM, Kuster DWD, van der Velden J, Wolters AHG, Giepmans BNG, Makarewich CA, et al. DWORF Extends Life Span in a PLN-R14del Cardiomyopathy Mouse Model by Reducing Abnormal Sarcoplasmic Reticulum Clusters. Circ Res. 2023;133:1006-1021. doi: 10.1161/CIRCRESAHA.123.323304
7. Te Rijdt WP, van Tintelen JP, Vink A, van der Wal AC, de Boer RA, van den Berg MP, Suurmeijer AJ. Phospholamban p.Arg14del cardiomyopathy is characterized by phospholamban aggregates, aggresomes, and autophagic degradation. Histopathology. 2016;69:542-550. doi: 10.1111/his.12963
8. van der Zwaag PA, van Rijsingen IA, Asimaki A, Jongbloed JD, van Veldhuisen DJ, Wiesfeld AC, Cox MG, van Lochem LT, de Boer RA, Hofstra RM, et al. Phospholamban R14del mutation in patients diagnosed with dilated cardiomyopathy or arrhythmogenic right ventricular cardiomyopathy: evidence supporting the concept of arrhythmogenic cardiomyopathy. Eur J Heart Fail. 2012;14:1199-1207. doi: 10.1093/eurjhf/hfs119
9. Posch MG, Perrot A, Geier C, Boldt L-H, Schmidt G, Lehmkuhl HB, Hetzer R, Dietz R, Gutberlet M, Haverkamp W, et al. Genetic deletion of arginine 14 in phospholamban causes dilated cardiomyopathy with attenuated electrocardiographic R amplitudes. Heart Rhythm. 2009;6:480-486. doi: https://doi.org/10.1016/j.hrthm.2009.01.016
10. van Lint FHM, Hassanzada F, Verstraelen TE, Wang W, Bosman LP, van der Zwaag PA, Oomen T, Calkins H, Murray B, Tichnell C, et al. Exercise does not influence development of phenotype in PLN p.(Arg14del) cardiomyopathy. Neth Heart J. 2023;31:291-299. doi: 10.1007/s12471-023-01800-4
11. van der Voorn SM, van Drie E, Proost V, Dimitrova K, Netherlands Acm/Pln R, Ernst RF, James CA, Tichnell C, Murray B, Calkins H, et al. Lack of Evidence for the Role of the p.(Ser96Ala) Polymorphism in Histidine-Rich Calcium Binding Protein as a Secondary Hit in

Cardiomyopathies. Int J Mol Sci. 2023;24. doi: 10.3390/ijms242115931
12. Lopera-Maya EA, Li S, de Brouwer R, Nolte IM, van Breen J, Jongbloed JDH, Swertz MA, Snieder H, Franke L, Wijmenga C, et al. Phenotypic and Genetic Factors Associated with Absence of Cardiomyopathy Symptoms in PLN:c.40_42delAGA Carriers. Journal of cardiovascular translational research. 2023;16:1251-1266. doi: 10.1007/s12265-022-10347-5
13. Eijgenraam TR, Boukens BJ, Boogerd CJ, Schouten EM, van de Kolk CWA, Stege NM, Te Rijdt WP, Hoorntje ET, van der Zwaag PA, van Rooij E, et al. The phospholamban p.(Arg14del) pathogenic variant leads to cardiomyopathy with heart failure and is unreponsive to standard heart failure therapy. Sci Rep. 2020;10:9819. doi: 10.1038/s41598-020-66656-9
14. Funk F, Kronenbitter A, Hackert K, Oebbeke M, Klebe G, Barth M, Koch D, Schmitt JP. Phospholamban pentamerization increases sensitivity and dynamic range of cardiac relaxation. Cardiovasc Res. 2023;119:1568-1582. doi: 10.1093/cvr/cvad037
15. Cleary SR, Teng ACT, Kongmeneck AD, Fang X, Phillips TA, Cho EE, Smith RA, Karkut P, Makarewich CA, Kekenes-Huskey PM, et al. Dilated cardiomyopathy variant R14del increases phospholamban pentamer stability, blunting dynamic regulation of calcium. J Biol Chem. 2025;301:108118. doi: 10.1016/j.jbc.2024.108118
16. Gurha P, Abreu-Goodger C, Wang T, Ramirez MO, Drumond AL, van Dongen S, Chen Y, Bartonicek N, Enright AJ, Lee B, et al. Targeted deletion of microRNA-22 promotes stress-induced cardiac dilation and contractile dysfunction. Circulation. 2012;125:2751-2761. doi: 10.1161/CIRCULATIONAHA.111.044354
17. Hu C, Dai F, Wang J, Jiang L, Wang D, Gao J, Huang J, Luo J, Tang F, Zhang Z, et al. Peroxiredoxin-5 Knockdown Accelerates Pressure Overload-Induced Cardiac Hypertrophy in Mice. Oxid Med Cell Longev. 2022;2022:5067544. doi: 10.1155/2022/5067544
18. Shirakabe A, Zhai P, Ikeda Y, Saito T, Maejima Y, Hsu CP, Nomura M, Egashira K, Levine B, Sadoshima J. Drp1-Dependent Mitochondrial Autophagy Plays a Protective Role Against Pressure Overload-Induced Mitochondrial Dysfunction and Heart Failure. Circulation. 2016;133:1249-1263. doi: 10.1161/CIRCULATIONAHA.115.020502
19. Melleby AO, Romaine A, Aronsen JM, Veras I, Zhang L, Sjaastad I, Lunde IG, Christensen G. A novel method for high precision aortic constriction that allows for generation of specific cardiac phenotypes in mice. Cardiovasc Res. 2018;114:1680-1690. doi: 10.1093/cvr/cvy141
20. Percie du Sert N, Hurst V, Ahluwalia A, Alam S, Avey MT, Baker M, Browne WJ, Clark A, Cuthill IC, Dirnagl U, et al. The ARRIVE guidelines 2.0: Updated guidelines for reporting animal research. PLoS Biol. 2020;18:e3000410. doi: 10.1371/journal.pbio.3000410
21. van Rijsingen IA, van der Zwaag PA, Groeneweg JA, Nannenberg EA, Jongbloed JD, Zwinderman AH, Pinto YM, Dit Deprez RH, Post JG, Tan HL, et al. Outcome in phospholamban R14del carriers: results of a large multicentre cohort study. Circ Cardiovasc Genet. 2014;7:455-465. doi: 10.1161/CIRCGENETICS.113.000374
22. de Brouwer R, Meems LMG, Verstraelen TE, Mahmoud B, Proost V, Wilde AAM, Bosman LP, van Drie E, van der Zwaag PA, van Tintelen JP, et al. Sex-specific aspects of phospholamban cardiomyopathy: The importance and prognostic value of low-voltage electrocardiograms. Heart Rhythm. 2022;19:427-434. doi: 10.1016/j.hrthm.2021.11.009
23. Eijgenraam TR, Stege NM, Oliveira Nunes Teixeira V, de Brouwer R, Schouten EM, Grote Beverborg N, Sun L, Spater D, Knoll R, Hansson KM, et al. Antisense Therapy Attenuates Phospholamban p.(Arg14del) Cardiomyopathy in Mice and Reverses Protein Aggregation. Int

J Mol Sci. 2022;23. doi: 10.3390/ijms23052427

24. Knipp BS, Ailawadi G, Sullivan VV, Roelofs KJ, Henke PK, Stanley JC, Upchurch GR, Jr. Ultrasound measurement of aortic diameters in rodent models of aneurysm disease. J Surg Res. 2003;112:97-101. doi: 10.1016/s0022-4804(03)00114-8
25. Zacchigna S, Paldino A, Falcao-Pires I, Daskalopoulos EP, Dal Ferro M, Vodret S, Lesizza P, Cannata A, Miranda-Silva D, Lourenco AP, et al. Towards standardization of echocardiography for the evaluation of left ventricular function in adult rodents: a position paper of the ESC Working Group on Myocardial Function. Cardiovasc Res. 2021;117:43-59. doi: 10.1093/cvr/cvaa110
26. Kranias EG, Hajjar RJ. Modulation of cardiac contractility by the phospholamban/SERCA2a regulatome. Circ Res. 2012;110:1646-1660. doi: 10.1161/CIRCRESAHA.111.259754
27. Vafiadaki E, Kranias EG, Eliopoulos AG, Sanoudou D. The phospholamban R14del generates pathogenic aggregates by impairing autophagosome-lysosome fusion. Cell Mol Life Sci. 2024;81:450. doi: 10.1007/s00018-024-05471-1
28. Taegtmeyer H, Sen S, Vela D. Return to the fetal gene program: a suggested metabolic link to gene expression in the heart. Ann N Y Acad Sci. 2010;1188:191-198. doi: 10.1111/j.1749-6632.2009.05100.x
29. Tracy E, Rowe G, LeBlanc AJ. Cardiac tissue remodeling in healthy aging: the road to pathology. Am J Physiol Cell Physiol. 2020;319:C166-C182. doi: 10.1152/ajpcell.00021.2020
30. Okada K, Minamino T, Tsukamoto Y, Liao Y, Tsukamoto O, Takashima S, Hirata A, Fujita M, Nagamachi Y, Nakatani T, et al. Prolonged endoplasmic reticulum stress in hypertrophic and failing heart after aortic constriction: possible contribution of endoplasmic reticulum stress to cardiac myocyte apoptosis. Circulation. 2004;110:705-712. doi: 10.1161/01.CIR.0000137836.95625.D4
31. Park CS, Cha H, Kwon EJ, Sreenivasaiah PK, Kim DH. The chemical chaperone 4-phenylbutyric acid attenuates pressure-overload cardiac hypertrophy by alleviating endoplasmic reticulum stress. Biochem Biophys Res Commun. 2012;421:578-584. doi: 10.1016/j.bbrc.2012.04.048
32. Feyen DAM, Perea-Gil I, Maas RGC, Harakalova M, Gavidia AA, Arthur Ataam J, Wu TH, Vink A, Pei J, Vadgama N, et al. Unfolded Protein Response as a Compensatory Mechanism and Potential Therapeutic Target in PLN R14del Cardiomyopathy. Circulation. 2021;144:382-392. doi: 10.1161/CIRCULATIONAHA.120.049844
33. Myrthe Y C vdH, Tom E V, Remco dB, Esmée vD, Virginnio M P, Freyja H M vL, Laurens P B, Arjan C H, Cathelijne D, Tjeerd G, et al. Identifying Predictors for Heart Failure Outcomes in Phospholamban p.(Arg14del)-Positive Individuals. JACC Heart Fail. 2025;13. doi: 10.1016/j.jchf.2025.102558

Supplemental material

Supplementary figures

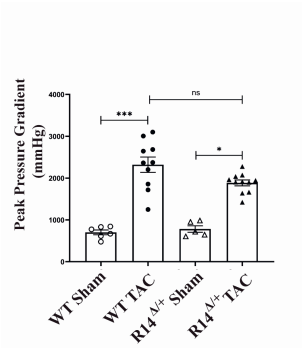

Fig S1. TAC results in similar cardiac pressure overload in WT and R14$^{\Delta/+}$ mice

Peak trans-TAC pressure gradients calculated from doppler velocity using the Bernoulli equation 1-week post-surgery. The data significance was analyzed using Kruskal-Wallis tests, followed by Dunn's multiple comparisons test. *p<0.05, ***p<0.001.

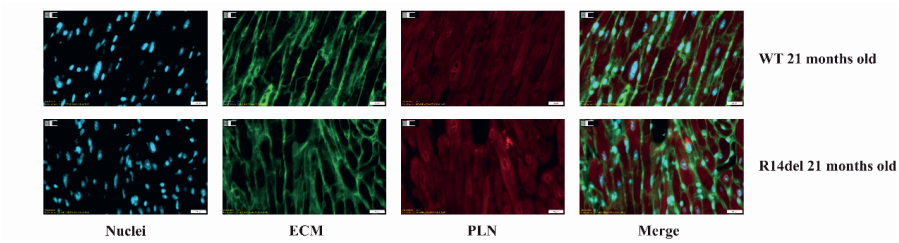

Fig S2. R14$^{\Delta/+}$ mice exhibit S/ER cluster in LV tissue of 21 months of age

Representative images immunofluorescence staining of PLN (red), together with extracellular matrix (green) and nuclei (blue) of the LV sections of WT, and R14$^{\Delta/+}$ mice 21 months of age (scale bar 20 µm).

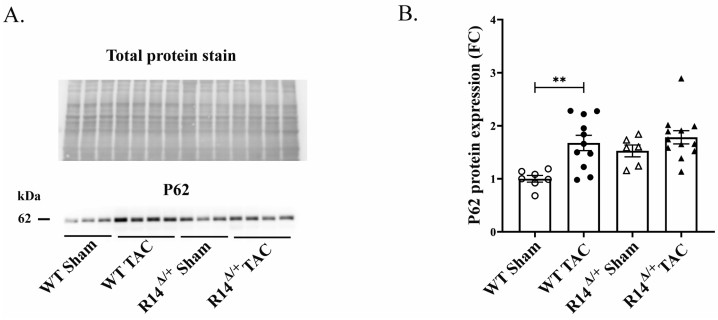

Figure S3. P62 protein level elevated after TAC surgery

(A) Representative Western blot images of total protein and P62 protein level in LVs. **(B)** P62 protein quantification corrected by total protein. The data significance was analyzed using Kruskal-Wallis tests, followed by Dunn's multiple comparisons test. **p<0.01. PVDF (polyvinylidene fluoride) membranes were sectioned according to the molecular weights of the target proteins and incubated with the corresponding antibodies. Full-length, uncropped Western blot images are included in the supplemental material for reference.

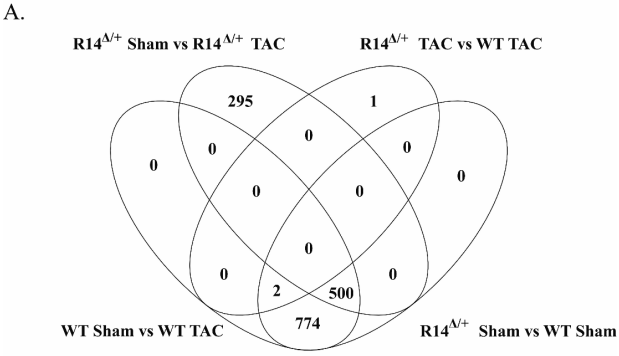

Fig S4. Gene expressed differently between TAC and Sham groups

Distinct patterns of gene expression between WT TAC versus WT sham and $R14^{\Delta/+}$ TAC versus $R14^{\Delta/+}$ sham. No separation between WT TAC versus. $R14^{\Delta/+}$ TAC, and WT sham versus. $R14^{\Delta/+}$ sham were observed.

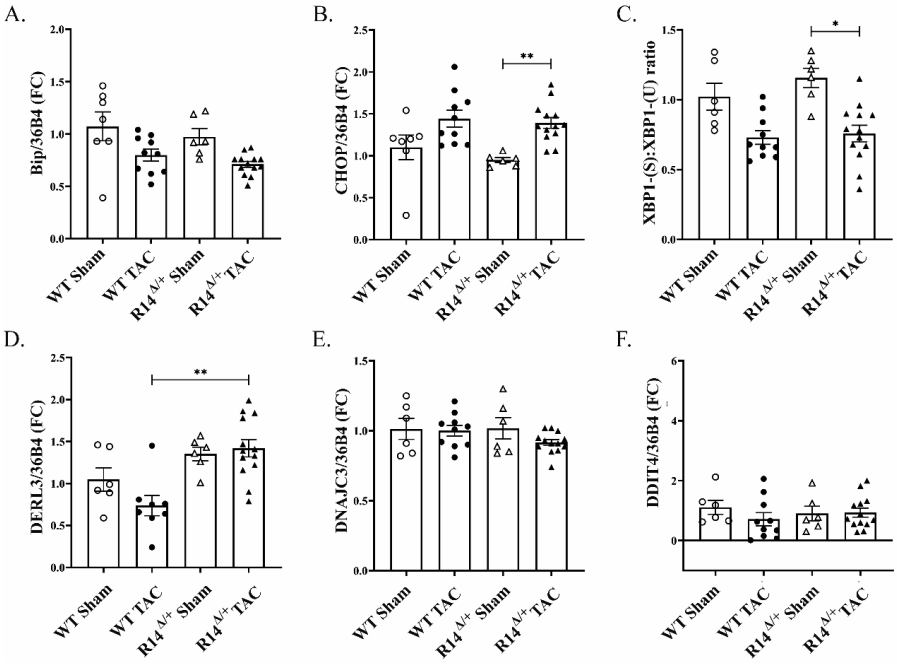

Figure 5 TAC did not induce ER stress in WT and PLN-R14$^{\Delta/+}$ mice

The relative ER related mRNA expressed in LV tissue. The significance of data was analyzed using Kruskal-Wallis test followed by Dunn's multiple comparisons test. *p<0.05, **p<0.01.

Supplementary tables

Table S1. Primer sequences used for RT-PCR

Gene	Protein		Sequence
PLN	phospholamban	Forward Reverse	GACGATCACCGAAGCCAAG CGAGCGAGTGAGGTATTGC
SERCA2a	Sarcoplasmic/endoplasmic reticulum Ca^{2+}-ATPase	Forward Reverse	TCAGTATGACGGGCTTGTAG CGGTAGCTTCTCCAACTTTC
NPPA	Atrial Natriuretic Peptide	Forward Reverse	GCTTCCAGGCCATATTGGAG GGTGGTCTAGCAGGTTCTTG
Timp1	Tissue Inhibitor of Metalloproteinases-1	Forward Reverse	CAACGAGACCACCTTATACC CATATCCACAGAGGCTTTCC
Col1a1	Collagen type 1 alpha 1 chain	Forward Reverse	AGAGCATGACCGATGGATTC CGCTGTTCTTGCAGTGATAG
Rplp0 (36B4)	Ribosomal protein, large P0	Forward Reverse	AACGGGTACAAACGAGTC AGATGGATCAGCCAAGAAG
Hspa5	Binding-immunoglobulin protein	Forward Reverse	TGCAGCAGGACATCAAGTTC GTTTGCCCACCTCCAATATC
CHOP (Ddit3)	CCAAT/enhancer-binding homologous protein	Forward Reverse	GGGCACCTATATCTCATCCC GGGCCATAGAACTCTGACTG
Xbp1 s	X-box binding protein 1 spliced	Forward Reverse	CTGAGTCCGAATCAGGTGCAG GTCCATGGGAAGATGTTCTGG
Xbp1 u	X-box binding protein 1 unspliced	Forward Reverse	CCGCAGCACTCAGACTATG GGTAGACCTCTGGGAGTTC
DERL3	Derlin-3	Forward Reverse	CCTCGTGGACCTGCTGG GGTCTGCAGGAGCCTCTTG
DNAJC3	DnaJ heat shock protein family (Hsp40) member C3	Forward Reverse	CGACGCCTTATCACAGTTTC CGGCAGTAAAGTCCATCTTC
DDIT4	regulated in development and DNA damage responses 1	Forward Reverse	GGATGGGGTGTCGTTGCCCG GGCAGCTCTTGCCCTGCTCC

Table S2. Antibodies used for Western blot

List of primary antibodies used in this study

Primary antibody	Host	Cat. No.	Supplier	Dilution	Blocking buffer	Molecular weight (kDa)
Anti-PLN	Rabbit	14562S	Cell Signalling	1:1,000	BSA	12 and 24
Anti-SERCA	Mouse	Ab2861	Abcam	1:1,000	Milk	110
Anti-P62	Mouse	Ab56416	Abcam	1:1,000	Milk	62

List of secondary antibodies used in this study

Secondary antibody	Antigen	Label	Cat. No	Supplier	Dilution
Rabbit anti-mouse	Mouse	HRP	P0260	Dako	1:2,000
Goat anti-rabbit	Rabbit	HRP	P044801	Dako/Agilent	1:2,000

Table S3. Common Genes expressed in positive enriched biological process

	Term name	Gene in WT TAC vs WT sham	Gene in $R14^{\Delta/+}$ TAC vs $R14^{\Delta/+}$ sham
1	monoatomic ion transport	Adcyap1r1,Anxa5,Aplnr,Bak1,Bmp4,Ccl21a,Ccr5,Cd63,Clic1,Cx3cl1,Ednrb,F2r,Fhl1,Fxyd5,Hes1,Lgals3,Pkd1,Pkd2,Plcg2,Prnp,Ptk2b,S100a6,Scn1b,Serpine2,Slc1a3,Slc38a2,Slc39a6,Tfrc,Ace,Anxa2,Atp6v0a4,Atp8b1,Bcl2,Calhm5,Ccn2,Clic5,Edn3,Fxyd6,Gnao1,Igf1,Kif5b,Mmgt2,Nppa,Panx1,Piezo2,Rrad,Sfxn1,Tgfb2,Tspo	Adora2a,Adra1a,Akt2,Camk2a,Clcn1,Cox7a1,Crhr2,Hcn4,Kcnj2,Kcnj3,Kcnj5,Klhl3,Maob,P2ry1,Scn4b,Slc22a3,Ano10,Atp1a2,Atp2a2,Atp5pf,Cngb3,Dhrs7c,Gstm7,Kcne1,Kcnip2,Kcnv2,mt-Nd5,Slc20a2,Slc25a4,Slc25a12,Slc25a22,Slc41a1,Strit1
2	monoatomic cation transport	Adcyap1r1,Anxa5,Aplnr,Bak1,Bmp4,Ccl21a,Ccr5,Cd63,Cx3cl1,Ednrb,F2r,Fhl1,Hes1,Lgals3,Pkd2,Plcg2,Prnp,Ptk2b,Serpine2,Slc1a3,Slc38a2,Slc39a6,Tfrc,Ace,Anxa2,Atp6v0a4,Bcl2,Calhm5,Ccn2,Edn3,Gnao1,Igf1,Kif5b,Mmgt2,Nppa,Panx1,Piezo2,Pkd1,Rrad,Scn1b,Sfxn1,Tgfb2,Tspo	Adora2a,Adra1a,Akt2,Camk2a,Cox7a1,Crhr2,Hcn4,Kcne1,Kcnj2,Kcnj3,Kcnj5,Klhl3,mt-Nd5,Scn4b,Slc20a2,Slc25a22,Ano10,Atp1a2,Atp2a2,Atp5pf,Cngb3,Dhrs7c,Gstm7,Kcnip2,Kcnv2,Slc25a4,Slc25a12,Slc41a1,Strit1
3	metal ion transport	Adcyap1r1,Anxa5,Aplnr,Bak1,Bmp4,Ccl21a,Ccr5,Cd63,Cx3cl1,Ednrb,F2r,Fhl1,Hes1,Lgals3,Pkd2,Plcg2,Prnp,Ptk2b,Serpine2,Slc1a3,Slc38a2,Slc39a6,Tfrc,Ace,Anxa2,Bcl2,Ccn2,Edn3,Gnao1,Igf1,Kif5b,Mmgt2,Nppa,Panx1,Pkd1,Rrad,Scn1b,Sfxn1,Tgfb2,Tspo	Adora2a,Adra1a,Akt2,Camk2a,Crhr2,Hcn4,Kcne1,Kcnj2,Kcnj3,Kcnj5,Scn4b,Atp1a2,Atp2a2,Dhrs7c,Gstm7,Kcnip2,Kcnv2,Klhl3,Slc20a2,Slc25a12,Slc41a1,Strit1
4	regulation of blood circulation	Cx3cl1,Ednrb,Egfr,F2r,Hif1a,Hsp90aa1,Itga9,Scn1b,Shox2,Ace,App,Ccn2,Edn3,Gnao1,Hbegf,Mmp2,Myh7,Nppa,Svep1,Tgfb2	Adra1a,Adra1b,Alox5,Crhr2,Hcn4,Kcne1,Kcnj2,Kcnj5,Rgs2,Rnf207,Scn4b,Tbx5,Apln,Atp1a2,Atp2a2,Atp5pf,Hopx,Kcnip2,Strit1,Tnni3

5	regulation of monoatomic ion transport	Adcyap1r1,Aplnr,Bak1,Bmp4,Cd63,Cx3cl1,F2r,Fhl1,Fxyd5,Hes1,Lgals3,Pkd2,Prnp,Ptk2b,Scn1b,Serpine2,Ace,Atp8b1,Bcl2,Edn3,Fxyd6,Gnao1,Igf1,Kif5b,Nppa,Rrad,Tgfb2,Tspo	Adora2a,Akt2,Camk2a,Crhr2,Kcnj2,Kcnj5,Maob,P2ry1,Scn4b,Atp1a2,Dhrs7c,Gstm7,Kcne1,Kcnip2,Kcnj3,Strit1
6	muscle system process	Bmp4,Ccn4,Col14a1,Cttn,Dbn1,Ednrb,F2r,Mybpc2,Myl1,Myl6,Ptger4,Scn1b,Tnfrsf1a,Tnfrsf1b,Acta1,Atp8a2,Ccn2,Comp,Edn3,Hsp90aa1,Igf1,Igfbp5,Myh7,Nppa,Nppb,Pi16,Sulf1,Tpm3,Tpm4	Adra1a,Adra1b,Clcn1,Hcn4,Kcnj2,Kcnj5,Meis1,P2ry1,Rnf207,Scn4b,Tnni2,Atp1a2,Atp2a2,Kcne1,Kcnip2,Rgs2,Slc25a4,Strit1,Tnni3
7	circulatory system process	Amot,Cx3cl1,Ednrb,Egfr,F2r,Gpx1,Hif1a,Hsp90aa1,Id2,Itga9,Myl1,Nppb,Plod3,Scn1b,Shox2,Sod3,Ace,App,Ccn2,Col1a2,Comp,Ddah1,Edn3,Emilin1,Gnao1,Hbegf,Mmp2,Myh7,Nox4,Nppa,Postn,Scpep1,Svep1,Tgfb2	Adora2a,Adra1a,Adra1b,Alox5,Crhr2,Hcn4,Kcnj2,Kcnj5,P2ry1,Rnf207,Scn4b,Slc27a1,Tbx5,Tnni2,Apln,Atp1a2,Atp2a2,Atp5pf,Emilin2,Hopx,Kcne1,Kcnip2,Rgs2,Strit1,Tnni3
8	phosphorus metabolic process	Adarb1,Adcy7,Adcyap1r1,Aplnr,Bak1,Bmp4,Cda,Ckb,Crlf1,Cx3cl1,Cx3cr1,Dclk1,Ednrb,Eef1a1,Egfr,Enpp1,Fgfr1,Gba1,Grk5,Hes1,Hif1a,Inhba,Itga6,Ldlr,Lrp8,Lrrk1,Mapk4,Nudt16,Pkd1,Pla2g4a,Plcg2,Prkag2,Prkcd,Ptger4,Ptk2b,Ptprf,Ptprn,Rap2b,S1pr2,Sox9,Syk,Tfrc,Tgfbr1,Thbs1,Tlr4,Tnfrsf1a,Upp1,Acot9,Anxa2,App,Bcl2,Ccn2,Ccnd2,Cd44,Cdkl2,Cfh,Clec4n,Dhdds,Dynll1,Ehd4,Fbln1,Fn1,Fndc1,Hbegf,Hsp90aa1,Igf1,Irak4,Lox,Mical1,Myh7,Nmrk2,Nox4,Nppa,Nppb,Nuak1,Nudt18,Nupr1,Pfkp,Ppm1e,Prnp,Sfrp1,Sfrp2,Srpx2,Thbs4,Tmem119,Tspan9,Tspo,Uck2,Ugp2	Acot1,Akt2,Camk2a,Dusp18,Enpp2,Entpd5,Il15,Isyna1,Mylk4,Ndufb11,P2ry1,Pdk2,Pdp2,Pim1,Pla2g5,Rgs2,Sema4d,Slc25a42,Slc27a1,Sord,Wnk2,Acaa2,Acot2,Acss1,Apln,Atp1a2,Atp5pf,Ces1d,Dgat2,Eno3,Epha4,Fbp2,Fitm1,Hadha,Impa2,mt-Nd5,Ndufa5,Nme6,Pink1,Ppm1k,Ppm1l,Sbk2,Slc25a12
9	blood circulation	Amot,Cx3cl1,Ednrb,Egfr,F2r,Gpx1,Hif1a,Hsp90aa1,Id2,Itga9,Myl1,Nppb,Plod3,Scn1b,Shox2,Sod3,Ace,App,Ccn2,Col1a2,Comp,Ddah1,Edn3,Emilin1,Gnao1,Hbegf,Mmp2,Myh7,Nppa,Postn,Scpep1,Svep1,Tgfb2	Adora2a,Adra1a,Adra1b,Alox5,Crhr2,Hcn4,Kcnj2,Kcnj5,P2ry1,Rgs2,Rnf207,Scn4b,Tbx5,Tnni2,Apln,Atp1a2,Atp2a2,Atp5pf,Emilin2,Hopx,Kcne1,Kcnip2,Strit1,Tnni3
10	phosphate-containing compound metabolic process	Adarb1,Adcy7,Adcyap1r1,Aplnr,Bak1,Bmp4,Cda,Ckb,Crlf1,Cx3cl1,Cx3cr1,Dclk1,Ednrb,Eef1a1,Egfr,Enpp1,Fgfr1,Gba1,Grk5,Hes1,Hif1a,Inhba,Itga6,Ldlr,Lrp8,Lrrk1,Mapk4,Nudt16,Pkd1,Pla2g4a,Plcg2,Prkag2,Prkcd,Ptger4,Ptk2b,Ptprf,Ptprn,Rap2b,S1pr2,Sox9,Syk,Tfrc,Tgfbr1,Thbs1,Tlr4,Tnfrsf1a,Upp1,Acot9,Anxa2,App,Bcl2,Cc	Acot1,Akt2,Camk2a,Dusp18,Enpp2,Entpd5,Il15,Isyna1,Mylk4,Ndufb11,P2ry1,Pdk2,Pdp2,Pim1,Pla2g5,Rgs2,Sema4d,Slc25a42,Slc27a1,Sord,Wnk2,Acaa2,Acot2,Acss1,Apln,Atp1a2,Atp5pf,Ces1d,Dgat2,Eno3,Epha4,Fbp2,Fitm1,Hadha,Impa2,mt-Nd5,Ndufa5,Nme6,Pink1,Ppm1k,Ppm1

		n2,Ccnd2,Cd44,Cdkl2,Cfh,Clec4n,Dhdds,Dynll1,Ehd4,Fbln1,Fn1,Fndc1,Hbegf,Hsp90aa1,Igf1,Irak4,Lox,Mical1,Myh7,Nmrk2,Nox4,Nppa,Nppb,Nuak1,Nudt18,Nupr1,Pfkp,Ppm1e,Prnp,Sfrp1,Sfrp2,Srpx2,Thbs4,Tmem119,Tspan9,Tspo,Uck2,Ugp2	l,Sbk2,Slc25a12
11	regulation of system process	Ccn4,Cttn,Cx3cl1,Ednrb,Egfr,F2r,Fgfr1,Gba1,Hif1a,Inhba,Nppb,Ptger4,Ptk2b,S1pr2,Scn1b,Shox2,Tnfrsf1a,Tnfrsf1b,Ace,App,Ccn2,Dbn1,Ecrg4,Edn3,Gnao1,Hbegf,Hsp90aa1,Igf1,Igfbp5,Itga9,Mmp2,Myh7,Nppa,Pi16,Svep1,Tgfb2,Tspo	
12	establishment of localization	Ildr2,Adcyap1r1,Anxa5,Aplnr,Arfgap3,Arhgap17,Arl4c,Aspscr1,Bak1,Bmp4,Ccl21a,Ccr5,Cd9,Cd63,Cnn2,Cttn,Cttnbp2nl,Cx3cl1,Dbn1,Ecrg4,Ednrb,Egfr,Enpp1,F2r,Fbln5,Fgfr1,Fhl1,Fxyd5,Gas1,Gpm6b,Hes1,Hif1a,Il4ra,Inhba,Lbp,Ldlr,Lgals3,Lima1,Lrp8,Ltbp4,Map1a,Map1b,Mrc2,Niban2,Nkd2,Ophn1,Pkd1,Pkd2,Pla2g4a,Plcg2,Pls3,Pou2f2,Prkar1a,Prkcd,Pros1,Ptger4,Ptk2b,Rab34,Rcn3,S100a6,S100a10,Scn1b,Serpine2,Slc1a3,Slc25a30,Slc38a2,Slc39a6,Star,Syk,Tfrc,Thbs1,Tlr4,Tnfrsf1a,Tnfrsf1b,Tnfrsf11a,Abra,Ace,Actn4,Ankrd1,Anxa1,Anxa2,Ap1s2,Apod,App,Aqp8,Atp6v0a4,Atp8a2,Atp8b1,Bcl2,Calhm5,Ccn2,Clic1,Clic5,Col1a1,Comp,Comt,Creb3l2,Cygb,Dipk2a,Dpysl2,Dync1li1,Dynll1,Edn3,Ehd4,Fndc1,Fxyd6,Gnao1,Grip1,Hsp90aa1,Ift122,Igf1,Kdelr3,Kif5b,Lman1l,Lpar1,Lrp1,Mical1,Mmgt2,Msn,Nppa,Nucb2,Panx1,Pcdh17,Phldb2,Piezo2,Prnp,Ptprn,Rab7b,Rab27b,Rab31,Rbp1,Rhoj,Rrad,Rtn4,Serpine1,Sfrp1,Sfxn1,Spcs3,Ssc5d,Tgfb2,Tgfb3,Tgm2,Tspan9,Tspan17,Tspo,Txnip,Uchl1,Zdhhc2	Adora2a,Adra1a,Akt2,Alox5,Aqp7,Bcl2l11,Car14,Cenpf,Clcn1,Cox7a1,Crhr2,Dusp18,Emc4,Enpp2,Hcn4,Il15,Kcnj2,Kcnj3,Kcnj5,Maob,Nectin2,P2ry1,Pim1,Pola2,Rgs2,Ruvbl2,Scn4b,Selenbp1,Slc7a1,Slc22a3,Slc25a42,Slc27a1,Spc24,Ston2,Syvn1,Tmed1,Wrap53,Acaa2,Ano10,Apln,Atp1a2,Atp2a2,Atp5pf,Camk2a,Ces1d,Cngb3,Dhrs7c,Gstm7,Hadh,Ift81,Kcne1,Kcnip2,Kcnv2,Klhl3,Lrpprc,mt-Nd5,Pex6,Pink1,Pla2g5,Ppm1k,Preb,Rtn2,Slc20a2,Slc25a4,Slc25a12,Slc25a22,Slc41a1,Stard10,Strit1,Syt7,Ttll1,Whrn

13	transport	Kif5b,Pls3,Scn1b,Mical1,Ccn2,Igf1,Rtn4,Prkar1a,Ace,Cygb,Hif1a,Fbln5,Tgfb3,Hsp90aa1,Atp8a2,Ptprn,Map1a,Ehd4,Edn3,Anxa5,Apod,App,Fhl1,Clic5,Rab27b,Anxa1,Ankrd1,Cd63,Lrp8,Uchl1,Ift122,Comt,S100a6,Col1a1,Slc1a3,Aqp8,Msn,Ap1s2,Sfrp1,Star,Gnao1,Comp,Rrad,Panx1,Anxa2,Dync1li1,Pkd1,Bcl2,Bak1,F2r,Mmgt2,Map1b,Actn4,Lman1l,Rab31,Piezo2,Nppa,Tspo,Abra,Aplnr,Dipk2a,Rbp1,Rhoj,Fxyd6,Fndc1,Pkd2,Grip1,Ssc5d,Pcdh17,Enpp1,Serpine1,Tgm2,Txnip,Atp6v0a4,Lpar1,Tlr4,Tgfb2,Lrp1,Ltbp4,Prnp,Clic1,Pou2f2,Dynll1,Fxyd5,Kdelr3,Lbp,Rcn3,Egfr,Mrc2,Syk,Sfxn1,Nkd2,Bmp4,Prkcd,Slc25a30,Dpysl2,Ednrb,Slc38a2,Ecrg4,Serpine2,Tnfrsf11a,Niban2,Hes1,Tfrc,Pros1,Lima1,Slc39a6,Aspscr1,Tnfrsf1b,Adcyap1r1,Tnfrsf1a,Cd9,Tspan9,Rab34,Cnn2,Nucb2,Il4ra,Arhgap17,Cttn,Ophn1,Gpm6b,Fgfr1,Cx3cl1,Ldlr,Ptk2b,Cttnbp2nl,Arl4c,Calhm5,Lgals3,Rab7b,Gas1,Arfgap3,Pla2g4a,Inhba,S100a10,Plcg2,Dbn1,Creb3l2,Zdhhc2,Atp8b1,Ptger4,Thbs1,Ildr2,Ccl21a,Ccr5	Adora2a,Adra1a,Akt2,Alox5,Aqp7,Bcl2l11,Camk2a,Car14,Cenpf,Clcn1,Cox7a1,Crhr2,Enpp2,Hcn4,Il15,Kcnj2,Kcnj3,Kcnj5,Maob,P2ry1,Pim1,Pola2,Preb,Rgs2,Scn4b,Selenbp1,Slc7a1,Slc22a3,Slc25a42,Slc27a1,Ston2,Syvn1,Tmed1,Acaa2,Ano10,Apln,Atp1a2,Atp2a2,Atp5pf,Ces1d,Cngb3,Dhrs7c,Gstm7,Hadh,Ift81,Kcne1,Kcnip2,Kcnv2,Klhl3,Lrpprc,mt-Nd5,Pex6,Pink1,Pla2g5,Ppm1k,Rtn2,Slc20a2,Slc25a4,Slc25a12,Slc25a22,Slc41a1, Stard10,Strit1,Syt7,Ttll1
14	localization	Kif5b,Etv5,Scn1b,Ccn2,Igf1,Rtn4,Prkar1a,Ace,Cygb,Fbln5,Tgfb3,Hsp90aa1,Tspan17,Ptprn,Cfh,Fbn1,Map1a,Ehd4,Edn3,Anxa5,Dclk1,Apod,App,Fhl1,Clic5,Myl12a,Rab27b,Anxa1,Ankrd1,Cd63,Lrp8,Uchl1,Ptn,Ift122,Comt,S100a6,Col1a1,Slc1a3,Aqp8,Msn,Ap1s2,Sfrp1,Star,Gnao1,Comp,Anxa2,Dync1li1,Bcl2,F2r,Tmsb4x,Map1b,Spcs3,Actn4,Lman1l,Rab31,Piezo2,Nppa,Tspo,Abra,Dipk2a,Rbp1,Rhoj,Fxyd6,Fndc1,Pkd2,Grip1,Ssc5d,Pcdh17,Enpp1,Serpine1,Tgm2,Atp6v0a4,Lpar1,Tlr4,Tgfb2,Lrp1,Ltbp4,Nbl1,Prnp,Tmsb10,Dynll1,Fxyd5,Kdelr3,Pls3,Mical1,Mrc2,Hif1a,Syk,Sfxn1,Nkd2,Atp8a2,Dpysl2,Serpine2,Hes1,Lima1,Tspan5,Tspan9,Plod3,Nucb2,Gpm6b,Rrad,Panx1,Ldlr,Pkd1,Bak1,Ptk2b,Mmgt2,Calhm5,Lgals3,Gas1,Pla2g4a,Amot,S100a10,Aplnr,Phldb2,Plcg2,Txnip,Creb3l2,Atp8b1,Ccl21a,Clic1,Pou2f2,Lbp,Rcn3,Egfr,Nin	Adora2a,Adra1a,Akt2,Alox5,Aqp7,Bcl2l11,Camk2a,Car14,Cenpf,Clcn1,Cox7a1,Crhr2,Dusp18,Emc4,Enpp2,Hcn4,Il15,Kcnj2,Kcnj5,Lama5,Maob,Nectin2,P2ry1,Pim1,Pola2,Rgs2,Ruvbl2,Scn4b,Selenbp1,Slc7a1,Slc22a3,Slc25a42,Slc27a1,Spc24,Ston2,Syvn1,Tmed1,Wdr45,Wrap53,Acaa2,Ano10,Apln,Atp1a2,Atp2a2,Atp5pf,Ces1d,Cngb3,Dgat2,Dhrs7c,Fitm1,Gstm7,Hadh,Ift81,Kcne1,Kcnip2,Kcnj3,Kcnv2,Klhl3,Lrpprc,mt-Nd5,Pex6,Pink1,Pla2g5,Ppm1k,Preb,Rtn2,Slc20a2,Slc25a4,Slc25a12,Slc25a22,Slc41a1,Stard10,Strit1,Syt7,Ttll1,Whrn

		,Bmp4,Prkcd,Slc25a30,Ednrb,Slc38a2,Ecrg4,Tnfrsf11a,Niban2,Tfrc,Pros1,Slc39a6,Aspscr1,Gba,Tnfrsf1b,Adcyap1r1,Tnfrsf1a,Cd9,Sox9,Mmp14,Rab34,Cnn2,Il4ra,Arhgap17,Ldaf1,Cttn,Ophn1,Fgfr1,Cx3cl1,Cttnbp2nl,Arl4c,Rab7b,Arfgap3,Inhba,Dbn1,Iqce,Dchs1,Cntln,Zdhhc2,Ptger4,Thbs1,Ildr2,Ccr5	
15	organonitrogen compound metabolic process	Fbln1,Dio2,Crlf1,Sulf1,Gpx3,Ccn2,Nuak1,Igf1,Tnip1,Rtn4,Ace,Trim47,Pfkp,Aopep,Thbs4,Samd4,Pdlim2,Itih5,Tspan17,Casp12,Igfbp5,Fn1,Ptprn,Pam,Cfh,Uck2,Vim,Pamr1,Ehd4,Sfrp2,Apod,App,Hbegf,Lox,Ddah1,Lrp8,Nppb,Uchl1,Cdkl2,Pcolce,Gxylt2,Ccnd2,Comt,Loxl3,Timp1,Grk5,Nmrk2,Cd44,Nox4,Nupr1,Cpxm2,Msn,Sfrp1,Adcy7,Mmp2,Comp,Anxa2,Dnaja4,Bcl2,Rpl3,Gpx1,F2r,Nlrc3,Cx3cr1,Myh7,Tmem119,Nppa,Tspo,Otulin,Fndc1,Qsox1,Loxl2,Adamts2,Hspb6,Enpp1,Tgm2,Tlr4,Tgfb2,Lrp1,Prnp,Ddah2,Tgfbr1,Dhdds,Mical1,Egfr,Adarb1,Upp1,Aebp1,Galc,Hif1a,Hsp90aa1,Traf3,Syk,Nkd2,Prkcd,Tars,Ecrg4,Mgat4a,Serpine2,Map1a,Dclk1,Hes1,Masp1,Clec4n,Adamts10,Ppic,Mapk4,Acot9,Rnf115,Ctsk,Tspan5,Hacd4,Tnfrsf1b,Prkag2,Mmp23,Tnfrsf1a,Tspan9,Scpep1,Sox9,Usp32,Mmp14,Ckb,Il17ra,Plod3,Slc1a3,Nucb2,Ophn1,Sh3bgrl,Psmb10,Ldlr,Pkd1,Chpf,Bak1,Ptk2b,Irak4,Gas1,Spcs3,C1ra,Pla2g4a,Hectd2,Inhba,S100a10,Serpinb6b,Naaladd2,Ctla2a,Aplnr,Nudt18,Ppm1e,Spsb4,Plcg2,Ttll7,Rap2b,Serpine1,Eef1a1,Dsel,Dap,Zdhhc2,Thbs1,Ccl21a,Col4a3,Lrrk1,Rcn3,Phlda1,Bmp4,Ednrb,Tfrc,Aspscr1,Gba,Cda,Tgfb1i1,Fgfr1,Cx3cl1,Nudt16,Numbl,S1pr2,Dact1,Ptprf,P3h2,Rbms3,Ptger4	P3h4,Atp1a2,Unc45b,Dglucy,Acot2,Entpd5,Aldh6a1,Mtr,Ttll1,Adhfe1,Epha4,Rgs2,Slc25a12,Acss1,P2ry1,Ppm1l,Oplah,Atp5pf,Ndufa5,Lrpprc,Pfdn6,Camk2a,Cpt2,Pink1,Gstk1,Rtn2,Dbt,Rpl3l,Crhr2,Gstm7,Akt2,Etfb,Dgat2,Ndufb11,Mmp15,Slc27a1,Bckdhb,Ces1d,Eno3,mt-Nd5,Lgals4,Pla2g5,Acot1,Acaa2,Ppm1k,Wnk2,Hjv,Pdk2,Mrps35,Kyat3,Gcat,Klhl3,Mtif2,Mif4gd,Sema4d,Tppp,Enpp2,Spta1,Aldh9a1,Eif3m,Mme,Gpt,Sharpin,Ppil1,Pim1,Anks1,Carnmt1,Syvn1,Rps6,Sbk2,Slc25a42,Fah,Gpt2,Il15,Adamts7,Nme6,Hhatl,Pdp2,Ggcx,Gzmm,Mylk4,Dusp18,Qsox2,Kyat1,Neurl2,Maob
16	regulation of transport	Adcyap1r1,Anxa5,Aplnr,Aspscr1,Bak1,Bmp4,Ccl21a,Cd63,Cnn2,Cttnbp2nl,Cx3cl1,Dpysl2,Egfr,Enpp1,F2r,Fgfr1,Fhl1,Fxyd5,Gpm6b,Hes1,Hif1a,Il4ra,Inhba,Lbp,Lgals3,Map1b,Pkd2,Pla2g4a,Plcg2,Pls3,Prkcd,Pros1,Ptger4,Ptk2b,S100a10,Serpine2,Syk,Thbs1,Tlr4,Tnfrsf1a,Tnfrsf1b,Tnfrsf11a,	Adora2a,Akt2,Alox5,Camk2a,Crhr2,Il15,Kcne1,Kcnj2,Kcnj3,Kcnj5,Maob,P2ry1,Pim1,Rgs2,Rtn2,Scn4b,Ston2,Acaa2,Apln,Atp1a2,Atp2a2,Atp5pf,Ces1d,Dhrs7c,Gstm7,Hadh,Kcnip2,Pink1,Slc25a4,Slc25a22,Strit1,Syt7

		Ace,Actn4,Ankrd1,Anxa1,Anxa2,Apod,App,Atp8a2,Atp8b1,Bcl2,Dbn1,Dync1li1,Dynll1,Ecrg4,Edn3,Ehd4,Fndc1,Fxyd6,Gas1,Gnao1,Hsp90aa1,Igf1,Kif5b,Lpar1,Lrp1,Mical1,Msn,Nppa,Nucb2,Ophn1,Prkar1a,Prnp,Rab27b,Rrad,Rtn4,Scn1b,Serpine1,Sfrp1,Slc38a2,Tgfb2,Tgfb3,Tgm2,Tspo,Zdhhc2	
17	cellular process	Crip1,Kif5b,Plekho1,Ppfibp1,Sparc,Dcn,Ccn2,Rtn4,Pfkp,Aspn,Vcan,Thbs4,Col14a1,Col5a2,Col3a1,Igfbp5,Pam,Cfh,Uck2,Vim,Xirp2,Fbn1,Ccn5,Postn,Sfrp2,Ccdc80,Fstl1,Enah,Clic5,Pi16,Myl12a,Dpysl3,Lox,Ankrd1,Col15a1,Angptl7,Mxra8,Uchl1,Col1a2,Pcolce,Mfap5,Emp1,Ccnd2,Loxl3,Serpinf1,S100a6,Timp1,Col1a1,Ugp2,Ltbp2,Nmrk2,Col4a1,Col4a2,Mmp2,Crispld2,Comp,Acta1,Itgbl1,Bcl2,Rpl3,Nrap,Myh7,Nppa,Cilp,Ecm2,Fxyd6,Col8a1,Fibin,Igfbp7,Hspb6,Tgm2,Itga9,Prune2,Tgfb2,Synpo2l,Lrrc17,Fgl2,Lrp1,Ltbp4,Prnp,Fbln1,Dio2,Crlf1,Nav1,Actn1,Cd34,Nuak1,Unc5b,Col6a2,Fstl3,Tnip1,Prkar1a,Ace,Cygb,Tgfb3,Samd4,Casp12,Fn1,Ptprn,Des,Col5a1,Frzb,Ehd4,Edn3,S100a11,Apod,App,Rcan1,Igfbp6,Fhl1,Hbegf,Ltbp3,Ddah1,Svep1,Cnksr1,Nppb,Arpc1b,Medag,Gxylt2,Mgp,Ift122,Comt,Meox1,Rhoc,Nox4,Nupr1,Msn,Tnmd,Srpx2,Sfrp1,Adcy7,Gnao1,Gpx1,Fbln2,F2r,Tmsb4x,Nlrc3,Sprr1a,Map1b,Tmem119,Col8a2,Piezo2,Tspo,Mfap4,Cox19,Otulin,Rbp1,Lgals1,Flnc,Fndc1,Qsox1,Loxl2,Adamtsl2,Adamts2,Pmepa1,Gdf15,Atp6v0a4,Tlr4,Col16a1,Nbl1,Dhdds,Etv5,Pcolce2,Sulf1,Mafk,Pmp22,Gpx3,Scn1b,Igf1,Fbln5,Hsp90aa1,Pdlim2,Shisa5,Tspan17,Nabp1,Cd55,Apbb1ip,Itga6,Map1a,Anxa5,Dclk1,Tbx15,Itgb5,Tnfrsf12a,Bambi,Anxa1,Cd63,Lrp8,Mmp23,Cdkl2,Ptn,Col6a1,Grk5,Gab2,Cd44,Slc1a3,Nid1,Aqp8,Ap1s2,Star,Tpm4,Anxa2,Dnaja4,Col12a1,Dync1li1,Rasl11b,Cx3cr1,Junb,Spcs3,Actn4,Lman1l,Rab31,Maff,Abra,Tuba1c,Naalad2,Tubb2b,Nudt18,Dipk2a,Ppm1e,Rhoj,Tecp	P3h4,Atp1a2,Rbfox1,Tbx5,Acadvl,Unc45b,Acot2,Entpd5,Aldh6a1,Mtr,Fbp2,Fitm1,Ttll1,Hadha,Adhfe1,Epha4,Rgs2,Cenpf,Kcnj3,Slc25a12,Sord,Acss1,P2ry1,Ppm1l,Hadh,Oplah,Atp5pf,Ndufa5,Lrpprc,Eci1,Pfdn6,Syt7,Kcnip2,Decr1,Cpt2,Pink1,Atp2a2,Ift81,Gstk1,Rtn2,Tcea3,Rpl3l,Efnb3,Akt2,Etfb,Pex11a,Star d10,Dgat2,Ndufb11,Slc25a4,Mmp15,Bckdhb,Dhrs7c,Ces1d,Hopx,Eno3,Retnla,mt-Nd5,Mlf1,Adra1b,Ech1,Lgals4,Pla2g5,Lgr6,Gal3st3,Cox7a1,Fam174b,Tnni3,Acaa2,Apbb1,Slc20a2,Ppm1k,Ano10,Wnk2,Hjv,Car14,Pdk2,Mrps35,Cmtm8,Strit1,Osgep,Gcat,Slc41a1,Klhl3,Pdcd2,Lama5,Cenpv,Ybx2,Slc25a22,Isyna1,Mtif2,Mif4gd,Coro6,Dglucy,Rgs7bp,Opn4,Ogdhl,Spta1,Lamb3,Aldh9a1,Eif3m,Bcl2l11,Slc22a3,Pim1,Emilin2,Anks1,Impa2,Camk2a,Syvn1,Pola2,Cyp4b1,Ablim2,Clcn1,Sbk2,Dbt,Crhr2,Ruvbl2,Gstm7,Col5a3,Fah,Tnni2,Stard8,Slc27a1,Kcnj5,Tmed1,Hcn4,Hhatl,Bcl11b,Pdp2,Foxo6,Ggcx,Gzmm,Mgmt,Slc7a1,Kcnj2,Mapk1ip1,Gpr22,Mylk4,Penk,Nqo2,Lrrc4b,Helt,Dusp18,Zfp358,Kcnv2,Hes6,Selenbp1,Acot1,Pde11a,Gramd4,Phpt1,Syde2,Apln,Ctnnal1,Whrn,Prdm16,Kcne1,Kyat3,Hsbp1l1,Snhg14,Meis1,Adora2a,Ccl11,Ston2,Sema4d,Tppp,Enpp2,Alox5,Esrrg,Emc4,Mme,Gpt,Sharpin,Ppil1,Carnmt1,Cryz,Aqp7,Rps6,Spa17,Slc25a42,Pex6,Ercc1,Gpt2,Il15,Adamts7,Nme6,Acbd4,Rnf207,Nectin2,Sox6,Dnaaf3,Cngb3,Wrap53,Preb,Adra

		r1,Scx,Pkd2,Grip1,Ssc5d,Haus8,Pcdh17,Igsf10,Lum,Cavin3,Enpp1,Serpine1,Prkab2,Lpar1,Mybpc2,Myl6,Eid1,Tmsb10,2410006H16Rik,Ddah2,Carhsp1,Dynll1,Fxyd5,Kdelr3,Bicc1,Pls3,Ptgis,Ro60,Mical1,Mrc2,Rflnb,Hif1a,Sfxn1,Atp8a2,Dpysl2,Sorbs3,Serpine2,Tpm3,Hes1,Masp1,Runx1,Adamts10,Rab27b,Ppic,Acot9,Gpatch4,Rnf115,Ctsk,Pdpn,Emilin1,Foxp2,Fscn1,Tspan9,Ckb,Sh3bgrl,Gpm6b,Rrad,Psmb10,Panx1,Mcam,Itga11,Lmo2,Pkd1,Bak1,Ptk2b,Irak4,Mmgt2,Myof,Calhm5,Cpne8,Gas1,Mllt11,Cnn3,C1ra,Pla2g4a,Fmod,Prelp,Amot,Phlda3,S100a10,Serpinb6b,Aplnr,Spsb4,Col6a3,Dok1,Cebpd,Sod3,Phldb2,Zfp267,Rtkn,Rrp12,Tacc3,Mical2,Tsr1,Rras,Txnip,Atp8b1,Ifi27l2a,Xirp1,Clic1,Tgfbr1,Fcrl2,P4ha1,Ntn4,Egfr,Csrp2,Adarb1,Aebp1,Id2,Galc,Nin,Traf3,Syk,Nkd2,Prkcd,Tars,Slc38a2,Sdc3,Il1r1,Tnfrsf11a,Shox2,Lima1,Tspan5,Hacd4,Tnfrsf1b,Prkag2,Srsf9,Adcyap1r1,Zyx,Bhlhe40,Tnfrsf1a,Cd9,Mmp14,Il17ra,Plod3,Ccn4,Nucb2,Il4ra,Rgs10,Cttn,Pdlim3,Mt2,Ldlr,Chpf,Septin11,Tubb2a,Arl4c,Lgals3,Rab7b,Creb5,Gemin6,Inhba,Ctla2a,Zbtb7c,Col27a1,Trim16,Ino80c,Col4a4,Sp110,Dnm3os,Plcg2,Dbn1,Sema3f,Rap2b,Eef1a1,Cntln,Creb3l2,Dsel,Dap,Isg20,Zdhhc2,Vasn,Thbs1,Emp3,Ildr2,Ccl21a,Ccr5,Col4a3,Snord13,Pou2f2,Lrrk1,Lbp,Rcn3,Nav3,Phlda1,Upp1,Tshz3,Cd180,Gpx8,Bmp4,Slc25a30,Ednrb,Matn2,Ecrg4,Mgat4a,Ifi211,Niban2,Lhx6,Tubgcp4,Skil,Ptgfrn,Tfrc,Pros1,Fmnl3,Clec4n,Slc39a6,Myot,Mapk4,Aspscr1,Gba,Glipr2,Cda,Eln,Wnt5b,Sox9,Sez6,Usp32,Rab34,Relb,Chn2,Cnn2,Zfp626,Arhgap17,Tgfb1i1,Ldaf1,Mki67,Ophn1,Fgfr1,Cx3cl1,Cotl1,Nudt16,Arap1,Atxn7l3,Cttnbp2nl,Numbl,Fzd2,Arfgap3,Pcdh9,Mcm3,S1pr2,Dact1,Shb,Zfp316,Slitrk4,Ankrd23,Ptprf,Vat1,Abi3bp,Sbno2,Iqce,Dchs1,Tnfrsf23,P3h2,Rbms3,Ptger4,Sema3d,Ms4a6c,Chaserr	1a,Scn4b,Spc24,Qsox2,Wdr45,Kyat1,Neurl2,Maob

18	regulation of biological quality	Kif5b,Dio2,Plekho1,Sparc,Dcn,Rtn4,Prkar1a,Ace,Samd4,Ptprn,Cfh,Vim,Edn3,Postn,App,Fhl1,Serping1,Myl12a,Ddah1,Svep1,Col1a2,Comt,Msn,Srpx2,Sfrp1,Mmp2,Gnao1,Comp,Bcl2,F2r,Tmsb4x,Map1b,Myh7,Nppa,Tspo,Rbp1,Atp6v0a4,Itga9,Ltbp4,Prnp,Fbln1,Carhsp1,Dynll1,Etv5,Scn1b,Igf1,Hif1a,Hsp90aa1,Syk,Atp8a2,Fn1,Serpine2,Cd55,Map1a,Anxa5,Tnfrsf12a,Bambi,Anxa1,Ctsk,Pdpn,Lrp8,Nppb,Emilin1,Ptn,Tspan9,Scpep1,Plod3,Star,Anxa2,Pkd1,Bak1,Septin11,Ptk2b,Gpx1,Cx3cr1,Mllt11,Pla2g4a,Piezo2,Amot,Aplnr,Rhoj,Sod3,Pkd2,Grip1,Serpine1,Lpar1,Tlr4,Atp8b1,Ccl21a,Tmsb10,Clic1,Lbp,Egfr,Id2,Bmp4,Prkcd,Ednrb,Ecrg4,Niban2,Shox2,Pros1,Fmnl3,Lima1,Gba,Tnfrsf1b,Eln,Adcyap1r1,Cd9,Sez6,Nucb2,Cttn,Ophn1,Fgfr1,Cx3cl1,Cotl1,Arap1,Numbl,Fzd2,Inhba,S1pr2,Dact1,Slitrk4,Ptprf,Plcg2,Dbn1,Sema3f,Abi3bp,Rap2b,Zdhhc2,Ptger4,Thbs1,Sema3d,Ildr2,Ccr5	Atp1a2,Tbx5,Slc25a22,Adora2a,Ccl11,Sema4d,Rgs7bp,Alox5,Epha4,Rgs2,Spta1,Kcnj3,Bcl2l11,P2ry1,Mme,Hadh,Atp5pf,Slc22a3,Pim1,Emilin2,Camk2a,Syt7,Syvn1,Kcnip2,Aqp7,Pink1,Atp2a2,Clcn1,Pex6,Crhr2,Efnb3,Akt2,Pex11a,Dgat2,Slc25a4,Kcnj5,Hcn4,Ces1d,Adra1b,Kcnj2,Adra1a,Scn4b,Lrrc4b,Tnni3,Acaa2,Apln,Ppm1k,Kcne1
19	positive regulation of multicellular organismal process	Abi3bp,Amot,Aplnr,Bmp4,Ccl21a,Ccn4,Ccr5,Cd55,Cttn,Cx3cl1,Cx3cr1,Ednrb,Egfr,Etv5,F2r,Fgfr1,Gba1,Glipr2,Gpm6b,Hes1,Hif1a,Id2,Il1r1,Il4ra,Il17ra,Inhba,Lbp,Lrp8,Map1b,Mmp14,Nin,Numbl,Pdpn,Pla2g4a,Plcg2,Pou2f2,Prkab2,Ptger4,Ptgis,Ptk2b,Ptprf,Rras,Runx1,Scx,Serpine2,Shb,Shox2,Skil,Slitrk4,Sox9,Star,Syk,Tfrc,Tgfb1i1,Tgfbr1,Thbs1,Tlr4,Tnfrsf1a,Tnfrsf1b,Tnfrsf11a,Tnfrsf12a,Traf3,Ace,Anxa1,Anxa2,App,Atp8a2,Bambi,Bcl2,Ccn2,Ccnd2,Cd34,Clec4n,Col1a1,Dbn1,Ddah1,Ecrg4,Edn3,Emilin1,Fn1,Grip1,Hsp90aa1,Hspb6,Igf1,Lgals1,Loxl2,Ltbp3,Lum,Nppa,Nppb,Panx1,Postn,Ptn,Rab7b,Rtn4,Serpine1,Serpinf1,Sfrp2,Srpx2,Sulf1,Svep1,Tgfb2,Tgfb3,Tgm2,Tmem119,Trim16,Tspo,Vim	Tbx5,Adora2a,Ccl11,Sema4d,Tppp,Enpp2,Alox5,Epha4,Rgs2,Spta1,Esrrg,Slc25a12,P2ry1,Mme,Hadh,Atp5pf,Pim1,Emilin2,Decr1,Cpt2,Crhr2,Efnb3,Slc25a4,Il15,Slc27a1,Nectin2,Sox6,Slc7a1,Penk,Adra1a,Lrrc4b,Apln,Slc20a2,Prdm16

20	regulation of multicellular organismal process	Ccnd2,Cd34,Col14a1,Cygb,Fgl2,Gnao1,Igfbp5,Itga9,Lox,Loxl3,Mmp2,Prnp,Rbp1,Serpinf1,Sfrp1,Sparc,Srpx2,Tgfb2,Tgm2,Timp1,Vim,Angptl7,Aspn,Bcl2,Ccn2,Col1a1,Col4a2,Comp,Dcn,Fbn1,Hspb6,Lrrc17,Myh7,Nppa,Pi16,Postn,Rtn4,Serping1,Sfrp2,Thbs4,Adcy7,Anxa2,Bambi,Cd63,Cx3cr1,F2r,Fbln1,Frzb,Gdf15,Lrp8,Ltbp3,Lum,Maff,Nppb,Prkab2,Ptn,Sulf1,Tgfb3,Tlr4,Tnfrsf12a,Ace,Apod,App,Ddah1,Dnaja4,Edn3,Fn1,Fstl3,Hbegf,Lgals1,Loxl2,Map1b,Mgp,Nlrc3,Nupr1,Prkar1a,Svep1,Tmem119,Tnmd,Tspo,Anxa5,Aplnr,Ccl21a,Ccn4,Col4a3,Ctsk,Fbln5,Gpm6b,Hes1,Hif1a,Lmo2,Ntn4,Pdpn,Pla2g4a,Plcg2,Ptgis,Ptk2b,Rras,Runx1,S100a10,Serpine2,Syk,Amot,Anxa1,Atp8a2,Cd55,Emilin1,Etv5,Grip1,Hsp90aa1,Igf1,Panx1,Phldb2,Rflnb,Rhoj,Scn1b,Scx,Serpine1,Ssc5d,Star,Tgfbr1,Pou2f2,Lbp,Egfr,Nav3,Id2,Nin,Traf3,Bmp4,Prkcd,Ednrb,Ecrg4,Il1r1,Tnfrsf11a,Skil,Shox2,Tfrc,Pros1,Clec4n,Gba,Glipr2,Tnfrsf1b,Bhlhe40,Tnfrsf1a,Cd9,Sox9,Mmp14,Il17ra,Relb,Il4ra,Tgfb1i1,Cttn,Fgfr1,Cx3cl1,Ldlr,Numbl,Lgals3,Rab7b,Inhba,S1pr2,Ctla2a,Shb,Slitrk4,Trim16,Ino80c,Ptprf,Dbn1,Sema3f,Abi3bp,Vasn,Ptger4,Thbs1,Sema3d,Ildr2,Ccr5	Adamts7,Adora2a,Adra1a,Alox5,Bcl2l11,Ccl11,Enpp2,Esrrg,Hcn4,Il15,Kcnj2,Kcnj5,Lama5,Meis1,Mme,Nectin2,P2ry1,Penk,Pim1,Ruvbl2,Scn4b,Sema4d,Slc27a1,Sox6,Spta1,Tbx5,Tppp,Adra1b,Apln,Atp1a2,Atp2a2,Atp5pf,Cpt2,Crhr2,Decr1,Efnb3,Emilin2,Epha4,Hadh,Helt,Hes6,Hopx,Kcne1,Kcnip2,Lrrc4b,Prdm16,Rgs2,Rnf207,Slc7a1,Slc20a2,Slc25a4,Slc25a12,Strit1,Syt7,Tnni3

Table S4. Common Genes expressed in negative enriched biological process

	Term name	Gene in WT TAC vs WT sham	Gene in $R14^{\Delta/+}$ TAC vs $R14^{\Delta/+}$ sham
1	monocarboxylic acid metabolic process	Abcd1,Acot1,Adh1,Akt2,Aldob,Appl2,Cbfa2t3,Cpt2,Etfdh,Flcn,Gcdh,Kyat1,Lipe,Mapk14,Npc1,Nudt7,Pfkfb1,Ppara,Ppargc1a,Prkab1,Scd4,Slc27a1,Sord,Acaa2,Acacb,Acad11,Acadm,Acadvl,Acot2,Acss1,Aldh5a1,Angptl3,Ces1d,Crat,Decr1,Dgat2,Ech1,Echs1,Eci1,Eno3,Etfb,Gstm7,Hadh,Hadha,Ldhb,Plin5	Acaa2,Acadvl,Acbd4,Acot1,Akt2,Alox5,Cpt2,Fah,Gstm7,Kyat1,Pdk2,Slc27a1,Sord,Acot2,Acss1,Ces1d,Decr1,Dgat2,Ech1,Eci1,Eno3,Etfb,Hadh,Hadha,Slc25a12
2	monocarboxylic acid catabolic process	Abcd1,Acaa2,Acad11,Akt2,Cpt2,Crat,Etfdh,Gcdh,Lipe,Nudt7,Sord,Acacb,Acadm,Acadvl,Acot2,Ces1d,Decr1,Ech1,Echs1,Eci1,Etfb,Hadh,Hadha,Plin5	Etfb,Acaa2,Acadvl,Akt2,Cpt2,Decr1,Fah,Hadh,Sord,Acot2,Ces1d,Ech1,Eci1,Hadha
3	cardiac muscle contraction	Adra1a,Adra1b,Cacnb2,Ctnna3,Dsg2,Fgf13,Hcn4,Kcne1,Kcnh2,Kcnj2,Kcnj5,Kcnq1,Rgs2,Rnf207,Abcc9,Atp2a2,Myh6,Ryr2,Scn4b,Smtn,Strit1,Tnni3,Tnni3k	Adra1a,Adra1b,Hcn4,Kcnj2,Kcnj5,Scn4b,Tnni2,Atp1a2,Atp2a2,Kcne1,Rgs2,Rnf207,Strit1,Tnni3
4	fatty acid catabolic process	Abcd1,Akt2,Appl2,Cpt2,Etfdh,Gcdh,Mapk14,Ppara,Ppargc1a,Acaa2,Acacb,Acad11,Acadm,Acadvl,Crat,Decr1,Dgat2,Ech1,Echs1,Eci1,Etfb,Hadh,Hadha,Plin5	Etfb,Acaa2,Acadvl,Akt2,Cpt2,Decr1,Hadh,Acot2,Ces1d,Ech1,Eci1,Hadha
5	regulation of blood circulation	Adra1a,Adra1b,Agtr1a,Cacnb2,Crhr2,Ctnna3,Dsg2,Fgf13,Hcn4,Kcnd2,Kcne1,Kcnh2,Kcnj2,Kcnj5,Kcnq1,Rgs2,Tbx5,Abcc9,Apln,Atp2a2,Hopx,Hrc,Kcnip2,Myh6,Pik3r1,Rnf207,Ryr2,Scn4b,Slc4a3,Smtn,Strit1,Tnni3,Tnni3k	Adra1a,Adra1b,Alox5,Crhr2,Hcn4,Kcne1,Kcnj2,Kcnj5,Rgs2,Rnf207,Scn4b,Tbx5,Apln,Atp1a2,Atp2a2,Atp5pf,Hopx,Kcnip2,Strit1,Tnni3
6	heart process	Adra1a,Adra1b,Cacnb2,Crhr2,Ctnna3,Dsg2,Fgf13,Hcn4,Kcnd2,Kcne1,Kcnh2,Kcnj2,Kcnj5,Kcnq1,Rgs2,Tbx5,Abcc9,Apln,Atp2a2,Hopx,Hrc,Kcnip2,Myh6,Pik3r1,Rnf207,Ryr2,Scn4b,Slc4a3,Smtn,Strit1,Tnni3,Tnni3k	Adra1a,Adra1b,Crhr2,Hcn4,Kcnj2,Kcnj5,Rgs2,Rnf207,Scn4b,Tbx5,Tnni2,Apln,Atp1a2,Atp2a2,Atp5pf,Hopx,Kcne1,Kcnip2,Strit1,Tnni3
7	heart contraction	Adra1a,Adra1b,Cacnb2,Crhr2,Ctnna3,Dsg2,Fgf13,Hcn4,Kcnd2,Kcne1,Kcnh2,Kcnj2,Kcnj5,Kcnq1,Rgs2,Tbx5,Abcc9,Apln,Atp2a2,Hopx,Hrc,Kcnip2,Myh6,Pik3r1,Rnf207,Ryr2,Scn4b,Slc4a3,Smtn,Strit1,Tnni3,Tnni3k	Adra1a,Adra1b,Crhr2,Hcn4,Kcnj2,Kcnj5,Rgs2,Rnf207,Scn4b,Tbx5,Tnni2,Apln,Atp1a2,Atp2a2,Atp5pf,Hopx,Kcne1,Kcnip2,Strit1,Tnni3

8	small molecule catabolic process	Abcd1,Adh1,Akt2,Aldh2,Aldh6a1,Aldob,Bckdha,Bckdhb,Cpt2,Crat,Dbt,Etfdh,Gcat,Gcdh,Gpt,Kyat1,Lipe,Mccc2,Nqo2,Nudt7,Sord,Acaa2,Acacb,Acad11,Acadm,Acadvl,Acot2,Adhfe1,Aldh5a1,Ces1d,Decr1,Ech1,Echs1,Eci1,Eno3,Etfb,Got1,Hadh,Hadha,Kyat3,Plin5	Acaa2,Acadvl,Akt2,Cpt2,Dbt,Dhdh,Fah,Gcat,Gpt,Gpt2,Kyat1,Nqo2,Sord,Acot2,Adhfe1,Aldh6a1,Bckdhb,Ces1d,Decr1,Ech1,Eci1,Eno3,Etfb,Hadh,Hadha,Kyat3,Slc25a12
9	regulation of heart contraction	Adra1a,Adra1b,Cacnb2,Crhr2,Ctnna3,Dsg2,Fgf13,Hcn4,Kcnd2,Kcne1,Kcnh2,Kcnj2,Kcnj5,Kcnq1,Rgs2,Tbx5,Abcc9,Apln,Atp2a2,Hopx,Hrc,Kcnip2,Myh6,Pik3r1,Rnf207,Ryr2,Scn4b,Slc4a3,Smtn,Strit1,Tnni3,Tnni3k	Adra1a,Adra1b,Crhr2,Hcn4,Kcne1,Kcnj2,Kcnj5,Rgs2,Rnf207,Scn4b,Tbx5,Apln,Atp1a2,Atp2a2,Atp5pf,Hopx,Kcnip2,Strit1,Tnni3
10	carboxylic acid catabolic process	Abcd1,Akt2,Aldh6a1,Bckdha,Bckdhb,Cpt2,Crat,Dbt,Etfdh,Gcat,Gcdh,Gpt,Kyat1,Lipe,Mccc2,Nudt7,Sord,Acaa2,Acacb,Acad11,Acadm,Acadvl,Acot2,Adhfe1,Aldh5a1,Ces1d,Decr1,Ech1,Echs1,Eci1,Etfb,Got1,Hadh,Hadha,Kyat3,Plin5	Acaa2,Acadvl,Akt2,Aldh6a1,Cpt2,Dbt,Fah,Gcat,Gpt,Gpt2,Kyat1,Kyat3,Sord,Acot2,Adhfe1,Bckdhb,Ces1d,Decr1,Ech1,Eci1,Etfb,Hadh,Hadha
11	organic acid catabolic process	Abcd1,Akt2,Aldh6a1,Bckdha,Bckdhb,Cpt2,Crat,Dbt,Etfdh,Gcat,Gcdh,Gpt,Kyat1,Lipe,Mccc2,Nudt7,Sord,Acaa2,Acacb,Acad11,Acadm,Acadvl,Acot2,Adhfe1,Aldh5a1,Ces1d,Decr1,Ech1,Echs1,Eci1,Etfb,Got1,Hadh,Hadha,Kyat3,Plin5	Acaa2,Acadvl,Akt2,Aldh6a1,Cpt2,Dbt,Fah,Gcat,Gpt,Gpt2,Kyat1,Kyat3,Sord,Acot2,Adhfe1,Bckdhb,Ces1d,Decr1,Ech1,Eci1,Etfb,Hadh,Hadha
12	organic acid metabolic process	Abcd1,Acot1,Adh1,Akt2,Aldh6a1,Aldob,Appl2,Bckdha,Carnmt1,Cbfa2t3,Cpt2,D2hgdh,Dbt,Etfdh,Flcn,Gcat,Gcdh,Gnmt,Gpt,Gstm7,Kyat1,Lipe,Mapk14,Mccc2,Npc1,Nudt7,Ogdhl,Pfkfb1,Pla2g5,Ppara,Ppargc1a,Prkab1,Scd4,Slc27a1,Acaa2,Acacb,Acad11,Acadm,Acadvl,Acot2,Acss1,Adhfe1,Aldh5a1,Angptl3,Bckdhb,Carns1,Ces1d,Crat,Decr1,Dgat2,Dglucy,Ech1,Echs1,Eci1,Eno3,Etfb,Got1,Hadh,Hadha,Kyat3,Ldhb,Plin5,Sord,Thap4	Acaa2,Acbd4,Acot1,Akt2,Alox5,Carnmt1,Cpt2,Dbt,Fah,Gcat,Gpt,Gpt2,Gstm7,Kyat1,Mtr,Ogdhl,Pdk2,Pla2g5,Slc27a1,Sord,Acadvl,Acot2,Acss1,Adhfe1,Aldh6a1,Bckdhb,Ces1d,Decr1,Dgat2,Dglucy,Ech1,Eci1,Eno3,Etfb,Hadh,Hadha,Kyat3,Slc25a12
13	oxoacid metabolic process	Abcd1,Acot1,Adh1,Akt2,Aldh6a1,Aldob,Appl2,Bckdha,Carnmt1,Cbfa2t3,Cpt2,D2hgdh,Dbt,Etfdh,Flcn,Gcat,Gcdh,Gnmt,Gpt,Gstm7,Kyat1,Lipe,Mapk14,Mccc2,Npc1,Nudt7,Ogdhl,Pfkfb1,Pla2g5,Ppara,Ppargc1a,Prkab1,Scd4,Slc27a1,Acaa2,Acacb,Acad11,Acadm,Acadvl,Acot2,Acss1,Adhfe1,Aldh5a1,Angptl3,Bckdhb,Carns1,Ces1d,Crat	Acaa2,Acbd4,Acot1,Akt2,Alox5,Carnmt1,Cpt2,Dbt,Fah,Gcat,Gpt,Gpt2,Gstm7,Kyat1,Mtr,Ogdhl,Pdk2,Pla2g5,Slc27a1,Sord,Acadvl,Acot2,Acss1,Adhfe1,Aldh6a1,Bckdhb,Ces1d,Decr1,Dgat2,Dglucy,Ech1,Eci1,Eno3,Etfb,Hadh,Hadha,Kyat3,Slc25a12

		,Decr1,Dgat2,Dglucy,Ech1,Echs1,Eci1,Eno3,Etfb,Got1,Hadh,Hadha,Kyat3,Ldhb,Plin5,Sord,Thap4	
14	carboxylic acid metabolic process	Abcd1,Acot1,Adh1,Akt2,Aldh6a1,Aldob,Appl2,Bckdha,Carnmt1,Cbfa2t3,Cpt2,D2hgdh,Dbt,Etfdh,Flcn,Gcat,Gcdh,Gnmt,Gpt,Gstm7,Kyat1,Lipe,Mapk14,Mccc2,Npc1,Nudt7,Ogdhl,Pfkfb1,Pla2g5,Ppara,Ppargc1a,Prkab1,Scd4,Slc27a1,Acaa2,Acacb,Acad11,Acadm,Acadvl,Acot2,Acss1,Adhfe1,Aldh5a1,Angptl3,Bckdhb,Carns1,Ces1d,Crat,Decr1,Dgat2,Dglucy,Ech1,Echs1,Eci1,Eno3,Etfb,Got1,Hadh,Hadha,Kyat3,Ldhb,Plin5,Sord,Thap4	Acaa2,Acbd4,Acot1,Akt2,Alox5,Carnmt1,Cpt2,Dbt,Fah,Gcat,Gpt,Gpt2,Gstm7,Kyat1,Mtr,Ogdhl,Pdk2,Pla2g5,Slc27a1,Sord,Acadvl,Acot2,Acss1,Adhfe1,Aldh6a1,Bckdhb,Ces1d,Decr1,Dgat2,Dglucy,Ech1,Eci1,Eno3,Etfb,Hadh,Hadha,Kyat3,Slc25a12
15	small molecule metabolic process	Abcd1,Acot1,Adh1,Akt2,Aldh2,Aldh6a1,Aldob,Appl2,Bckdha,Car14,Carnmt1,Cbfa2t3,Cpt2,D2hgdh,Dbt,Dut,Etfdh,Fbp2,Flcn,Gcat,Gcdh,Gnmt,Gpt,Hectd4,Hmgcs2,Hsd11b1,Kcnq1,Kyat1,Lipe,Mapk14,Mccc2,Mme,Nadk2,Naprt,Npc1,Nqo2,Ogdhl,P2ry1,Pde4a,Pdss2,Pfkfb1,Ppara,Ppargc1a,Prkab1,Scd4,Slc25a42,Slc27a1,Acaa2,Acacb,Acad11,Acadm,Acadvl,Acot2,Acss1,Adhfe1,Aldh5a1,Angptl3,Bckdhb,Carns1,Ces1d,Crat,Decr1,Dgat2,Dglucy,Ech1,Echs1,Eci1,Eno3,Entpd5,Etfb,Fitm2,Got1,Gstm7,Hadh,Hadha,Impa2,Isyna1,Kyat3,Ldhb,Myh6,Nudt7,Oard1,Pank1,Pik3r1,Pla2g5,Plin5,Ppip5k2,Retsat,Sord,Stard3,Thap4	Acbd4,Acot1,Akt2,Alox5,Car14,Carnmt1,Cpt2,Dbt,Dhdh,Entpd5,Fah,Gcat,Gpt,Gpt2,Isyna1,Kyat1,Mme,mt-Nd5,Mtr,Ndufb11,Nqo2,Ogdhl,P2ry1,Pdk2,Pla2g5,Slc25a42,Slc27a1,Sord,Acaa2,Acadvl,Acot2,Acss1,Adhfe1,Aldh6a1,Atp1a2,Atp5pf,Bckdhb,Ces1d,Decr1,Dgat2,Dglucy,Ech1,Eci1,Eno3,Etfb,Fbp2,Ggcx,Gstm7,Hadh,Hadha,Impa2,Kyat3,Ndufa5,Nme6,Slc25a12

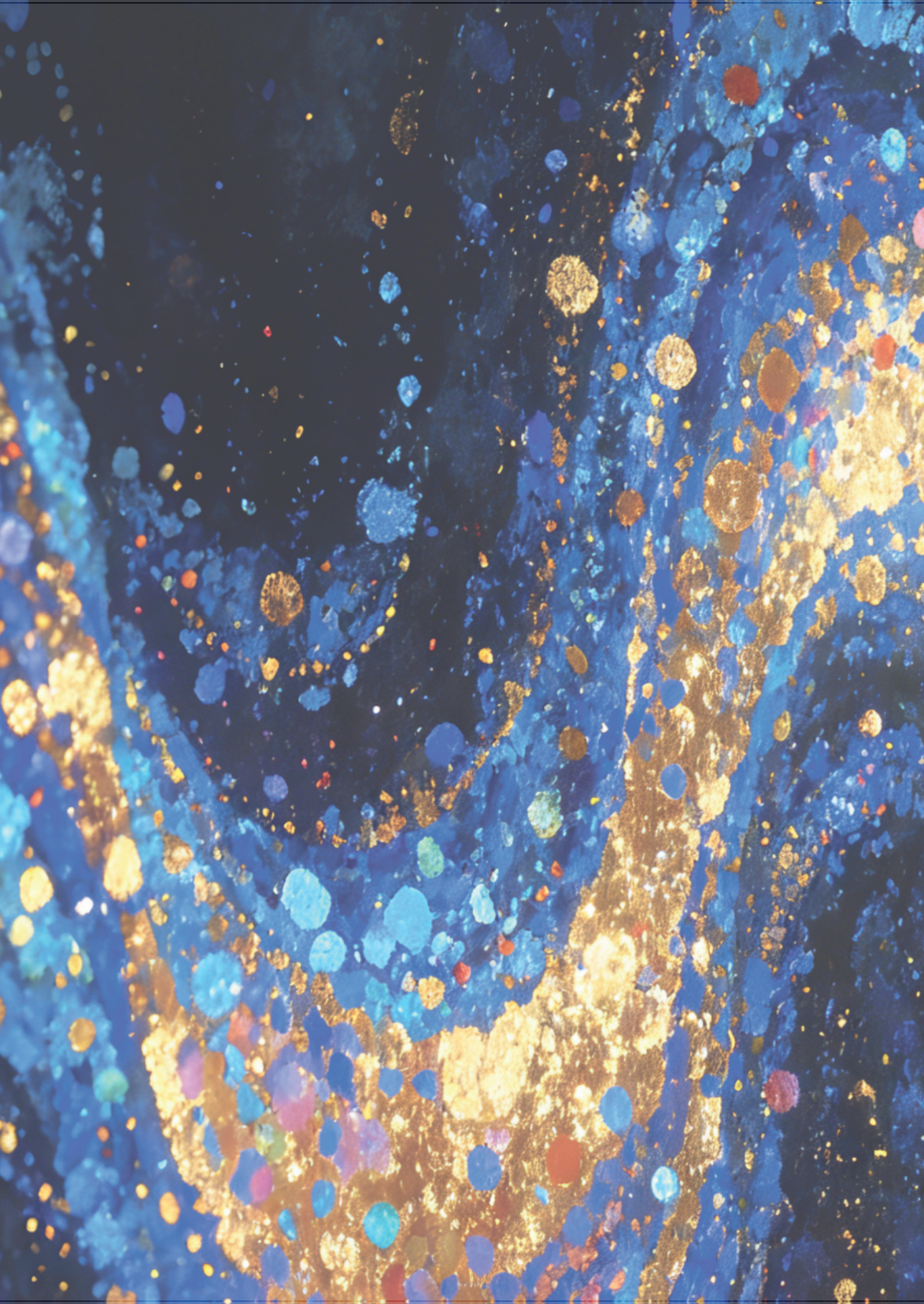

Chapter 4

An Inducible Mouse Model of PLN-R14del Cardiomyopathy Reveals Early Proteomic Changes in the Sarco/Endoplasmic Reticulum

Liu Sun #, Vivian Oliveira Nunes Teixeira #, Sietske Zijlstra, Peter van der Meer, Herman H.W. Silljé*

Department of Cardiology, University Medical Center Groningen, University of Groningen, Groningen, the Netherlands

(*In preparation*)

Abstract:

The inherited pathogenic variant PLN-R14del of the sarco/endoplasmic reticulum (S/ER) protein phospholamban can cause arrhythmogenic cardiomyopathy (ACM) and dilated cardiomyopathy (DCM), often leading to severe heart failure. While advanced disease features, such as fibrosis and abnormal cardiomyocyte S/ER cluster formation, are well-documented, the early molecular triggers of PLN-R14del driven cardiomyopathy remain elusive. In this study, we used a novel inducible mouse model to investigate the initial events underlying PLN-R14del associated cardiac pathology.
A conditional knockin (cKI) mouse strain with a floxed wildtype PLN exon and a downstream PLN-R14del exon (PLN-R14del$^{fl/fl}$) and with cardiomyocyte specific MerCreMer expression was generated. Two weeks after tamoxifen injection in adult mice, >97% of wildtype PLN mRNA was replaced by PLN-R14del mRNA. At four weeks post-induction, small S/ER clusters became visible in the cardiomyocytes of these mice, but cardiac function and tissue morphology remained normal. Over time, these clusters increased in size and abundance, coinciding with the onset of cardiac dysfunction. Control mice expressing the MerCreMer construct without the floxed PLN locus showed none of these alterations, confirming that the observed phenotype is PLN-R14del specific.

To identify early molecular changes of this cardiomyopathy, cardiomyocytes were isolated from 4-week-induced PLN-R14del mice and matched controls. Transcriptomic and proteomic analyses revealed predominantly early proteome alterations, primarily affecting S/ER-specific processes. These findings provide, for the first time, insight in the early pathogenic alterations triggered by PLN-R14del.

In conclusion, our study identifies early PLN-R14del-specific proteome changes in distinct S/ER pathways, offering novel insights and potential therapeutic targets for this cardiomyopathy.

1. Introduction

Phospholamban (PLN) is a regulator of calcium cycling by inhibiting the sarco/endoplasmic reticulum calcium ATPase (SERCA). Through this inhibition, PLN regulates Ca^{2+} reuptake into the sarco/endoplasmic reticulum (S/ER), ensuring proper myocardial relaxation and contraction cycles.[1,2] The p.Arg14del (R14del) variant, has a deletion of the arginine codon at position 14 in the PLN protein, and is the most prevalent PLN pathogenic mutation. Carriers of the PLN-R14del mutation are at risk of developing arrhythmogenic cardiomyopathy (ACM) and/or dilated cardiomyopathy (DCM), potentially progressing to severe heart failure (HF).[3,4] In patients and in a PLN-R14del mouse model, aberrant S/ER morphology, characterized by prominent accumulation of PLN-positive S/ER clusters, is closely associated with cardiomyocyte death and heart failure development.[5,6] This distinctive PLN localization has emerged as a pathological hallmark of PLN-R14del cardiomyopathy, consistently observed in both patients and mouse models, but absent in other forms of ACM or DCM.[7,8] Therefore, elucidating the mechanisms underlying S/ER malformation represents a key research focus in understanding the pathogenesis of this disease.

A PLN-R14del mouse model that presents similar disease characteristics as humans was designed to investigate the mechanism of PLN-R14del cardiomyopathy.[9] The rate of Ca^{2+} uptake was found to be enhanced in homozygous PLN-R14del ($R14^{\Delta/\Delta}$) and in heterozygous ($R14^{+/\Delta}$) cardiomyocytes compared to wild-type (WT) mice.[5,10] Inhibition of SERCA-PLN interaction or PLN silencing by antisense oligonucleotide (ASO) therapy did not, or only partially, elevated S/ER Ca^{2+} uptake in R14del cardiomyocytes.[10,11] Since PLN silencing did prevent cardiac dysfunction and improved survival of $R14^{\Delta/\Delta}$ mice, mechanisms beyond SERCA regulation must be involved. The formation of aberrant S/ER clusters was halted and reversed by ASO treatment, suggesting that it may be a key pathological mechanism driving PLN-R14del cardiomyopathy.

In homozygous $R14^{\Delta/\Delta}$ mice, pathological alterations already become visible a few weeks after birth and mice die within 8 weeks. Conversely, heterozygous $R14^{+/\Delta}$ mice closely mimic the human carrier state, but their slow and less synchronous disease progression makes it difficult to study the earliest pathogenic changes.[9] To overcome these limitations, an inducible PLN-R14del model was generated, allowing temporal control of PLN-R14del expression and enabling detailed investigation of the initiation and progression of S/ER malformation.

A transgenic mouse model was designed using the LoxP/ α-myosin heavy chain (α-MHC)-MerCreMer system to enable conditional allele conversion.[12] In this new model, mice have a floxed PLN-WT exon followed by the same exon containing the R14del mutation. This allows tamoxifen induced MerCreMer recombination of the LoxP site, resulting in the excision of the WT PLN allele and consequent replacement by the PLN-R14del allele. This tamoxifen-inducible PLN-$R14del^{fl/fl}$ system provides time

dependent and synchronous expression of the PLN-R14del allele, allowing the identification of early underlying pathogenic processes.

This study aimed to investigate the development of S/ER clustering in a novel inducible PLN-R14del mouse model and to explore the underlying S/ER-associated mechanisms. We demonstrate that upon onset of gene conversion, abnormal S/ER clusters originate as small speckles and progressively enlarge over time. Importantly, at this early stage we observed S/ER proteome alterations, without corresponding transcriptional changes, and these can be linked to post-transcriptional Endoplasmic Reticulum-Associated Degradation (ERAD).

2. Method

2.1 Study design and animal model

Male and female inducible MerCreMer PLN-R14del mice were housed under a 12-hour light/dark cycle with ad libitum access to food and water, as previously described.[9] Baseline echocardiography was performed at 10 weeks of age, before initiation of tamoxifen injections. All mice were randomized based on sex, body weight, and echocardiographic parameters into five experimental groups. Mice received tamoxifen (45 mg/kg/day) via intraperitoneal injection for five consecutive days and were sacrificed at 3, 4, 5, or 6 weeks after the first injection. The efficiency of gene conversion was measured 2 weeks after the first injection. MerCreMer PLN-R14del homozygous ($R14^{fl/fl}$) mice treated with vehicle and MerCreMer PLN-WT mice treated with tamoxifen were sacrificed at 6 weeks after first injection and served as age-matched controls. An additional group of untreated MerCreMer PLN-R14del homozygous ($R14^{fl/fl}$) mice was sacrificed at 10 weeks of age and served as the baseline control. Endpoint echocardiography was performed before sacrifices. Echocardiography and termination were performed under anesthesia with 2-2.5% isoflurane mixed with oxygen. This study was approved by the Dutch Central Committee for animal experiments (CCD; license number AVD1050020199105) and the animal ethical committee of the University of Groningen (permit numbers IVD199105-01-016, IVD199105-01-019, IVD199105-01-023, IVD199105-01-025) and followed the guidelines set out in the Directive 2010/63/EU of the European Parliament for using animals in research. It also followed the Animal Research: Reporting of In Vivo Experiments (ARRIVE) guidelines for reporting on experiments done with animals.[13]

2.2 Tissue collection at termination

The morphology and function of the left ventricle (LV) were assessed using a Vevo 3100 preclinical imaging system equipped with a 40-MHz MXX550D linear array transducer (FUJIFILM VisualSonics, Canada), as detailed in previous studies.[5] Subsequent hemodynamic evaluations were carried out using Vevo LAB software version 5.7.1 (FUJIFILM VisualSonics). Data collection and analysis followed the

recommendations outlined by the European Society of Cardiology Working Group on Myocardial Function and were conducted in a blinded fashion.[14]

2.3 Euthanasia

Euthanasia was performed under anesthesia using a mixture of oxygen and 2.5% isoflurane. After confirming the depth of anesthesia, the abdominal and thoracic cavities were opened. Blood was draw from the abdominal aorta, then saline was perfused through the heart to flush the circulatory system. The heart was removed, and rinsed with ice-cold 1 M potassium chloride (KCl) solution (Merck Millipore, Germany). A transverse mid-slide was preserved for histological analysis, several small pieces (1 mm^3) from the left ventricle (LV) myocardium were collected for electron microscopy processing, and the remaining tissue was immediately snap-frozen in liquid nitrogen for further molecular studies. Electron microscopy was performed for mice sacrificed at 4 and 6 weeks after tamoxifen injection.

2.4 Histological staining

Transverse sections of ventricles were fixed in 4% formaldehyde (10% neutral buffered formalin; Klinipath, The Netherlands) for a minimum of 24 hours. Following fixation, tissues were dehydrated using an automated tissue processor (Leica TP1020; Leica Microsystems, Germany), embedded in paraffin, and cut into 4-µm-thick sections. Prior to staining, the tissue sections were deparaffinized according to standard protocols.

To assess PLN clustering, ventricular tissue sections were immunostained with a rabbit anti-PLN primary antibody (Cell Signaling Technology, MA, USA), followed by an Alexa Fluor 555-conjugated secondary antibody. Cardiomyocyte boundaries were visualized using fluorescein isothiocyanate (FITC)-conjugated wheat germ agglutinin (WGA), and nuclei were counterstained with 4',6-diamidino-2-phenylindole (DAPI). Whole-slide imaging was performed using a NanoZoomer 2.0-HT digital slide scanner (Hamamatsu Photonics, Japan). PLN clusters were quantified in 25 cardiomyocytes per mouse (Ctrl, n = 6; Tamoxifen-treated, n = 8 per group). Cluster size was expressed in square micrometers (µm²), and cluster positivity was reported as the percentage (%) of cardiomyocytes. Only clusters with an area above 5 µm² were included in the analysis, as smaller clusters were difficult to distinguish on the stained images.

For co-localization analysis of PLN with other sarcoplasmic reticulum (SR) proteins in mouse cardiac tissue, immunofluorescence staining was performed using antibodies against P62, MFGE8, PDIA, EMC2, and SEL1L, along with anti-PLN. Fluorescently labeled secondary antibodies were used for signal detection. Details of the primary and secondary antibodies are provided in **Supplementary table 1**. Images were acquired using a Leica TCS SP8X confocal microscope (Leica Microsystems) with a 63X oil immersion objective (numerical aperture 1.4; pinhole size 95.5 µm).

2.5 Quantitative Polymerase Chain Reaction (q-PCR)

Total RNA was isolated from snap-frozen left ventricular tissue using TRI Reagent

(Sigma-Aldrich, MO, USA) following the manufacturer's instructions. Complementary DNA (cDNA) was synthesized using the QuantiTect Reverse Transcription Kit (Qiagen, Germany). Quantitative real-time PCR (qPCR) was performed using iQ SYBR Green Supermix (Bio-Rad, CA, USA) on a C1000 Touch Thermal Cycler with a CFX384 Real-Time PCR Detection System (Bio-Rad). Gene expression data were analyzed using Bio-Rad CFX Manager 3.0 software. All target gene expression levels were normalized to the reference gene Rplp0 (36B4) and presented as fold changes relative to the untreated control group. Primer sequences are listed in **Supplementary table 2**.

Specific Taqman probes for mouse PLN wildtype and R14del was generated via the online tool of the Thermoscientific-Taqman probe website, allowing us to distinguish the gene expression between WT and R14del of PLN-R14$^{fl/fl}$ mice (Assay ID: ANRWUHK).
(https://www.thermofisher.com/order/custom-genomic-products/tools/genotyping/).

2.6 Cardiomyocytes isolation

Cardiomyocytes were isolated using a Langendorf perfusion free system.[15] Both vehicle-treated and tamoxifen-treated mice (n = 5 per group) were included as age-matched controls and experimental groups, respectively. To investigate proteomic and transcriptomic changes during the early stage of disease progression, all mice were sacrificed 4 weeks after the first day of injection.

2.7 Protein isolation and immunoblotting

Total protein was extracted from snap-frozen left ventricular (LV) tissue using radioimmunoprecipitation assay (RIPA) lysis buffer as previously described.[9] Protein concentrations were determined using the Pierce BCA Protein Assay Kit (Thermo Scientific, MA, USA). Protein samples were normalized to equal concentrations for subsequent Western blot analysis. After heating, samples were loaded onto sodium dodecyl sulfate-polyacrylamide gels (SDS-PAGE) for electrophoretic separation, followed by transfer to Immun-Blot polyvinylidene fluoride (PVDF) membranes using a semi-dry transfer system (Amersham Biosciences, UK).

Total protein normalization was performed using Revert 700 Total Protein Stain (LI-COR #926-11021), according to the manufacturer's protocol. Membranes were then blocked in blocking buffer (5% milk or 5% BSA in TBST, prepared according to the manufacturer's instructions) and incubated overnight at 4°C with primary antibodies, followed by incubation with species-specific secondary antibodies for 1 hour at room temperature. Protein bands were visualized using enhanced chemiluminescence (ECL) with Western Lightning Ultra Chemiluminescent Substrate (Cytiva, #204-22101), and images were captured using the Amersham ImageQuant 800 system. Densitometric quantification of target proteins was performed using Image Studio Lite Software (Version 5.2; LI-COR). Protein expression values were reported as fold changes (FC) relative to the 0-week control group. Primary and secondary antibodies that were used are presented in **Supplementary table 3**.

2.8 Electron microscopy

Electron microscopy with PLN quantum dot immunolabeling was performed as reported previously.[5]

2.9 Proteomics and transcriptome analysis of isolated cardiomyocytes

Proteins were isolated from cardiomyocytes, followed by denaturation, reduction, alkylation, and tryptic digestion. Afterwards, proteins were fractionated by high-pH reversed-phase liquid chromatography, and analyzed by liquid chromatography-mass spectrometry using an UltiMate 3000 chromatography system and an Orbitrap Fusion Lumos Tribrid mass spectrometer (Thermo Scientific). To identify differentially expressed proteins between the experimental groups, label-free quantification (LFQ) intensity values obtained from mass spectrometry were first log2-transformed to approximate a normal distribution and reduce heteroscedasticity. Differential expression analysis was performed using an unpaired two-tailed Student's t-test (R 4.4.2), comparing tamoxifen-treated mice with vehicle-treated controls (n = 5 per group). To account for multiple hypothesis testing, false discovery rate (FDR) adjustment was applied using the Benjamini-Hochberg procedure. Proteins with an absolute log2FC > 1 and adjusted p-value (FDR) < 0.05 were considered significantly differentially expressed.

RNA Library preparation and sequencing were performed by Lexogen NGS services (Vienna, Austria). Data filtering and differential expression analysis were performed using the ggplot2 package in R (version 4.4.3). Differentially expressed genes (DEGs) were defined by a P value of <0.05 and an absolute log2FC >1.

GO term enrichment analysis for cellular components was performed using g:Profiler (https://biit.cs.ut.ee/gprofiler/gost). Differentially expressed genes (DEGs) with an absolute log2FC > 1 and P < 0.05 were selected for analysis and visualization.

Statistical analyses

Data are presented as mean ± standard error of the mean (SEM). Statistical analyses were performed using GraphPad Prism version 10.5.0. For comparisons among multiple groups, the Kruskal-Wallis test followed by Dunn's post hoc multiple comparisons test was used. Non-treated mice served as the control group. P-values < 0.05 were considered statistically significant. All data acquisition and analysis were performed in a blinded manner.

3. Result

3.1 Tamoxifen converts mice to homozygosity in 2 weeks and leads to cardiac dysfunction from 5 weeks post-injection.

A mouse model with cardiomyocyte specific MerCreMer expression (α-MHC promoter) and floxed wildtype PLN coding exons followed by a PLN-R14del pathogenic coding exon was established ($R14^{fl/fl}$). In this model tamoxifen administration can activate Cre-

loxP recombination, resulting in the replacement of the mouse PLN-WT alleles to the homozygous PLN-R14del alleles **(Figure 1A)**. To test this, ten-week-old mice were injected with tamoxifen or vehicle for one week. Two weeks after the first injection, WT PLN and PLN-R14del cardiac gene expression was analyzed using allele specific TaqMan probes. Tamoxifen injection resulted in an almost complete (97%) change from WT to PLN-R14del gene transcript **(Figure 1B)**. Since no allele specific antibodies exist, we do not know how fast WT PLN is replaced by R14del PLN protein, but a study using myoblasts suggests turnover rates of less than 24 hours.[16] Based on this, we conducted an experiment in which we randomly assigned mice to either a non-treatment group or a tamoxifen-treated group and terminated the latter at 3, 4, 5 and 6 weeks after the first tamoxifen injection **(Figure 1C)**.

Prior to genotype conversion, baseline cardiac function of all experimental groups was within the normal range, with an average ejection fraction (EF) > 55%. Additionally, MerCreMer PLN-WT mice (no floxed allele) treated with tamoxifen and PLN-R14$^{fl/fl}$ mice treated with vehicle were included and terminated at 6 weeks after first injection as controls. Cardiac function remained normal in these two control groups in comparison with the baseline (0 weeks induction) PLN-R14$^{fl/fl}$ mice **(Supplemental figure 1A-B)**. In tamoxifen-treated MerCreMer PLN-R14$^{fl/fl}$ mice, echocardiographic assessments were performed prior to sacrifice at 3, 4, 5 or 6 weeks after injections. EF mean of the group remained within the normal range up to 4 weeks post-injection. A marked decline was first detected at week 5, and by week 6, the average EF had dropped below 20%. This deterioration in systolic function was accompanied by progressive increases in both left ventricular (LV) diastolic and systolic diameters from week 5 onward, indicative of ventricular dilation and contractile dysfunction **(Figure 1D-F)**.

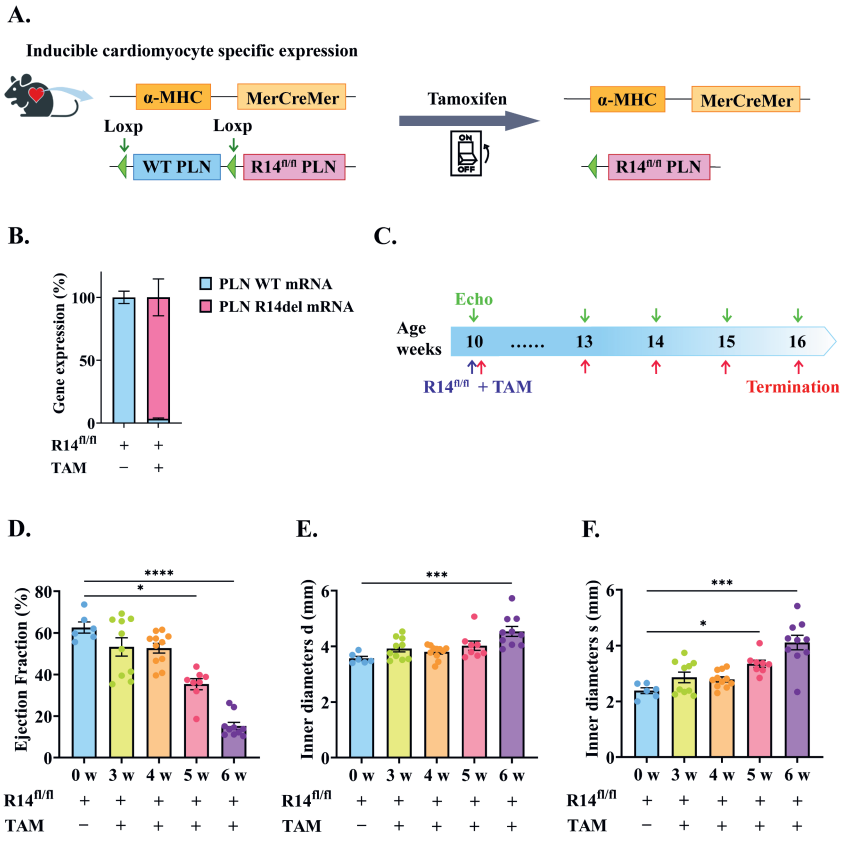

Figure 1. Tamoxifen induces PLN-R14del homozygosity and progressive cardiac dysfunction.

(A) Schematic representation of the tamoxifen-inducible MerCreMer system used to activate PLN-R14del expression. **(B)** Gene conversion efficiency following tamoxifen induction. **(C)** Schematic overview of the *in vivo* study design (TAM=tamoxifen). **(D)** Ejection fraction, **(E)** LV inner diastolic diameter, and **(F)** LV inner systolic diameter at the indicated weeks(w) of inducible PLN-R14$^{fl/fl}$ mice either non-treated (0w) or tamoxifen-treated (3w, 4w, 5w, 6w) (non-treated, n=6; Tamoxifen-treated, n ≥ 8 per group). $^{*}p<0.05$, $^{***}p<0.001$, $^{****}p<0.0001$ compared to untreated mice. Kruskal-Wallis with Dunn's multiple comparisons test.

3.2 SR cluster emerges three weeks after conversion

A key hallmark of PLN-R14del cardiomyopathy in both humans and mice is the formation of pathological sarco/endoplasmic reticulum (S/ER) PLN clusters.[5,7-9] In the heterozygous situation these clusters are formed in a very heterogenous manner with some cells forming clusters while others still have normal PLN distribution. In homozygous mice this is more synchronous, but already starts very early in life (3 weeks of age). Using the current model, we could now investigate how PLN S/ER clusters would develop in a synchronous manner upon tamoxifen mediated induction.

At 3 weeks after injection, immunofluorescent PLN/WGA/DAPI staining revealed very small scattered PLN speckles in nearly all cardiomyocytes, with most speckles measuring less than 5 µm². For cluster quantification, 25 longitudinal cardiomyocytes were randomly selected from the scanned ventricular staining image of each animal. With disease progression, the size of PLN clusters (only PLN clusters >5 µm² counted) progressively increased **(Figure 2A-B)**, along with a gradual rise in the percentage of cluster-positive cells **(Figure 2C)**.

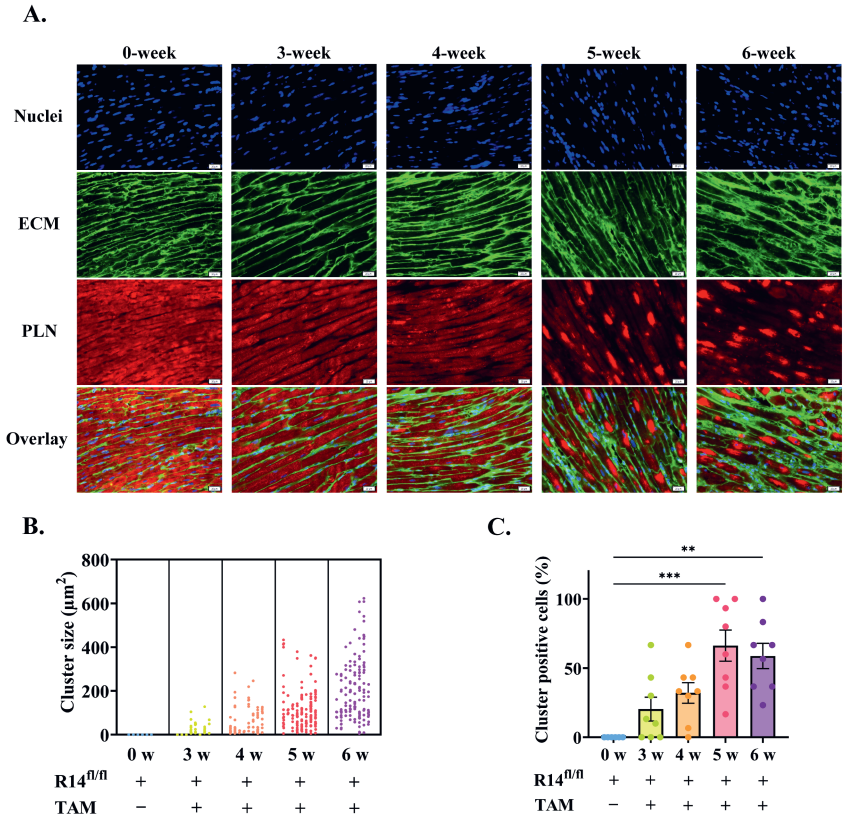

Figure 2. Progressive accumulation of PLN-positive clusters during disease progression.

(A) Representative immunofluorescence (IF) staining of PLN, together with wheat germ agglutinin (WGA) staining of extracellular matrix and 4',6-diamidino-2-phenylindole (DAPI) staining of nuclei in ventricular tissue sections of non-treated (0w) and tamoxifen-treated (3w, 4w, 5w, 6w) inducible PLN-R14$^{fl/fl}$ mice terminated at different timepoints (non-treated, n=6; Tamoxifen, n = 8 per group) (scale bars, 20 µm). **(B)** Quantification of the size of PLN clusters in cardiomyocytes (only PLN clusters >5 µm² counted) and **(C)** the percentage of PLN-cluster positive cells in 25 longitudinal cardiomyocytes from each animal stained tissue sections at different weeks(w) after induction (non-treated, n=6; Tamoxifen, n ≥ 8 per group). Statistical comparison between non-treated versus tamoxifen-treated inducible PLN-R14$^{fl/fl}$ mice. $^{**}p<0.01$, $^{***}p<0.001$ Kruskal-Wallis with Dunn's multiple comparisons test.

3.3 Progressive accumulation of S/ER clusters following Tamoxifen-induced conversion in PLN-R14$^{fl/fl}$ mice.

To further obtain structural insights into SR formation and organization electron microscopy was performed on ventricular tissue. Based on the findings from fluorescent staining, we anticipated that structural alterations would be difficult to detect using electron microscopy at the 3-week time point. Moreover, by the 4-week time point, cardiac function remained normal, making it a suitable stage for further analysis. Therefore, we investigated the 4-week time point to enhance the likelihood of capturing ultrastructural changes. Quantum dot labeling with an anti-PLN antibody enabled detailed visualization of these clusters in electron microscopy samples. At 4 weeks post-TAM injection, electron microscopy revealed the presence of PLN dot-positive sarcoplasmic reticulum (SR) cluster structures in the mitochondrial region **(Figure 3A)**, along with a small number of similar PLN labeled membranous structures located between adjacent sarcomeres **(Figure 3B)**. By 6 weeks, these SR membranes had largely disappeared from the inter-sarcomeric space **(Figure 3D)** and accumulated extensively in the mitochondrial area **(Figure 3C)**. This redistribution suggests a progressive mislocalization or reorganization of SR structures during disease progression, which may contribute to impaired excitation-contraction coupling in PLN-R14$^{fl/fl}$ cardiomyopathy.

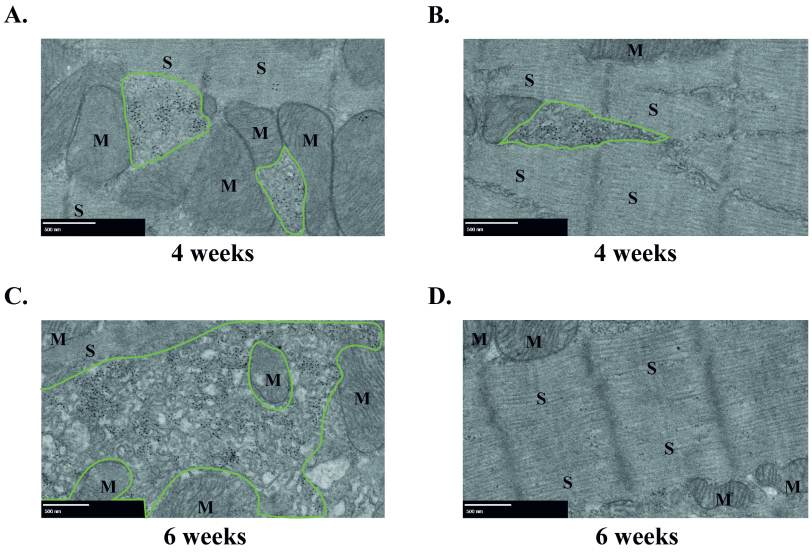

Figure 3. Progressive mislocalization and accumulation of S/ER clusters in PLN-R14$^{fl/fl}$ mice. Representative electron micrographs of cardiac ventricular tissue from tamoxifen-treated R14$^{fl/fl}$ mice at 4 weeks **(A, B)** and 6 weeks **(C, D)** post-injection (scale bars, 500 nm). At 4 weeks, small PLN-positive membranous clusters (solid line circled) were observed dispersed within the mitochondrial region **(A)** and between adjacent sarcomeres (S) **(B)**. By 6 weeks, mislocalized clustered S/ER structures **(C)**, indicated by circles, were predominantly found surrounding mitochondria (M), accompanied by a marked reduction of SR area between adjacent sarcomeres **(D)**.

3.4 Cardiac remodeling in converted PLN-R14del mice starts at 4 weeks.

Molecular changes associated with cardiac remodeling were examined. In line with the observed deterioration in cardiac function, expression of atrial natriuretic peptide (*Nppa*), a well-established marker of cardiac wall stress and hypertrophy, was significantly upregulated after 5 and 6 weeks of tamoxifen-treatment as compared to non-treated baseline controls in $R14^{fl/fl}$ mice **(Figure4 A)**. Similarly, ventricular mRNA levels of fibrosis-related genes, including Tissue Inhibitor of Metalloproteinases 1 (*Timp1*) and Collagen Type I Alpha 1 Chain (*Col1a1*), were also elevated in tamoxifen-treated mice **(Figure4 B-C)**. Notably, all of these molecular changes became significant after 5 weeks post-injection. Together, these results indicate that the conversion from wild-type to homozygous PLN-R14del genotype leads to progressive cardiac remodeling, characterized by impaired cardiac function, molecular activation of hypertrophy and fibrosis pathways, thereby corroborating the in vivo functional decline.

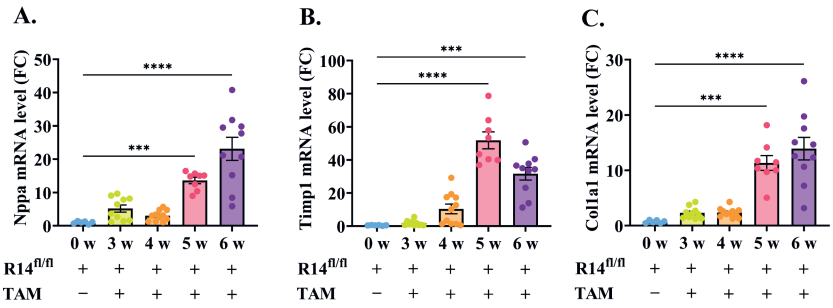

Figure 4. Cardiac remodeling in converted PLN-R14del mice starts at 4 weeks.

Ventricular gene expression of markers of cardiac remodeling. **(A)** atrial natriuretic peptide (*Nppa*), **(B)** Tissue Inhibitor of Metalloproteinases 1 (*Timp1*) and **(C)** collagen type I alpha 1 chain (*Col1a1*) of non-treated (0w) mice and tamoxifen-treated (3w, 4w, 5w, 6w) inducible PLN-$R14^{fl/fl}$ mice at different weeks(w) after induction (non-treated, n=6; Tamoxifen-treated, n ≥ 8 per group), normalized to 36B4 (*Rplp0*) housekeeping gene levels and shown relative fold change to non-treated mice. $^{***}p<0.001$, $^{****}p<0.0001$, Kruskal-Wallis with Dunn's multiple comparisons test.

3.5 PLN R14del cardiomyopathy is closely associated with post-transcriptional dysregulation of S/ER-related proteins

Since PLN is specifically expressed in cardiomyocytes, the onset of PLN-R14del cardiomyopathy must originate from dysfunctional processes within these cells. Nevertheless, previous transcriptomic and proteomic studies have been performed on whole tissue and primarily revealed broad features of cardiac remodeling, such as fibrosis and immune activation. These are, however, likely secondary processes and do not address the initial problem that arises from the affected cardiomyocytes.[17] To address this gap, we performed proteomics and transcriptomic analyses at 4 weeks after induction, a time point when PLN clusters were already evident but before the

appearance of other disease markers **(Figure 5A)**. Moreover, by specifically isolating cardiomyocytes, we were able to minimize indirect effects arising from non-cardiomyocyte cell types. Vehicle-treated $R14^{fl/fl}$ mice were included as controls and terminated at the same time point. Proteomic and transcriptomic analyses were performed on protein lysates and purified RNA, respectively, from these isolated cardiomyocytes.

Proteomic analysis identified 63 significantly upregulated (>2-fold change) and 19 downregulated proteins in $R14^{fl/fl}$ tamoxifen-treated mice compared to vehicle-treated controls **(Figure 5B)**. Two proteins showed a particularly strong and significantly upregulation, namely p62 (*SQSTM1*) and Mfge8. P62 is a known upregulated protein in both human and PLNR14del cardiomyopathy and co-localizes with PLN-R14del clusters. This confirms the validity of this inducible model and importantly shows that p62 protein increase is an early effect in this disease. Western blotting of whole lysates revealed a very strong increase at a later time point, corresponding with co-localization at large PLN-positive clusters **(Supplemental figure 2A-D)**. As described in the next paragraph, Mfge8 and other identified proteins were also followed up **(Supplementary figure S3)**. Importantly, Gene Ontology (GO, cellar component) analyses revealed that ER related proteins were predominantly enriched, including some specific ER protein complexes, the oligosaccharyltransferase complex and EMC for targeting proteins to the ER **(Figure 5C)**. Together with the histological findings this suggest that dysregulation of ER related processes occur first in PLN-R14del cardiomyopathy. In contrast only a limited number of proteins were downregulated and these were related to mitochondrial and cytosolic functions **(Figure 5C)**.

Transcriptomic analysis revealed much less significant changes in the gene expression profile comparison did only reveal small differences **(Figure 5D)**, and confirmed the absence of cardiac remodeling gene expression markers at this stage **(Figure 4A-C)**.[17] The genes that did show significant upregulated expression were not related to any specific process and included mostly cytosolic and nuclear protein encoding genes and downregulated genes encoded mostly mitochondrial and cytosolic proteins **(Figure 5E)**. The complete list of differentially expressed genes is provided in the **Supplemental material**. Interestingly, many proteins that showed significant upregulation by proteome analyses, including p62 and MFGE8, did not show a significant transcriptional upregulation at this stage.

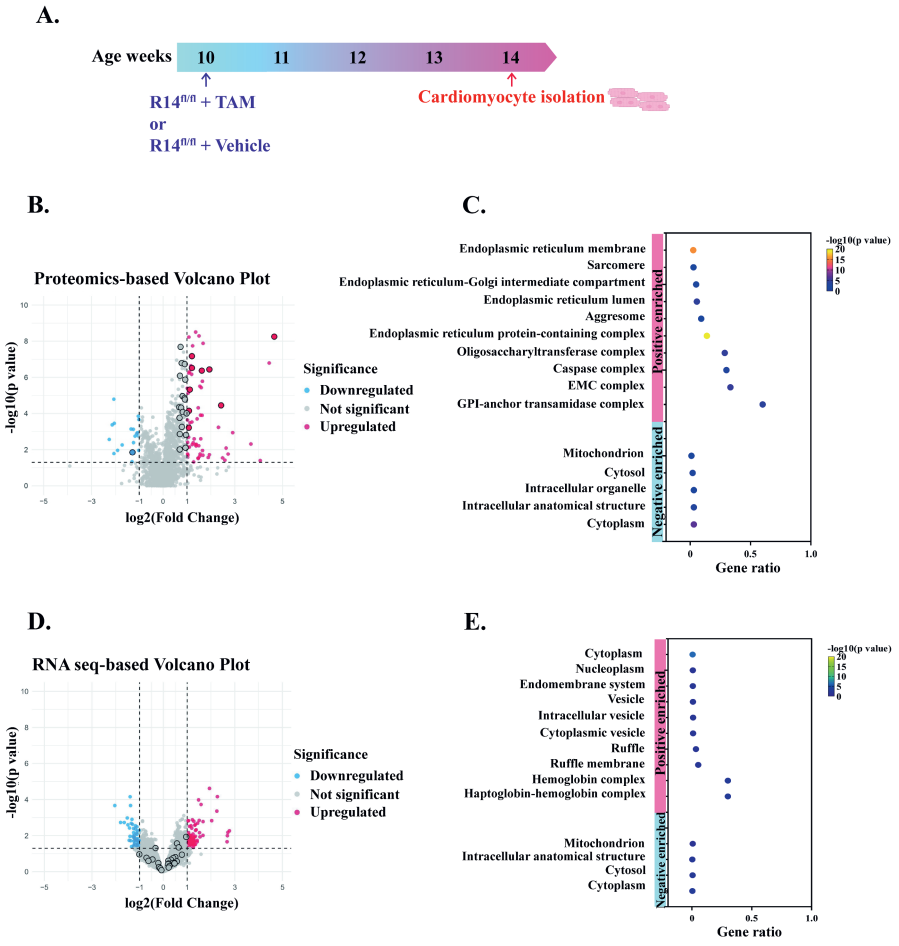

Figure 5. ER-associated protein upregulation identified by cardiomyocyte proteomics is not reflected at the transcriptomic level.

(A) Schematic overview of the cardiomyocytes isolation performed at 4 weeks after treatment. **(B)** Volcano plot based on proteomic analysis showing significantly upregulated and downregulated proteins between tamoxifen-treated and non-treated $R14^{fl/fl}$ mice. **(C)** Gene Ontology (GO) enrichment analysis of cellular component significantly altered between groups based on proteomic analysis. (**D)** Volcano plot based on RNA sequencing showing significantly upregulated and downregulated transcripts between tamoxifen-treated and non-treated mice. **(E)** GO enrichment analysis of cellular component based on transcriptomic data. In volcano plots, red dots indicate significantly upregulated proteins/transcripts, and blue dots indicate significantly downregulated ones. For proteomics, differential protein expression was assessed by two-tailed unpaired Student's t-tests. Resulting p-values were adjusted using the Benjamini-Hochberg method to control the false discovery rate. For RNA sequencing, differential gene expression was analyzed using DESeq2 with the Wald test and Benjamini-Hochberg correction for multiple testing. (n = 5 per group).

3.5 Validation of ERAD substrates in the SEL1L-HRD1 pathway

The upregulation of S/ER proteins in the absence of corresponding transcriptional changes was indicative for altered S/ER protein homeostasis. The endoplasmic reticulum-associated degradation (ERAD) pathway, plays an important role for maintaining protein homeostasis within the S/ER. Although several ERAD pathways exist we focused on the Suppressor/Enhancer of Lin-12-Like Protein 1-Like (SEL1L) and (HMG-CoA reductase degradation protein 1 (HRD1) complex pathway, which has been extensively studied. SEL1L is a single-pass ER membrane protein that has a critical role in substrate recruitment to HRD1, a multi-span transmembrane E3 ligase, which facilitates substrate retrotranslocation and ubiquitination, which marks proteins for proteasome mediated degradation.[18] An extensive list of SEL1L-HRD1 substrates has been published[19] and we therefore compared this list to the proteome dataset generated here. Notably, of the 28 matched SEL1L-HRD1-associated proteins, many exhibited robust upregulation at the protein level, without corresponding changes at the transcript level, indicative for post-transcriptional regulation by ERAD **(Figure 6A and Supplemental table 4)**.

To further validate the proteomic findings of ERAD-associated protein upregulation, we performed Western blot analysis and immunofluorescence staining. Western blot was conducted on whole heart tissue lysates collected from tamoxifen treated PLN-R14$^{fl/fl}$ mice at multiple time points and untreated controls, providing a temporal profile of ERAD protein expression during disease progression. Consistent with the finding above, we observed a progressive increase in the expression levels of bonafide SEL1L-HRD substrates Mfge8 and Ddost following genetic conversion **(Figure 6B-D)**. In parallel, immunofluorescence double staining on isolated cardiomyocytes from tamoxifen-treated and vehicle-treated mice at 4 weeks post-injection, further confirmed the co-localization of some key ERAD components (SEL1L, EMC2, PDIA, and Mfge8) with PLN-positive S/ER clusters **(Figure 6E)**. Consistent with the proteomics and western blot result, histological staining also confirmed progressive accumulation of Mfge8, which co-localized with PLN clusters **(Supplemental figure 3A)**. Since Mfge8 is also a secreted protein, we investigated blood plasma levels, but did not observe a significant increase in late-stage homozygous PLN-R14$^{fl/fl}$ mice compared to WT controls **(Supplemental figure 3B)**. These results suggest that the upregulation of ERAD-related proteins is a dynamic and progressive process during disease development in PLN-R14$^{fl/fl}$ hearts. The demonstrated spatial association of these ERAD components with PLN-positive SR clusters may indicate that altered ERAD pathway activity may contribute to PLN-R14del cardiomyopathy.

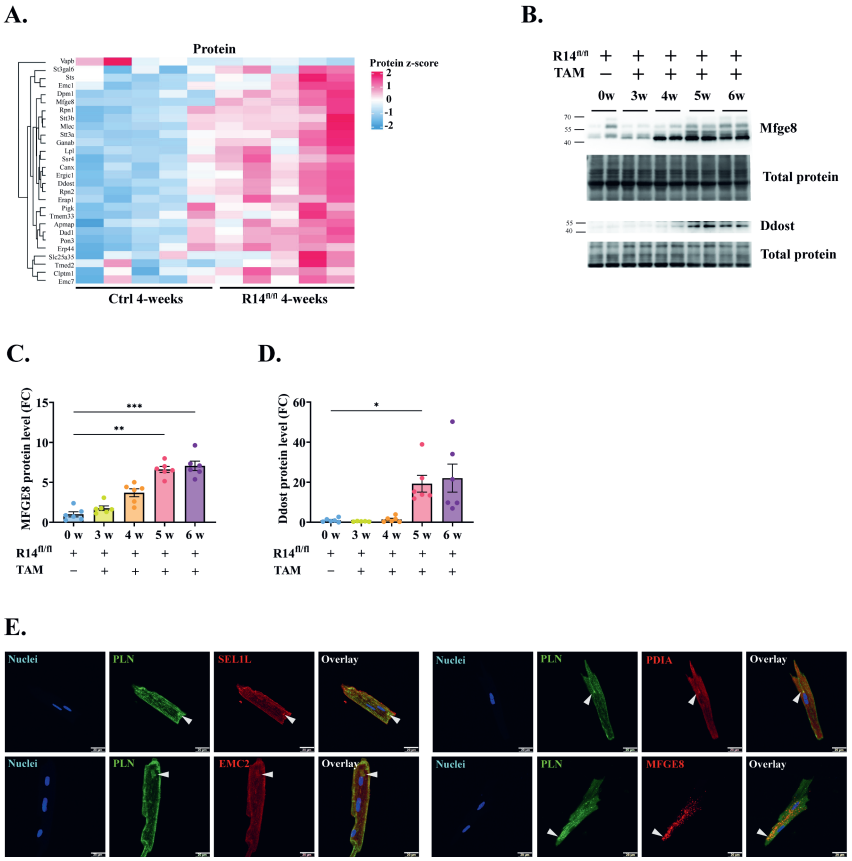

Figure 6. Dynamic upregulation of ERAD substrates and co-localization with PLN-positive clusters. **(A)** Heatmap comparing protein Z-scores $\log_2$ fold changes (FC) for the 28 matched ERAD substrate candidates in cardiomyocytes isolated 4 weeks post-injection from vehicle-treated and tamoxifen-treated PLN-R14$^{fl/fl}$ mice. **(B)** Representative averaged Western blot images of Mfge8 (top) and Ddost (bottom), along with corresponding total protein staining, in ventricular tissue collected from tamoxifen-treated PLN-R14$^{fl/fl}$ at different weeks after conversion. Quantification of protein levels is presented as fold change (FC) for and Mfge8 **(C)** and Ddost **(D)** (n = 6 per group). **(E)** Representative immunofluorescent double staining for PLN (green) together with Suppressor/Enhancer of Lin-12-like protein 1 (SEL1L), ER membrane protein complex subunit 2 (EMC2), Protein disulfide-isomerase A4 (PDIA), or Milk fat globule-EGF factor 8 protein (Mfge8) (red) in cardiomyocytes of tamoxifen-treated PLN-R14$^{fl/fl}$ mice at 4 weeks post-conversion. Nuclei are stained blue with 4',6-diamidino-2-phenylindole (DAPI). Merged images (overlay) demonstrate the spatial co-localization of ERAD-related proteins with PLN-positive structures. White arrows indicate clusters of the target protein (scale bars, 20 µm). $^{*}p<0.05$, $^{**}p<0.01$, $^{***}p<0.001$ (Kruskal-Wallis with Dunn's multiple comparisons test).

4. Discussion

In this study, we characterized the pathological features of PLN-R14del cardiomyopathy using an MerCreMer inducible PLN-R14del mouse model. The inducible model ensured synchronized disease onset in adult animals, allowing for a more accurate temporal analysis of the emerging pathological features, including early disease onset. Notably, early hallmarks of PLN-R14del cardiomyopathy,[7] small sarcoplasmic reticulum (SR) clusters, are already detectable as early as 3-4 weeks after induction, albeit in limited and subtle forms. These initial SR clusters progressively enlarge and accumulate, reflecting disease progression over time. Furthermore, transcriptomic and proteomic analyses of isolated cardiomyocytes from converted mice four weeks after injections revealed a significant upregulation of ERAD components at the protein level, without corresponding changes at the mRNA level, suggesting that altered S/ER proteostasis is an important early disease mechanism. Together, these findings highlight S/ER clustering as an early pathological hallmark, and point toward dysregulated protein homeostasis, rather than transcriptional reprogramming, as a key driver of disease initiation.

Induced PLN-R14del$^{fl/fl}$ mice developed cardiac remodeling and dysfunction by 5 weeks post-induction, and progressed to severe heart failure by 6 weeks, with similar characteristics as constitutive homozygous PLN-R14del mice.[17] Immunofluorescence staining revealed that PLN clusters progressively enlarged as the disease advanced. To more clearly visualize these structures, electron microscopy combined with PLN labeling was employed. This revealed that by 4 weeks, PLN-labeled membrane structures were reduced in the sarcomere region and began to accumulate in the vicinity of mitochondria. By 6 weeks, large areas of PLN-labeled membranes were predominantly found in the mitochondrial zone, while such structures were rarely detected near sarcomeres. These findings suggest that, as the disease progresses, intracellular membrane remodeling occurs in cardiomyocytes, ultimately leading to the formation of larger clusters that may compromise overall cardiomyocyte function.

To investigate the pathological processes that cardiomyocytes undergo prior to the onset of cardiac remodeling and heart failure, we isolated cardiomyocytes from PLN-R14$^{fl/fl}$ mice at 4 weeks post-induction and performed both proteome and transcriptome analyses. In a previous study, proteomic profiling of whole heart tissue revealed many alterations, including inflammatory responses, fibrotic remodeling, mitochondrial dysfunction, and amino acid metabolism.[17] However, these changes were likely influenced by non-cardiomyocyte populations such as fibroblasts and endothelial cells, potentially obscuring cardiomyocyte-specific pathological signatures. In this study, by analyzing purified cardiomyocytes, we uncovered for the first time a distinct upregulation of proteins that localize to the sarcoplasmic/endoplasmic reticulum (S/ER) in PLN-R14del cardiomyopathy. These included molecular chaperones and quality control proteins such as CANX, ERP44, GANAB, and MLEC, which are critical for glycoprotein folding and ER quality control.[20-22] Subunits of the endoplasmic reticulum

membrane protein complex (EMC1, EMC7, TMEM)[23] and the oligosaccharyltransferase (OST) complex (STT3A, STT3B, DAD1, DDOST, RPN1, RPN2)[24] were also upregulated, consistent with increased demand for membrane protein biogenesis and N-linked glycosylation. Additional enrichment of TMED2, ERGIC1, and PIGK suggested alterations in ER-Golgi trafficking,[25-27] while metabolic regulators such as APMAP, LPL, and MFGE8 indicated broader changes in lipid and glycoprotein homeostasis.[28-30] Together, the enrichment of these processes indicates increased burden on ER folding capacity, enhanced demand for glycosylation, and structural remodeling of intracellular membranes during the early stages of disease.

Among the ER-related alterations identified in purified cardiomyocytes, a notable upregulation of substrates of the endoplasmic reticulum-associated degradation (ERAD) machinery, SEL1L-HRD1, were observed.[31-33] The accumulation of proteins from this ERAD axis, without corresponding mRNA elevation, suggests that cardiomyocytes bearing the PLN-R14del mutation experience significant ER stress, or alternatively, are hampered in these control pathways to maintain ER homeostasis. Since these two options are interrelated, we currently cannot distinguish between them.

Our findings that p62 is markedly upregulated and co-localizes with PLN clusters in cardiomyocytes are consistent with previous reports linking PLN-R14del to impaired proteins homeostasis and potential impaired autophagic clearance of protein aggregates.[17,34] Interestingly, the HRD1 ubiquitin-ligase has also been shown to be able to stimulate p62-dependent selective autophagy.[35] Whether the accumulation of p62 reflects a blockade in this selective autophagy rather than enhanced recruitment by the HRD1 ubiquitin-ligase requires further investigations. Altogether, this spatial association suggests that the malfunction of the ERAD system induced by PLN-R14del leads to enhanced recruitment of p62-mediated autophagic pathways to mitigate proteotoxic stress. Such compensatory mechanisms may be essential in maintaining cardiomyocyte proteostasis during early disease stages.

Previous studies have identified MFGE8 as an endogenous negative regulator of pathological cardiac hypertrophy, and it has been proposed as both a potential biomarker and a therapeutic target for cardiac remodeling.[36] The increased Mfge8 levels observed PLN-R14del cardiomyocytes may represent a protective response, similar to elevation of natriuretic peptides, or alternatively reflect an impaired secretory pathway. Given that Mfge8 is an ER luminal protein whereas PLN is localized to the cytosolic face of the sarcoplasmic reticulum, a direct molecular interaction between them is highly unlikely. Therefore, the observed colocalization more likely reflects close spatial proximity within S/ER microdomains or indirect association through other membrane or luminal factors.

While activation of the ERAD pathway has been extensively documented in neurodegenerative and metabolic diseases, this study, to our knowledge, is the first to demonstrate its involvement in a genetic cardiomyopathy model driven by the PLN-

R14del mutation. These findings uncover a previously unrecognized aspect of PLN-R14del pathogenesis, highlighting the contribution of ER protein quality control mechanisms to cardiomyocyte dysfunction. Moreover, they suggest that therapeutic strategies aimed at modulating the ERAD machinery, either by enhancing its efficiency or preventing its exhaustion, may represent a novel avenue for treating this otherwise intractable condition.

This study has several limitations. First, the inducible MerCreMer system carries a potential risk of Cre-related toxicity, which could confound certain aspects of disease progression. However, tamoxifen addition to MerCreMer mice without the floxed PLN locus did not show cardiac impairment in our study, the observed alterations must be predominantly PLN-R14del specific. Second, homozygous $R14^{fl/fl}$ mice were used, whereas patients carry the PLN R14del mutation in a heterozygous state. Moreover, the model is restricted to cardiomyocytes, while in humans the mutation affects all cell types. Despite these limitations, the use of an inducible, cardiomyocyte-specific model provides important advantages, enabling mechanistic investigations that cannot be performed in human subjects. Finally, due to antibody availability and specificity, our validation was restricted to a limited number of ERAD-related proteins in this study.

In summary, this study demonstrates that the pathogenesis of PLN-R14del cardiomyopathy is characterized by early alterations in the S/ER proteome, occurring independently of changes in gene expression. Many of the affected S/ER proteins are substrates of the HRD1-ERAD pathway and accumulate upon the onset of abnormal S/ER cluster formation.

References

1. MacLennan DH, Kranias EG. Phospholamban: a crucial regulator of cardiac contractility. Nat Rev Mol Cell Biol 2003;4:566-577.
2. Rathod N, Bak JJ, Primeau JO, Fisher ME, Espinoza-Fonseca LM, Lemieux MJ, Young HS. Nothing Regular about the Regulins: Distinct Functional Properties of SERCA Transmembrane Peptide Regulatory Subunits. Int J Mol Sci 2021;22.
3. van der Zwaag PA, van Rijsingen IA, Asimaki A, Jongbloed JD, van Veldhuisen DJ, Wiesfeld AC, Cox MG, van Lochem LT, de Boer RA, Hofstra RM, Christiaans I, van Spaendonck-Zwarts KY, Lekanne dit Deprez RH, Judge DP, Calkins H, Suurmeijer AJ, Hauer RN, Saffitz JE, Wilde AA, van den Berg MP, van Tintelen JP. Phospholamban R14del mutation in patients diagnosed with dilated cardiomyopathy or arrhythmogenic right ventricular cardiomyopathy: evidence supporting the concept of arrhythmogenic cardiomyopathy. Eur J Heart Fail 2012;14:1199-1207.
4. Kobra H, Fotis K, Anthony O G, Jason R W, Luke P, Roy A L, Guo-Chang F, Dimitris T, Rohan R P, Gerald W 2nd D, David H M, Dimitrios Th K, Evangelia G K. A mutation in the human phospholamban gene, deleting arginine 14, results in lethal, hereditary cardiomyopathy. Proc Natl Acad Sci U S A 2006;103.
5. Stege NM, Eijgenraam TR, Oliveira Nunes Teixeira V, Feringa AM, Schouten EM, Kuster DWD, van der Velden J, Wolters AHG, Giepmans BNG, Makarewich CA, Bassel-Duby R, Olson EN, de Boer RA, Sillje HHW. DWORF Extends Life Span in a PLN-R14del Cardiomyopathy Mouse Model by Reducing Abnormal Sarcoplasmic Reticulum Clusters. Circ Res 2023;133:1006-1021.
6. Stege NM, de Boer RA, Makarewich CA, van der Meer P, Sillje HHW. Reassessing the Mechanisms of PLN-R14del Cardiomyopathy: From Calcium Dysregulation to S/ER Malformation. JACC Basic Transl Sci 2024;9:1041-1052.
7. Te Rijdt WP, van Tintelen JP, Vink A, van der Wal AC, de Boer RA, van den Berg MP, Suurmeijer AJ. Phospholamban p.Arg14del cardiomyopathy is characterized by phospholamban aggregates, aggresomes, and autophagic degradation. Histopathology 2016;69:542-550.
8. Te Rijdt WP, van der Klooster ZJ, Hoorntje ET, Jongbloed JDH, van der Zwaag PA, Asselbergs FW, Dooijes D, de Boer RA, van Tintelen JP, van den Berg MP, Vink A, Suurmeijer AJH. Phospholamban immunostaining is a highly sensitive and specific method for diagnosing phospholamban p.Arg14del cardiomyopathy. Cardiovasc Pathol 2017;30:23-26.
9. Eijgenraam TR, Boukens BJ, Boogerd CJ, Schouten EM, van de Kolk CWA, Stege NM, Te Rijdt WP, Hoorntje ET, van der Zwaag PA, van Rooij E, van Tintelen JP, van den Berg MP, van der Meer P, van der Velden J, Sillje HHW, de Boer RA. The phospholamban p.(Arg14del) pathogenic variant leads to cardiomyopathy with heart failure and is unreponsive to standard heart failure therapy. Sci Rep 2020;10:9819.
10. Claudia M, Marem E, Chiara F, Mara F, Paolo B, Elena S, Valentina P, Angela S M, Giulio P, Vivian Oliveira Nunes T, Rudolf A dB, Herman H W S, Francesco L, Antonio Z. Early consequences of the phospholamban mutation PLN-R14del(+/-) in a transgenic mouse model. Acta Physiol (Oxf) 2024;240.
11. Sun L, Eijgenraam TR, Amilon C, Janzen D, Hansson KM, Kubli DA, Spater D, Mullick AE, van der Meer P, Nunes Teixeira VO, Sillje HHW. In PLN-R14del mice, SR structure restoration,

rather than calcium cycling, is the dominant effector of PLN-ASO treatment. Cardiovasc Res 2025.

12. D S S, M N, M A C, S A W, T R K, K M T, J M P, J D M. Temporally regulated and tissue-specific gene manipulations in the adult and embryonic heart using a tamoxifen-inducible Cre protein. Circ Res 2001;89.
13. Percie du Sert N, Hurst V, Ahluwalia A, Alam S, Avey MT, Baker M, Browne WJ, Clark A, Cuthill IC, Dirnagl U, Emerson M, Garner P, Holgate ST, Howells DW, Karp NA, Lazic SE, Lidster K, MacCallum CJ, Macleod M, Pearl EJ, Petersen OH, Rawle F, Reynolds P, Rooney K, Sena ES, Silberberg SD, Steckler T, Wurbel H. The ARRIVE guidelines 2.0: Updated guidelines for reporting animal research. PLoS Biol 2020;18:e3000410.
14. Zacchigna S, Paldino A, Falcao-Pires I, Daskalopoulos EP, Dal Ferro M, Vodret S, Lesizza P, Cannata A, Miranda-Silva D, Lourenco AP, Pinamonti B, Sinagra G, Weinberger F, Eschenhagen T, Carrier L, Kehat I, Tocchetti CG, Russo M, Ghigo A, Cimino J, Hirsch E, Dawson D, Ciccarelli M, Oliveti M, Linke WA, Cuijpers I, Heymans S, Hamdani N, de Boer M, Duncker DJ, Kuster D, van der Velden J, Beauloye C, Bertrand L, Mayr M, Giacca M, Leuschner F, Backs J, Thum T. Towards standardization of echocardiography for the evaluation of left ventricular function in adult rodents: a position paper of the ESC Working Group on Myocardial Function. Cardiovasc Res 2021;117:43-59.
15. Ackers-Johnson M, Li PY, Holmes AP, O'Brien SM, Pavlovic D, Foo RS. A Simplified, Langendorff-Free Method for Concomitant Isolation of Viable Cardiac Myocytes and Nonmyocytes From the Adult Mouse Heart. Circ Res 2016;119:909-920.
16. Teng AC, Miyake T, Yokoe S, Zhang L, Rezende LM, Jr., Sharma P, MacLennan DH, Liu PP, Gramolini AO. Metformin increases degradation of phospholamban via autophagy in cardiomyocytes. Proc Natl Acad Sci U S A 2015;112:7165-7170.
17. Eijgenraam TR, Boogerd CJ, Stege NM, Oliveira Nunes Teixeira V, Dokter MM, Schmidt LE, Yin X, Theofilatos K, Mayr M, van der Meer P, van Rooij E, van der Velden J, Sillje HHW, de Boer RA. Protein Aggregation Is an Early Manifestation of Phospholamban p.(Arg14del)-Related Cardiomyopathy: Development of PLN-R14del-Related Cardiomyopathy. Circ Heart Fail 2021;14:e008532.
18. Wang HH, Biunno I, Sun S, Qi L. SEL1L-HRD1-mediated ERAD in mammals. Nat Cell Biol 2025;27:1063-1073.
19. Wei X, Lu Y, Lin LL, Zhang C, Chen X, Wang S, Wu SA, Li ZJ, Quan Y, Sun S, Qi L. Proteomic screens of SEL1L-HRD1 ER-associated degradation substrates reveal its role in glycosylphosphatidylinositol-anchored protein biogenesis. Nat Commun 2024;15:659.
20. Tiziana A, Massimo A, Alexandre M, Thomas S, Fabio T, Angela B, Roberto S. ERp44, a novel endoplasmic reticulum folding assistant of the thioredoxin family. EMBO J 2002;21.
21. Jingru C, Piaopiao W, Yu-He T, Hanjie L, Zibo W, Xiuyuan W, Xiaoman Z, Xiao-Dong G, Morihisa F, Ganglong Y. Proteome and Glycoproteome Analyses Reveal Regulation of Protein Glycosylation Site-Specific Occupancy and Lysosomal Hydrolase Maturation by N-Glycan-Dependent ER-Quality Control. J Proteome Res 2024;23.
22. Galli C, Bernasconi R, Solda T, Calanca V, Molinari M. Malectin participates in a backup glycoprotein quality control pathway in the mammalian ER. PLoS One 2011;6:e16304.
23. Qi Z, Xianjun Z, Lin Z. ER membrane complex (EMC): Structure, functions, and roles in diseases. FASEB J 2024;38.

24. Harada Y, Ohkawa Y, Kizuka Y, Taniguchi N. Oligosaccharyltransferase: A Gatekeeper of Health and Tumor Progression. Int J Mol Sci 2019;20.
25. Anwar MU, Sergeeva OA, Abrami L, Mesquita FS, Lukonin I, Amen T, Chuat A, Capolupo L, Liberali P, D'Angelo G, van der Goot FG. ER-Golgi-localized proteins TMED2 and TMED10 control the formation of plasma membrane lipid nanodomains. Dev Cell 2022;57:2334-2346 e2338.
26. Garcia-Cazorla A, Oyarzabal A, Saudubray JM, Martinelli D, Dionisi-Vici C. Genetic disorders of cellular trafficking. Trends Genet 2022;38:724-751.
27. Muniz M, Riezman H. Trafficking of glycosylphosphatidylinositol anchored proteins from the endoplasmic reticulum to the cell surface. J Lipid Res 2016;57:352-360.
28. Blessy P, Holly M, Rupali U-B, Monica R H, Son T, Goncalo Dias dV, Lauren Z, Charles K H, Jeffrey G M, Joan F-B, Thomas P M, Steven A F, W Mike H. Paraoxonase-like APMAP maintains endoplasmic-reticulum-associated lipid and lipoprotein homeostasis. Dev Cell 2025;60.
29. Ren Y, Liu W, Zhang J, Bi J, Fan M, Lv Y, Wu Z, Zhang Y, Wu R. MFG-E8 Maintains Cellular Homeostasis by Suppressing Endoplasmic Reticulum Stress in Pancreatic Exocrine Acinar Cells. Front Cell Dev Biol 2021;9:803876.
30. Yagyu H, Chen G, Yokoyama M, Hirata K, Augustus A, Kako Y, Seo T, Hu Y, Lutz EP, Merkel M, Bensadoun A, Homma S, Goldberg IJ. Lipoprotein lipase (LpL) on the surface of cardiomyocytes increases lipid uptake and produces a cardiomyopathy. Journal of Clinical Investigation 2003;111:419-426.
31. Bhattacharya A, Qi L. ER-associated degradation in health and disease - from substrate to organism. J Cell Sci 2019;132.
32. Qi L, Tsai B, Arvan P. New Insights into the Physiological Role of Endoplasmic Reticulum-Associated Degradation. Trends Cell Biol 2017;27:430-440.
33. Hwang J, Qi L. Quality Control in the Endoplasmic Reticulum: Crosstalk between ERAD and UPR pathways. Trends Biochem Sci 2018;43:593-605.
34. Vafiadaki E, Kranias EG, Eliopoulos AG, Sanoudou D. The phospholamban R14del generates pathogenic aggregates by impairing autophagosome-lysosome fusion. Cell Mol Life Sci 2024;81:450.
35. Feng L, Zhang J, Zhu N, Ding Q, Zhang X, Yu J, Qiang W, Zhang Z, Ma Y, Huang D, Shen Y, Fang S, Yu Y, Wang H, Shen Y. Ubiquitin ligase SYVN1/HRD1 facilitates degradation of the SERPINA1 Z variant/alpha-1-antitrypsin Z variant via SQSTM1/p62-dependent selective autophagy. Autophagy 2017;13:686-702.
36. Deng KQ, Li J, She ZG, Gong J, Cheng WL, Gong FH, Zhu XY, Zhang Y, Wang Z, Li H. Restoration of Circulating MFGE8 (Milk Fat Globule-EGF Factor 8) Attenuates Cardiac Hypertrophy Through Inhibition of Akt Pathway. Hypertension 2017;70:770-779.

Supplementary Figures

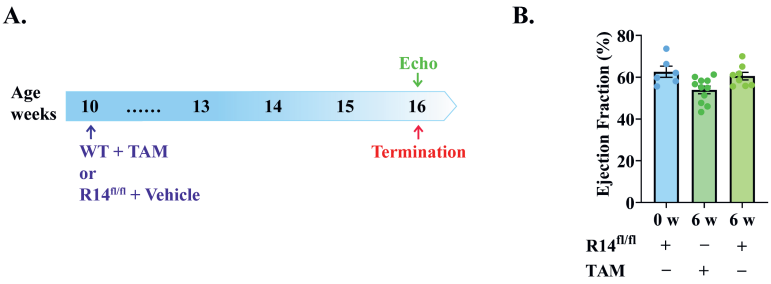

Supplementary Figure S1. Cardiac function remained comparable between control groups.
(A) Schematic overview of the *in vivo* study design of control mice. **(B)** Ejection fraction of non-treated PLN-R14$^{fl/fl}$ mice terminated at 0 week after injection (10 weeks of age), PLN-WT mice treated with tamoxifen and PLN-R14$^{fl/fl}$ mice treated with vehicle were terminated at 6 weeks after first injection (n ≥ 6 per group) (Kruskal-Wallis with Dunn's multiple comparisons test).

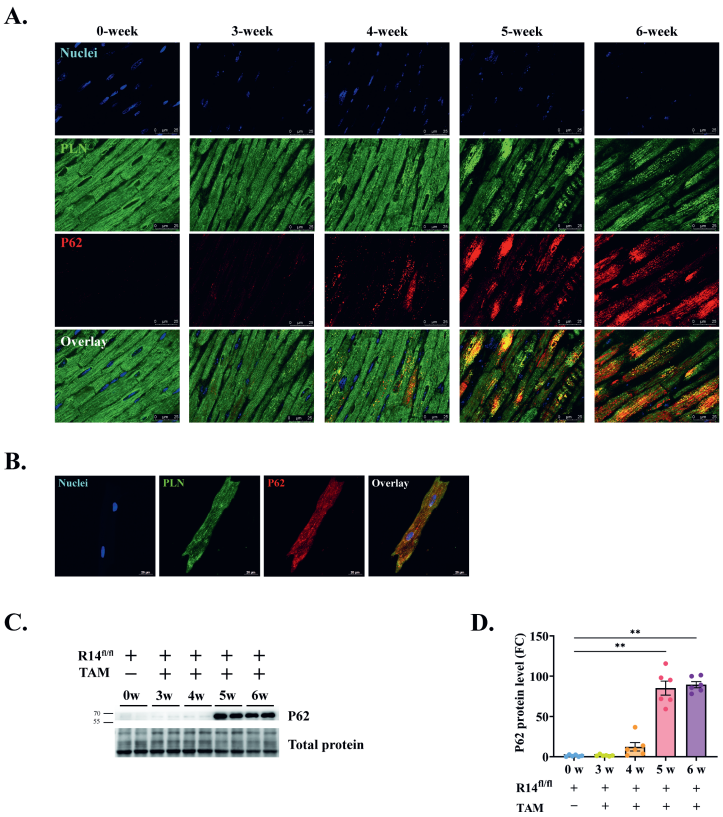

Supplementary Figure S2. Progressive upregulation of P62 and its colocalization with PLN clusters in cardiomyocytes.

(A) Representative immunofluorescent staining of PLN (green) together with P62 (SQSTM1) (red) in ventricular tissue of tamoxifen treated PLN-R14del$^{fl/fl}$ mice collected at different weeks after conversion (scale bars, 25 µm). **(B)** Immunofluorescent double staining of PLN (green) and P62 (SQSTM1) (red) in cardiomyocytes isolated from tamoxifen-treated PLN-R14$^{fl/fl}$ mice at 4 weeks post-conversion. Nuclei are stained blue with 4',6-diamidino-2-phenylindole (DAPI). (scale bars, 20 µm). **(C)** Representative averaged Western blot images of P62 (top) and corresponding total protein staining (bottom) in ventricular tissue collected at different weeks after conversion. Quantification of protein levels is presented as fold change (FC) of P62 **(D)** (n = 6 per group). $^{**}p<0.01$ (Kruskal-Wallis with Dunn's multiple comparisons test).

A.

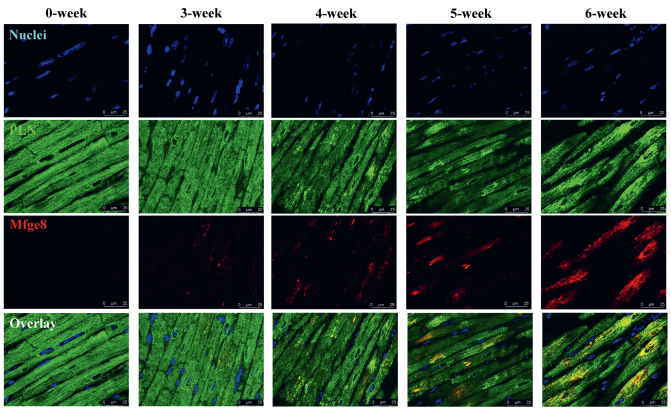

B.

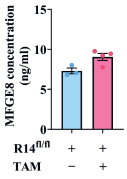

Supplementary Figure S3. Mfge8 upregulation and colocalization with PLN clusters during disease progression.

(A) Representative immunofluorescent staining of PLN (green) together with Mfge8 (red) in ventricular tissue of PLN-R14del$^{fl/fl}$ mice collected at different weeks after conversion (scale bars, 25 µm). **(B)** Plasma Mfge8 concentration measured by ELISA in WT and 6-weeks old homozygous PLN-R14$^{fl/fl}$ mice (this is not inducible). Data are presented as mean ± SEM (WT, n = 3; PLN-R14$^{fl/fl}$ n=4). Statistical analysis was performed using the Mann-Whitney test.

Supplementary Tables

Supplementary Table S1. Antibodies used for histological staining.

Primary antibody	Host	Cat. No.	Supplier	Dilution
Anti-PLN	Rabbit	ab219626	Abcam	1:1,000
Anti-PLN	Mouse	MA3-922	Thermo Fisher Scientific	1:200
Anti-SEL1L	Rabbit	ab78298	Abcam	1:100
Anti-EMC2	Rabbit	25443-1-AP	Proteintech	1:100
Anti-PDIA	Rabbit	#3501S	Cell signaling	1:100
Anti-Mfge8	Goat	AF2805	R&D Systems	1:100
Anti-P62	Rabbit	ab109012	Abcam	1:100

Secondary antibody	Antigen	Label	Cat. No.	Supplier	Dilution
Donkey anti-rabbit	Rabbit	Alexa488	A21206	Thermo Fisher Scientific	1:100
Donkey anti-mouse	Mouse	Alexa555	A31570	Thermo Fisher Scientific	1:100
Donkey anti-mouse	Mouse	Alexa488	A21202	Thermo Fisher Scientific	1:100
Donkey anti-rabbit	Rabbit	Alexa555	A31572	Thermo Fisher Scientific	1:100
Donkey anti-goat	Goat	Alexa555	A21432	Thermo Fisher Scientific	1:100

Supplementary Table S2. Primer sequences used for qPCR.

Gene	Protein		Sequence (5'-3')
Nppa	Atrial Natriuretic Peptide	Forward Reverse	GCTTCCAGGCCATATTGGAG GGTGGTCTAGCAGGTTCTTG
Timp1	Tissue Inhibitor of Metalloproteinases-1	Forward Reverse	CAACGAGACCACCTTATACC CATATCCACAGAGGCTTTCC
Col1a1	Collagen type 1 alpha 1 chain	Forward Reverse	AGAGCATGACCGATGGATTC CGCTGTTCTTGCAGTGATAG
Rplp0	Ribosomal protein, large P0 (36B4)	Forward Reverse	AACGGGTACAAACGAGTC AGATGGATCAGCCAAGAAG

Supplementary Table S3. Antibodies used for Western blot.

Primary antibody	Host	Cat. No.	Supplier	Dilution	Molecular weight (kDa)
Anti-Mfge8	Goat	AF2805	R&D Systems	1:800	60-70
Anti-OST48(DDOST)	Mouse	sc-74408	Santa cruz	1:100	48

Secondary antibody	Antigen	Label	Cat. No	Supplier	Dilution
Rabbit anti-mouse	Mouse	HRP	P0260	Dako	1:2,000
Goat anti-rabbit	Rabbit	HRP	P0448	Dako	1:2,000
Donkey anti-goat	goat	HRP	A21432	Invitrogen	1:2,000

Supplementary Table S4. Substrate matched with ERAD pathway.

		RNA-sequencing			Proteomics		
name	**Descriptions**	**log2FC**	**P-value**	**-log10(Pvalue)**	**log2FC**	**P-value**	**-log10(Pvalue)**
Mfge8	Lactadherin	0.193	0.388	0.411	4.653	5.60E-09	8.251
Sts	Steryl-sulfatase	Na	Na	Na	2.428	3.53E-05	4.452
Ergic1	Endoplasmic reticulum-Golgi intermediate compartment protein 1	-0.183	0.564	0.249	1.936	3.65E-07	6.438
Dpm1	Dolichol-phosphate mannosyltransferase subunit 1	-1.011	0.109	0.961	1.619	4.24E-07	6.372
Stt3a	Dolichyl-diphosphooligosaccharide--protein glycosyltransferase subunit STT3A	0.460	0.320	0.495	1.206	3.03E-07	6.519
Ddost	Dolichyl-diphosphooligosaccharide--protein glycosyltransferase 48 kDa subunit	0.363	0.348	0.458	1.205	6.71E-08	7.173
Dad1	Dolichyl-diphosphooligosaccharide--protein glycosyltransferase subunit DAD1	0.218	0.354	0.451	1.117	4.76E-06	5.322
Clptm1	Putative lipid scramblase CLPTM1	0.413	0.176	0.754	1.084	7.04E-05	4.153
Pigk	GPI-anchor transamidase	0.778	0.114	0.941	1.076	0.000608	3.216
Ssr4	Translocon-associated protein subunit delta	0.571	0.027	1.566	0.986	9.8E-05	4.009
St3gal6	Type 2 lactosamine alpha-2,3-sialyltransferase	0.253	0.492	0.308	0.959	0.001532	2.815
Tmed2	Transmembrane emp24 domain-containing protein 2	0.316	0.218	0.661	0.939	0.007886	2.103
Rpn2	Dolichyl-diphosphooligosaccharide--protein glycosyltransferase subunit 2	0.957	0.012	1.929	0.924	1.34E-06	5.874
Mlec	Malectin	0.643	0.045	1.344	0.913	1.67E-05	4.776
Lpl	Lipoprotein lipase	-0.329	0.049	1.308	0.907	1.84E-07	6.735
Stt3b	Dolichyl-diphosphooligosaccharide--protein glycosyltransferase subunit STT3B	0.224	0.594	0.226	0.898	1.40E-05	4.853
Erp44	Endoplasmic reticulum resident protein 44	-0.081	0.829	0.082	0.821	8.23E-05	4.085
Rpn1	Dolichyl-diphosphooligosaccharide--protein glycosyltransferase subunit 1	0.500	0.156	0.807	0.813	1.10E-05	4.959
Tmem33	Transmembrane protein 33	-0.458	0.210	0.677	0.784	0.000549	3.261
Erap1	Endoplasmic reticulum aminopeptidase 1	Na	Na	Na	0.779	1.63E-07	6.789
Emc1	ER membrane protein complex subunit 1	0.468	0.349	0.457	0.754	4.76E-05	4.322
Canx	Calnexin	0.204	0.250	0.602	0.731	2.06E-08	7.685
Ganab	Neutral alpha-glucosidase AB	0.566	0.267	0.573	0.706	8.15E-07	6.089
Slc25a35	Solute carrier family 25 member 35	Na	Na	Na	0.700	0.001369	2.864
Pon3	Serum paraoxonase/lactonase 3	-0.708	0.170	0.770	0.696	0.009711	2.013
Emc7	ER membrane protein complex subunit 7	-0.130	0.664	0.178	0.687	0.000173	3.762
Apmap	Adipocyte plasma membrane-associated protein	-0.627	0.252	0.598	0.676	4.45E-05	4.352
Vapb	Vesicle-associated membrane protein-associated protein B	-0.213	0.332	0.478	-1.283	0.014096	1.851

Chapter 5

In PLN-R14del mice, SR structure restoration, rather than calcium cycling, is the dominant effector of PLN-ASO treatment

Liu Sun [1], Tim R. Eijgenraam [1], Carl Amilon [2], David Janzén [2], Kenny M. Hansson [3], Dieter A. Kubli [4], Daniela Später [3], Adam E. Mullick [5], Peter van der Meer [1], Vivian Oliveira Nunes Teixeira [1], Herman H.W. Silljé [1]*

[1]Department of Cardiology, University Medical Center Groningen, University of Groningen, Groningen, The Netherlands
[2]Drug Metabolism and Pharmacokinetics, Research and Early Development, Cardiovascular, Renal and Metabolism, BioPharmaceuticals R&D, AstraZeneca, Gothenburg, Sweden
[3]Bioscience Cardiovascular, Research and Early Development, Cardiovascular, Renal and Metabolism (CVRM), BioPharmaceuticals R&D, AstraZeneca, Gothenburg, Sweden
[5]Ionis Pharmaceuticals, Carlsbad, CA, USA

Cardiovasc Research. 2025 Sep 4;121(13):2042–2054

Abstract

Aims

Phospholamban (PLN) acts as an inhibitory regulator of calcium uptake in the sarco-/endoplasmic reticulum (SR) of cardiomyocytes. The pathogenic variant, PLN-R14del, leads to dilated and/or arrhythmogenic cardiomyopathy. Previous studies demonstrated that PLN-targeting antisense oligonucleotides (ASOs) can mitigate disease progression in mice. However, it remains unclear whether the protective effects of PLN-ASO therapy are due to improved calcium homeostasis or via reduction of abnormal PLN-SR clusters, a hallmark of this disease.

Methods and results

Homozygous PLN-R14del ($R14^{\Delta/\Delta}$) mice were randomized to injections with various doses of PLN-ASO (3, 7, 15 or 25 mg/kg) or a scrambled control. Consistent with previous findings, $R14^{\Delta/\Delta}$ mice exhibited severe cardiac dysfunction, myocardial fibrosis, and aberrant SR clusters by 7 weeks of age. ASO-treated $R14^{\Delta/\Delta}$ mice displayed a dose-dependent preservation of cardiac function with diminished remodeling and extended lifespan. Correspondingly, abnormal PLN-SR clustering was diminished by ASO therapy in a dose-dependent manner, and SR structure returned to a normal state. Calcium dynamics were investigated separately on isolated cardiomyocytes from treated mice. In wild-type (WT) mice, ASO (25 mg/kg) mediated PLN depletion significantly enhanced calcium and contractile dynamics, confirming effective target engagement. In $R14^{\Delta/\Delta}$ cardiomyocytes, however, ASO treatment showed limited effects on calcium dynamics. Calcium transient decay and sarcomeric shortening were already enhanced in $R14^{\Delta/\Delta}$ cardiomyocytes compared to WT, suggesting a partial loss of the PLN-R14del calcium inhibitory function. This preexisting acceleration of calcium dynamics likely accounts for the limited impact of ASO therapy on calcium regulation in $R14^{\Delta/\Delta}$ mice.

Conclusions

PLN-ASO treatment demonstrated a dose-dependent restoration of SR organization and a concomitant increase in lifespan in PLN-R14del mice. The enhanced SR calcium uptake in PLN-R14del mice suggests a partial loss of inhibitory function, limiting ASO therapy's effects on calcium dynamics. This implies that PLN-ASO therapy acts predominantly via restoration of SR structure in PLN-R14del cardiomyopathy.

Translational Perspective

Human carriers of a p.Arg14del (R14del) variant of the phospholamban (PLN) gene face high risk of developing dilated and/or arrhythmogenic cardiomyopathy, progressing to severe heart failure. As patients are mostly non-responsive to standard care and no specific treatment for exists, heart transplantation is often a last option. PLN antisense therapy shows promise as the first precision medicine, targeting the root cause of the disease. Our data indicate that, at optimal dosing, PLN antisense therapy halts disease progression and extends lifespan in mice. While PLN-ASO enhances calcium cycling, its primary therapeutic effect in PLN-R14del cardiomyopathy is by reducing harmful PLN-SR clusters.

1. Introduction

Phospholamban (PLN) is a small protein that resides in the membrane of the sarcoplasmic reticulum (SR) and is predominantly expressed in ventricular cardiomyocytes. Its primary role is to inhibit the uptake of calcium ions (Ca^{2+}) from the cytosol into the SR by interacting with the sarco/endoplasmic reticulum Ca^{2+}-ATPase 2a (SERCA2a) pump.[1,2] Several pathogenic mutations in the gene encoding PLN have been linked to cardiomyopathies.[2] Among these, the p.Arg14del (R14del) variant is the most well-known and frequently occurring mutation, which can lead to dilated and/or arrhythmogenic cardiomyopathy, often culminating in severe heart failure (HF).[3] Currently, there is no specific treatment for this form of cardiomyopathy, and heart transplantation is often required as a last option.[4-6]

Using a PLN-R14del mouse model that has similar disease characteristics as in humans, we recently showed that silencing therapy with an antisense oligonucleotide (ASO), targeting *Pln* mRNA for degradation, could halt disease development and prolong lifespan of PLN-R14del mice.[7] This was true for a prophylactic treatment, starting before disease development, but also for a therapeutic treatment, starting at the time of early or advanced disease.[7,8] Therapeutic treatment at the early disease stage could halt further decline in cardiac function, attenuated cardiac fibrosis and hence extended survival of PLN-R14del mice. Moreover, PLN immunohistochemistry showed that dense PLN staining of abnormal SR clusters, a hallmark of this disease,[9] was observed at the start of treatment but was strongly reduced after ASO treatment.[8] This might indicate that normal SR structure is restored by ASO treatment, but this needs confirmation beyond PLN (mis)localization. Also, until now, calcium cycling has not been investigated in the context of ASO treatment, while this is particularly interesting for PLN-related cardiomyopathies. Originally, it was thought that PLN-R14del would be a super-inhibitor of SERCA2a.[10] Badone et al,[11] however, contradicted this superinhibition theory using human PLN-R14del iPSC derived cardiomyocytes and reported reduced inhibitory activity. Subsequently, also studies in mice carrying a genomic PLN-R14del locus reported reduced inhibitory activity on SERCA2a in cardiomyocytes and this was true for both heterozygous and homozygous PLN-R14del mice.[9,12] Studies utilizing PLN-targeting antisense therapy could further unravel the impact of PLN silencing on cardiomyocyte calcium handling and SR clustering in PLN-R14del cardiomyopathy, potentially offering deeper insights into the disease mechanism.[13]

Previous studies showed therapeutic effects in PLN-R14del mice using PLN-ASO.[4,7,8] In this study, we aim to demonstrate the dose-dependent therapeutic effects of a novel PLN-ASO in PLN-R14del mice, with the potential for these findings to translate into meaningful benefits for human PLN-R14del cardiomyopathy. Subsequently, we show for the first time that abnormal SR clustering is resolved and SR organization is rescued in these mice in a dose-dependent manner, which directly correlates with disease progression. Finally, this study shows that PLN-ASO treatment does enhance SR

calcium uptake in wild-type (WT) mice, but to a far lesser extent in PLN-R14del mice. Together, these data indicate that the therapeutic effect of PLN silencing in PLN-R14del cardiomyopathy is primarily mediated by improvements in SR structure rather than by enhanced calcium cycling.

2. Methods

2.1 Study design and animal model

The generation and phenotypic characterization of the PLN-R14del mouse model, and housing of mice have been described before.[5] Male and female WT and homozygous PLN-R14del ($R14^{\Delta/\Delta}$) mice were enrolled in this study. Before treatment initiation at 5 weeks of age, baseline echocardiography was performed. Based on sex, weight and baseline cardiac function, $R14^{\Delta/\Delta}$ mice were subsequently randomized to six different groups receiving PLN-ASO (5'-GCATATCAATTTCCTG-3') injections, at a dose of 0 (vehicle only; Dulbecco's PBS), 3, 7, 15 or 25 mg/kg/injection or a scrambled-ASO (5'-GGCCAATACGCCGTCA-3') of 25 mg/kg/injection (n=8 per group). Doses were selected based on dose response-modelling from previous in vivo studies[7,8] and were chosen to cover PLN inhibition between 20% to 70%. The time to initiate treatment with ASO was informed by previous studies to give optimal opportunity to show a treatment effect. ASOs were designed and produced by Ionis Pharmaceuticals (CA, USA). Six WT mice were included as healthy controls, receiving vehicle injections. Injections started at 5 weeks of age, with four injections in the first week, followed by a weekly maintenance injection of the same dose in the subsequent weeks. $R14^{\Delta/\Delta}$ mice were monitored until they reached the humane endpoint (ejection fraction (EF) <10%, >20% weight loss or lethargy and dyspnea), which generally occurs at 7-8 weeks of age.[5] In addition, when the average EF of an ASO dosing group was <20% or when >30% of the mice of an ASO dosing group reached the humane endpoint, the entire experimental group was terminated. Surviving $R14^{\Delta/\Delta}$ groups, together with the WT mice, were kept until 21 weeks of age, with follow-up echocardiograms at 7, 15 and 21 weeks of age. At sacrifice, hearts were collected for histological and molecular analyses. Echocardiography and termination were conducted under anesthesia with 2.5% isoflurane mixed with oxygen. In a separate experiment for calcium handling and sarcomere measurements in isolated cardiomyocytes, an additional 10 WT and 10 $R14^{\Delta/\Delta}$ mice were treated with vehicle or 25 mg/kg PLN-ASO between 3 and 5 weeks of age, following the abovementioned regimen. This study was approved by the Dutch Central Authority for Scientific Procedures on Animals (license numbers AVD1050020199105 and AVD10500202115446) and the Animal Welfare Body of the University of Groningen (permit numbers IVD199105-01-011 and IVD2115446-02-003), followed the guidelines set out in the Directive 2010/63/EU of the European Parliament for using animals in research and were reported in line with the Animal Research: Reporting of *In Vivo* Experiments (ARRIVE) guidelines.[14]

2.2 Echocardiography

Left ventricular (LV) morphology and function were monitored using a Vevo 3100 preclinical imaging system equipped with a 40-MHz MX550D linear array transducer (FUJIFILM VisualSonics, Canada), as previously described.[9] Recordings were analyzed using Vevo LAB software version 5.7.1 (FUJIFILM VisualSonics). Data acquisition and analysis adhered to the guidelines provided by the European Society of Cardiology Working Group on Myocardial Function.[15]

2.3 Euthanasia

Euthanasia was performed under anesthesia using a mixture of oxygen and 2.5% isoflurane. After ensuring deep anesthesia, the abdominal and thoracic cavities were opened, blood was collected via the abdominal aorta, and saline was used to flush the circulatory system via the heart. The heart was carefully excised, rinsed in an ice-cold 1 M potassium chloride (KCl) solution (Merck Millipore, Germany). A transverse mid-section of the heart was preserved for histological examination, and the remaining tissue samples were promptly snap-frozen in liquid nitrogen for further molecular analyses.

2.4 Histological staining

Transverse cardiac slices of both ventricles were preserved in a 4% formaldehyde solution (10% formalin; Klinipath, The Netherlands) for at least 24 h. After fixation, heart tissues were dehydrated using an automated system (Leica TP1020; Leica Microsystems, Germany), embedded in paraffin, and sectioned into 4-µm thick slices for histological analysis. Tissue sections were deparaffinized before proceeding with staining procedures.

Masson's trichrome staining was performed to identify collagen deposition, adhering to standard protocols. Subsequently, the entire stained sections were scanned using a Nanozoomer 2.0-HT digital slide scanner (Hamamatsu Photonics, Japan). Quantification of fibrosis in each section was accomplished by analyzing the percentage of the total section area occupied by fibrotic tissue using the positive Pixel Count v9 algorithm of Aperio's ImageScope software version 12.4.0 (Leica Microsystems).

To evaluate PLN clustering, ventricular tissue sections were stained with a rabbit anti-PLN primary antibody (Cell Signaling Technologies, MA, USA), followed by labeling with an Alexa 555-conjugated secondary antibody. Cell boundaries were visualized using fluorescein isothiocyanate (FITC)-conjugated wheat germ agglutinin (WGA), and nuclei were stained with 4',6-diamidino-2-phenylindole (DAPI). PLN clusters were quantified in 30-50 cardiomyocytes per mouse (n=6 per group). The cluster-positive cells were presented as per 0.1 mm^2, as indicated by the scale bar.

To show the co-localization of PLN and other SR proteins in mouse cardiac tissue samples, SERCA2a or HRC (histidine-rich calcium-binding protein) were co-stained with PLN using fluorescently-labeled secondary antibodies. Specific antibodies used in immunohistochemistry are listed in **Supplementary Table S1**.

Fluorescent staining images were acquired using a Leica TCS SP8X confocal microscope (Leica Microsystems). PLN/WGA/DAPI localization and colocalization of SERCA2a or HRC with PLN were captured using a 63x objective (numerical aperture 1.4, pinhole size 95.5 µm).

2.5 Quantitative Polymerase Chain Reaction (qPCR)

Total RNA was extracted from snap-frozen ventricular tissue using TRI Reagent (Sigma-Aldrich, MO, USA) according to the manufacturer's protocol. Complementary DNA (cDNA) synthesis was performed using the QuantiTect reverse transcription kit (Qiagen, Germany). Quantitative polymerase chain reaction (qPCR) was conducted with iQ SYBR Green Supermix (Bio-Rad, CA, USA) on a C1000 Thermal Cycler CFX 384 Real-Time PCR Detection System (Bio-Rad). Gene expression levels were analyzed using Bio-Rad CFX Manager 3.0 software. All gene expression levels were normalized to the reference gene *Rplp0* (36B4) and reported as fold changes relative to the WT control group. The primer sequences used for qPCR are listed in Supplementary **Table S2**. The qPCR primers used for PLN mRNA quantification were designed downstream of the R14del mutation site. Primer binding and amplification efficiency are therefore similar for the WT and PLN-R14del transcript.

2.6 Western blot

Total protein from snap-frozen ventricular tissue was extracted using Radioimmunoprecipitation Assay (RIPA) buffer as described previously.[5] Protein concentrations were measured using a Pierce bicinchoninic acid (BCA) protein assay kit (Thermo Scientific, MA, USA). Samples were heated to 95°C for 5 min for PLN or 50°C for 15 min for SERCA2a, followed by loading onto a sodium dodecyl sulfate-polyacrylamide gel electrophoresis (SDS-PAGE) system. Equal amounts of protein were loaded, with 5 µg per well for PLN and 10 µg per well for SERCA2a. Proteins separated by SDS-PAGE were then transferred to an Immuno-Blot polyvinylidene fluoride (PVDF) membrane (Bio-Rad) using a semi-dry transfer system (Amersham Biosciences, UK). The total protein level in each sample was determined using the Revert 700 Total Protein Stain Kit (LI-COR Biosciences, NE, USA), which was subsequently used for protein normalization. Membranes were blocked with blocking buffer and incubated overnight at 4°C with a primary antibody, followed by a one-hour incubation at room temperature with a secondary antibody. Detection was carried out using enhanced chemiluminescence with the Western Lightning Ultra Chemiluminescent Substrate (PerkinElmer, MA, USA) and visualized with the Amersham ImageQuant 800 Western blot imaging system (Cytiva, MA, USA). Quantification of target proteins was performed using Image Studio Lite Software version 5.2 (LI-COR Biosciences). Protein expression values were reported as fold changes relative to the WT control group. Primary and secondary antibodies that were used are presented in Supplementary **Table S3**.

Total protein from snap-frozen isolated cardiomyocytes was extracted using RIPA buffer. To quantify PLN protein levels, a 12-230 kDa Separation Module (ProteinSimple, CA, USA) was used on an automated Western blot system (Jess Simple Western; ProteinSimple) following the manufacturer's instructions. Protein lysates were used at 1 mg/ml together with an anti-PLN antibody (1:50, Cell Signaling Technologies) and an Anti-Rabbit Detection Module (ProteinSimple). Protein expression was normalized by protein normalization module (ProteinSimple) following the manufacturer's protocol.

2.7 Electron microscopy

Electron microscopy (EM) was performed as reported previously.[9,16] Briefly, LV myocardial tissue was cut into 1 mm^3 pieces and fixed in EM fixative (2% paraformaldehyde and 2% glutaraldehyde in 0.1M sodium cacodylate (PH 7.4)) overnight at 4°C. The fixative was subsequently replaced with fresh buffer (0.5% paraformaldehyde and 2% glutaraldehyde in 0.1 M sodium cacodylate, pH 7.4) to allow for prolonged storage and improved preservation of cellular ultrastructure. Post-fixation was carried out using 1% osmium tetroxide and 1.5% potassium ferrocyanide. The samples were then sectioned, mounted on single-slot cupper grids, and contrasted with 4% neodymium acetate. Sections were imaged using scanning transmission electron microscopy (STEM) (Zeiss Supra55, Germany).

2.8 Contraction and calcium measurements in isolated cardiomyocytes

Cardiomyocytes were isolated using a Langendorff-free method.[17] Cardiomyocytes were loaded with the calcium fluorophore Fura-2, AM and single cell calcium transients and sarcomere shortening were recorded using a MultiCell High Throughput system (IonOptix, MA, USA) under pacing conditions (1.5 Hz, 20 V) at 37 °C. At least 40 cells were included per mouse (n=5 per group). Measurements were done at baseline and following beta-adrenergic stimulation using 100 nM isoproterenol. Calcium and contractility data were analyzed using CytoSolver with default settings, while excluding cells with <5 transients and outliers outside mean ± 1.5 * interquartile range (IQR).

2.9 Statistical analyses

Data are presented as means ± standard error of the mean (SEM). Sarcomere length and ratiometric calcium transients are shown as line graphs. Quantification of SR-EM parameters and contractile and calcium parameters are displayed in SuperPlots presenting both individual cell values (transparent dots) and mean values per mouse (solid dots) with the matching colors.[18] Data of isolated cardiomyocytes were log-transformed and a hierarchical test with Bonferroni correction was applied in R version 4.4.0.[18] All other statistical analyses were performed using GraphPad Prism version 9.1.0. For statistical analysis of survival curves, a log-rank test was performed. For all other comparisons, nonparametric tests were performed due to small group sizes (n=5-8). Echocardiographic parameters at each timepoint were compared separately to the WT group of the same age using a Kruskal-Wallis test with post-hoc Dunn's multiple

comparisons test. At the 7-week time point, comparisons were made among all PLN-R14$^{\Delta/\Delta}$ groups. For other assays, a Mann-Whitney test was used to compare vehicle-treated R14$^{\Delta/\Delta}$ mice to WT mice (to evaluate differences between genotypes), followed by a Kruskal-Wallis test with post-hoc Dunn's multiple comparisons test for comparisons among the vehicle-treated and ASO-treated R14$^{\Delta/\Delta}$. P-values <0.05 were considered statistically significant. All data acquisition and analyses were performed in a blinded manner.

3. Results

3.1 PLN-ASO treatment rescues R14$^{\Delta/\Delta}$ mice from HF and premature death in a dose-dependent manner

PLN-ASO or vehicle treatment started at 5 weeks of age, in accordance to a previous study,[8] with four injections during the first week of treatment, followed by weekly injections of the indicated doses (**Figure 1A**). As expected, vehicle-treated R14$^{\Delta/\Delta}$ mice reached the humane endpoint at 7 weeks of age, which is in agreement with previous studies.[5] PLN-ASO treatment showed a dose dependent increase in survival of R14$^{\Delta/\Delta}$ mice, with the 3 mg/kg group surviving until 9 weeks of age, while those receiving 7 mg/kg reached the humane endpoint and were terminated at 11 weeks of age (**Figure 1B**). Importantly, the higher ASO dose groups of 15 and 25 mg/kg did not reach the humane endpoint and remained viable until the end of the experiment, except for one mouse in the 15 mg/kg group. All WT mice remained viable until the end of the experiment (**Figure 1B**).

Investigation of cardiac function, using echocardiography, also revealed a clear dose-response effect in the R14$^{\Delta/\Delta}$ mice (**Figure 1C-F**). From 5 weeks (start of treatment) to 7 weeks of age, a rapid decline in LVEF was observed in the vehicle-treated R14$^{\Delta/\Delta}$ group (R14$^{\Delta/\Delta}$ Ctrl), whereas the EF of WT mice remained >60% (**Figure 1C**). ASO treatment prevented heart function decline and with increasing doses, a more preserved EF was observed. Since it takes some time to reach sufficient depletion of PLN by ASO-mediated silencing, an immediate stabilizing effect on cardiac function was not expected. No additional echocardiograms were made of the R14$^{\Delta/\Delta}$ mice receiving vehicle and 3 mg/kg of ASO, because these animals reached the humane endpoint within 2 weeks after the first follow-up measurement. As R14$^{\Delta/\Delta}$ mice receiving 7 mg/kg of ASO became lethargic around 11 weeks of age, we performed an additional echo and this revealed a further decline in cardiac function compared to the previous analysis at 7 weeks of age (**Figure 1C**). Subsequently, these mice were terminated at this time point, because this group reached the predefined humane endpoint (group average EF <20%). Importantly, the EF of the 15 and 25 mg/kg groups did not decline further after the first follow-up echocardiogram (7 weeks of age), indicating stabilization of cardiac function (**Figure 1C**). This was even more profound in the highest dose group, suggesting that at this dose even some improvement may occur. LV end-systolic and end-diastolic internal diameters were significantly increased in vehicle-treated R14$^{\Delta/\Delta}$ mice as compared to WT mice, indicating ventricular dilatation,

which was dose-dependently rescued by PLN-ASO administration (**Figure 1D, E**). All observed effects were specific to PLN-ASO administration, as R14$^{\Delta/\Delta}$ mice injected with a scrambled ASO at the highest dose (25 mg/kg) showed the same rapid decline in cardiac function as untreated mice with an average EF of 13.0±1.1%, and reached the humane endpoint by 7 weeks of age (**Supplementary, Figure S1**). Together, these data demonstrate that PLN-ASO therapy exerts a dose-dependent effect on cardiac function and lifespan in PLN-R14$^{\Delta/\Delta}$ mice.

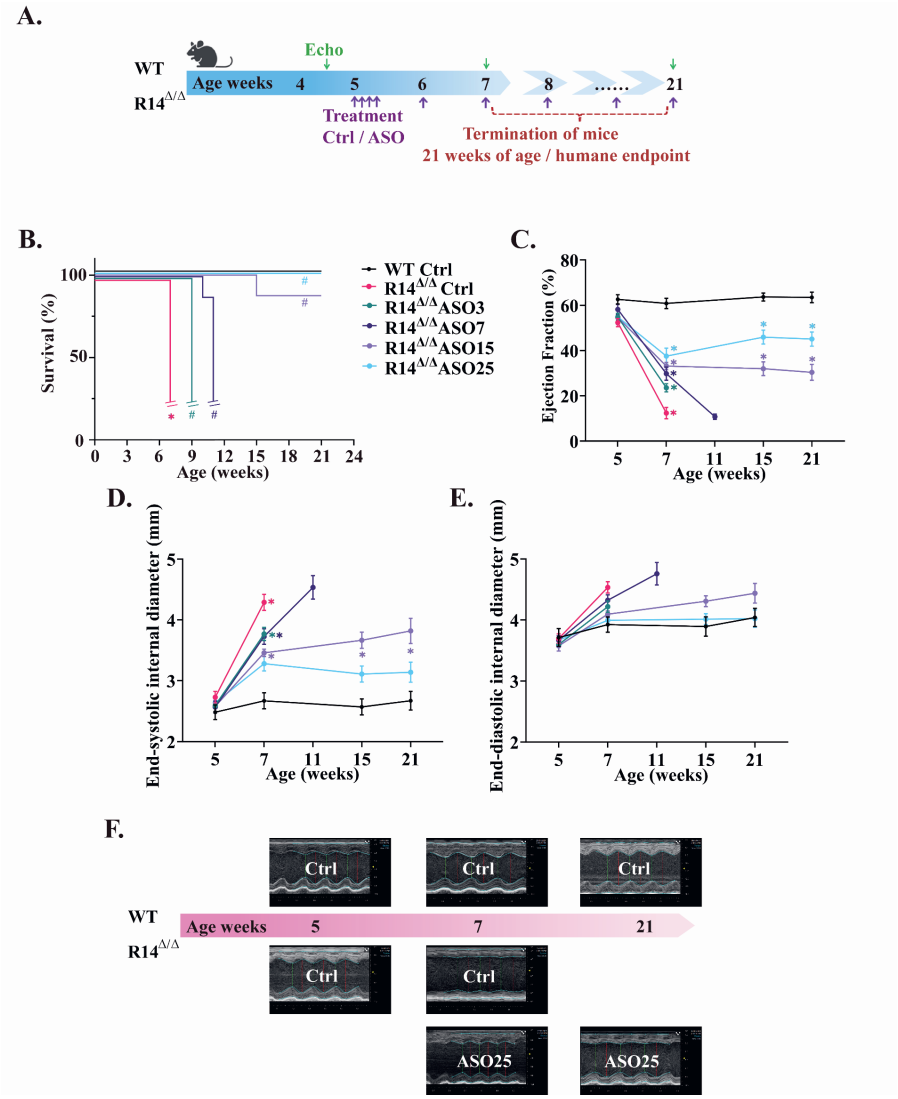

Figure 1. PLN-ASO therapy extends the lifespan and improves cardiac function of PLN-R14$^{\Delta/\Delta}$ mice.

(A) Schematic overview of the *in vivo* study design. **(B)** Survival curve of WT mice receiving vehicle injections (Ctrl; n=6) and PLN-R14$^{\Delta/\Delta}$ mice receiving vehicle injections (Ctrl) or 3, 7, 15 or 25 mg/kg of PLN-ASO (n=8 per group). The interrupted lines of the vehicle and low dose groups indicate that the predefined humane end-point was reached in these groups. *p=0.0001 compared to WT Ctrl; $^{\#}$p=0.0001 compared to R14$^{\Delta/\Delta}$ Ctrl (Log-rank test). **(C)** Ejection fraction, **(D)** end-systolic internal diameter, and **(E)** end-diastolic internal diameter of WT mice receiving vehicle injections (Ctrl; n=6) and PLN-R14$^{\Delta/\Delta}$ mice receiving vehicle injections (Ctrl) or 3, 7, 15 or 25 mg/kg of PLN-ASO (n=8 per group) at 5, 7, 11, 15 and 21 weeks of age. *p<0.05 compared to WT mice of corresponding age. Kruskal-Wallis with Dunn's multiple comparisons test). **(F)** Representative echocardiographic images of WT Ctrl, PLN-R14$^{\Delta/\Delta}$ Ctrl and PLN-R14$^{\Delta/\Delta}$ ASO25 mice at 5 (baseline), 7 and 21 weeks of age.

3.2 PLN depletion effectively mitigates cardiac remodeling in a dose-dependent manner

Next, to confirm effective depletion of PLN following PLN-ASO treatment, PLN expression was determined at both mRNA and protein level. Since R14$^{\Delta/\Delta}$ mice receiving vehicle or 3 or 7 mg/kg PLN-ASO did not survive until the 21-week time point, it is important to note that these cardiac samples are from time points corresponding to their maximal lifespan (**Figure 1B**). As shown, both gene (**Supplementary, Figure S2A**) and protein (**Figure 2A**) expression levels were dose-dependently decreased in hearts of ASO-treated R14$^{\Delta/\Delta}$ mice. We like to note that at 7 weeks of age, PLN levels are also lower in the R14$^{\Delta/\Delta}$ vehicle group as compared to the WT group (**Figure 2A** and **Supplementary, Figure S2A**). This has been observed before and is at least partially related to downregulation of PLN in this animal model, as present in this group at 7 weeks.[19] At the protein level this difference may also partly be explained by differences in antibody binding to wildtype PLN and PLN-R14del and therefore we have to be cautious with direct protein comparisons between WT and R14$^{\Delta/\Delta}$ groups. Moreover, cardiomyocyte density was approximately 25% lower in the R14$^{\Delta/\Delta}$ vehicle group compared to WT, consistent with previously reported cell death, which may contribute to the observed reduction in PLN levels (**Supplementary Figure S3**). However, a direct comparison of immunohistochemical staining for PLN and cardiac troponin revealed a pronounced decrease in PLN expression within cardiomyocytes (**Supplementary Figure S3**). While some bias in this quantification cannot be excluded, due to certain PLN clusters being out of focus, Western blot analyses corrected for cardiac troponin I and α-actinin levels also confirmed reduced PLN protein levels in the R14$^{\Delta/\Delta}$ vehicle group (**Supplementary Figure S4**). These findings corroborate earlier reports of cellular PLN downregulation in the context of heart failure.[8] The dose-dependent efficacy of ASO-mediated PLN protein depletion, calculated as percent reduction compared to vehicle-treated R14$^{\Delta/\Delta}$ mice, is shown in Supplementary **Table S4**. Besides PLN, also SERCA2a protein and gene (*Atp2a2*) expression levels were investigated (**Figure 2B**, **Supplementary Figure S2B**). SERCA2a was reduced in the R14$^{\Delta/\Delta}$ vehicle group and in the low dose ASO3 and

ASO7 treatment groups, but was restored by the high dose ASO treatment. The observed reduction in SERCA2a is consistent with findings in both mice and human, where decreased SERCA2a expression is associated with heart failure.[20,21] The restoration of SERCA2a expression in the high dose groups therefore aligns with improved cardiac function. Since a low SERCA2a/PLN ratio may contribute to heart failure,[20] we also measured the ratio in this study. Although no significant decrease was observed in vehicle-treated R14$^{\Delta/\Delta}$ mice, at high ASO doses SERCA2a/PLN ratios were increased (**Figure 2C**). Similar changes were also observed for SERCA2a gene expression and the ratio between gene expression levels of SERCA2a and PLN (**Supplementary Figure S2C**). Overall, these results confirm the expected dose-dependent reduction of cardiac PLN-R14del levels following PLN-ASO administration.

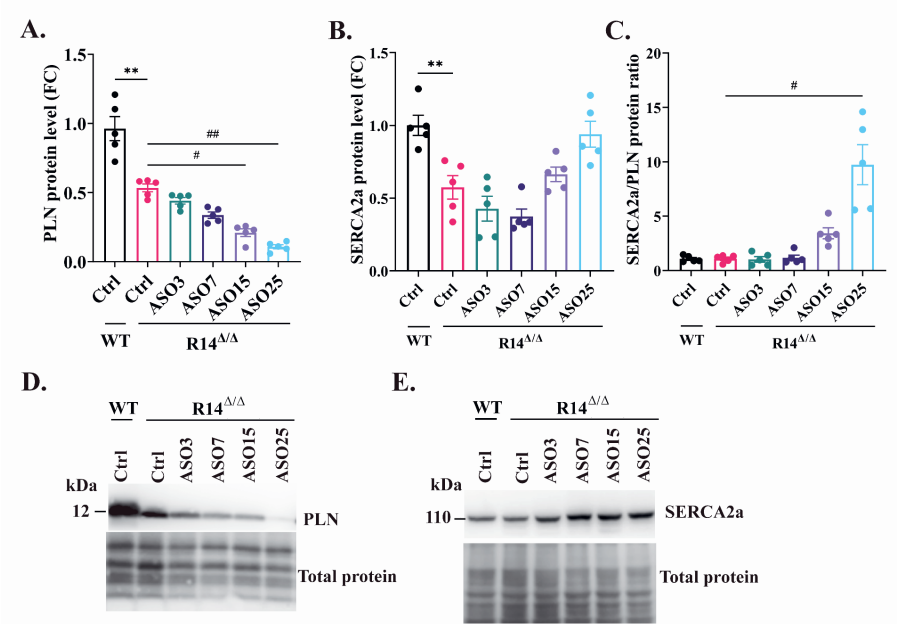

Figure 2. PLN-ASO administration effectively reduces the expression of PLN and increases the SERCA2a/PLN ratio in a dose-dependent manner.

Protein quantification of **(A)** PLN and **(B)** SERCA2a and **(C)** their ratio (SERCA2a/PLN) in ventricular tissue of vehicle-treated WT (Ctrl) and vehicle-treated PLN-R14$^{\Delta/\Delta}$ (Ctrl) mice and PLN-ASO-treated (3, 7, 15 or 25 mg/kg) PLN-R14$^{\Delta/\Delta}$ mice (n=5 per group). Ventricular tissue was collected at 21 weeks of age, except for those groups that reached the humane endpoint earlier (R14$^{\Delta/\Delta}$: Ctrl at 7 weeks, ASO3 at 9 weeks and ASO7 at 11 weeks). Protein expression normalized to total protein levels, is shown as fold change (FC) compared to WT Ctrl. Representative (average based) Western immunoblot images of **(D)** PLN (top), **(E)** SERCA2a (top) and their total protein staining (bottom). Cardiac tissue from mice was collected at various ages for protein isolation, as outlined in the study design. **p<0.01 (Mann-Whitney test), #p<0.05, ##p<0.01 (Kruskal-Wallis with Dunn's multiple comparisons test).

Molecular changes related to cardiac remodeling were also investigated. Gene expression of the cardiac wall stress and hypertrophy biomarker atrial natriuretic peptide (encoded by the *Nppa* gene) was significantly elevated in R14$^{\Delta/\Delta}$ vehicle group compared to WT (**Figure 3A**). Consistent with improved cardiac function in the 25 mg/kg PLN-ASO-treated R14$^{\Delta/\Delta}$ groups, *Nppa* was significantly reduced as compared to the vehicle-treated R14$^{\Delta/\Delta}$ group (**Figure 3A**). A similar dose-response effect was observed for fibrotic gene expression (*Timp1* and *Col1a1*), indicative of diminished fibrosis formation (**Figure 3B, C**). To corroborate this finding, histochemistry was performed, using Masson's trichrome staining to visualize myocardial fibrosis in ventricular sections (**Figure 3D**). As shown before,[5] in vehicle-treated R14$^{\Delta/\Delta}$ mice, cardiac fibrosis was significantly elevated as compared to WT mice (**Figure 3D, E**). Hearts from R14$^{\Delta/\Delta}$ mice treated with 3 and 7 mg/kg of ASO showed more collagen deposition as compared to the vehicle-treated R14$^{\Delta/\Delta}$ group. We believe that the increased lifespan of these low dose groups, as compared to the vehicle group, provides an increased time window for fibrosis development, ultimately resulting in higher levels of extracellular matrix. Most importantly, however, is that in fibrosis was not further elevated in the high dose groups. Thus, PLN-ASO therapy dose-dependently reduces natriuretic peptide expression and halts fibrosis formation in hearts of R14$^{\Delta/\Delta}$ mice, corroborating our *in vivo* findings.

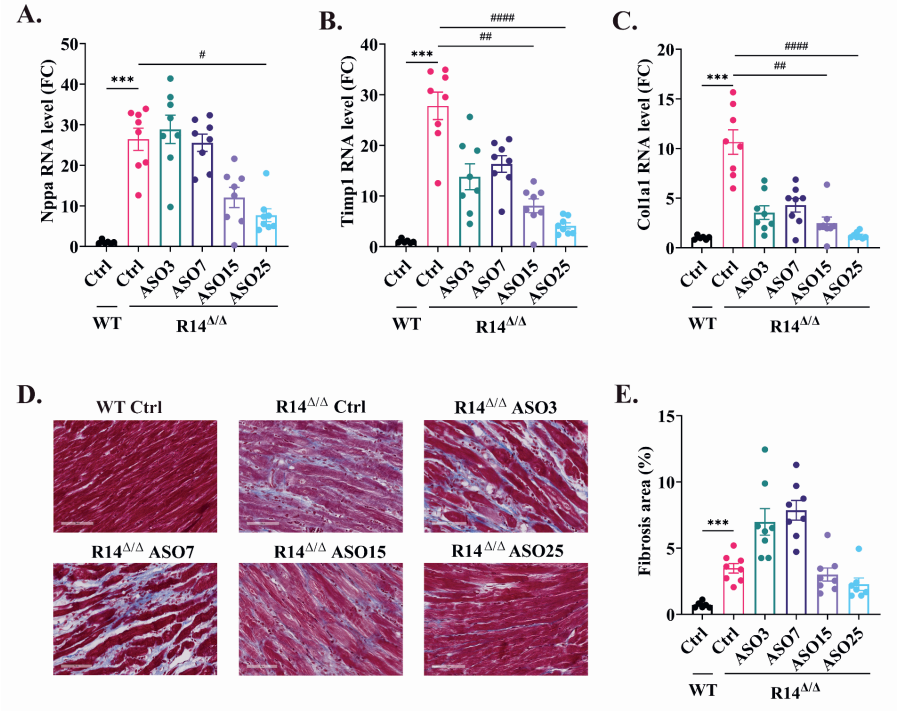

Figure 3. PLN depletion dose-dependently mitigates cardiac remodeling in hearts of PLN-R14$^{\Delta/\Delta}$ mice.

Ventricular gene expression of markers of cardiac remodeling. **(A)** atrial natriuretic peptide (*Nppa*), **(B)** Tissue Inhibitor of Metalloproteinases 1 (*Timp1*) and **(C)** collagen type I alpha 1 chain (*Col1a1*) of vehicle-treated WT (n=6) and ASO-treated (3, 7, 15 or 25 mg/kg) PLN-R14$^{\Delta/\Delta}$ mice (n=8 per group), normalized to 36B4 (*Rplp0*) housekeeping gene levels and shown relative fold change to WT Ctrl. **(D)** Representative (average based) Masson's trichrome-stained cardiac tissue sections of vehicle-treated WT and ASO-treated (3, 7, 15 or 25 mg/kg) PLN-R14$^{\Delta/\Delta}$ mice (scale bars, 70 μm). **(E)** Quantification of cardiac fibrosis in Masson's trichrome-stained cardiac tissue sections of vehicle-treated WT (n=6) and ASO-treated (3, 7, 15 or 25 mg/kg) PLN-R14$^{\Delta/\Delta}$ mice (n=8 per group), displayed as percentage of total stained area. Ventricular tissue was collected at 21 weeks of age, except for those groups that reached the humane endpoint earlier (R14$^{\Delta/\Delta}$: Ctrl at 7weeks, ASO3 at 9 weeks and ASO7 at 11 weeks). ***p<0.001 (Mann-Whitney test), $^{\#}$p<0.05, $^{\#\#}$p<0.01, $^{\#\#\#\#}$p<0.0001 (Kruskal-Wallis with Dunn's multiple comparisons test).

3.3 PLN silencing dose-dependently resolves detrimental SR clusters in PLN-R14$^{\Delta/\Delta}$ mice

A key hallmark of PLN-R14del cardiomyopathy in humans and mice is the occurrence of detrimental cardiac SR clusters, as evidenced by strong perinuclear PLN staining in R14$^{\Delta/\Delta}$ cardiomyocytes.[5,9] In vehicle-treated R14$^{\Delta/\Delta}$ mice, PLN clusters were highly prevalent with 17.7±1.3 cluster-positive cells per 0.1mm^2, whereas such clusters were not observed in WT mice (**Figure 4A, B**). Importantly, these SR clusters were dose-dependently reduced after ASO treatment and were nearly absent at the highest doses. Absence of PLN-positive clusters suggests that the organization of the SR is restored. We previously demonstrated that HRC and SERCA2a colocalize with PLN in aberrant SR clusters.[9] To confirm restructuring of reticulum membranes, we performed immunohistochemical double staining for SERCA2a/PLN and HRC/PLN in cardiomyocytes from both WT and R14$^{\Delta/\Delta}$ mice treated with either vehicle or 25 mg/kg ASO, assessing protein colocalization. (**Figure 5A, B**). Confocal imaging validated colocalization of these proteins and showed enrichment in the SR clusters of R14$^{\Delta/\Delta}$ mice. Importantly, ASO treatment normalized SERCA2a and HRC localization in the majority of R14$^{\Delta/\Delta}$ cardiomyocytes, confirming that ASO treatment restored SR organization. As PLN is not completely silenced upon ASO administration, low amounts of PLN and small SR clusters were observed in some cardiomyocytes of ASO-treated R14$^{\Delta/\Delta}$ mice. Together, these findings demonstrate that PLN-ASO therapy resulted in dose-dependent restoration of SR structure in hearts of PLN-R14$^{\Delta/\Delta}$ mice.

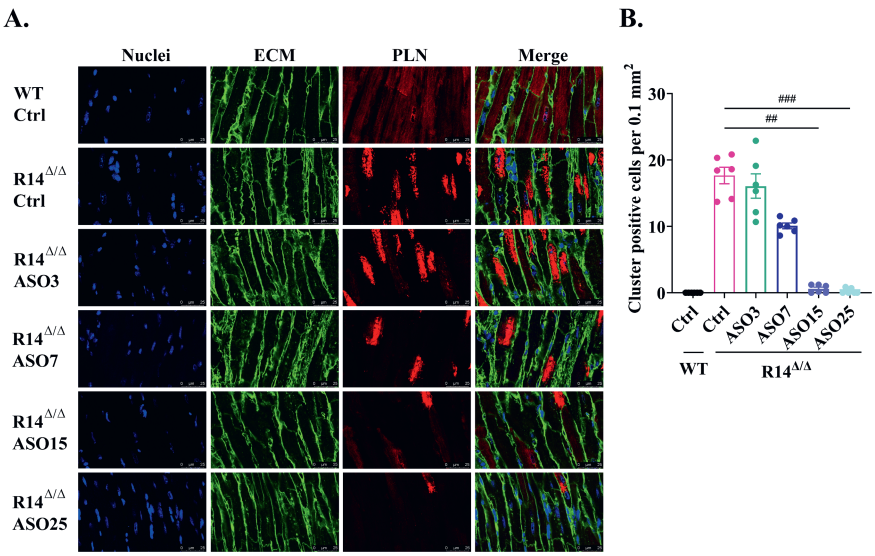

Figure 4. Silencing of PLN results in dose-dependent removal of abnormal intracardiomyocyte SR clusters in PLN-R14$^{\Delta/\Delta}$ mice.

(A) Representative (average based) immunofluorescence (IF) staining of PLN (red), together with wheat germ agglutinin (WGA) staining of extracellular matrix (green) and 4',6-diamidino-2-phenylindole (DAPI) staining of nuclei (blue) in ventricular tissue sections of vehicle-treated WT and ASO-treated (3, 7, 15 or 25 mg/kg) R14$^{\Delta/\Delta}$ mice (scale bars, 25 µm). **(B)** PLN-cluster-positive cardiomyocytes per 0.1 mm^2 of stained tissue sections (n=6 per group). Statistical comparison between WT and R14$^{\Delta/\Delta}$ mice receiving vehicle treatment was not performed as no SR clusters were found in WT hearts. $^{\#\#}p<0.01$, $^{\#\#\#}p<0.001$ (Kruskal-Wallis with Dunn's multiple comparisons test).

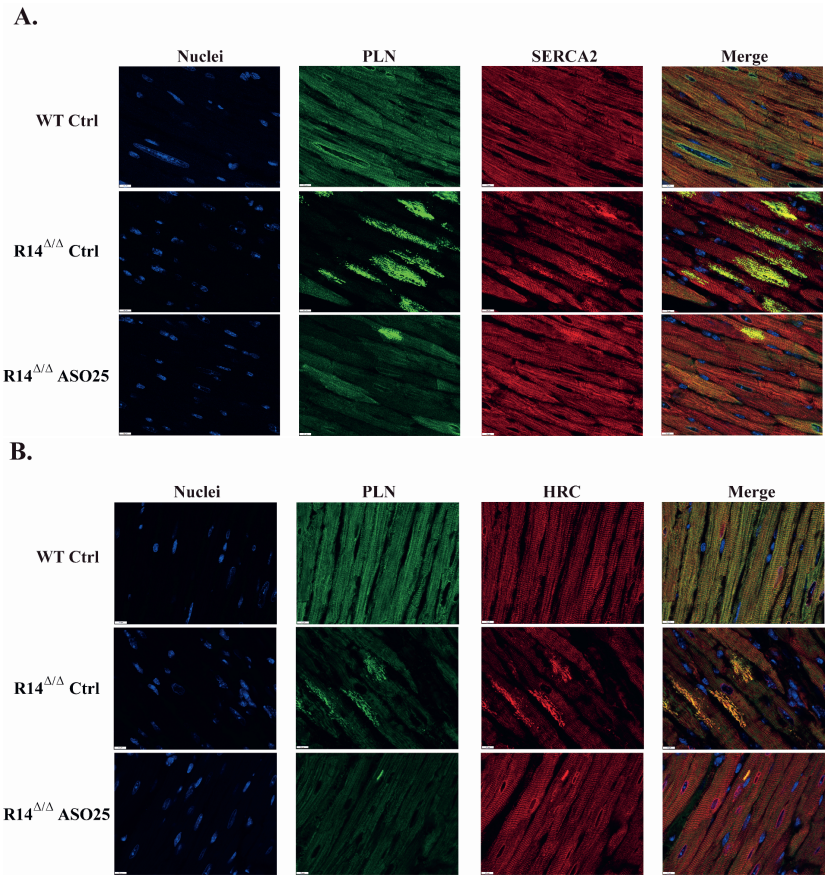

Figure 5. Treatment with PLN-ASO recovers SR organization in hearts of PLN-R14$^{\Delta/\Delta}$ mice. Representative immunofluorescent double staining for PLN (green) together with **(A)** SERCA2a (sarcoplasmic reticulum Ca^{2+} ATPase 2) or **(B)** HRC (histidine-rich calcium binding protein) (red) in ventricular tissue sections of WT Ctrl, R14$^{\Delta/\Delta}$ Ctrl and PLN-ASO (25 mg/kg) PLN-R14$^{\Delta/\Delta}$ mice (scale bars, 10 μm). Nuclei are stained blue using 4',6-diamidino-2-phenylindole (DAPI).

3.4 PLN-ASO treatment normalized SR structure in PLN-R14$^{\Delta/\Delta}$ mice

To visualize the sarcoplasmic reticulum (SR) structure in greater detail, electron microscopy (EM) was performed. Ventricular tissue from vehicle-treated wild-type (WT) mice and from both vehicle- and ASO25-treated R14$^{\Delta/\Delta}$ mice (all terminated at 7 weeks of age) was analyzed to assess SR restoration following ASO treatment (**Figure 6A–C**). In vehicle-treated R14$^{\Delta/\Delta}$ mice, cardiomyocytes exhibited a markedly aberrant and SR distribution, in contrast to the well-organized SR network seen in WT mice. Notably, SR density between sarcomeres was significantly reduced (**Figure 6B**), while SR accumulation around mitochondria was increased and appeared disorganized (**Figure 6C**). Strikingly, irregular membrane-like structures were frequently observed

near mitochondria, reflecting severe SR disarray. PLN-ASO25 treatment largely restored the normal SR architecture. Minimal distances between the SR and mitochondria, as well as the relative SR–T-tubule distances, were unchanged across groups (**Supplementary Figure 5**). Collectively, these findings indicate a pronounced remodeling of the longitudinal SR in R14$^{\Delta/\Delta}$ mice, which is substantially reversed by ASO treatment.

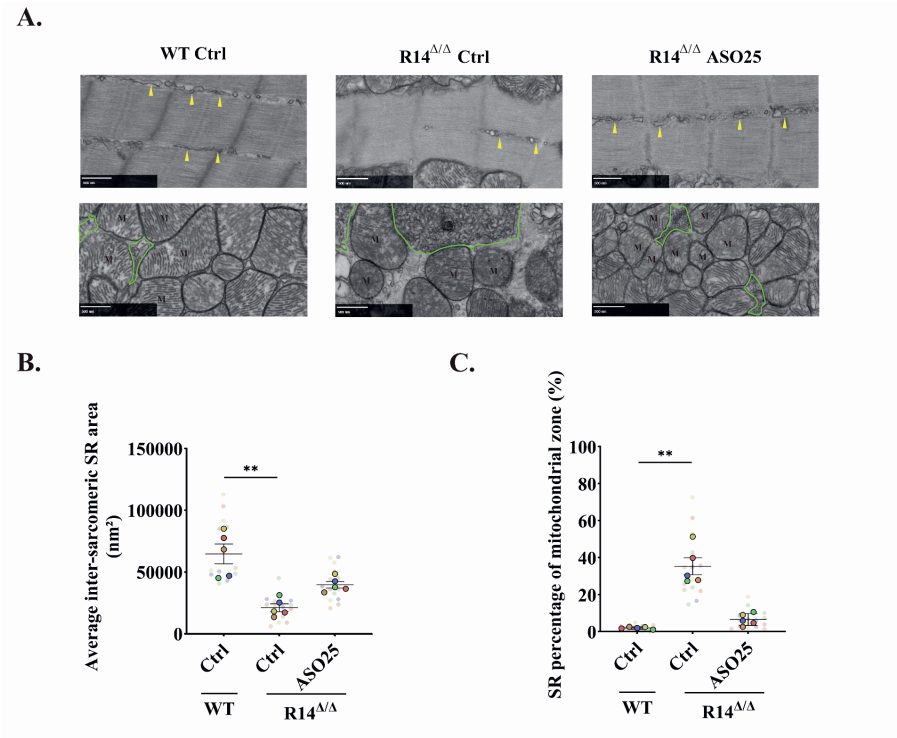

Figure 6. PLN-ASO treatment normalized SR structure in PLN-R14$^{\Delta/\Delta}$ mice.

(A) Representative electron microscopic images from cardiac ventricle of WT Ctrl, R14$^{\Delta/\Delta}$ Ctrl and PLN-ASO (25 mg/kg) PLN-R14$^{\Delta/\Delta}$ mice (scale bars, 500 nm) showing a reduced SR area (yellow arrow) between adjacent sarcomeres and clustered SR (green line circled) mislocalized around mitochondria (M). Quantification of SR area as the average SR area between adjacent sarcomeres **(B)** and a percentage within the mitochondrial zone **(C)**. (n=5 per group). *p<0.05, ***p<0.001, ****p<0.0001 (One-way ANOVA test with Turkey's multiple comparisons test). In panels B, C the colors of the individual cell values (transparent dots) match the colors of the average values (solid dots) of the same mouse.

3.5 The PLN-R14del pathogenic variant results in a partial loss of SERCA2a inhibitory function

Since PLN regulates SERCA2a activity and the effect of PLN-R14del on SERCA2a has been debated, we investigated calcium cycling and sarcomere contraction in isolated cardiomyocytes of vehicle- and ASO-treated WT and R14$^{\Delta/\Delta}$ mice. Due to the

challenges of isolating cardiomyocytes in advanced disease, including the presence of extensive cardiac fibrosis and the frailty of diseased cardiomyocytes, cardiomyocyte isolation was performed at 5 weeks of age (an early disease stage). To reach sufficient PLN depletion, ASO treatment (with the same frequency as in the abovementioned experiment) was initiated at 3 weeks of age with the highest ASO dose (25 mg/kg) (**Figure 7A**). This two-week treatment period resulted in strong reduction of PLN protein expression in cardiomyocytes isolated from WT and $R14^{\Delta/\Delta}$ mice, as compared to the vehicle-treated mice of the same genotype (**Supplementary Figure S6**). For calcium measurements, cardiomyocytes were loaded with the ratiometric calcium fluorophore Fura-2, after which calcium transients and sarcomere shortening were measured simultaneously in single cells. As expected, silencing of PLN and subsequent relief of SERCA2a inhibition resulted in faster SR calcium uptake in ASO-treated WT cardiomyocytes as evidenced by significantly smaller tau (time constant of calcium transient decay) values and significantly greater calcium peak amplitudes (**Figure 7B-D**). In $R14^{\Delta/\Delta}$ cardiomyocytes, tau was significantly lower and calcium transients were significantly higher than in WT cardiomyocytes, indicating a loss of SERCA2a inhibitory function in mice carrying the PLN-R14del pathogenic variant. Consistently, ASO-mediated depletion of PLN had a much smaller effect on calcium transient decay and did not alter calcium transient amplitudes in $R14^{\Delta/\Delta}$ mice. The ASO effects on calcium cycling were also reflected in cardiomyocyte relaxation, resulting in significantly accelerated sarcomere relaxation (tau) and significantly increased shortening amplitude in WT cardiomyocytes (**Figure 7E-G**). $R14^{\Delta/\Delta}$ cardiomyocytes demonstrated significantly smaller tau for sarcomere relaxation and sarcomeric shortening amplitude was significantly stronger as compared to WT cardiomyocytes. Consequently, the PLN silencing effects on contraction and relaxation were significant, though less pronounced in $R14^{\Delta/\Delta}$ compared to WT cardiomyocytes. We also performed beta-adrenergic stimulation using isoproterenol, which had a profound effect on all indicated parameters in vehicle treated WT cardiomyocytes (**Supplementary Figure S7**). The effect of isoproterenol is partially dependent on protein kinase A (PKA)-mediated phosphorylation of PLN, resulting in reduced SERCA2a inhibition and enhanced calcium cycling, contraction and relaxation.[22] Not surprisingly, isoproterenol had only limited additive effect on these parameters in ASO-treated WT cardiomyocytes (**Supplementary Figure S7**). Similarly, isoproterenol had limited additive effects in $R14^{\Delta/\Delta}$ cardiomyocytes with or without ASO treatment (**Supplementary Figure S7**), indicating that the R14del pathogenic variant of PLN is a partial loss-of-function mutation. Nevertheless, isoproterenol stimulation of ASO-treated WT and $R14^{\Delta/\Delta}$ cardiomyocytes further increase calcium transient amplitude, showing that PLN depletion did not deplete cardiac reserve. Altogether, the current study shows that PLN-ASO therapy has limited effects on calcium handling in PLN-R14del cardiomyopathy.

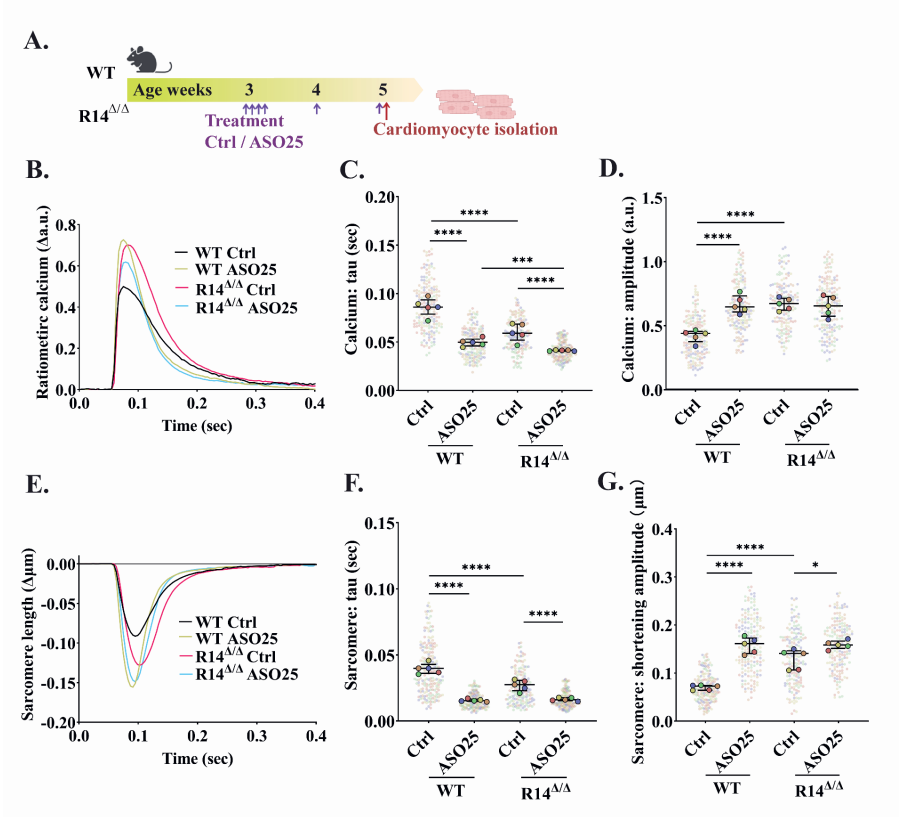

Figure 7. Isolated cardiomyocytes of PLN-R14$^{\Delta/\Delta}$ mice demonstrate accelerated calcium decay and sarcomeric relaxation with limited effect of PLN depletion.

(A) Schematic overview of the isolated cardiomyocyte study design. **(B)** Normalized ratiometric calcium transients under pacing conditions in cardiomyocytes isolated from WT and R14$^{\Delta/\Delta}$ mice treated with vehicle or ASO (25 mg/kg; averaged transients of 5 mice per group). **(C)** Calcium decay time constant (tau) and **(D)** calcium amplitude (n=5 per group). **(E)** Normalized sarcomere lengths under pacing conditions in cardiomyocytes isolated from WT and R14$^{\Delta/\Delta}$ mice treated with vehicle or ASO (25 mg/kg; averaged transients of 5 mice per group). **(F)** Sarcomere decay time constant (tau) and **(G)** sarcomere shortening amplitude (n=5 per group). *p<0.05, ***p<0.001, ****p<0.0001 (hierarchical statistical test with Bonferroni correction).[17] In panels C, D, F and G, the colors of the individual cell values (transparent dots) match the colors of the average values (solid dots) of the same mouse.

4. Discussion

In this study, we showed a dose dependent treatment effect with PLN-ASO on cardiac remodeling and survival in a murine PLN-R14del cardiomyopathy model. Our results revealed that PLN-R14$^{\Delta/\Delta}$ mice benefit already from ASO treatment at low doses (3 and 7 mg/kg) with a delay in cardiac functional decline and death. At higher doses (15 and 25 mg/kg), cardiac function was stabilized and lifespan was prolonged from 7 weeks to 21 weeks (the predefined endpoint of the experiment). Detrimental SR cluster formation, a hallmark of PLN-R14del cardiomyopathy,[9,23] showed a corresponding dose-dependent reduction. Investigation of other SR marker proteins showed that PLN depletion restored SR structure in R14$^{\Delta/\Delta}$ mice. Finally, we demonstrated that sarcomere relaxation and SR Ca^{2+} uptake was accelerated in isolated cardiomyocytes from WT mice after ASO treatment. In R14$^{\Delta/\Delta}$ mice, however, these parameters were already enhanced and ASO treatment had limited additional effect. This indicates that the PLN-R14del mutation is a partial loss-of-function variant. Therefore, the beneficial ASO effects do not primarily relate to enhanced SERCA2a-mediated calcium transport. Instead, the PLN-R14del mutation appears to gain a pathogenic function, disrupting normal SR structure, which ASO treatment helps to restore.

Previously, we have demonstrated that a high dose of ASO (≥50 mg/kg) significantly improved survival in R14$^{\Delta/\Delta}$ mice.[7,8] While this demonstrated proof of concept, we had not yet explored the dose-response effects or the underlying mechanisms. One proposed mechanism is the relief of PLN-R14del-mediated super-inhibition of SERCA2a following PLN depletion. Normally, phosphorylation of PLN by PKA alleviates SERCA2a inhibition, but PLN-R14del lacks the PKA consensus site and cannot be phosphorylated upon beta-adrenergic stimulation.[24] This led to the suggestion that PLN-R14del might constitutively inhibit SERCA2a.[10] However, while some studies support this idea, recent evidence suggests that PLN-R14del is a (partial) loss-of-function mutation with reduced or no inhibitory activity on SERCA2a.[12,25] If the PLN-R14del variant results in loss of inhibitory function, further alleviation of SERCA2a inhibition by ASO-mediated depletion of PLN would have limited therapeutic benefit. To investigate this further, we examined calcium cycling and contraction in isolated cardiomyocytes from WT and R14$^{\Delta/\Delta}$ mice, with and without ASO treatment, and in the presence and absence of beta-adrenergic stimulation. Consistent with recent studies,[9,12] we found that R14$^{\Delta/\Delta}$ cardiomyocytes exhibit enhanced SR calcium uptake compared to WT cardiomyocytes, indicating that PLN-R14del has reduced SERCA2a inhibitory activity. The effect of ASO treatment on calcium transient decay in R14$^{\Delta/\Delta}$ cardiomyocytes was therefore less pronounced, supporting the notion that PLN-R14del is a partial loss-of-function mutation. Additional studies with beta-adrenergic stimulation (isoproterenol) showed positive inotropic effects in WT cardiomyocytes consistent with, amongst others, PKA-mediated PLN phosphorylation relieving SERCA2a inhibition.[9] However, the response to isoproterenol stimulation was reduced in R14$^{\Delta/\Delta}$ cardiomyocytes, because these cells showed enhanced SR calcium uptake at baseline, similar to findings in PLN knockout (KO) mouse cardiomyocytes.[26,27]

Enhanced calcium dynamics were reflected by improved sarcomere relaxation parameters in R14$^{\Delta/\Delta}$ cardiomyocytes. Overall, our results provide evidence that PLN-R14del is a partial loss-of-function mutation.

As mentioned above, cardiomyocytes from PLN-KO mice exhibit accelerated SR calcium uptake,[26,27] similar to what we observed in PLN-R14del cardiomyocytes. Additionally, the inotropic response to beta-adrenergic stimulation is either absent or nearly absent in both PLN-KO and PLN-R14del cardiomyocytes.[26,27] However, while PLN-KO mice are viable and age normally up to 24 months,[28] PLN-R14$^{\Delta/\Delta}$ mice develop severe HF within 8 weeks after birth. This indicates that loss of SERCA2a inhibitory function of PLN-R14del cannot account for the rapid cardiac decline and shortened lifespan observed in these mice. In agreement with others,[9,11,12] this suggests that PLN-R14del has acquired a novel pathogenic function. Abnormal perinuclear localization of PLN has been identified as a hallmark of PLN-R14del cardiomyopathy, and we have recently demonstrated that this abnormality is associated with structurally altered SR.[9] Cardiomyocytes with these abnormal SR structures eventually undergo necrosis, leading to replacement fibrosis.[9] Treatment with ASO resulted in a dose-dependent reduction of perinuclear PLN staining, with other SR markers also returning to normal localization post-treatment. Therefore, the induction of abnormal PLN-SR clustering represents a novel pathological gain-of-function of the PLN-R14del protein, which explains why reducing this protein through ASO therapy effectively halts disease progression.

In this study, we established, for the first time, a clear dose-response relationship between ASO treatment and PLN clustering and survival in PLN-R14$^{\Delta/\Delta}$ mice. Even with a limited reduction of PLN, there was a delay in the decline of cardiac function and a modest extension of survival in the R14$^{\Delta/\Delta}$ mouse model. Importantly, humans with the heterozygous PLN-E2stop (p.Glu2Ter) variant, showing a 50% reduction in PLN levels are healthy.[29] A single homozygous individual from consanguineous parents did, however, developed DCM. However, the generalizability of this finding in unclear, as animal studies have shown normal cardiac function in the absence of PLN under both rest and stress conditions.[27,30] Collectively, this highlights that partial PLN reduction through silencing can have therapeutic potential in humans. Our results demonstrate that reducing PLN-R14del is beneficial without full elimination, even in this aggressive R14$^{\Delta/\Delta}$ model, underscoring the viability of partial PLN reduction as a treatment strategy.

We acknowledge several limitations of this study. First, the use of mice as a model organism to study PLN pathophysiology has inherent challenges. While PLN function is well conserved between humans and mice, there may be differences in the exact contribution of PLN in calcium homeostasis in each species. Additionally, we used homozygous PLN-R14del mice, whereas human patients are heterozygous for this variant. The decision to use homozygous PLN-R14del mice was driven by their accelerated disease progression and the demonstrated efficacy of ASO treatment in

prior studies. Importantly, these homozygous mice also recapitulate most of the key pathological features observed in the human disease.[5] Although, initially it was suggested that PLN-R14del would localize to the plasma membrane in the absence of wildtype PLN,[31] more recent studies have not confirmed this.[9, 32] This has recently been discussed and provides further support for the use of a homozygous mouse model for accelerated and synchronous disease development.[6] Human PLN-R14del induced pluripotent stem cell (iPSC)-derived cardiomyocytes have been studied, including viral miRNA-mediated PLN silencing (~50% reduction).[33] However in these in vitro models it is challenging to recapitulate the key phenotypes observed in patients, including abnormal SR clustering; thus, therapeutic validation in such in vitro models still has limitations.[6]

In conclusion, this study demonstrates a dose-dependent protective effect of ASO treatment in PLN-R14del cardiomyopathy mice. This protective effect does primarily not result from improved calcium cycling, but is likely due to a reduction in abnormal SR structures caused by the altered pathogenic function of the PLN-R14del protein.

Additional Information

Funding
This work was supported by the Dutch Heart Foundation [2018-30 (CVON-PREDICT2) to H.H.W.S. and V.O.N.T., 01-003-2022-0358 (CarMa) to H.H.W.S. and V.O.N.T.] ; Fondation Leducq [18CVD01 (CURE-PLaN), to H.H.W.S. and V.O.N.T.]; the PLN Foundation [Crazy ideas, to HHWS and VONT]; China Scholarship Council Grant [202008230186 to L.S.]. Part of the work has been performed at the UMCG Imaging and Microscopy Center (UMIC), which is sponsored by ZonMW grant 91111.006.

Author Contribution Statement
H.H.W.S. and V.O.N.T. conceived the hypothesis and designed the project together with TE, ; L.S and V.O.N.T. performed the main experiments. L.S., T.R.E., and V.O.N.T. acquired data; L.S., T.R.E., V.O.N.T. and H.H.W.S. were involved in data analysis and interpretation; L.S. drafted the manuscript; H.H.W.S., T.R.E. and V.O.N.T. revised the manuscript critically for important intellectual contents; C.A., D.J., K.M.H., D.S, A.E,M., D.A.K. contributed to the study design, interpretation of data, and reviewed the manuscript. AstraZeneca and Ionis Pharmaceuticals oversaw the experiments and provided the primary funding for the project. Ionis Pharmaceuticals provided ASOs used in this study. All authors approved of the final version to be published.

Data availability
All data that support the findings of this study are available from the corresponding author upon reasonable request.

Acknowledgements
The authors would like to thank Martin Dokter, and Susanne Feringa for their excellent technical assistance and Anouk Wolters for her expert help in electron miscroscopy. We would like to thank animal caretakers and staff from the UMCG central animal facility (CDP) for their services.

Conflict of Interest
The UMCG which employed/employs several of the authors received research grants and/or fees from AstraZeneca, Ionis Pharmaceuticals, Inc., Abbott, Boehringer Ingelheim, Cardior Pharmaceuticals GmbH, Novo Nordisk, and Roche. D.J., K.M.H., D.S. are employees of AstraZeneca. D.K. and A.E.M. are employees of Ionis Pharmaceuticals. C.A. is a former employee of AstraZeneca and a current employee of Novo Nordisk.

References

1. Rathod N, Bak JJ, Primeau JO, Fisher ME, Espinoza-Fonseca LM, Lemieux MJ, Young HS. Nothing Regular about the Regulins: Distinct Functional Properties of SERCA Transmembrane Peptide Regulatory Subunits. Int J Mol Sci 2021;22.
2. MacLennan DH, Kranias EG. Phospholamban: a crucial regulator of cardiac contractility. Nature Reviews Molecular Cell Biology 2003;4:566-577.
3. van der Zwaag PA, van Rijsingen IAW, Asimaki A, Jongbloed JDH, van Veldhuisen DJ, Wiesfeld ACP, Cox MGPJ, van Lochem LT, de Boer RA, Hofstra RMW, Christiaans I, van Spaendonck-Zwarts KY, Lekanne dit Deprez RH, Judge DP, Calkins H, Suurmeijer AJH, Hauer RNW, Saffitz JE, Wilde AAM, van den Berg MP, van Tintelen JP. Phospholamban R14del mutation in patients diagnosed with dilated cardiomyopathy or arrhythmogenic right ventricular cardiomyopathy: evidence supporting the concept of arrhythmogenic cardiomyopathy. Eur J Heart Fail 2014;14:1199-1207.
4. Deiman FE, Bomer N, van der Meer P, Grote Beverborg N. Review: Precision Medicine Approaches for Genetic Cardiomyopathy: Targeting Phospholamban R14del. Curr Heart Fail Rep 2022;19:170-179.
5. Eijgenraam TR, Boukens BJ, Boogerd CJ, Schouten EM, van de Kolk CWA, Stege NM, Te Rijdt WP, Hoorntje ET, van der Zwaag PA, van Rooij E, van Tintelen JP, van den Berg MP, van der Meer P, van der Velden J, Sillje HHW, de Boer RA. The phospholamban p.(Arg14del) pathogenic variant leads to cardiomyopathy with heart failure and is unreponsive to standard heart failure therapy. Sci Rep 2020;10:9819.
6. Stege NM, de Boer RA, Makarewich CA, van der Meer P, Sillje HHW. Reassessing the Mechanisms of PLN-R14del Cardiomyopathy: From Calcium Dysregulation to S/ER Malformation. JACC Basic Transl Sci 2024;9:1041-1052.
7. Grote Beverborg N, Spater D, Knoll R, Hidalgo A, Yeh ST, Elbeck Z, Sillje HHW, Eijgenraam TR, Siga H, Zurek M, Palmer M, Pehrsson S, Albery T, Bomer N, Hoes MF, Boogerd CJ, Frisk M, van Rooij E, Damle S, Louch WE, Wang QD, Fritsche-Danielson R, Chien KR, Hansson KM, Mullick AE, de Boer RA, van der Meer P. Phospholamban antisense oligonucleotides improve cardiac function in murine cardiomyopathy. Nat Commun 2021;12:5180.
8. Eijgenraam TR, Stege NM, Oliveira Nunes Teixeira V, de Brouwer R, Schouten EM, Grote Beverborg N, Sun L, Spater D, Knoll R, Hansson KM, Amilon C, Janzen D, Yeh ST, Mullick AE, van der Meer P, de Boer RA, Sillje HHW. Antisense Therapy Attenuates Phospholamban p.(Arg14del) Cardiomyopathy in Mice and Reverses Protein Aggregation. Int J Mol Sci 2022;23.
9. Stege NM, Eijgenraam TR, Oliveira Nunes Teixeira V, Feringa AM, Schouten EM, Kuster DWD, van der Velden J, Wolters AHG, Giepmans BNG, Makarewich CA, Bassel-Duby R, Olson EN, de Boer RA, Sillje HHW. DWORF Extends Life Span in a PLN-R14del Cardiomyopathy Mouse Model by Reducing Abnormal Sarcoplasmic Reticulum Clusters. Circ Res 2023;133:1006-1021.
10. Haghighi K, Kolokathis F, Gramolini AO, Waggoner JR, Pater L, Lynch RA, Fan GC, Tsiapras D, Parekh RR, Dorn GW, 2nd, MacLennan DH, Kremastinos DT, Kranias EG. A mutation in the human phospholamban gene, deleting arginine 14, results in lethal, hereditary cardiomyopathy. Proc Natl Acad Sci U S A 2006;103:1388-1393.

11. Badone B, Ronchi C, Lodola F, Knaust AE, Hansen A, Eschenhagen T, Zaza A. Characterization of the PLN p.Arg14del Mutation in Human Induced Pluripotent Stem Cell-Derived Cardiomyocytes. Int J Mol Sci 2021;22.
12. Maniezzi C, Eskandr M, Florindi C, Ferrandi M, Barassi P, Sacco E, Pasquale V, Maione AS, Pompilio G, Teixeira VON, de Boer RA, Sillje HHW, Lodola F, Zaza A. Early consequences of the phospholamban mutation PLN-R14del(+/-) in a transgenic mouse model. Acta Physiol (Oxf) 2024;240:e14082.
13. Lauffer MC, van Roon-Mom W, Aartsma-Rus A, Collaborative N. Possibilities and limitations of antisense oligonucleotide therapies for the treatment of monogenic disorders. Commun Med (Lond) 2024;4:6.
14. Percie du Sert N, Hurst V, Ahluwalia A, Alam S, Avey MT, Baker M, Browne WJ, Clark A, Cuthill IC, Dirnagl U, Emerson M, Garner P, Holgate ST, Howells DW, Karp NA, Lazic SE, Lidster K, MacCallum CJ, Macleod M, Pearl EJ, Petersen OH, Rawle F, Reynolds P, Rooney K, Sena ES, Silberberg SD, Steckler T, Wurbel H. The ARRIVE guidelines 2.0: Updated guidelines for reporting animal research. PLoS Biol 2020;18:e3000410.
15. Zacchigna S, Paldino A, Falcao-Pires I, Daskalopoulos EP, Dal Ferro M, Vodret S, Lesizza P, Cannata A, Miranda-Silva D, Lourenco AP, Pinamonti B, Sinagra G, Weinberger F, Eschenhagen T, Carrier L, Kehat I, Tocchetti CG, Russo M, Ghigo A, Cimino J, Hirsch E, Dawson D, Ciccarelli M, Oliveti M, Linke WA, Cuijpers I, Heymans S, Hamdani N, de Boer M, Duncker DJ, Kuster D, van der Velden J, Beauloye C, Bertrand L, Mayr M, Giacca M, Leuschner F, Backs J, Thum T. Towards standardization of echocardiography for the evaluation of left ventricular function in adult rodents: a position paper of the ESC Working Group on Myocardial Function. Cardiovasc Res 2021;117:43-59.
16. Kuipers J, de Boer P, Giepmans BN. Scanning EM of non-heavy metal stained biosamples: Large-field of view, high contrast and highly efficient immunolabeling. Exp Cell Res 2015;337:202-207.
17. Ackers-Johnson M, Li PY, Holmes AP, O'Brien SM, Pavlovic D, Foo RS. A Simplified, Langendorff-Free Method for Concomitant Isolation of Viable Cardiac Myocytes and Nonmyocytes From the Adult Mouse Heart. Circ Res 2016;119:909-920.
18. Sikkel MB, Francis DP, Howard J, Gordon F, Rowlands C, Peters NS, Lyon AR, Harding SE, MacLeod KT. Hierarchical statistical techniques are necessary to draw reliable conclusions from analysis of isolated cardiomyocyte studies. Cardiovasc Res 2017;113:1743-1752.
19. Nakagawa T, Yokoe S, Asahi M. Phospholamban degradation is induced by phosphorylation-mediated ubiquitination and inhibited by interaction with cardiac type Sarco(endo)plasmic reticulum Ca(2+)-ATPase. Biochem Biophys Res Commun 2016;472:523-530.
20. Davide G, Joachim C, Judith K G, Federica dM, Roger J H. SERCA2a in heart failure: role and therapeutic prospects. J Bioenerg Biomembr 2006;37.
21. Lipskaia L, Keuylian Z, Blirando K, Mougenot N, Jacquet A, Rouxel C, Sghairi H, Elaib Z, Blaise R, Adnot S, Hajjar RJ, Chemaly ER, Limon I, Bobe R. Expression of sarco (endo) plasmic reticulum calcium ATPase (SERCA) system in normal mouse cardiovascular tissues, heart failure and atherosclerosis. Biochim Biophys Acta 2014;1843:2705-2718.
22. Pallien T, Klussmann E. New aspects in cardiac L-type Ca2+ channel regulation. Biochem Soc Trans 2020;48:39-49.

23. Wouter P TR, J Peter vT, Aryan V, Allard C vdW, Rudolf A dB, Maarten P vdB, Albert J H S. Phospholamban p.Arg14del cardiomyopathy is characterized by phospholamban aggregates, aggresomes, and autophagic degradation. Histopathology 2016;69.
24. Ceholski DK, Trieber CA, Holmes CFB, Young HS. Lethal, Hereditary Mutants of Phospholamban Elude Phosphorylation by Protein Kinase A. J Biol Chem 2012;287:26596-26605.
25. Ceholski DK, Trieber CA, Young HS. Hydrophobic imbalance in the cytoplasmic domain of phospholamban is a determinant for lethal dilated cardiomyopathy. J Biol Chem 2012;287:16521-16529.
26. L L, G C, E G K, D M B. Cardiac myocyte calcium transport in phospholamban knockout mouse: relaxation and endogenous CaMKII effects. Am J Physiol 1998;274.
27. Luo W, Grupp IL, Harrer J, Ponniah S, Grupp G, Duffy JJ, Doetschman T, Kranias EG. Targeted ablation of the phospholamban gene is associated with markedly enhanced myocardial contractility and loss of beta-agonist stimulation. Circ Res 1994;75:401-409.
28. Slack J, Grupp I, Dash R, Holder D, Schmidt A, Gerst M, Tamura T, Tilgmann C, James P, Johnson R, Gerdes A, Kranias E. The enhanced contractility of the phospholamban-deficient mouse heart persists with aging. J Mol Cell Cardiol 2001;33.
29. Li Z, Chen P, Xu J, Yu B, Li X, Wang DW, Wang DW. A PLN nonsense variant causes severe dilated cardiomyopathy in a novel autosomal recessive inheritance mode. Int J Cardiol 2019;279:122-125.
30. Heinis FI, Thompson BR, Gulati R, Wheelwright M, Metzger JM. Myofilament-based physiological regulatory compensation preserves diastolic function in failing hearts with severe Ca2+ handling deficits. JCI Insight 2024;9.
31. Haghighi K, Pritchard T, Bossuyt J, Waggoner JR, Yuan Q, Fan GC, Osinska H, Anjak A, Rubinstein J, Robbins J, Bers DM, Kranias EG. The human phospholamban Arg14-deletion mutant localizes to plasma membrane and interacts with the Na/K-ATPase. J Mol Cell Cardiol 2012;52:773-782.
32. Vafiadaki E, Haghighi K, Arvanitis DA, Kranias EG, Sanoudou D. Aberrant PLN-R14del Protein Interactions Intensify SERCA2a Inhibition, Driving Impaired Ca(2+) Handling and Arrhythmogenesis. Int J Mol Sci 2022;23.
33. Karakikes I, Stillitano F, Nonnenmacher M, Tzimas C, Sanoudou D, Termglinchan V, Kong CW, Rushing S, Hansen J, Ceholski D, Kolokathis F, Kremastinos D, Katoulis A, Ren L, Cohen N, Gho J, Tsiapras D, Vink A, Wu JC, Asselbergs FW, Li RA, Hulot JS, Kranias EG, Hajjar RJ. Correction of human phospholamban R14del mutation associated with cardiomyopathy using targeted nucleases and combination therapy. Nat Commun 2015;6:6955.

Supplemental material

1. Supplementary figures

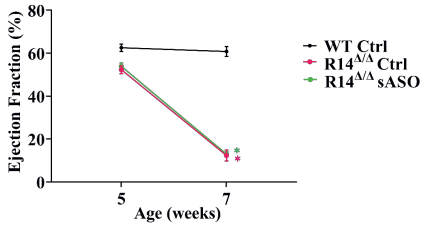

Supplementary Figure S1. Scrambled ASO administration does not alter cardiac function of PLN-R14$^{\Delta/\Delta}$ mice.

Ejection fraction of WT Ctrl (n=6) and R14$^{\Delta/\Delta}$ Ctrl or scrambled ASO (sASO) (n=8 per group) at 5 and 7 weeks of age. *p<0.05 vs. WT mice of the same age (Kruskal-Wallis with Dunn's multiple comparisons test).

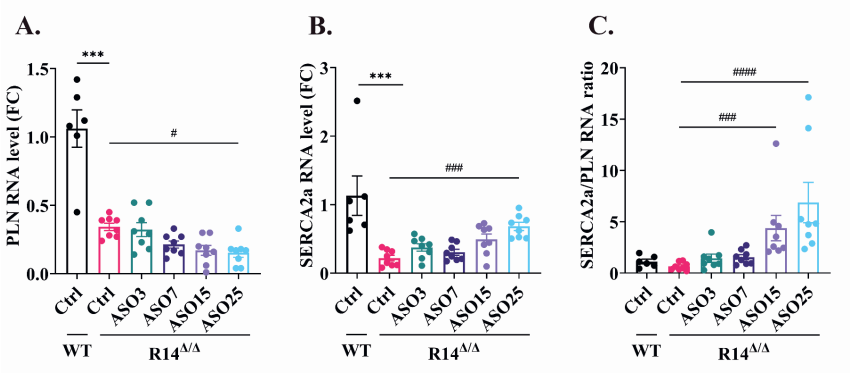

Supplementary Figure S2. PLN-ASO administration effectively reduces the RNA level of PLN and increases the SERCA2a/PLN ratio in a dose-dependent manner.

Relative ventricular mRNA levels of **(A)** PLN (*Pln*) and **(B)** SERCA2a (*Atp2a2*), normalized to housekeeping gene *Rplp0* (36B4), and **(C)** SERCA2a/PLN ratio of vehicle-treated WT (n=6), PLN-R14$^{\Delta/\Delta}$ mice (n=8) and PLN-ASO-treated (3, 7, 15 or 25 mg/kg) R14$^{\Delta/\Delta}$ mice (n=8), depicted as fold changes (FC) compared to WT Ctrl. Ventricular tissue was harvested at the predetermined termination time points, either upon reaching the humane endpoint or at 21 weeks of age. ***p<0.001 (Mann-Whitney test), $^{\#}$p<0.05, $^{\#\#\#}$p<0.001, $^{\#\#\#\#}$p<0.0001 (Kruskal-Wallis with Dunn's multiple comparison test).

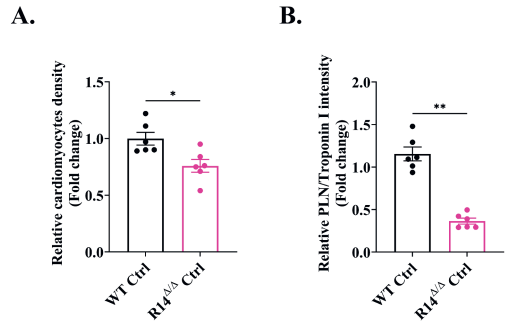

Supplementary Figure S3. Cardiomyocyte cell density and PLN expression decreased in R14$^{\Delta/\Delta}$ vehicle group

Cardiomyocyte cell density and PLN expression in WT and R14$^{\Delta/\Delta}$ vehicle groups determined by immunofluorescence microscopy (A). Cardiomyocyte density was determined by counting the number of cardiac Troponin I stained cells in a transverse cut section and corrected by the area. n=6 per group. (B) The amount of PLN fluorescence and cardiac Troponin I fluorescence were determined in cardiomyocytes in a longitudinal cut section. The ratio between PLN and cardiac Troponin I are shown for the WT and R14$^{\Delta/\Delta}$ groups (n=6). *p<0.05, **p<0.01 (Mann-Whitney test).

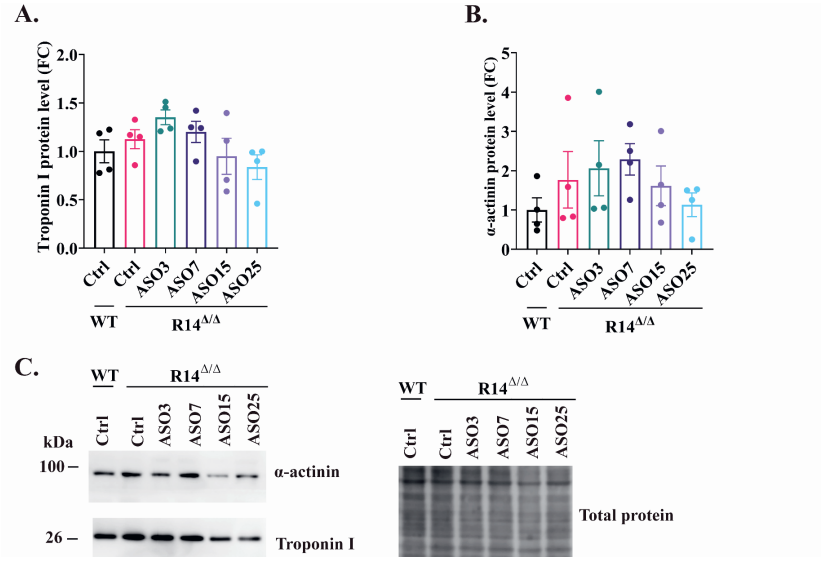

Supplementary Figure S4. Cardiac expression of troponin I and α-actinin is not affected by heart failure.

Protein quantification of **(A)** cardiac troponin I and **(B)** α-actinin in ventricular tissue of vehicle-treated WT (Ctrl) and R14$^{\Delta/\Delta}$ (Ctrl) mice and PLN-ASO-treated (3, 7, 15 or 25 mg/kg) R14$^{\Delta/\Delta}$ mice (n=4 per group). Protein expression was normalized to total protein levels and shown as fold change (FC) compared to WT Ctrl. **(C)** Representative (average based) Western immunoblot images of α-actinin (left top), troponin I (left bottom) and total protein staining (right). The PVDF membrane was cut into sections based on the expected molecular weights of the target proteins, and each section was incubated with specific antibody accordingly.

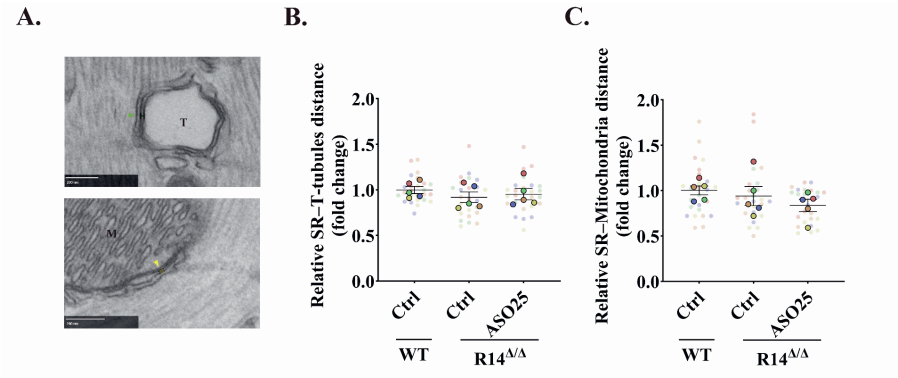

Supplementary Figure S5. PLN- R14$^{\Delta/\Delta}$ mice exhibit preserved spatial association between the SR, T-tubules, and mitochondria.

(A) Representative electron micrographs showing the measured distances between the SR and T-tubules (top, green bar) and between the SR and mitochondria (bottom, yellow bar) (scale bar 200nm). **(B-C)** Quantification of the relative distance between SR–T-tubules **(B)** and SR–mitochondria **(C)**. (n = 5 per group). In panels B, C the colors of the individual cell values (transparent dots) match the colors of the average values (solid dots) of the same mouse.

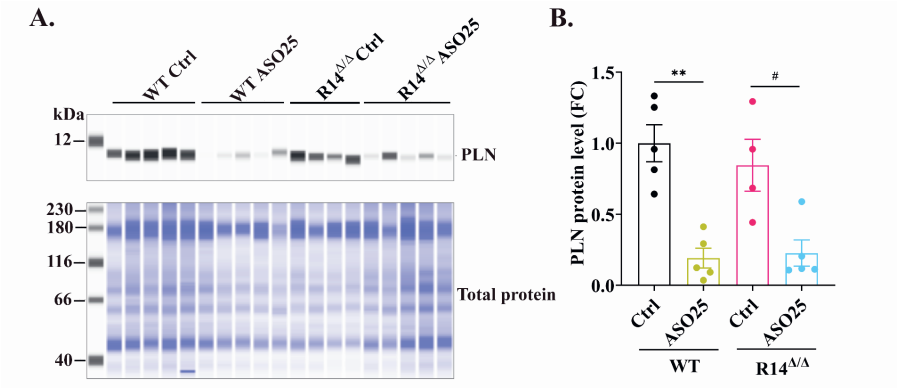

Supplementary Figure S6. Efficient knockdown of PLN protein in isolated cardiomyocytes following PLN-ASO administration.

Jess Western immunoblot images of **(A)** PLN (top), and its total protein (bottom) **(B)** PLN protein levels in cardiomyocytes isolated from WT and R14$^{\Delta/\Delta}$ mice treated with vehicle or 25 mg/kg PLN-ASO, normalized to total protein levels and shown as fold change (FC) compared to vehicle-treated WT cardiomyocytes (n=5 per group, except n=4 for vehicle-treated R14$^{\Delta/\Delta}$ cardiomyocytes). **p<0.01, #p<0.05 (Mann-Whitney test).

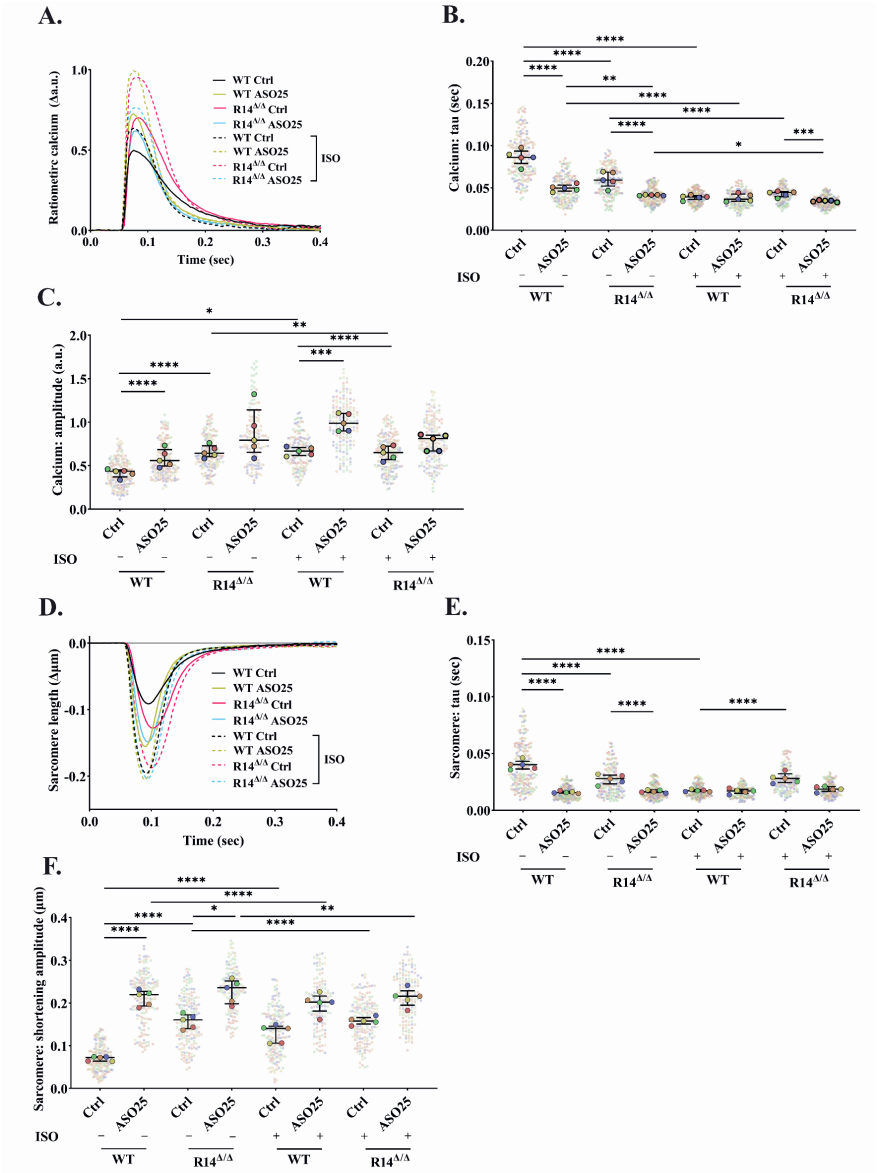

Supplementary Figure S7. Isolated cardiomyocytes from PLN-R14$^{\Delta/\Delta}$ mice exhibit enhanced contractile and calcium dynamics, with limited response to isoproterenol stimulation.

(A) Normalized ratiometric calcium transients under pacing conditions in cardiomyocytes isolated from WT and R14$^{\Delta/\Delta}$ mice treated with vehicle or PLN-ASO (25 mg/kg; n=5 per group), before (solid lines) and after addition (dashed lines) of isoproterenol (ISO). **(B)** Calcium decay time constant (tau) and **(C)** calcium amplitude (n=5 per group). **(D)** Normalized sarcomere lengths under pacing conditions in cardiomyocytes isolated from WT and R14$^{\Delta/\Delta}$ mice treated with vehicle or PLN-ASO (25 mg/kg; n=5 per group), before (solid lines) and after addition (dashed lines) of isoproterenol (ISO). **(E)** Sarcomere decay time constant (tau) and **(F)** sarcomere shortening amplitude (n=5 per group). *p<0.05, **p<0.01,

***p<0.001, ****p<0.0001 (hierarchical statistical test with Bonferroni correction).[17] In panels B, C, E and F, the colors of the individual cell values (transparent dots) match the colors of the average values (solid dots) of the same mouse.

Supplementary Tables

Supplementary Table S1. Antibodies used for histological staining.

Primary antibody	Host	Cat. No.	Supplier	Dilution
Anti-PLN	Rabbit	ab219626	Abcam	1:1,000
Anti-PLN	Mouse	MA3-922	Thermo Fisher Scientific	1:200
Anti-SERCA2	Mouse	MA3-919	Thermo Fisher Scientific	1:100
Anti-HRC	Rabbit	HPA004833	Sigma	1:100

Secondary antibody	Antigen	Label	Cat. No.	Supplier	Dilution
Donkey anti-rabbit	Rabbit	Alexa488	A21206	Thermo Fisher Scientific	1:100
Donkey anti-mouse	Mouse	Alexa555	A31570	Thermo Fisher Scientific	1:100
Donkey anti-mouse	Mouse	Alexa488	A21202	Thermo Fisher Scientific	1:100
Donkey anti-rabbit	Rabbit	Alexa555	A31572	Thermo Fisher Scientific	1:100

Supplementary Table S2. Primer sequences used for qPCR.

Gene	Protein		Sequence (5'-3')
Pln	Phospholamban	Forward Reverse	GACGATCACCGAAGCCAAG CGAGCGAGTGAGGTATTGC
Atp2a2	Sarcoplasmic/endoplasmic reticulum Ca^{2+}-ATPase 2	Forward Reverse	TCAGTATGACGGGCTTGTAG CGGTAGCTTCTCCAACTTTC
Nppa	Atrial Natriuretic Peptide	Forward Reverse	GCTTCCAGGCCATATTGGAG GGTGGTCTAGCAGGTTCTTG
Timp1	Tissue Inhibitor of Metalloproteinases-1	Forward Reverse	CAACGAGACCACCTTATACC CATATCCACAGAGGCTTTCC
Col1a1	Collagen type 1 alpha 1 chain	Forward Reverse	AGAGCATGACCGATGGATTC CGCTGTTCTTGCAGTGATAG
Rplp0	Ribosomal protein, large P0 (36B4)	Forward Reverse	AACGGGTACAAACGAGTC AGATGGATCAGCCAAGAAG

Supplementary Table S3. Antibodies used for Western blot.

Primary antibody	Host	Cat. No.	Supplier	Dilution	Molecular weight (kDa)
Anti-PLN	Rabbit	14562S	Bioke	1:1,000	12
Anti-SERCA2	Mouse	MA3-919	Thermo Fisher Scientific	1:1,000	110
Anti-α-actinin	Mouse	A7811	Sigma	1:1,000	100
Anti-Troponin	Rabbit	Ab47003	Abcam	1:2,000	26

Secondary antibody	Antigen	Label	Cat. No	Supplier	Dilution
Rabbit anti-mouse	Mouse	HRP	P0260	Dako	1:2,000
Goat anti-rabbit	Rabbit	HRP	P0448	Dako	1:2,000

Supplementary Table S4. ASO-mediated PLN protein depletion.

	Mean of PLN protein depletion compared to PLN-R14$^{\Delta/\Delta}$ Ctrl ± SEM	**p value**
PLN-R14$^{\Delta/\Delta}$ Ctrl	0.00 ± 5.37	
PLN-R14$^{\Delta/\Delta}$ ASO3	17.59 ± 4.45	ns
PLN-R14$^{\Delta/\Delta}$ ASO7	37.09 ± 4.32	ns
PLN-R14$^{\Delta/\Delta}$ ASO15	60.79 ± 5.19	0.0127
PLN-R14$^{\Delta/\Delta}$ ASO25	79.88 ± 2.85	0.0005

Chapter 6

Simulating the impact of phospholamban (PLN) silencing on PLN complexes in PLN-R14del cardiomyopathy

Liu Sun [1], Laurens A. Silljé [2], Vivian Oliveira Nunes Teixeira [1], Herman H.W. Silljé[1]*

[1]Department of Cardiology, University Medical Center Groningen, University of Groningen, Groningen, The Netherlands
[2]Science and Engineering, Biology, University of Groningen, Groningen, The Netherlands

(*In preparation*)

Abstract

Introduction

Phospholamban (PLN) is predominantly expressed in cardiomyocytes, and several pathogenic variants contribute to heart disease. The best-studied variant, PLN-R14del, is associated with dilated and/or arrhythmogenic cardiomyopathy. Previous work has shown that PLN-targeting antisense oligonucleotides (ASOs) can mitigate disease progression in a PLN-R14del mouse model. Because PLN exists in equilibrium between pentameric and monomeric states and forms complexes with the Sarco/(Endo)plasmic Reticulum Calcium ATPase 2a (SERCA), we simulated the effects of PLN silencing on these complexes to identify differential sensitivities to PLN depletion.

Methods

PLN wildtype (PLN-WT) and PLN-R14del form pentamers and bind as monomers to SERCA. Previously determined equilibrium constants from fluorescence resonance energy transfer (FRET) microscopy were used to model steady-state equilibria of these interactions across a range of total PLN levels.

Results

Simulated linear reductions in PLN-WT and PLN-R14del levels revealed marked differences in the behavior of free and complexed species. Pentameric complexes declined almost linearly with decreasing total PLN. In contrast, free PLN and PLN–SERCA complexes were more resilient to PLN depletion, remaining relatively stable across a wide range before decreasing more sharply at high depletion levels. This likely reflects the second-order kinetics of pentamer formation compared with the first-order PLN-SERCA interaction. PLN-WT and PLN-R14del behaved similarly overall, although PLN-R14del showed a modestly higher propensity for pentamer formation and reduced SERCA binding.

Conclusion

Our simulations indicate that pentameric PLN is more sensitive to PLN silencing than free or SERCA-bound PLN. These differential effects should be considered when designing PLN-targeted therapies, and it will be essential to determine which PLN pool drives PLN-R14del cardiomyopathy.

Abbreviations:

PLN = Phospholamban
PLN-R14del = Pathogenic PLN-R14del variant
SERCA = Sarco/(Endo)plasmic Reticulum Calcium ATPase 2a
WT = wildtype PLN
R14 = PLN-R14del variant
PLNfree = free wildtype PLN
PLNtotal = total wildtype PLN pool
PLNpent = wildtype PLN pentamer pool
PLN-SERCA = wildtype PLN - SERCA pool
R14free = free PLN-R14del pool
R14total = total PLN-R14del pool
R14pent = PLN-R14del pentamer pool
R14-SERCA = PLN-R14del - SERCA pool
PLN_x-$R14_y$pent = PLN and PLN-R14del were modeled as mixed pentamers, with x and y representing the number of molecules of each species incorporated into the pentamer

Introduction

Phospholamban (PLN) is highly expressed in cardiomyocytes within the heart and numerous pathogenic variants have been described that can cause heart disease. The PLN-R14del variant, lacks one codon, resulting in a PLN protein in which Arginine 14 (R14) is missing. This is the most well studied autosomal dominant inherited variant and at least two different founder mutations have been identified.[1,2] PLN-R14del carriers are prone to develop arrhythmogenic and/or dilated cardiomyopathy often resulting in severe heart failure development.[1,3] Currently, no specific therapy exists for these patients and the only cure is heart transplantation.

Phospholamban can interact with the Sarco/Endoplasmic reticulum Calcium ATPase 2a (SERCA2a) and acts as an inhibitory regulator of calcium uptake in the sarco/endoplasmic reticulum (S/ER) of cardiomyocytes. It was originally proposed that PLN-R14del would act as a superinhibitor of SERCA2a.[1] However, more recent data indicate that PLN-R14del has (partially) lost its SERCA2a inhibitory action.[4-7] The exact effect of this pathogenic variant on SERCA2a remains therefore elusive, and it is not yet known whether its pathogenicity is actually mediated via unbalancing SERCA2a activity.

PLN does not only interact with SERCA2a, but also with itself resulting in the formation of pentameric structures within the SR membrane. Also, PLN-R14del can form these pentamers, and it is currently unknown whether pentameric structures with PLN-R14del may contribute to disease development. Importantly, in hearts of PLN-R14del patients so called “PLN aggregates” are detected in cardiomyocytes and are considered a hallmark of this disease.[8,9] More recent studies have revealed that these aggregates consist of abnormal S/ER containing PLN clusters.[5] Studies with a PLN-R14del mouse model suggest that cardiomyocytes with these clusters are prone to necrotic cell death, which can explain the severe replacement fibrosis in hearts of PLN-R14del patients.[10] Although, the mechanisms underlying PLN cluster formation remain unclear, it is plausible that this process contributes to disease development.

A PLN-R14del mouse model with similar disease characteristics as observed in patients, including PLN-clustering, cell death, replacement fibrosis and heart failure development has been used to study therapeutic approaches.[4,5] PLN silencing using antisense oligonucleotides (ASOs) has proven highly effective, halting disease progression even in a severe homozygous model with accelerated pathology.[4,11,12] Since SR calcium uptake is already elevated in this disease model, PLN silencing did not further affect this process. Interestingly, however, silencing did result in a strong reduction of cardiomyocytes with abnormal SR clusters, suggesting that these clusters may represent the primary pathogenic driver.

Reduction of PLN levels, via PLN silencing, will have different effects on the different complexes, but this is difficult to investigate in cells due to the transient nature of these

interactions. Using excellent FRET-based cellular studies, the research group of Robia defined the different molecular binding constants for PLN and PLN-R14del with SERCA, and between the PLN molecules.[13] We therefore decided to model the effects of PLN silencing on the different complexes and relate this to our knowledge on disease development. As shown, in this simulation study the WT PLN and R14del PLN pentameric complexes are much more sensitive to PLN silencing, as compared to the WT PLN/SERCA and R14del PLN/SERCA complexes and the free PLN molecules.

Methods

Equilibria of different complexes

We used standard association/dissociation equilibrium kinetics based on molecule A and B interaction, as follow:

$$[A] + [B] \rightleftharpoons [AB]$$

and with dissociation constant K_D for AB:

$$KdAB = \frac{[A] * [B]}{[AB]}$$

With three different molecules, PLN, PLN-R14del and SERCA2a, that compete for interaction, and the tendency of PLN and PLN-R14del to assemble into pentameric complexes additional complexity is added, resulting in additional equations. The following equilibrium expressions, where A represents PLN wild-type (WT), B represents PLN-R14del (R14) and C represents SERCA2a (SERCA) were used:

[A] + [C]	⇌	[AC]	(WT and SERCA interaction)
[B] + [C]	⇌	[BC]	(R14 and SERCA interaction)
5[A]	⇌	[A_5]	(WT pentamer formation)
5[B]	⇌	[B_5]	(R14 pentamer formation)
4[A] + [B]	⇌	[A_4B]	(4xWT + 1xR14 pentamer formation)
3[A] + 2[B]	⇌	[A_3B_2]	(3xWT + 2xR14 pentamer formation)
2[A] + 3[B]	⇌	[A_2B_3]	(2xWT + 3xR14 pentamer formation)
[A] + 4[B]	⇌	[AB_4]	(1xWT + 4xR14 pentamer formation)

Equilibrium constants

The dissociation constant (K_D) for most of these equilibria have been determined experimentally by the Robia group,[13] using cellular FRET based assays and are depicted in **Table 1**. Since the K_D for mixed PLN WT-R14 pentamers is an average value, it does not distinguish between the different possible PLN WT and R14 mixed complexes. We therefore estimated these with the following formula:

K_D A4B = (K_D AA^(4/5)* K_D AB^(1/5))

K_D A3B2 = K_D AA^(3/5)* K_D AB^(2/5)

K_D A2B3 = K_D AA^(2/5)* K_D AB^(3/5)

K_D AB4 = K_D AA^(1/5)* K_D AB^(4/5)

The final estimated K_Ds for mixed pentamers were corrected by the measured FRET based value divided by the the mean value of these mixed K_Ds (0.97 correction factor) and are included in **Table 2**.

Calculations of steady state concentrations:

The equations shown below, represent the total concentration of each molecule as the sum of its free forms and its bound forms in various complexes. The equations account for a wide range of complexes (e.g. PLN-SERCA interactions and different PLN pentamer stoichiometries), capturing the complexity of multi-protein interactions with different stoichiometries. The equations are nonlinear due to the high-order terms of complex formation that are related to the free unbound concentrations. The model does not include cooperative or allosteric interactions, and dynamic posttranslational modifications that might require more complex models and more knowledge on this system.

$$[Atotal] = [Afree] + 5 * \frac{[Afree]^5}{K_D\,A5} + 4 * \frac{[Afree]^4 * [Bfree]}{K_D\,A4B} + 3 * \frac{[Afree]^3 * [Bfree]^2}{K_D\,A3B2} + 2 * \frac{[Afree]^2 * [Bfree]^3}{K_D\,A2B3} + \frac{[Afree] * [Bfree]^4}{K_D\,AB4} + \frac{[Afree] * [Cfree]}{K_D\,AC}$$

$$[Btotal] = [Bfree] + 5 * \frac{[Bfree]^5}{K_D\,B5} + 4 * \frac{[Bfree]^4 * [Afree]}{K_D\,AB4} + 3 * \frac{[Bfree]^3 * [Afree]^2}{K_D\,A2B3} + 2 * \frac{[Bfree]^2 * [Afree]^3}{K_D\,A3B2} + \frac{[Bfree] * [Afree]^4}{K_D\,A4B} + \frac{[Bfree] * [Cfree]}{K_D\,BC}$$

$$[Ctotal] = [Cfree] + \frac{[Afree] * [Cfree]}{K_D\,AC} + \frac{[Bfree] * [Cfree]}{K_D\,BC}$$

To explore the system behavior and solve the equations numerically these formulas were incorporated into a computational model and solved using Python and SciPy by incorporating the K_D values shown in Table 2. While the exact concentrations of PLN and SERCA molecules in the two-dimensional cellular S/ER membrane bilayer are unknown, it is widely accepted that the PLN:SERCA ratio is between 4:1 and 1:1. We therefore included a 2:1 ratio in our calculations. PLN depletion was always modeled as a linear decline and with SERCA remaining constant. All outcomes were reinserted into the formulas for validation, ensuring that the total percentage of all molecules across different complexes always summed to 100%.

Results

Simulation parameters and effect of PLN concentrations on PLN pentameric structures.

We used binding constants from previously published studies,[13] as depicted in **Table 1** and calculated corresponding K_D's for mixed PLN complexes as shown in **Table 2**, and included these into our equilibrium equations. Based on experimental evidence, indicating that the PLN:SERCA2a ratio is between 4:1 to 1:1 under baseline conditions (without PLN silencing) we used an average standard 2:1 ratio for all calculations.[14] Experimental findings have shown that approximately 40% of SERCA is functionally regulated by PLN in native mouse SR membranes.[15] Therefore concentrations needed to be identified in the model at which about 40% of SERCA was bound to PLN. This was performed by modelling a broad concentration range of PLN and SERCA concentrations (a.u) with different fixed 2:1 PLN:SERCA ratios. With increasing SERCA and PLN concentrations, the percentages PLN pentamers increased rapidly followed by an increase in the PLN-SERCA complex concentrations **(Figure 1)**. At this 2:1 PLN:SERCA ratio, 40% SERCA binding was obtained at a PLN concentration of 45 (a.u.) and a corresponding SERCA concentration of 22.5 (a.u).

Table 1. Equilibrium constants (Kd) derived from FRET-based assays[13]

Interaction	**Experimental equilibrium constant (Kd) in AU***
PLN-SERCA	2,13
R14del-SERCA	3,12
PLN-PLN	0,87
R14del-PLN	0,54
R14del-R14del	0,34

**AU = Arbitrary Units*

Table 2. Dissociation constants used in the equilibrium equations for mixed PLN-R14del pentamers

Equilibrium constant	**Equilibrium constant (Kd) used for calculations in AU***
PLN_4-$R14del_1$	0,70
PLN_3-$R14del_2$	0,58
PLN_2-$R14del_3$	0,48
PLN_1-$R14del_4$	0,40

**AU = Arbitrary Units*

These values were calculated based on the Kd values shown in Table 1, as described in the Materials and Methods section.

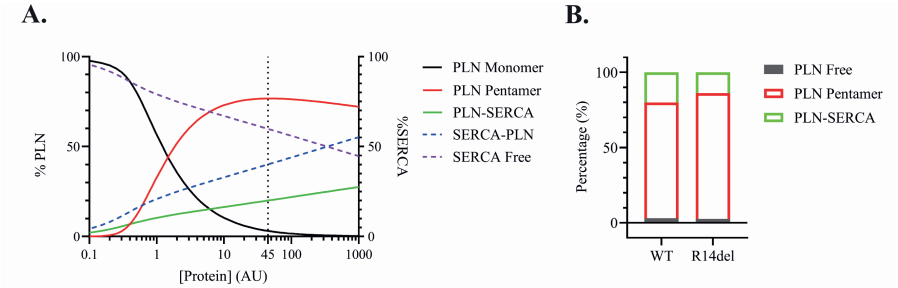

Figure 1. Modeling of PLN–SERCA equilibria reveals ~40% SERCA binding at a 2:1 PLN:SERCA ratio

(A) PLN and SERCA concentrations (arbitrary units, a.u.) were screened at a fixed 2:1 PLN:SERCA ratio to evaluate the distribution of PLN monomers, pentamers, as well as the percentage of SERCA bound to PLN or remaining free. Increasing protein concentrations resulted in a rapid rise of PLN pentamers, followed by an increase in PLN-SERCA complexes, accompanied by a decline in PLN monomers. At a PLN concentration of 45 a.u., ~40% of SERCA was bound to PLN, as indicated by the broken vertical line. Solid lines (left vertical axis) and dashed lines (right vertical axis). **(B)** Distribution of PLN between free PLN, PLN pentamers, and PLN-SERCA complexes under baseline conditions based on the dotted vertical line of figure 1A.

Effect of PLN silencing on PLN and SERCA complexes in a wildtype situation

Using the determined baseline condition, we next, investigated the effect of PLN silencing. First a condition in which all PLN consisted of wildtype PLN (WT) was investigated. In this setting, stable SERCA2a protein levels were assumed, also in the presence of PLN silencing, meaning that upon 50% reduction of PLN the PLN:SERCA2a ratio would increase 2 folds. The total baseline PLN levels were set to 100% and the response of the different PLN pools to a linear decrease of total PLN were calculated. As shown in **Figure 1A**, at baseline (no PLN depletion) about 76.7% of all PLN was present in pentamers, whereas the percent of PLN bound to SERCA was 20.1% and the percent of free PLN was 3.2% **(Figure 1B)**.

The amount of PLN present in pentamers showed a very direct response to PLN depletion and decreased almost linearly over a broad range. At about 90% of total PLN depletion the pentameric pools were nearly absent (0.2% PLN in pentamers). In contrast, the PLN-SERCA and free PLN pools were much less responsive to PLN depletion, showing only a gradual decrease with decreasing total PLN levels **(Figure 2A)**. A pronounced, steep decline was observed only when total PLN was reduced by more than 80%. These data suggest that PLN pentamers serve as a reservoir that buffers changes in SERCA-bound PLN.

The percentage of free SERCA and SERCA bound to PLN was about 60% and 40% at baseline (no PLN depletion), respectively, in accordance with the predefined characteristics of the model **(Figure 2B)**. Upon PLN depletion the percentage of

SERCA bound to PLN only gradually declined with a concomitant increase of free SERCA. Again, a pronounced, steep decline in SERCA bound to PLN was observed only when total PLN was reduced by more than 80% and this resulted in a similar steep increase in free SERCA **(Figure 2B)**.

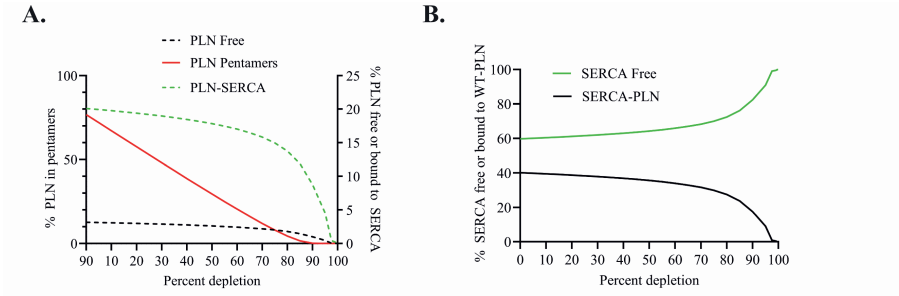

Figure 2. Effect of PLN depletion on PLN oligomeric pools and SERCA binding in a wildtype situation

(A) Effect of PLN silencing on free, pentameric PLN and SERCA-PLN complexes in the Wildtype state. Solid line (left vertical axis) and dashed lines (right vertical axis). **(B)** Relative proportion of free SERCA and SERCA-PLN complexes in response to PLN depletion.

Effect of PLN silencing on R14del PLN and SERCA complexes in a homozygous R14del situation

Although no homozygous human patients have been identified till now, mouse experiments have revealed strongly accelerated disease development in PLN-R14del homozygous mice as compared to heterozygous mice. We therefore simulated the effects of this more extreme and simpler R14del homozygous situations, before looking into a more complex heterozygous situation. Similar to the WT situation, PLNR14del (R14) was predominantly present in pentamers, and even more than in the WT situation (83,4% vs 76.7% for homozygous R14del and WT situation, respectively) **(Figure 2A, 3A)**. The percent R14 bound to SERCA was only 13.9% and the percent free R14 was 2.7%. In particular the amount of R14 bound to SERCA was much lower as compared to the WT bound to SERCA (13.9% vs 20.1%, respectively) **(Figure 3B)**. The amount of SERCA bound to R14 was therefore also lower (27.9%) as compared to the similar WT baseline situation (40% SERCA bound to PLN). This may, to some extent, explain the reduced SERCA inhibitory activity of R14 as compared to WT PLN.[4,5] Like in the WT situation the percent of free (unbound) R14 was low at baseline (2.7%). Upon PLN depletion, similar effects as in the wildtype situation were observed with a fast, almost linear decrease of R14 present in pentamers and a much more gradual decrease R14 bound to SERCA, with a steeper decrease after about 80% PLN reduction. The same was observed for free R14. Also, the effects on SERCA bound to R14 and free SERCA showed a similar behavior under this condition, upon PLN depletion.

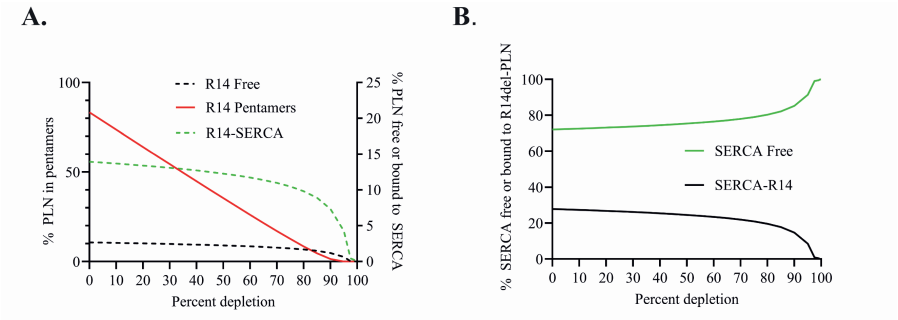

Figure 3. Effect of PLN depletion on PLN oligomeric pools and SERCA binding in a homozygous PLN-R14del situation

(A) Effect of PLN silencing on free, pentameric R14del PLN and SERCA-R14del PLN complexes in the homozygous R14del state. Solid line (left vertical axis) and dashed lines (right vertical axis). **(B)** Relative proportion of free SERCA and SERCA-R14del PLN complexes in response to PLN depletion in the homozygous R14del state. Effect of total PLN reduction on pentamers in a heterozygous situation in which both WT and R14del PLN are present.

PLN-R14del cardiomyopathy is an autosomal dominant disease, making it essential to investigate the effects of total PLN reduction in the heterozygous state. This is a more complex situation, as equal amounts of PLN WT and PLN-R14del are assumed to be present, and both are expected to decrease linearly upon silencing. When PLN WT and R14 are considered as a single pool and plotted together, the outcome closely resembles that of the WT and homozygous models: most WT and R14 molecules are incorporated into pentamers, and approximately 21% are bound to SERCA **(Figure 4A)**.

However, when PLN WT and R14 are analyzed separately and pentamer composition is taken into account, a different picture emerges **(Figure 4B)**. The majority of PLN WT and R14 molecules are incorporated into mixed pentamers, while pure WT and pure R14 pentamers contain only 9.9% and 15.1% of their respective molecules. Consequently, the concentration of pure R14del pentamers is 5.5-fold lower in the heterozygous compared to the homozygous condition. The mixed pentamers exhibit similar behavior, as shown in **Supplemental figure 1**. Thus, although the overall PLN pentamer pool declines almost linearly with total PLN depletion, similar to the WT and homozygous state, the decline of the specific pentameric forms is much more gradual in the heterozygous condition.

Approximately 21% of the total PLN pool is bound to SERCA, which corresponds to 13% WT and 8% R14, respectively **(Figure 4C)**. The total percentage of free PLN is about 4%, with both WT and R14 contributing almost equally (~2% each). PLN depletion affects these pools in a similar manner as observed under the other conditions. When examining SERCA binding, about 41% of SERCA is bound to PLN, of which 25.9% is bound to WT and 16.0% to R14 **(Figure 4D)**. Compared to the PLN-R14del

homozygous state, 42% less SERCA is bound to R14 in the heterozygous condition, a smaller reduction than the expected 50%.

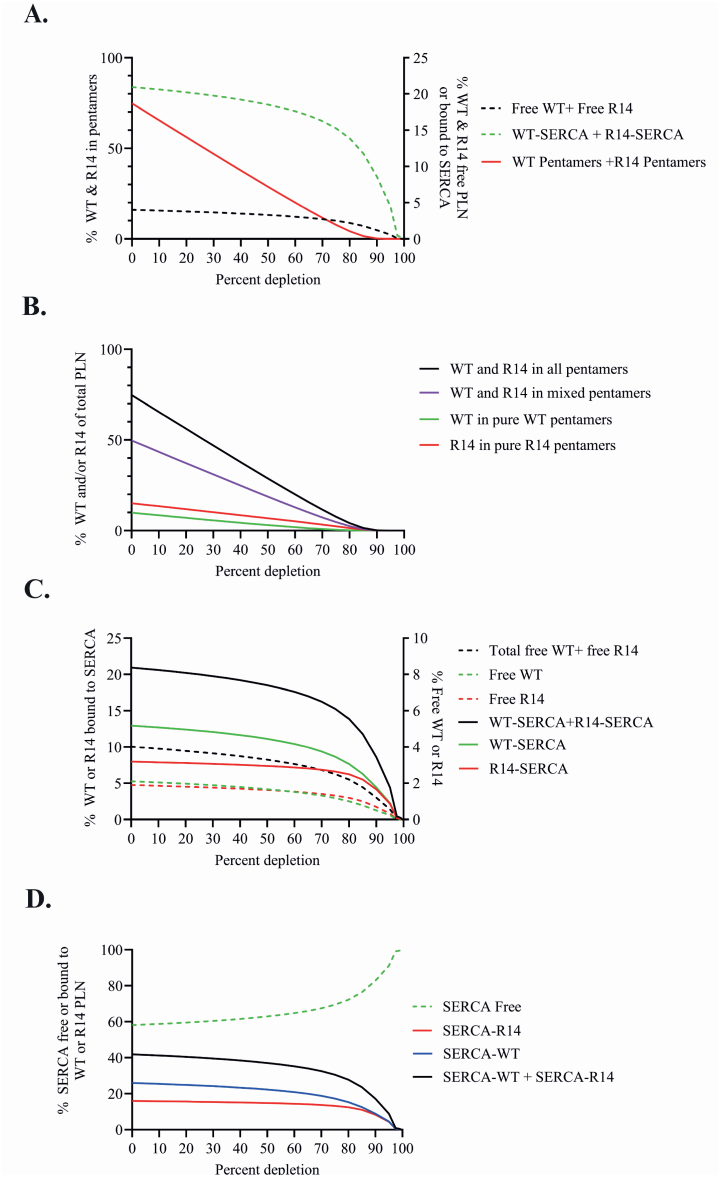

Figure 4. Effect of total PLN reduction on pentamer formation and SERCA binding in the heterozygous PLN WT/R14 state.

(A) Total PLN reduction in the heterozygous condition (equal amounts of WT PLN and R14del PLN) modeled as a single combined pool. Solid line (left vertical axis) and dashed lines (right vertical axis). **(B)** The PLN pentamer population comprises mixed pentamers (containing both WT and R14del PLN),

pure WT PLN pentamers, or pure R14del PLN pentamers, with their sum representing the total PLN pentamer population. Solid line (left vertical axis) and dashed lines (right vertical axis). **(C)** WT and/or R14del PLN bind to SERCA in the heterozygous state. **(D)** SERCA bound to WT and/or R14del PLN in the heterozygous state.

Discussion

Despite extensive investigations using patient material as well as cell and animal models, the underlying mechanism of PLN-R14del cardiomyopathy remains poorly understood. This may be due to the complex and dynamic interactions of this small protein with SERCA and with itself within the sarcoplasmic reticulum membrane, and possibly with other molecules. Such interactions are difficult to capture in experimental systems. Therefore, we turned to in silico simulation, to study how different PLN complexes are altered in relation to PLN silencing, which has shown therapeutic potential in animal studies.[4,11,12] Our simulations revealed that PLN pentamers are more sensitive to silencing compared with SERCA-PLN complexes and free PLN. These pentamers appear to act as a buffer, helping to maintain relatively stable levels of the other PLN pools. It will therefore be critical to identify which PLN pool drives disease in PLN-R14del cardiomyopathy. For other forms of heart failure, PLN silencing has also been suggested as a therapeutic strategy, but this may involve different PLN pools and requires further exploration.

It is remarkable that the PLN pentameric pool decreases almost linearly with the reduction in total PLN levels, whereas free PLN and SERCA-PLN complex remain relatively stable across a wide concentration range. This likely reflects the secondary nature of pentamer formation, which requires multiple PLN molecules to assemble, making it more sensitive to PLN abundance than the one-to-one interaction between PLN and the relatively constant amount of SERCA. Our simulations therefore support earlier suggestions that most PLN resides in pentamers, and that this pool functions as a buffer to stabilize PLN-SERCA levels.[16]

This has important implications for PLN silencing as a therapeutic strategy in PLN-R14del cardiomyopathy and other forms of heart failure. If the SERCA-R14del complex is the primary disease driver, higher levels of silencing may be required than if pentameric PLN is the main pathogenic species. For PLN-R14del cardiomyopathy, however, the disease-causing pool remains uncertain. Initially, the SERCA-R14del complex was considered the key target, but recent evidence indicates a reduced inhibitory action of PLN-R14del on SERCA and makes this explanation therefore less convincing.4,5 It is therefore tempting to speculate that the R14del pentamer may contribute to disease development. Supporting this idea, heterozygous R14del mice develop cardiomyopathy only at an advanced age (>15 months), whereas homozygous mice present with severe heart failure as early as 8 weeks.[17] Our simulations show that SERCA-R14del complexes are only 1.7-fold lower in the heterozygous state compared with homozygous condition, whereas pure PLN-R14del pentamers decrease by nearly 5.5-fold. These findings may suggest that pentamers, rather than SERCA complexes,

may play a more prominent role in disease development, and that wildtype PLN could exert a dampening effect by interfering with pure PLN-R14del pentamer formation.
PLN silencing is also considered an attractive strategy for common forms of heart failure, as several studies have reported reduced SERCA protein levels and diminished activity. Lowering PLN in such conditions could, in principle, enhance SERCA activity.[18,19] However, a recent study suggested that SERCA levels may actually remain stable during heart failure, an observation that requires further investigation.[20] Since our primary focus was to examine PLN-R14del cardiomyopathy, we did not simulate other types of heart failure in which SERCA might be reduced.

It is important to note that simulation studies have clear limitations and can only provide an indirect and simplified view of the real-life in vivo situation. Our model is based on equilibrium constants determined using fluorescently tagged PLN and SERCA proteins overexpressed in non-cardiomyocytes. These tags may interfere with normal PLN behavior, and in cardiomyocytes additional regulatory mechanisms are likely involved. Furthermore, our simulation only considers interactions between PLN and SERCA, while it is well known that these proteins interact with numerous other molecules, such as DWORF.[21] We modeled steady-state levels of PLN-SERCA and PLN-PLN complexes, but in reality, these complexes are dynamically influenced by posttranslational modifications, diastolic calcium concentrations, and beating frequency.[22] Notably, Robia and colleagues, using the same parameters applied here, demonstrated that in the PLN-R14del context the dynamic range of complex formation in response to beating frequency is reduced.[13] This may also contribute to disease development, including arrhythmogenesis. Finally, we do not know how pentamer formation occurs and whether this is a linear or non-linear process. Simulations of PLN-SERCA and PLN-PLN interactions in relation to PLN silencing should therefore be interpreted with caution and not used to define therapeutic windows for PLN-R14del cardiomyopathy. Instead, these investigations are meant to help us to understand the underlying processes and provide guidance for further research.

Altogether, the key conclusion we wish to emphasize is that PLN silencing affects different PLN pools in distinct ways, and it will be essential to determine which pool is the actual driver of PLN-R14del cardiomyopathy.

Supplemental figure

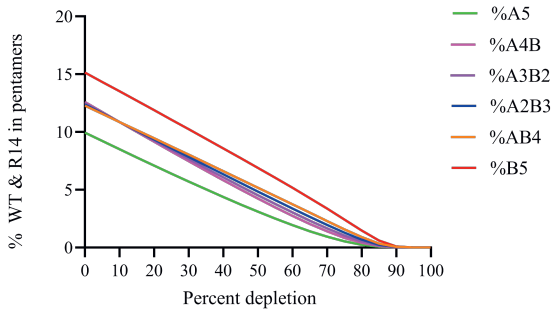

Supplemental figure 1. Differential decline of PLN pentamer subtypes during total PLN reduction in heterozygous states

Simulated decline of different PLN pentamer subtypes during total PLN reduction in heterozygous conditions.

Additional Information

Acknowledgements

We would like to thank Seth L. Robia and Peter M Kekenes-Huskey for fruitful discussions and scientific insights on PLN dynamics.

Funding

This work was supported by the Dutch Heart Foundation [2018-30 (CVON-PREDICT2) to H.H.W.S., 01-003-2022-0358 (CarMa) to H.H.W.S. and V.O.N.T.]; and a China Scholarship Council Grant [202008230186 to L.S.].

References

1. Kobra H, Fotis K, Anthony O G, Jason R W, Luke P, Roy A L, Guo-Chang F, Dimitris T, Rohan R P, Gerald W 2nd D, David H M, Dimitrios Th K, Evangelia G K. A mutation in the human phospholamban gene, deleting arginine 14, results in lethal, hereditary cardiomyopathy. Proc Natl Acad Sci U S A 2006;103.
2. van der Zwaag PA, van Rijsingen IA, de Ruiter R, Nannenberg EA, Groeneweg JA, Post JG, Hauer RN, van Gelder IC, van den Berg MP, van der Harst P, Wilde AA, van Tintelen JP. Recurrent and founder mutations in the Netherlands-Phospholamban p.Arg14del mutation causes arrhythmogenic cardiomyopathy. Neth Heart J 2013;21:286-293.
3. van der Zwaag PA, van Rijsingen IA, Asimaki A, Jongbloed JD, van Veldhuisen DJ, Wiesfeld AC, Cox MG, van Lochem LT, de Boer RA, Hofstra RM, Christiaans I, van Spaendonck-Zwarts KY, Lekanne dit Deprez RH, Judge DP, Calkins H, Suurmeijer AJ, Hauer RN, Saffitz JE, Wilde AA, van den Berg MP, van Tintelen JP. Phospholamban R14del mutation in patients diagnosed with dilated cardiomyopathy or arrhythmogenic right ventricular cardiomyopathy: evidence supporting the concept of arrhythmogenic cardiomyopathy. Eur J Heart Fail 2012;14:1199-1207.
4. Sun L, Eijgenraam TR, Amilon C, Janzen D, Hansson KM, Kubli DA, Spater D, Mullick AE, van der Meer P, Nunes Teixeira VO, Sillje HHW. In PLN-R14del mice, SR structure restoration, rather than calcium cycling, is the dominant effector of PLN-ASO treatment. Cardiovasc Res 2025.
5. Stege NM, Eijgenraam TR, Oliveira Nunes Teixeira V, Feringa AM, Schouten EM, Kuster DWD, van der Velden J, Wolters AHG, Giepmans BNG, Makarewich CA, Bassel-Duby R, Olson EN, de Boer RA, Sillje HHW. DWORF Extends Life Span in a PLN-R14del Cardiomyopathy Mouse Model by Reducing Abnormal Sarcoplasmic Reticulum Clusters. Circ Res 2023;133:1006-1021.
6. Badone B, Ronchi C, Lodola F, Knaust AE, Hansen A, Eschenhagen T, Zaza A. Characterization of the PLN p.Arg14del Mutation in Human Induced Pluripotent Stem Cell-Derived Cardiomyocytes. Int J Mol Sci 2021;22.
7. Claudia M, Marem E, Chiara F, Mara F, Paolo B, Elena S, Valentina P, Angela S M, Giulio P, Vivian Oliveira Nunes T, Rudolf A dB, Herman H W S, Francesco L, Antonio Z. Early consequences of the phospholamban mutation PLN-R14del(+/-) in a transgenic mouse model. Acta Physiol (Oxf) 2024;240.
8. Te Rijdt WP, van Tintelen JP, Vink A, van der Wal AC, de Boer RA, van den Berg MP, Suurmeijer AJ. Phospholamban p.Arg14del cardiomyopathy is characterized by phospholamban aggregates, aggresomes, and autophagic degradation. Histopathology 2016;69:542-550.
9. Te Rijdt WP, van der Klooster ZJ, Hoorntje ET, Jongbloed JDH, van der Zwaag PA, Asselbergs FW, Dooijes D, de Boer RA, van Tintelen JP, van den Berg MP, Vink A, Suurmeijer AJH. Phospholamban immunostaining is a highly sensitive and specific method for diagnosing phospholamban p.Arg14del cardiomyopathy. Cardiovasc Pathol 2017;30:23-26.
10. Stege NM, de Boer RA, Makarewich CA, van der Meer P, Sillje HHW. Reassessing the echanisms of PLN-R14del Cardiomyopathy: From Calcium Dysregulation to S/ER Malformation. JACC Basic Transl Sci 2024;9:1041-1052.
11. Eijgenraam TR, Stege NM, Oliveira Nunes Teixeira V, de Brouwer R, Schouten EM, Grote

Beverborg N, Sun L, Spater D, Knoll R, Hansson KM, Amilon C, Janzen D, Yeh ST, Mullick AE, van der Meer P, de Boer RA, Sillje HHW. Antisense Therapy Attenuates Phospholamban p.(Arg14del) Cardiomyopathy in Mice and Reverses Protein Aggregation. Int J Mol Sci 2022;23.

12. Grote Beverborg N, Spater D, Knoll R, Hidalgo A, Yeh ST, Elbeck Z, Sillje HHW, Eijgenraam TR, Siga H, Zurek M, Palmer M, Pehrsson S, Albery T, Bomer N, Hoes MF, Boogerd CJ, Frisk M, van Rooij E, Damle S, Louch WE, Wang QD, Fritsche-Danielson R, Chien KR, Hansson KM, Mullick AE, de Boer RA, van der Meer P. Phospholamban antisense oligonucleotides improve cardiac function in murine cardiomyopathy. Nat Commun 2021;12:5180.
13. Cleary SR, Teng ACT, Kongmeneck AD, Fang X, Phillips TA, Cho EE, Smith RA, Karkut P, Makarewich CA, Kekenes-Huskey PM, Gramolini AO, Robia SL. Dilated cardiomyopathy variant R14del increases phospholamban pentamer stability, blunting dynamic regulation of calcium. J Biol Chem 2025;301:108118.
14. Glaves JP, Primeau JO, Espinoza-Fonseca LM, Lemieux MJ, Young HS. The Phospholamban Pentamer Alters Function of the Sarcoplasmic Reticulum Calcium Pump SERCA. Biophys J 2019;116:633-647.
15. Brittsan AG, Carr AN, Schmidt AG, Kranias EG. Maximal inhibition of SERCA2 Ca(2+) affinity by phospholamban in transgenic hearts overexpressing a non-phosphorylatable form of phospholamban. J Biol Chem 2000;275:12129-12135.
16. Funk F, Kronenbitter A, Hackert K, Oebbeke M, Klebe G, Barth M, Koch D, Schmitt JP. Phospholamban pentamerization increases sensitivity and dynamic range of cardiac relaxation. Cardiovasc Res 2023;119:1568-1582.
17. Eijgenraam TR, Boukens BJ, Boogerd CJ, Schouten EM, van de Kolk CWA, Stege NM, Te Rijdt WP, Hoorntje ET, van der Zwaag PA, van Rooij E, van Tintelen JP, van den Berg MP, van der Meer P, van der Velden J, Sillje HHW, de Boer RA. The phospholamban p.(Arg14del) pathogenic variant leads to cardiomyopathy with heart failure and is unreponsive to standard heart failure therapy. Sci Rep 2020;10:9819.
18. Mattiazzi A, Kranias EG. Unleashing the Power of Genetics: PLN Ablation, Phospholambanopathies and Evolving Challenges. Circ Res 2024;134:138-142.
19. Federica dM, Sian E H, G William D, Judith K G, Roger J H. Targeting phospholamban by gene transfer in human heart failure. Circulation 2002;105.
20. Ragone I, Barallobre-Barreiro J, Takov K, Theofilatos K, Yin X, Schmidt LE, Domenech N, Crespo-Leiro MG, van der Voorn SM, Vink A, van Veen TAB, Bodor C, Merkely B, Radovits T, Mayr M. SERCA2a Protein Levels Are Unaltered in Human Heart Failure. Circulation 2023;148:613-616.
21. Phillips TA, Hauck GT, Pribadi MP, Cho EE, Cleary SR, Robia SL. Micropeptide hetero-oligomerization adds complexity to the calcium pump regulatory network. Biophys J 2023;122:301-309.
22. Guo J, Aonuma K, Kovacs R, Chen Z. Calcium-dependent levels of phospholamban pentamer in native heart membranes reflect interactions of monomers with calcium-free SERCA2a. Arch Biochem Biophys 2025;769:110432.

Chapter 7

General discussion and future perspectives

Summary and discussion

In this thesis, we aimed to ***I)*** summarize the identified PLN variants in clinical studies and discuss their potential pathogenic mechanisms; ***II)*** explore if cardiac stress could accelerate the onset of PLN-R14del cardiomyopathy in a heterozygous mouse model. ***III)*** Identify early disease mechanisms using an inducible PLN-R14del mouse model to. ***IV)*** Investigate PLN antisense oligonucleotide (ASO) dose effects and the disease modulatory mechanism in a PLN-R14del homozygous mouse model. ***V)*** Utilize *in silico* simulation to explore how balances in different PLN complex are affected by PLN gene silencing.

I) Clinical PLN variant and potential mechanisms

Phospholamban (PLN) is a small regulatory protein that modulates the activity of the sarco/endoplasmic reticulum Ca^{2+}-ATPase (SERCA2a), thereby controlling Ca^{2+} re-uptake into the sarcoplasmic reticulum (SR) and regulating the contraction–relaxation cycle of cardiomyocytes.[1] PLN acts as a reversible inhibitor of SERCA2a under physiological conditions, showing inhibitory activity in its dephosphorylated state, while phosphorylation at Ser16 relieves inhibition to facilitate rapid Ca^{2+} sequestration during diastole. This regulatory mechanism contributes to maintain proper calcium homeostasis and cardiac performance.

In **Chapter 2**, we summarized the currently reported clinical PLN variants and discussed their phenotypic spectrum and potential pathogenic mechanisms. Various types of PLN mutations, including truncation, missense, and deletion variants such as R14del, L39stop, R9C, R9H, and R9L, have been identified in patients with dilated, hypertrophic, and arrhythmogenic cardiomyopathies. Although these variants were initially believed to share a common molecular target, SERCA2a, they display remarkable heterogeneity in clinical manifestation, penetrance, and disease progression. Such diversity likely reflects distinct effects of each variant on PLN's structural conformation, oligomerization, membrane insertion, post-translational modification and protein interactions. For example, while some variants disrupt PLN's ability to form pentamers, others likely alter its phosphorylation dynamics or stability within the lipid bilayer, thereby leading to variant-specific structural alterations, including changes in PLN conformation and tilt angle within the membrane, as well as shifts in the equilibrium between monomeric and oligomeric states. Regarding protein interactions, R9C has been proposed to sequester PKA, thereby reducing the phosphorylation and effectively dampening PLN's regulatory responsiveness. R14del induces a profound structural defect characterized by misfolded sarco(endo)plasmic reticulum membrane and formation of aberrant PLN clusters. These structural perturbations ultimately compromise essential cardiomyocyte functions, leading to cellular stress, progressive cardiomyocyte injury and death, and consequently driving adverse cardiac remodeling and the development of heart failure. The L39Stop transcript is stable and actively translated, but the resulting truncated protein undergoes rapid proteasomal degradation, indicating that accelerated protein turnover, rather than mRNA instability, accounts for

the reduced detectability of this PLN variant. This suggests that continuous synthesis and degradation of the mutant peptide may itself represent a pathogenic mechanism unique to this variant.

Emerging evidence indicates that the pathogenicity of PLN variants can extend beyond the classical SERCA2a inhibition hypothesis and involves disturbances in PLN pentamer-monomer equilibrium, aberrant conformational transition states, and abnormal clustering within the sarcoplasmic/endoplasmic reticulum membranes. These structural perturbations may impair membrane integrity, protein trafficking, and proteostasis, ultimately triggering maladaptive stress pathways such as ER stress, mitochondrial dysfunction, and autophagy dysregulation. The complexity of these processes highlights that PLN-related cardiomyopathies represent a multifaceted proteopathic disorder rather than a simple defect in calcium handling. Given this mechanistic diversity, it becomes evident that PLN variants exert their pathogenic effects through multiple, variant-specific mechanisms, underscoring the need for mutation-tailored therapeutic strategies that precisely target the underlying molecular defect rather than relying on generalized heart failure treatment approaches.

II) Pressure overload as a trigger and accelerator of PLN-R14del cardiomyopathy

Among all known PLN mutations, the p.Arg14del (R14del) variant is the most prevalent and best-characterized pathogenic allele.[2] Initially, the PLN-R14del mutation was believed to cause super-inhibition of SERCA2a and abnormal Ca^{2+} uptake. However, accumulating evidence has challenged this classical view.[3,4] A striking feature of PLN-R14del cardiomyopathy is its remarkable heterogeneity in disease onset and severity. Heterozygous PLN-R14del carriers commonly present with arrhythmogenic and/or dilated cardiomyopathy, leading to progressive ventricular dilation, systolic dysfunction, and ultimately heart failure.[5,6] While most carriers develop disease during mid-adulthood, some experience early and severe manifestations, whereas others remain mildly affected until late life.[7,8] Heterozygous PLN-R14del mouse model ($R14^{\Delta/+}$) faithfully recapitulates the human disease phenotype. These mice exhibit abnormal PLN clustering, progressive contractile dysfunction, cardiomyocyte hypertrophy, fibrosis, and cardiac dilation starting around one year of age, mirroring the disease onset observed in middle-aged human carriers.[9] The relatively slow disease progression in this model allows investigation of secondary triggers that might exacerbate disease development.

Recent studies have shown that perturbation of PLN pentamer formation can sensitize the heart to hemodynamic stress.[10] In a transgenic mouse model unable to form PLN pentamers, transverse aortic constriction (TAC) led to markedly reduced survival and aggravated cardiac dysfunction, attributed to a restricted dynamic range of SERCA2a modulation.[11]

Indeed, pressure overload has been reported to aggravate cardiac dysfunction in multiple genetic cardiomyopathy models by activating stress pathways involving

calcium homeostasis, myofibrillar remodeling, oxidative stress, and mitochondrial autophagy.[12-14] Given that altered balances PLN oligomeric complexes have also been observed in PLN-R14del cardiomyopathy, pressure overload might similarly act as an external accelerator of disease progression. Additionally, cardiomyocyte hypertrophy and interstitial fibrosis are common features of both TAC-induced cardiac stress and PLN-R14del cardiomyopathy, it is plausible that mechanical overload could lower the threshold for disease manifestation. Based on this hypothesis, we subjected $R14^{\Delta/+}$ mice to TAC surgery to investigate whether cardiac pressure overload accelerates onset of PLN-R14del cardiomyopathy.

In **Chapter 3**, our results demonstrated that transverse aortic constriction (TAC) triggered compensatory cardiomyocyte hypertrophy and interstitial fibrosis, which collectively contributed to progressive cardiac remodeling and eventually heart failure. In TAC-operated mice, the hallmark PLN-positive clusters were absent in both WT and $R14^{\Delta/+}$ mice. Since these clusters normally emerge in heterozygous $R14^{\Delta/+}$ mice at around 18 months of age, their absence under TAC conditions indicates that mechanical stress alone is insufficient to trigger the formation of such pathological structures and therefore does not initiate or exacerbate the disease process. In the TAC-operated groups, both WT and $R14^{\Delta/+}$ mice exhibited a comparable reduction in ejection fraction (EF) and developed similar degrees of cardiac remodeling. This indicates that cardiac pressure overload triggers a largely TAC-specific compensatory response, without any additional mutation-dependent effect attributable to R14del.

Previous studies have reported that TAC can induce endoplasmic reticulum (ER) stress and activate unfolded protein response (UPR) signaling in various cardiac models,[15,16] contributing to maladaptive remodeling and heart failure. However, in **Chapter 3**, ER stress-related markers were not significantly activated in either PLN-R14del or WT mice following TAC. Therefore, based on the current findings, it cannot be excluded whether ER stress serves as an accelerator of disease progression in PLN-R14del cardiomyopathy. Activation of the UPR is a well-recognized feature of PLN-R14del cardiomyopathy in both humans and mice.[17,18] Notably, in vitro experiments using human iPSC-derived cardiomyocytes have shown that pharmacological induction of the ER chaperone Binding immunoglobulin protein (BiP) can improve cellular function in PLN-R14del models, suggesting a potential protective role of enhanced ER proteostasis.[17] Moreover, although TAC induced cellular stress and cardiac remodeling, as reflected by elevated ANP levels and altered fibrotic gene expression, these changes did not translate into an accelerated or mutation-specific pathological response in PLN-R14del mice. Taken together, these findings suggest that the activation threshold for overt disease in PLN-R14del cardiomyopathy may require additional or chronic stressors beyond the acute biomechanical load imposed by TAC. Future investigations incorporating diverse stress models will therefore be essential, as factors such as ageing, oxidative stress, inflammation, and altered lipid metabolism may exert a more decisive influence in priming PLN-R14del cardiomyocytes toward dysfunction and disease progression.

III) Early Pathogenic Mechanisms Revealed by the Inducible PLN-R14del Mouse Model

To better delineate the temporal sequence of pathological events and characterize disease manifestations at different stages of onset in PLN-R14del cardiomyopathy, in **Chapter 4** we developed an inducible mouse model that enables temporal control of mutant expression through a tamoxifen-inducible MerCreMer Loxp system.[19] In this model, cardiomyocytes initially express wild-type PLN, which can be synchronously replaced by the R14del allele following tamoxifen administration. This approach enabled us to study disease initiation under controlled conditions, independent of developmental or secondary influences.

Using this model, we demonstrated that the earliest detectable abnormality after gene conversion is the appearance of small PLN-positive clusters within the S/ER, which gradually expand into characteristic perinuclear clusters. Under electron microscopy, we further observed that as the disease progressed, the distribution of the S/ER shifted from a uniform alignment between sarcomeres to a progressively aggregated pattern around mitochondria and the perinuclear region. Importantly, these structural alterations arise before detectable changes in mRNA expression or functional impairment, indicating that S/ER malformation constitutes the primary pathogenic event in PLN-R14del cardiomyopathy. Different from **Chapter 3**, in **Chapter 4** we isolated primary cardiomyocytes from PLN-R14del mice and performed comprehensive proteomic and transcriptomic analyses. By excluding the influence of non-cardiomyocyte populations and interstitial tissue, this approach enabled us to capture cardiomyocyte-specific molecular alterations. Proteomic profiling of the isolated cells revealed a selective upregulation of ER chaperones, glycoprotein-processing enzymes, and substrates of the SEL1L-HRD1 endoplasmic reticulum–associated degradation (ERAD) pathway, indicating disrupted proteostasis and compensatory activation of ER quality-control mechanisms. However, at the mRNA level, we did not observe activation of any known cardiac-specific of ER-related pathways. The mismatch between mRNA and protein expression further suggests post-transcriptional regulation and/or impaired degradation capacity.

SQSTM1 (p62) is consistently upregulated in both human and murine PLN-R14del cardiomyopathy and co-localizes with PLN-positive aggregates, suggesting that defective autophagic clearance contributes to the accumulation of misfolded PLN proteins.[20] Additionally, accumulation of p62 and its colocalization with PLN clusters point to defective autophagic clearance, which may link impaired ERAD function to secondary autophagy dysfunction. The concurrent activation of ERAD substrates and accumulation of p62 imply that PLN-R14del cardiomyocytes experience an imbalance between protein folding and degradation, resulting in chronic proteotoxic stress. Such maladaptive responses likely represent a cell-autonomous attempt to maintain homeostasis but ultimately contribute to disease progression when clearance mechanisms become saturated.

From a mechanistic perspective, the inducible model therefore provides a unique opportunity to capture the earliest molecular disturbances driving disease onset. Future work should aim to elucidate the role of the ERAD pathway and p62-dependent autophagy in PLN-R14del pathology, particularly given the accumulation of ERAD-related substrates observed in our model. Additional studies will be needed to determine whether modulating these protein-quality-control pathways can influence remodeling processes or disease progression.

IV)Therapeutic Implications of PLN-R14del Cardiomyopathy

To date, there are no disease-specific therapies available for PLN-R14del cardiomyopathy, and clinical management largely follows the general guidelines for dilated or arrhythmogenic cardiomyopathies.[9,21] The primary therapeutic goal remains the stabilization of cardiac function and prevention of malignant arrhythmias. Standard heart failure (HF) therapies, including β-blockers, ACE inhibitors, angiotensin receptor–neprilysin inhibitors, and mineralocorticoid receptor antagonists, are routinely prescribed to reduce hemodynamic stress, fibrosis, and ventricular remodeling. However, these conventional interventions primarily target the secondary consequences of contractile dysfunction rather than the underlying molecular pathology of the disease. Their efficacy in delaying disease onset or preventing progression in asymptomatic PLN-R14del mutation carriers remains uncertain. Implantable cardioverter-defibrillators (ICDs) are widely used for sudden cardiac death prevention, particularly in patients with severe arrhythmias or reduced left ventricular ejection fraction. In advanced disease stages, heart transplantation remains the only curative option. More recently, clinical trials and observational studies have explored eplerenone and other antifibrotic agents, but these approaches have not demonstrated significant benefit in modifying disease trajectory in PLN-R14del carriers.[22]

Given the pathogenic mechanism of PLN-R14del cardiomyopathy, characterized by aberrant protein clustering, and disorganization of the E/SR structure, current therapeutic efforts are increasingly shifting toward mechanism-based and genetic strategies. Among these, antisense oligonucleotide (ASO) therapy targeting PLN mRNA has shown strong preclinical efficacy by silencing mutant PLN expression, reducing pathological aggregates, and improving cardiac function.[18,23] In **Chapter 5**, ASO administration on homozygous mouse effectively suppressed PLN levels in cardiomyocytes, resulting in a significant attenuation of disease pathology in a dose dependent manner. Mice receiving the highest dose of ASO (25/mg/kg) in this chapter, exhibited reduced fibrosis, preserved contractile function, and prolonged survival, even when therapy was initiated at advanced disease stages. Importantly, the beneficial effects were accompanied by a marked decrease in the number of cardiomyocytes containing PLN-positive aggregates, while calcium reuptake kinetics remained largely unchanged in PLN-R14del cardiomyocytes. The latter reflects the previously observed accelerated calcium uptake in PLN-R14del cardiomyocytes, which in contrast to WT cells, cannot be significantly further enhanced in these cardiomyocytes by PLN-ASO treatment. This further confirms that SERCA inhibition is (partially) lost by PLN-

R14del. These observations suggest that the primary therapeutic effect of ASO treatment is the restoration of SR structural integrity rather than direct correction of calcium-handling defects in this cardiomyopathy.[24] In other words, disease progression appears to be primarily driven by structural disorganization and proteotoxic stress rather than by reducing SERCA2a activity. By lowering total PLN abundance, ASO therapy alleviates aggregate burden and stabilized SR membranes thereafter improving cell survival. As discussed below our complementary *in silico* simulation **Chapter 6** further supports this concept. Simulations incorporating experimentally derived binding constants revealed that PLN pentameric assemblies are particularly sensitive to PLN reduction, whereas SERCA–PLN complexes and monomeric PLN are less affected. This preferential destabilization of pentamers may explain the selective clearance of aggregates observed in vivo following ASO treatment. These findings reinforce the notion that PLN-R14del cardiomyopathy is primarily a structural proteinopathy, driven by abnormal oligomerization and clustering, with calcium dysregulation emerging as a secondary consequence rather than the initiating trigger.

V) In Silico Insights

The pathogenesis of PLN-R14del cardiomyopathy arises from complex and dynamic interactions of mutant PLN molecules with each other, with SERCA2a, and potentially with additional protein partners within the S/ER membrane. Our *in silico* simulation **Chapter 6,** integrated with experimental evidence, how different PLN and SERCA pools redistribute in response to PLN silencing, thereby clarifying the dynamic balance among these molecular states rather than providing direct insight into disease mechanisms. Under physiological conditions, PLN exists in an equilibrium between pentamers, SERCA-bound monomers, and a small fraction of free PLN. In **Chapter 2**, we discussed the various PLN variants and proposed that alterations in the balance between PLN oligomeric and pentameric states, as well as changes in PLN-SERCA binding affinity, may critically influence PLN function. Our simulation confirms that the pentameric PLN pool acts as a dynamic reservoir that stabilizes the balance of SERCA-bound PLN and buffers fluctuations in PLN abundance. Upon PLN silencing or depletion, pentamers decrease almost linearly, while SERCA-bound PLN remains relatively stable until PLN levels are reduced by more than 80%, indicating that pentamers are more sensitive to quantitative changes and serve as a buffering pool.

In the PLN-R14del context, several key differences emerge. The mutant protein forms pentamers even more efficiently than wild-type PLN, resulting in a higher fraction of PLN-R14del incorporated into oligomeric assemblies and a lower proportion available to interact with SERCA. This correlates with experimental findings that PLN-R14del exhibits reduced inhibitory potency toward SERCA, suggesting that altered PLN-SERCA coupling alone cannot fully explain disease development. Instead, excessive and aberrantly stable pentamer formation, particularly within the S/ER membrane, may disrupt local proteostasis and membrane organization, ultimately triggering maladaptive stress signaling. In the heterozygous state, where both PLN-WT and PLN-R14del coexist, mixed pentamers predominate, and the fraction of pure PLN-R14del

pentamers is markedly reduced compared to the homozygous condition. Despite this, SERCA binding to PLN-R14del remains only moderately decreased (≈38%), while disease progression in vivo is substantially delayed.

Together, these data support the hypothesis that the imbalance between PLN production, pentamer formation, and/or ER-stress may lead to accumulation of PLN clustering and misfolded S/ER membrane. This, in turn, compromises cardiomyocyte function and viability over time. Understanding how PLN structural states and turnover dynamics contribute to cellular stress will be essential for identifying which PLN pool-SERCA-bound, free, or pentameric, is the key driver of pathology. This simulation provides a conceptual framework that can guide future research, and further refinement of the model, such as incorporating dynamic calcium fluctuations and post-translational modifications, will be valuable for advancing our understanding of this complex regulatory system.

Future Perspectives

The remaining mechanistic and therapeutic challenges

The mechanistic insights presented in this thesis redefine PLN-R14del cardiomyopathy as a structural and proteostasis disorder rather than a pure calcium-handling defect. The identification of early S/ER disorganization and proteotoxic stress highlights the need for therapeutic strategies that directly target these upstream molecular abnormalities. Interventions that address the primary cause, such as PLN silencing, gene correction, or stabilization of ER proteostasis, are likely to offer the greatest therapeutic benefit. However, translating these approaches to the clinic remains challenging. Gene therapy and gene-editing technologies, while conceptually powerful, still face limitations related to cardiac tissue specificity, delivery efficiency, and potential off-target effects. Until these strategies reach clinical maturity, alternative or complementary treatments targeting mechanistic intermediates, such as aberrant PLN clustering or disrupted ER quality control, may serve as practical interim solutions.

Bridging towards translational application

Among emerging targeted strategies, antisense oligonucleotides (ASOs) directed against PLN mRNA have shown the most advanced preclinical efficacy, robustly attenuating or even reversing cardiomyopathy in PLN-R14del mouse models by lowering PLN expression, reducing aggregate burden, and restoring SR architecture. However, these data also highlight that timing, dosing, and the extent of PLN knockdown must be carefully titrated to preserve physiological SERCA2a regulation and avoid long-term consequences of excessive PLN depletion. Additionally, sustained supraphysiological SERCA activation may predispose the heart to maladaptive remodeling or arrhythmias, thereby limiting the suitability of such interventions for long-term therapeutic use. Our *in silico* investigations do, however, suggest that PLN-SERCA pool is less sensitive to silencing as compared to the pentameric PLN pool,

indicating that this may be a less strong concern for a therapeutic silencing strategy in PLN-R14del cardiomyopathy.

The challenge of treatment timing and personalized intervention

Another key challenge is determining the optimal timing of intervention. Evidence from the PLN-ASO studies indicates that early initiation, before overt cardiac dysfunction, achieves the best preservation of contractile function and minimizes tissue damage. However, preventive treatment in asymptomatic carriers poses ethical and clinical dilemmas due to potential side effects and uncertain disease penetrance. Therefore, treatment should ideally commence shortly before disease onset, guided by reliable early biomarkers. Developing a biomarker panel combining advanced cardiac imaging, circulating protein markers of ER stress, and genetic risk profiling may enable personalized treatment initiation for PLN-R14del carriers. In our inducible PLN-R14del mouse model, we observed intracellular accumulation of Mfge8 within cardiomyocytes, whereas no significant changes were detected in plasma mfge8 levels compare to WT mice, suggesting that this protein may not serve as a reliable circulating biomarker. Nevertheless, its intracellular redistribution highlights the possibility that other ER-associated or secretory proteins could reflect early pathogenic remodeling, warranting further exploration of alternative biomarkers for early disease detection and risk stratification in PLN-R14del cardiomyopathy.

As genetic screening and family-based cascade testing expand, identifying presymptomatic carriers of pathogenic PLN variants has become more feasible. Integrating regular biomarker monitoring into clinical follow-up will facilitate precision-medicine strategies, allowing early and individualized therapeutic intervention to prevent irreversible myocardial damage. Continued collaboration between basic science, translational research, and clinical genetics will be crucial to translate these mechanistic discoveries into tangible clinical benefit for patients with PLN-associated cardiomyopathies.

Conclusion

In this thesis, we demonstrate that the PLN-R14del mutation, as a primary genetic cause, induces a mechanistic defect characterized by aberrant clustering of PLN and S/ER structure misfolding, leading to progressive disruption of cardiomyocyte proteostasis and function. This structural disorganization triggers a cascade of molecular alterations, including activation of endoplasmic reticulum stress responses, dysregulated autophagy, and maladaptive remodeling. Histological analyses revealed cardiomyocyte loss, interstitial fibrosis, and compensatory hypertrophy, ultimately manifesting as a clinical phenotype that spans the spectrum of arrhythmogenic and dilated cardiomyopathies. Together, these findings indicate that PLN-R14del cardiomyopathy is not merely a Ca^{2+}-handling disorder but a complex S/ER structural disease.

Although the PLN-R14del mutation represents a primary genetic driver of disease, its phenotypic manifestation exhibits considerable heterogeneity among heterozygous patients. Heterozygous PLN-R14del mice subjected to TAC surgery developed myocardial fibrosis and systolic dysfunction, but showed no acceleration of the characteristic PLN-R14del cardiomyopathy phenotype. This suggests that pressure overload alone is insufficient to trigger the mutation-specific pathogenic cascade. In the inducible PLN-R14del mouse model, isolated cardiomyocytes displayed clear upregulation of ER-stress-related proteins, suggesting that intrinsic cellular stress responses are a key component of the mutation's pathogenic mechanism. Notably, TAC failed to induce ER stress signaling in heterozygous PLN-R14del mice, providing a mechanistic explanation for why pressure overload did not exacerbate disease progression in this model.

Current therapeutic strategies for PLN-related cardiomyopathy rely largely on standard heart failure management. Encouragingly, our work and others' preclinical studies demonstrate that PLN silencing can be effective in PLN cardiomyopathy models, supporting the view that gene-based interventions are moving from concept to actionable therapeutic avenues. Although not all PLN variants share the same pathogenic mechanism-highlighting the importance of variant-specific PLN silencing may ultimately prove beneficial for a broader spectrum of PLN-associated cardiomyopathy and could even inform treatment strategies for heart failure beyond PLN cardiomyopathy.

Reference

1. Eisner DA, Caldwell JL, Kistamas K, Trafford AW. Calcium and Excitation-Contraction Coupling in the Heart. Circ Res 2017;121:181-195.
2. Vafiadaki E, Glijnis PC, Doevendans PA, Kranias EG, Sanoudou D. Phospholamban R14del disease: The past, the present and the future. Front Cardiovasc Med 2023;10:1162205.
3. Stege NM, de Boer RA, Makarewich CA, van der Meer P, Silljé HHW. Reassessing the Mechanisms of PLN-R14del Cardiomyopathy. JACC: Basic to Translational Science 2024.
4. Badone B, Ronchi C, Lodola F, Knaust AE, Hansen A, Eschenhagen T, Zaza A. Characterization of the PLN p.Arg14del Mutation in Human Induced Pluripotent Stem Cell-Derived Cardiomyocytes. Int J Mol Sci 2021;22.
5. Haghighi K, Kolokathis F, Gramolini AO, Waggoner JR, Pater L, Lynch RA, Fan GC, Tsiapras D, Parekh RR, Dorn GW, 2nd, MacLennan DH, Kremastinos DT, Kranias EG. A mutation in the human phospholamban gene, deleting arginine 14, results in lethal, hereditary cardiomyopathy. Proc Natl Acad Sci U S A 2006;103:1388-1393.
6. van der Zwaag PA, van Rijsingen IA, de Ruiter R, Nannenberg EA, Groeneweg JA, Post JG, Hauer RN, van Gelder IC, van den Berg MP, van der Harst P, Wilde AA, van Tintelen JP. Recurrent and founder mutations in the Netherlands-Phospholamban p.Arg14del mutation causes arrhythmogenic cardiomyopathy. Neth Heart J 2013;21:286-293.
7. van der Zwaag PA, van Rijsingen IA, Asimaki A, Jongbloed JD, van Veldhuisen DJ, Wiesfeld AC, Cox MG, van Lochem LT, de Boer RA, Hofstra RM, Christiaans I, van Spaendonck-Zwarts KY, Lekanne dit Deprez RH, Judge DP, Calkins H, Suurmeijer AJ, Hauer RN, Saffitz JE, Wilde AA, van den Berg MP, van Tintelen JP. Phospholamban R14del mutation in patients diagnosed with dilated cardiomyopathy or arrhythmogenic right ventricular cardiomyopathy: evidence supporting the concept of arrhythmogenic cardiomyopathy. Eur J Heart Fail 2012;14:1199-1207.
8. Posch MG, Perrot A, Geier C, Boldt L-H, Schmidt G, Lehmkuhl HB, Hetzer R, Dietz R, Gutberlet M, Haverkamp W, Özcelik C. Genetic deletion of arginine 14 in phospholamban causes dilated cardiomyopathy with attenuated electrocardiographic R amplitudes. Heart Rhythm 2009;6:480-486.
9. Eijgenraam TR, Boukens BJ, Boogerd CJ, Schouten EM, van de Kolk CWA, Stege NM, Te Rijdt WP, Hoorntje ET, van der Zwaag PA, van Rooij E, van Tintelen JP, van den Berg MP, van der Meer P, van der Velden J, Sillje HHW, de Boer RA. The phospholamban p.(Arg14del) pathogenic variant leads to cardiomyopathy with heart failure and is unreponsive to standard heart failure therapy. Sci Rep 2020;10:9819.
10. Cleary SR, Teng ACT, Kongmeneck AD, Fang X, Phillips TA, Cho EE, Smith RA, Karkut P, Makarewich CA, Kekenes-Huskey PM, Gramolini AO, Robia SL. Dilated cardiomyopathy variant R14del increases phospholamban pentamer stability, blunting dynamic regulation of calcium. J Biol Chem 2025;301:108118.
11. Funk F, Kronenbitter A, Hackert K, Oebbeke M, Klebe G, Barth M, Koch D, Schmitt JP. Phospholamban pentamerization increases sensitivity and dynamic range of cardiac relaxation. Cardiovasc Res 2023;119:1568-1582.
12. Gurha P, Abreu-Goodger C, Wang T, Ramirez MO, Drumond AL, van Dongen S, Chen Y, Bartonicek N, Enright AJ, Lee B, Kelm RJ, Jr., Reddy AK, Taffet GE, Bradley A, Wehrens XH,

Entman ML, Rodriguez A. Targeted deletion of microRNA-22 promotes stress-induced cardiac dilation and contractile dysfunction. Circulation 2012;125:2751-2761.

13. Hu C, Dai F, Wang J, Jiang L, Wang D, Gao J, Huang J, Luo J, Tang F, Zhang Z, Tang C. Peroxiredoxin-5 Knockdown Accelerates Pressure Overload-Induced Cardiac Hypertrophy in Mice. Oxid Med Cell Longev 2022;2022:5067544.
14. Shirakabe A, Zhai P, Ikeda Y, Saito T, Maejima Y, Hsu CP, Nomura M, Egashira K, Levine B, Sadoshima J. Drp1-Dependent Mitochondrial Autophagy Plays a Protective Role Against Pressure Overload-Induced Mitochondrial Dysfunction and Heart Failure. Circulation 2016;133:1249-1263.
15. Okada K, Minamino T, Tsukamoto Y, Liao Y, Tsukamoto O, Takashima S, Hirata A, Fujita M, Nagamachi Y, Nakatani T, Yutani C, Ozawa K, Ogawa S, Tomoike H, Hori M, Kitakaze M. Prolonged endoplasmic reticulum stress in hypertrophic and failing heart after aortic constriction: possible contribution of endoplasmic reticulum stress to cardiac myocyte apoptosis. Circulation 2004;110:705-712.
16. Park CS, Cha H, Kwon EJ, Sreenivasaiah PK, Kim DH. The chemical chaperone 4-phenylbutyric acid attenuates pressure-overload cardiac hypertrophy by alleviating endoplasmic reticulum stress. Biochem Biophys Res Commun 2012;421:578-584.
17. Feyen DAM, Perea-Gil I, Maas RGC, Harakalova M, Gavidia AA, Arthur Ataam J, Wu TH, Vink A, Pei J, Vadgama N, Suurmeijer AJ, Te Rijdt WP, Vu M, Amatya PL, Prado M, Zhang Y, Dunkenberger L, Sluijter JPG, Sallam K, Asselbergs FW, Mercola M, Karakikes I. Unfolded Protein Response as a Compensatory Mechanism and Potential Therapeutic Target in PLN R14del Cardiomyopathy. Circulation 2021;144:382-392.
18. Eijgenraam TR, Stege NM, Oliveira Nunes Teixeira V, de Brouwer R, Schouten EM, Grote Beverborg N, Sun L, Spater D, Knoll R, Hansson KM, Amilon C, Janzen D, Yeh ST, Mullick AE, van der Meer P, de Boer RA, Sillje HHW. Antisense Therapy Attenuates Phospholamban p.(Arg14del) Cardiomyopathy in Mice and Reverses Protein Aggregation. Int J Mol Sci 2022;23.
19. D S S, M N, M A C, S A W, T R K, K M T, J M P, J D M. Temporally regulated and tissue-specific gene manipulations in the adult and embryonic heart using a tamoxifen-inducible Cre protein. Circ Res 2001;89.
20. Vafiadaki E, Kranias EG, Eliopoulos AG, Sanoudou D. The phospholamban R14del generates pathogenic aggregates by impairing autophagosome-lysosome fusion. Cell Mol Life Sci 2024;81:450.
21. Arbelo E, Protonotarios A, Gimeno JR, Arbustini E, Barriales-Villa R, Basso C, Bezzina CR, Biagini E, Blom NA, de Boer RA, De Winter T, Elliott PM, Flather M, Garcia-Pavia P, Haugaa KH, Ingles J, Jurcut RO, Klaassen S, Limongelli G, Loeys B, Mogensen J, Olivotto I, Pantazis A, Sharma S, Van Tintelen JP, Ware JS, Kaski JP, Group ESCSD. 2023 ESC Guidelines for the management of cardiomyopathies. Eur Heart J 2023;44:3503-3626.
22. de Brouwer R, Te Rijdt WP, Hoorntje ET, Amin A, Asselbergs FW, Cox M, van der Heijden JF, Hillege H, Karper JC, Mahmoud B, van der Meer P, Oomen A, Te Riele A, Sillje HHW, Tan HL, van Tintelen JP, van Veldhuisen DJ, Westenbrink BD, Wiesfeld ACP, Willems TP, van der Zwaag PA, Wilde AAM, de Boer RA, van den Berg MP. A randomized controlled trial of eplerenone in asymptomatic phospholamban p.Arg14del carriers. Eur Heart J 2023;44:4284-4287.

23. Grote Beverborg N, Spater D, Knoll R, Hidalgo A, Yeh ST, Elbeck Z, Sillje HHW, Eijgenraam TR, Siga H, Zurek M, Palmer M, Pehrsson S, Albery T, Bomer N, Hoes MF, Boogerd CJ, Frisk M, van Rooij E, Damle S, Louch WE, Wang QD, Fritsche-Danielson R, Chien KR, Hansson KM, Mullick AE, de Boer RA, van der Meer P. Phospholamban antisense oligonucleotides improve cardiac function in murine cardiomyopathy. Nat Commun 2021;12:5180.
24. Sun L, Eijgenraam TR, Amilon C, Janzen D, Hansson KM, Kubli DA, Spater D, Mullick AE, van der Meer P, Nunes Teixeira VO, Sillje HHW. In PLN-R14del mice, SR structure restoration, rather than calcium cycling, is the dominant effector of PLN-ASO treatment. Cardiovasc Res 2025;121:2042-2054.
25. Stege NM, Eijgenraam TR, Oliveira Nunes Teixeira V, Feringa AM, Schouten EM, Kuster DWD, van der Velden J, Wolters AHG, Giepmans BNG, Makarewich CA, Bassel-Duby R, Olson EN, de Boer RA, Sillje HHW. DWORF Extends Life Span in a PLN-R14del Cardiomyopathy Mouse Model by Reducing Abnormal Sarcoplasmic Reticulum Clusters. Circ Res 2023;133:1006-1021.
26. Dave J, Raad N, Mittal N, Zhang L, Fargnoli A, Oh JG, Savoia ME, Hansen J, Fava M, Yin X, Theofilatos K, Ceholski D, Kohlbrenner E, Jeong D, Wills L, Nonnenmacher M, Haghighi K, Costa KD, Turnbull IC, Mayr M, Cai CL, Kranias EG, Akar FG, Hajjar RJ, Stillitano F. Gene editing reverses arrhythmia susceptibility in humanized PLN-R14del mice: modelling a European cardiomyopathy with global impact. Cardiovasc Res 2022;118:3140-3150.

A

Netherlandse samenvatting

Dankwoord

Curriculum vitae

Dutch summary

Acknowledgements

About the author

Nederlandse samenvatting

Cardiomyopathieën vormen een heterogene groep aandoeningen van de hartspier die worden gekenmerkt door structurele en/of functionele afwijkingen van het hart. Deze afwijkingen kunnen leiden tot progressieve contractiestoornissen, hartritmestoornissen, hartfalen en plotselinge hartdood. Een belangrijk deel van deze aandoeningen heeft een genetische oorzaak. Binnen deze groep neemt phospholamban (PLN)-gerelateerde cardiomyopathie een voorname plaats in. In het bijzonder is de pathogene variant **PLN-R14del** van groot klinisch belang, omdat deze in Nederland relatief frequent voorkomt en gepaard gaat met een verhoogd risico op zowel aritmogene als gedilateerde cardiomyopathie. De klinische expressie is echter sterk variabel: sommige dragers ontwikkelen al op jonge leeftijd ernstige ziekte, terwijl anderen pas laat of slechts in milde vorm symptomen krijgen. Deze heterogeniteit wijst erop dat de pathogenese van PLN-R14del-cardiomyopathie complex is en niet volledig kan worden verklaard vanuit één enkel mechanisme.

PLN is een klein regulatoir membraaneiwit dat in hartspiercellen de activiteit van de calcium pomp SERCA2a in het sarco(endo)plasmatisch reticulum (SR/ER) moduleert en daarmee de calcium opname vanuit het cytoplasma naar het SR/ER beïnvloedt. Lange tijd werd aangenomen dat de ziekte vooral het gevolg was van een verstoorde calciumhuishouding door afwijkende remming van SERCA2a door PLN. Recente resultaten, waaronder die in dit proefschrift, laten echter zien dat deze klassieke verklaring onvoldoende is. In plaats daarvan wijzen de experimentele en conceptuele bevindingen op een breder ziektebeeld, waarin verstoring van SR/ER-structuur, afwijkende eiwitorganisatie, ontregeling van proteostase en mutatie-specifieke cellulaire stressresponsen centraal staan. Daarmee verschuift het perspectief van een louter calcium-georiënteerd model naar een model waarin structurele en proteotoxische processen een doorslaggevende rol spelen in het ontstaan van ziekte.
In dit proefschrift stond daarom de vraag centraal welke moleculaire en pathofysiologische mechanismen ten grondslag liggen aan PLN-R14del-cardiomyopathie, en in hoeverre deze mechanismen aanknopingspunten bieden voor gerichte therapie. Hiertoe zijn vijf samenhangende onderzoekslijnen uitgewerkt: 1) een overzicht van klinisch beschreven PLN-varianten en hun vermoedelijke werkingsmechanismen; 2) een analyse van cardiale stress als mogelijke ziektemodifier; 3) de ontwikkeling van een induceerbaar muismodel om vroege ziekteprocessen te bestuderen; 4) een evaluatie van dosisafhankelijke effecten van PLN-gerichte antisense oligonucleotiden (ASO's); 5) een *in silico*-analyse van de gevolgen van PLN-silencing voor verschillende PLN-complexen.

Het overzicht van bekende pathogene PLN-varianten in hoofdstuk 2, laat zien dat PLN-gerelateerde cardiomyopathie niet kan worden beschouwd als één uniforme aandoening. Verschillende varianten, waaronder truncaties, missense-mutaties en deleties zoals R14del, R9C, R9H, R9L en L39stop, leiden tot uiteenlopende fenotypes en waarschijnlijk ook tot verschillende onderliggende moleculaire defecten. De

verschillen betreffen onder meer oligomerisatie, fosforylering, membraaninsertie, stabiliteit en eiwit-eiwitinteracties. Deze bevindingen onderstrepen dat niet alle PLN-varianten via hetzelfde mechanisme pathogeen zijn, en dat een uniforme therapeutische benadering waarschijnlijk niet voor alle dragers optimaal zal zijn. Dit heeft belangrijke implicaties voor toekomstige precisiegeneeskunde binnen het veld van erfelijke cardiomyopathieën.

Vervolgens is in hoofdstuk 3 onderzocht of verhoogde cardiale belasting het ontstaan van PLN-R14del-cardiomyopathie kan versnellen. Omdat dragers een sterke variatie vertonen in leeftijd van ziekte-onset en ernst, werd verondersteld dat bijkomende stressoren de drempel voor ziekteactivatie mogelijk kunnen verlagen. In een heterozygoot PLN-R14del-muismodel werd hiervoor drukbelasting geïnduceerd met transverse aorta constrictie (TAC). Hoewel TAC, zoals verwacht, leidde tot hypertrofie, fibrose en afname van de cardiale functie, veroorzaakte het geen versnelde vorming van de kenmerkende PLN-positieve SR/ER-clusters en ook geen extra mutatie-specifieke verslechtering bovenop de algemene respons op drukbelasting. Deze resultaten laten zien dat acute biomechanische belasting op zichzelf onvoldoende is om het specifieke ziekteproces van PLN-R14del te initiëren of te versnellen. Daarmee lijkt algemene cardiale stress niet een simpele verklaring voor de klinische heterogeniteit bij dragers te zijn.

Om de vroegste gebeurtenissen in het ziekteproces beter te kunnen bestuderen, werd in dit proefschrift een nieuw induceerbaar PLN-R14del-muismodel ontwikkeld, zoals beschreven in hoofdstuk 4. In dit model kon de expressie van wildtype PLN in volwassen cardiomyocyten synchroon worden omgezet naar expressie van PLN-R14del door middel van een tamoxifen-afhankelijke MerCreMer/LoxP-strategie. Hierdoor werd het mogelijk om ziekte-initiatie in de tijd gecontroleerd te volgen, zonder verstoring door ontwikkelingsprocessen of asynchrone expressie. Met dit model werd aangetoond dat de eerste detecteerbare afwijking bestaat uit het ontstaan van kleine PLN-positieve clusters in het SR/ER, die in de loop van de tijd uitgroeien tot de karakteristieke perinucleaire structuren die kenmerkend zijn voor deze cardiomyopathie. Belangrijk is dat deze structurele veranderingen al zichtbaar waren voordat duidelijke functionele achteruitgang of uitgesproken weefselafwijkingen optraden. Dit wijst erop dat SR/ER-misvorming een vroege en waarschijnlijk primaire gebeurtenis is in de pathogenese van PLN-R14del-cardiomyopathie.

Aanvullende transcriptoom en proteoom analyses van geïsoleerde cardiomyocyten uit dit induceerbare model lieten zien dat de vroege moleculaire veranderingen zich vooral op eiwitniveau manifesteren. Terwijl op mRNA-niveau relatief weinig veranderingen werden waargenomen, toonde het proteoom duidelijke verstoringen in SR/ER-gerelateerde processen. Daarbij werden onder meer veranderingen gevonden die passen bij activering of overbelasting van kwaliteitscontrolemechanismen in het endoplasmatisch reticulum, inclusief accumulatie van eiwitten die verband houden met ER-geassocieerde afbraak (ERAD). Ook werd een discrepantie zichtbaar tussen

transcriptie en eiwitexpressie, wat wijst op een belangrijke rol voor post-translationele en/of afbraak-gerelateerde regulatie. Samen ondersteunen deze bevindingen het concept dat PLN-R14del-cardiomyopathie vroeg wordt gekenmerkt door verstoorde proteostase en een ontregeld intracellulair kwaliteitscontrolesysteem, gevolgd door latere transcriptoom veranderingen.

Een volgende centrale vraag was hoe verlaging van PLN-expressie therapeutisch ingrijpt op dit ziekteproces. In een homozygoot PLN-R14del-muismodel werd daarom het effect van verschillende doseringen van PLN-gerichte antisense oligonucleotiden onderzocht, zoals beschreven in hoofdstuk 5. Deze experimenten toonden een duidelijke dosisafhankelijke bescherming: ASO-behandeling leidde tot verbetering van de cardiale functie, afname van remodellering, verlenging van de overleving en reductie van de pathologische PLN-positieve SR-clusters. Opvallend was echter dat de invloed op calciumdynamiek in mutante hartspiercellen beperkt bleef. In wildtype-cellen leidde PLN-depletie wel tot de verwachte versnelling van calcium- en contractiedynamiek, maar in PLN-R14del-hartspiercellen waren deze parameters reeds versneld en nauwelijks verder te verbeteren. Dit ondersteunt de conclusie dat het therapeutisch effect van PLN-ASO bij deze mutatie niet primair berust op herstel van calciumregulatie, maar vooral op herstel van SR-structuur.

Om beter te begrijpen waarom PLN-silencing vooral de structurele pathologie lijkt te beïnvloeden, is in hoofdstuk 6 aanvullend een *in silico*-model ontwikkeld waarin verschillende moleculaire vormen van PLN werden gesimuleerd: vrije monomeren, pentameren en SERCA-gebonden complexen. Deze simulaties lieten zien dat pentamere PLN-complexen gevoeliger zijn voor afname van totale PLN-concentratie dan vrije of SERCA-gebonden PLN-vormen. Dat is relevant, omdat juist de pentameer of geclusterde PLN-pool vermoedelijk sterk bijdraagt aan de abnormale intracellulaire accumulatie die bij PLN-R14del wordt gezien. De modelresultaten bieden daarmee een mechanistische verklaring voor de experimentele observatie dat PLN-silencing gepaard gaat met afname van abnormale clustering en herstel van SR-architectuur, terwijl de functionele SERCA-gerelateerde pool relatief langer behouden blijft. Deze bevindingen ondersteunen het idee dat niet alle PLN-pools even gevoelig zijn voor afname van totale PLN-concentratie en dat de pentameer vorm, die het gevoeligst reageert, wellicht de meest pathologische component van het systeem is.

Gezamenlijk geven de resultaten in dit proefschrift aanleiding tot een herijking van het ziekteconcept van PLN-R14del-cardiomyopathie. In plaats van een aandoening die hoofdzakelijk wordt gedreven door afwijkende calciumremming van SERCA2a, komt er een beeld naar voren van een structurele proteinopathie van het sarco(endo)plasmatisch reticulum. Een centrale vroege gebeurtenis is de vorming van afwijkende PLN-positieve SR/ER-clusters, gevolgd door ontregeling van proteostase, activatie van intracellulaire stressroutes en uiteindelijk progressieve cardiale remodellering en functieverlies. Deze interpretatie verbindt de histologische, moleculaire, functionele en therapeutische bevindingen binnen dit proefschrift tot één

samenhangend geheel.

De resultaten hebben daarnaast duidelijke translationele implicaties. Ten eerste ondersteunen zij verdere ontwikkeling van PLN-gerichte silencingstrategieën als veelbelovende therapeutische route, waarbij optimaliseren van de juiste dosering in de mens een belangrijk aandachtspunt zal zijn. Ten tweede benadrukken onze resultaten het belang van vroege detectie, omdat interventie vóór het ontstaan van irreversibele structurele schade waarschijnlijk het meest effectief zal zijn. Ten derde suggereren zij dat toekomstige biomarkerontwikkeling zich niet uitsluitend moet richten op globale hartfunctiemetingen, maar ook op vroege indicatoren van SR/ER-stress,. Tot slot hebben we beschreven dat er PLN-variant-specifieke verschillen in onderliggend pathologische mechanismen kunnen zijn. Hiermee dient rekening te worden gehouden bij de ontwikkeling van nieuwe therapieën.

Samenvattend toont dit proefschrift aan dat de pathogene variant PLN-R14del leidt tot een vroeg optredende ontregeling van de intracellulaire SR/ER-organisatie, met daaropvolgende verstoring van proteostase en progressieve achteruitgang van hartspiercel functie. De bevindingen verschuiven het pathogenetische paradigma van een overwegend calcium-georiënteerde verklaring naar een model waarin structurele ontregeling en abnormale eiwitorganisatie centraal staan. Daarmee levert dit proefschrift niet alleen nieuwe inzichten in de biologie van PLN-R14del-cardiomyopathie, maar ook een basis voor de verdere ontwikkeling van mechanisme-gedreven en mutatie-specifieke behandelstrategieën.

Acknowledgements

Five years ago, with a deep passion for medicine and an aspiration to pursue cardiovascular research, I boarded the flight from Beijing to Amsterdam. At that time, my vision of the future was still somewhat unclear, and I did not yet know what path I would take after my master's degree, yet I was full of hope. One thing I knew clearly was that, at some point in my life, I wanted to pursue a study experience in another country. Groningen was a place I had never heard of before, but life is sometimes full of unexpected chance and coincidence. Over the subsequent five years in Groningen, I experienced many ups and downs and grew through both life and research. These unique experiences, whether in good times or difficult ones, have carried forward my past and laid a foundation for my future. Each step has quietly brought me closer to the person I aspire to become.

Looking back on this journey, I have gradually grown from a fresh and inexperienced student into an independent researcher capable of critical thinking, and I am now approaching a major milestone of my PhD path. I would like to express my heartfelt gratitude to my supervisors, family, friends, and colleagues who have accompanied and supported me along the way. Without your trust, encouragement, and help, I could not have made it this far on my own.

First and foremost, I would like to send my deepest gratitude to all my supervisors, **Prof. dr. Herman H.W. Silljé** and **Dr. Oliveira Nunes Teixeira V**. This PhD journey would not have been possible without your continuous guidance, encouragement, and unwavering support.

Dear **Herman**, I feel incredibly fortunate to have you as my supervisor during my PhD. When I started this journey, coming from a clinical background, I often felt lost in the lab and unsure about experimental work. You patiently guided me through those early stages and helped transform a rather naive beginner into an independent researcher. The way you approach scientific questions has also shaped my own thinking in subtle but lasting ways. Even when I did not always show much excitement about my results on the outside, you consistently encouraged me to view my work with more optimism and to take pride in each step forward. Thank you for your patience in shaping my scientific thinking and for your timely advice whenever I encounter challenges. Your dedication to rigorous research and high standards has profoundly influenced the way I approach science. Although I did not fully realize the extent of my growth at the time, I came to see clearly, especially during my new job interviews, how much I have changed and matured under your mentorship over these years. I am truly grateful for everything you have taught me, both academically and personally.

Dear **Vivian**, Working and living in a second language was both exciting and unfamiliar for me when I first arrived in the Netherlands. I still remember my very first day in the

lab, you welcomed me with such warmth, enthusiasm, and an easy, talkative openness, and it immediately made me feel that this new environment might not be as hard to settle into as I had feared. As my daily supervisor, you supported me in countless practical details of both work and life, many of the small but essential things that helped me stay grounded and move forward. Beyond the lab, we also shared many conversations about everyday life, personal thoughts, and the ups and downs of life. You often checked in to see whether everything was going well. And because I am not always the type to say everything out loud, your initiative meant even more to me. It gave me a deep sense of reassurance. I knew that whatever happened, you would be the person willing to step in, help me find a way through, and make sure I never had to handle things entirely on my own.

Here, I would like to extend my sincere gratitude to the members of the thesis assessment committee, **Prof. R.A. de Boer, Prof. A. J. A. van de Sluis, and Prof. J. P. van Tintelen**, for their time and effort in reviewing my thesis and providing valuable feedback.

I would like to specially thank my paranymphs: **Rani Puspitarani, Xuanxuan Guo**, for accepting my proposal and helping me arrange and offering help during my thesis defense.

Dear **Rani**, it surprised me that you were a little scared of me in the beginning, because I actually liked you from our very first conversation on the way to the lunch meeting room. I do not fully remember what exactly brought us closer and closer but knowing that you are such a social butterfly/caterpillar, it somehow makes perfect sense. When I first moved into our office, I did not expect much from the people around me. But apparently, life treated me much better than I had expected from that moment on. We have had so many kinds of "dates" together, as well as countless discussions about our "projects". We supported each other and somehow managed to make our PhD lives much better than average level. You have always been someone with a clear sense of purpose and direction. I truly hope that in the future, you will achieve the life you have envisioned for yourself and realize all your dreams. But please do not be a GP only gives paracetamol.

Dear **Xuanxuan**, your straightforward personality has always been one of the most distinctive presences in the lab. Although it felt a little sharp to me at first, the longer I got to know you, the more I realized that you were actually very easy to get along with.

In a way, it also seemed as if having Guoguo had somehow softened and "buffered"

you. During the last couple of months of my PhD, when the pressure became especially intense, having you as both a lunch buddy and a gossip buddy made those days feel shorter, lighter, and much more enjoyable. Whenever I needed to vent, you were always on my side, which made me feel much better. Although we both used to complain that Groningen is far away from anywhere and a little boring, I am glad that we both found

interests outside of work and truly enjoyed them. That made life there feel much richer than we had once imagined. In the coming months, you may also face a great deal of pressure as you approach graduation, but I wish that everything will go smoothly and that you will successfully achieve your goal.

Peter van der Meer, **Daan Westenbrink**, **Nils Bömer**, **Laura Meems**, thank you for your support and for your contributions to the academic environment in which I carried out my PhD research.

I would like to express my sincere gratitude to the technical and administrative support team for their invaluable assistance throughout this project. I am especially thankful to **Daniëlle Groenhagen** for her administrative support and departmental coordination, and to **Silke Oberdorf-Maass** for her management and coordination of the technical staff. I am also deeply grateful to **Sietske-Nyncke Zijlstra**, **Marloes Schouten**, and **Alianne Dunnink** for their outstanding technical support with sample processing, genotyping, mouse echocardiography, and mouse surgery. I would like to thank **Martin Dokter** for his support in histopathological analysis. Their expertise, dedication, and continued support, including technical assistance and equipment maintenance, were indispensable for the successful completion of this work.

Dear **Jumo Zhu**, thank you for all the support you gave me during my PhD, after my PhD, and even up until now. I especially want to thank you for taking care of Xiaomi for me during a particularly difficult period. Perhaps because we share a similar medical background and the same uncertainty about the future, our conversations could range from career plans and personal interests to the most random topics. It is amazing how diverse our conversations have been, and yet how naturally they always seemed to flow. I am also very grateful that you lent me your computer during my gap period and stayed up all night playing games with me. Without you, I probably would have finished writing my thesis at least three months earlier than this, but my life would also have been much less fun.

Tingting Chen, our friendship began on a wildly windy day, and I feel very lucky that you became my classmate, neighbor, and roommate. Over the past five years, we have shared so many personal thoughts and scientific discussions, and in this faraway country, you gradually became like a sister to me. We have also gone through many difficulties together. Although I would not describe you as the most optimistic person, I have always admired your strength and your ability to find a way through challenges. I truly hope that in the future you will find the path you want and build a life that suits you best. **Xiaodan Guo**, I truly appreciate your encouragement to start my horse-riding journal, as it would have been a great pity if I had never done so. Thank you for all the conversations we shared during the times when I felt lost, and for the thoughtful gifts and tea you brought back to Groningen from your trips. I have always known that you would be there for me whenever I needed help, and that reassurance has meant so much to me. Your kindness, warmth, and generosity have always brought me comfort. I

sincerely wish you and Mr. Ding a happy, peaceful, and beautiful life together.

I extend my gratitude to my friends in China, **MoMo,** thank you for your patience with me every day, for listening to my daily stories and complaints, and for always being there with your emotional support. It was a lot of fun having holiday together with you. Without you, I would not have come this far. **Pengyu Duan**, thank you for your daily support and for your willingness to help me financially during a difficult time. You have always been one of my strongest pillars. And thank you as well for being my ChatGPT VIP buddy, without that, we might never have finished our PhD theses. **Jialiang Gao**, thank you for submitting my documents during the COVID period. Without your help, I would not have been able to come to the Netherlands to pursue my dream.

PLN group, **Tim Eijgenraam**, thank you for your help and guidance during the final year of my PhD. I am truly grateful for your support with all the animal experiments, for your important contribution to cardiomyocyte isolation, and for the many conversations we shared. Your assistance and discussions were of great value to my research and to me personally during this final stage of my PhD journey. **Nienke Stege**, I am grateful for our honest conversations, which I always found refreshing and meaningful. Your attitude toward science has been truly inspiring to me, and I have greatly admired your thoughtful and genuine approach to research. Thank you also for your insightful suggestions during our PLN meetings. **Niharika Adak**, thank you for being part of the team and for helping to create such a pleasant and supportive working environment. I wish you all the best and every success in your future research. **Rui Li**, wish you all the best in scientific research.

I extend my gratitude to my officemates. **Annet Linders**, your handmade creations always brought me lovely surprises, and I enjoyed our conversations about your rabbit. **Itamar Braga Dias**, you are an amazing researcher, and I benefited greatly from your opinions and insights. Your energetic presence also had a positive influence on the working environment and made it even better. **Joris van den Hurk,** thank you for helping me participate in and translate during the Huurcommissie meeting, and for your scientific support in PLN research. **José Antonio Esquivel Gaytán**, thank you for your valuable advice about my future career during the final period of my PhD, and for sharing your Dutch textbook with me. I am also deeply grateful for your support during a difficult time. **Kirsten Nijholt,** you always made me feel at home in the office. I hope you succeeded and enjoyed the journal after your graduation. **Navin Suthahar**, I enjoyed the time we shared as officemates, and I always appreciated your thoughtful and insightful perspective on science.

I would also like to sincerely thank my graduated Chinese friends, whose companionship and support have meant a great deal to me. **Canxia Shi**, thank you for arranging our trip to Barcelona and so many other delightful day trips. **Hailun Qin**, thank you for the wonderful moments we shared in Papendal and Madrid**. Ming Wai Yeung,** thank you for so generously sharing your experience and knowledge. **Sunhuo**

Li, thank you for your support in my scientific work. **Xuanyi Jin**, thank you for your kindness, care, and encouragement during my PhD and in the gap period afterward.

Aad Withaar, thank you for teaching me how to analyze RNA-sequencing data. **Kalina Andrysiak,** I always enjoyed our conversations, and I greatly appreciated your kindness, comfort, and support during a difficult time. **Pablo Ignacio Sánchez Aguilera**, thank you for your help whenever I had problem during my experiment. **Susanne Feringa,** thank you for your contribution and all the arrangements for my project. **Constantin Palm**, **Eva Pet**, **Just Dronkers**, thank you for your kindness and for being part of the friendly and supportive atmosphere in the lab, truly appreciated your kindness and inclusiveness, which always made me feel comfortable and welcome. I really enjoyed our journey in Heidelberg. **Lotte Geerlings,** your active vibe always brings me up, and your contribution of organizing of lunch meeting and social event. **Karla Fernanda Arevalo Gomez**, thank you for helping me process the data of TAC study. **Mathilde Vermeer**, thank you for your academic support and assistance throughout my work. **Imran Ertugrul,** wish you succeed in your very cool transplantation project. **Ali A. Al-Mubarak**, **Belend Mahmoud, Cindya Iswandi**, **Ferdy Lambregtse**, **Frits Deiman**, **Huitzilihuitl Saucedo Orozco**, **Remco de Brouwer**, **Sam Majoor**, **Sanne de Wit**, and **Stascha Kuipers**, I would also like to thank you all for your kindness and for contributing to such a pleasant and supportive atmosphere in the department.

感谢我的父亲**孙志三**先生和母亲**刘静波**女士，感谢他们三十年来给予我的爱与培养。正是他们这些年来始终如一、毫无保留的爱，和他们一直以来对我梦想的支持，以及对我每一个决定的信任，我才有机会走出熟悉的生活，去见识这个世界更广阔、更多元的可能。 在人生的许多个十字路口，我也曾无数次感到迷茫，看不清前方的方向。但我始终知道，家人永远是我最坚强的后盾，是我在面对未知与挑战时最大的底气与依靠。很遗憾，爸爸没有机会亲眼见证我博士毕业的这一刻。但我始终相信，无论是在过去，还是此时此刻，我一直都是他的骄傲。

感谢我的舅舅**刘静涛**先生，你一直是我追梦途中指引方向的灯塔。那一盒来自英国的巧克力，像一扇轻轻打开的窗，让我第一次对远方与世界有了朦胧的想象，也由此踏上了探索世界的旅程。你用亲身经历带给我的启发与激励，支持我走到今天。

舅妈**于燕**女士，感谢你无论顺境还是逆境，都始终给予我支持。过去四年里，每次回国对我而言都并不容易。然而，每一次回去，你总会热情地接待我，带我出去玩，让我在艰难的时刻依然感受到家人带来的温暖与慰藉。

我的猫，咪小咪。在北部苦寒之地读博的这些年里，没有你的陪伴，生活大概会变得了无生趣。你用自己的方式，安静地参与了这段时光。在无数疲惫、孤独和情绪低落的时刻，你的存在让日子多了一点温柔，一点盼头，也让我在琐碎而艰难的生活里，依然能够感受到被陪伴的幸福。

最后，也是最重要的，我想感谢那个在面对困难时依然努力挣扎、咬牙前行的自己。一路走来，虽然有过迷茫、疲惫、委屈与无助，但我始终没有真正停下脚步。无论未来的道路通向何方，都希望自己能够不忘初心，始终保有内心的热爱、勇气与坚持，在经历中继续成长，在风雨中依然坚定地走下去。

About the author

Liu Sun was born on August 11, 1993, in Jilin, China, a city blanketed in snow for nearly half of the year. She began her academic journey at Harbin Medical University and subsequently earned her Bachelor's degree in 2017 and Master's degree in 2020 in Clinical Medicine (Cardiology). During her master's training, she also completed the required clinical residency rotations and obtained the corresponding training certificate.

In 2020, Liu Sun was awarded the joint China Scholarship Council (CSC)–University of Groningen scholarship to pursue doctoral training as a PhD researcher in the Department of Experimental Cardiology at the University Medical Center Groningen (UMCG), the Netherlands. Supervised by Prof. Dr. Herman Silljé and Dr. V. Oliveira Nunes Teixeira, the PhD research focused on elucidating the molecular mechanisms of PLN-R14del cardiomyopathy and identifying novel therapeutic strategies using an established transgenic PLN-R14del mouse model. Throughout the doctoral training, Liu Sun actively took part in scientific conferences in Europe and presented research findings at international congresses.

During her academic career, she matured into an independent researcher and contributed to the field through multiple scientific publications. Moving forward, she plans to apply her background in clinical medicine, animal models and cardiovascular research to the advancement of translational medicine and pre-clinical innovation. Her long-term goal is to develop effective therapeutic strategies for pressing cardiac problems and to make a meaningful contribution to biomedical science as a researcher and a doctor.